ARROW ENERGY PTY LTD

PL253 Groundwater Impact Assessment - Clynes Road FDP

Document no. Rev 0: 411001-00917-REP-HG-002

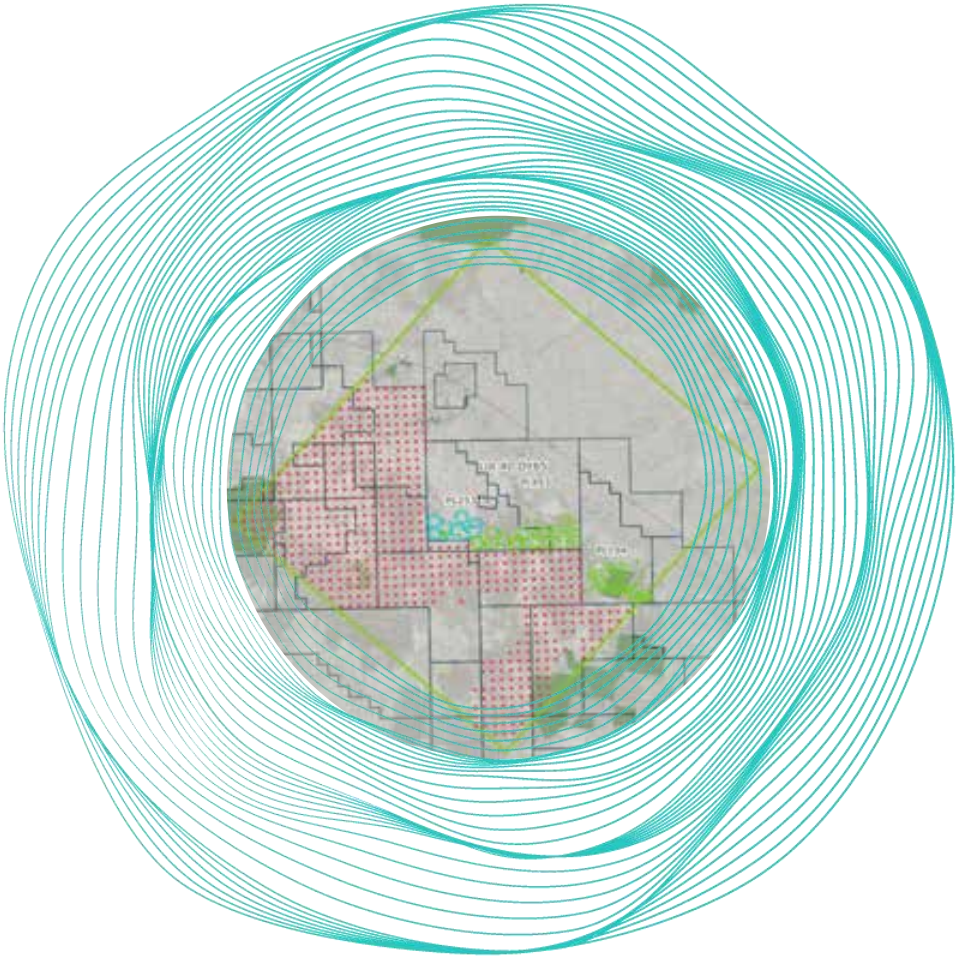

29 April 2026

Level 23, 123 Albert Street
Brisbane QLD 4000
PO Box 15081, City East QLD 4002
Australia
T: +61 7 3377 7000
Worley Consulting Pty Ltd
ABN 50 098 008 818

worley.com

Disclaimer

This report has been prepared on behalf of and for the exclusive use of Arrow Energy Pty Ltd, and is subject to and issued in accordance with the agreement between Arrow Energy Pty Ltd and Worley Consulting Pty Ltd. Worley Consulting Pty Ltd accepts no liability or responsibility whatsoever for it in respect of any use of or reliance upon this report by any third party. Copying this report without the permission of Arrow Energy Pty Ltd or Worley Consulting Pty Ltd is not permitted.

The information contained in these documents is protected by the Global Data Protection Regulation (GDPR). Worley complies with the provisions of the Regulation and the information is disclosed on the condition that the Recipient also complies with the provisions of the (GDPR). In particular, all of the resumes and the information contained therein, must be kept securely, must be used only for the purposes of assessing the suitability of the individuals to perform the tasks proposed and/or assessing the overall capabilities of Worley to undertake the Work proposed and must be destroyed upon completion of those purposes.

Details on how personal information provided to Worley is processed can be found at https://www.worley.com/site-services/privacy.

PROJECT - 411001-00917-REP-HG-002: PL253 Groundwater Impact Assessment - Clynes Road FDP							
Rev	**Description**	**Originator**	**Reviewer**	**Worley Approver**	**Revision Date**	**Customer Approver**	**Approval Date**
Rev B	Draft report	M. Azadi	G. Jacobs	M. Azadi	17 April 2026		
Rev 0	Final report	M. Azadi	G. Jacobs	M. Azadi	29 April 2026		

-

29 April 2026

Level 23, 123 Albert Street
Brisbane QLD 4000
PO Box 15081, City East QLD 4002
Australia
T: +61 7 3377 7000
Worley Consulting Pty Ltd
ABN 50 098 008 818

worley.com

Table of contents

Appendices

List of tables

List of figures

Acronyms and abbreviations

Acronym/abbreviation	Definition
BGL	Below Ground Level
COC	Contaminants of Concern
CSG	Coal Seam Gas
FDP	Field Development Plan
GHB	General Head Boundary
HSU	Hydrostratigraphic Units
LOR	Limit of Reporting
OGIA	Office of Groundwater Impact Assessment
QOI	Quantities of Interest
SCM	Site Conceptual Model
UCG	Underground Coal Gasification
WCM	Walloon Coal Measures

1. Introduction

Arrow Energy Pty Ltd (Arrow) proposes to undertake coal seam gas (CSG) production activities within Production Licence 253 (PL253), Queensland. The PL253 area includes the former Hopeland Underground Coal Gasification (UCG) site located on Lot 40 DY85, where historical UCG operations undertaken by Linc Energy resulted in residual hydrocarbon contamination and other UCG by-products within the groundwater system.

Arrow has conducted groundwater monitoring, numerical modelling, and annual reporting in and around the former UCG site since 2018 to characterise groundwater conditions, contaminant behaviour, and potential risks to surrounding receptors. Environmental Authority EA0001401, in effect since November 2023, authorises Stage 1 development activities within PL253, including the drilling and operation of 55 CSG production wells (Kogan Creek development).

Arrow is proposing additional development under an expanded Field Development Plan (FDP) associated with the Jammat project and is seeking regulatory approval for further 55 CSG wells along Clynes Road.

The location of the PL253 project area, the former Hopeland UCG site, and the distribution of Arrow (approved wells and proposed Clynes Road wells) and non-Arrow abstraction wells relevant to this assessment are shown in Figure 1-1.

As part of the Environmental Authority application process, updated groundwater modelling is required to assess the potential impacts of Arrow's proposed activities on groundwater flow, contaminant migration, and long-term groundwater recovery associated with the former Hopeland UCG site. Based on Arrow's previous studies (GHD, 2019; AGE, 2021, 2023; Intera, 2024, 2025), this assessment has been prepared by Worley to support Arrow's application for approval of the proposed expansion.

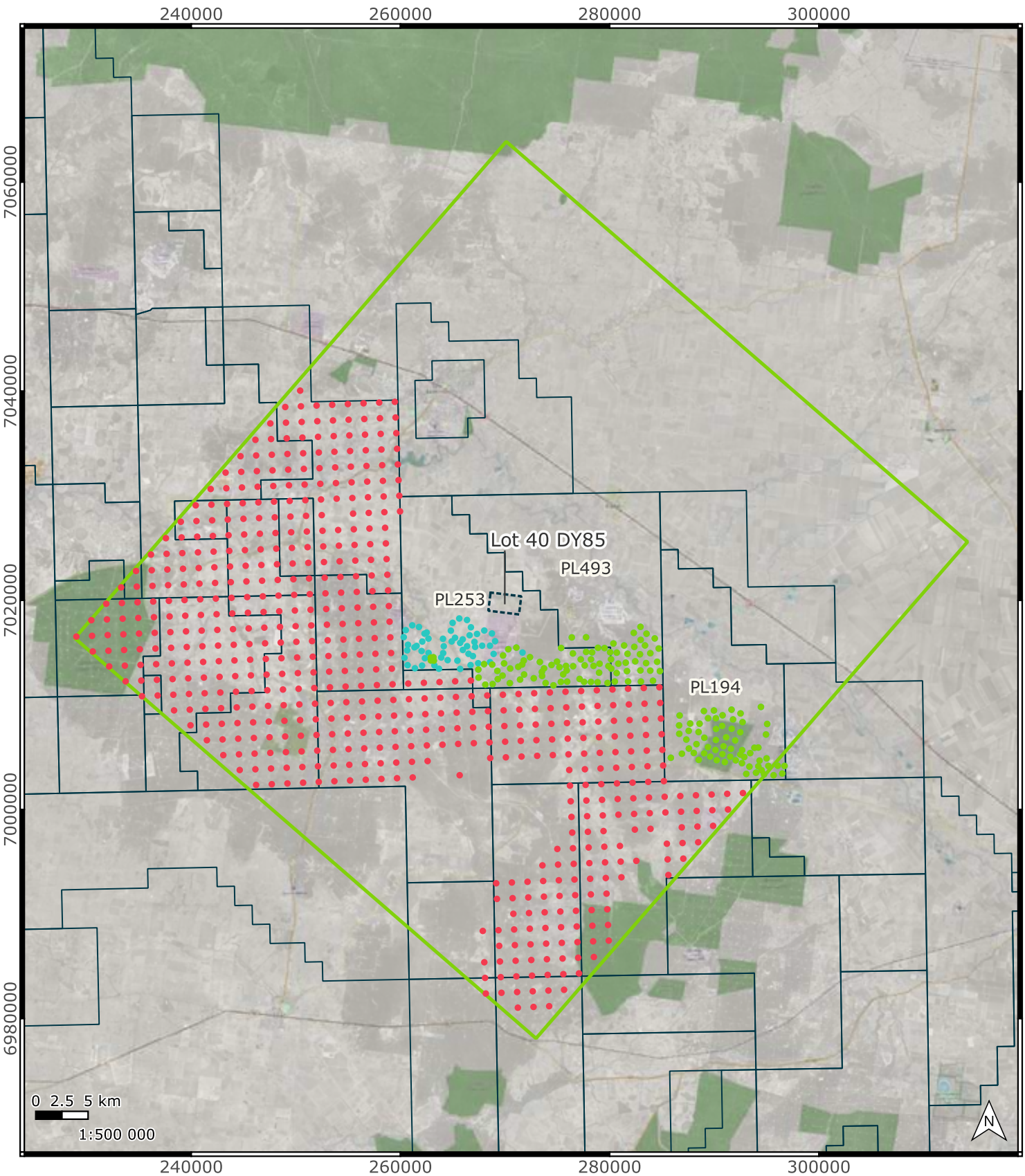

Legend

- Groundwtaer model extent
- Lot 40 DY85
- Petroleum Leases

Well groups

- Approved Arrow wells
- Arrow Clynes Rd wells
- Non-Arrow abstraction points (from UWIR 2021)

Project location and distribution of Arrow and non-Arrow wells

Project No.	Client	Figure No.
411001-00917	Arrow	1-1

Notes:
Project CRS: GDA94 / MGA zone 56
Last Saved: 12:58 25/02/2026
Filename: Figure_1-1
Exported by User: Mohsen.Azadi
Project Exported: 13:15 25/02/2026

References:
N/A

File Path: C:\modelling\Arrow\deliverables\Figures_REP-HG-001\Figure_1-1.qgz

worley consulting

1.1 Scope of work

The scope of work of this study is to assess the potential impacts of Arrow's proposed activities on groundwater flow, contaminant migration, and long-term groundwater recovery associated with the former Hopeland UCG site. The scope includes:

Site conceptual model development

Building on Arrow's previous investigations and modelling studies (GHD, 2019; AGE, 2021, 2023; Intera, 2024, 2025), the Site Conceptual Model (SCM) was updated to incorporate the latest hydrostratigraphic units defined in Arrow's geology model and to refine the understanding of groundwater flow and contaminant behaviour at Lot 40 DY85. The updated SCM integrates groundwater monitoring data from existing bores located both within and beyond Lot 40 DY85 and incorporates current interpretation of residual contaminant source zones associated with historical UCG activities.

The updated SCM was developed to identify potential contaminant mobilisation pathways and to characterise groundwater flow directions and concentration distributions in the vicinity of Lot 40 DY85. This refined conceptualisation provides a robust and informed basis for subsequent numerical model development, history matching, and impact assessment.

Groundwater flow and transport model development

A numerical groundwater flow and contaminant transport model was developed to represent aquifers on and in the vicinity of Lot 40 DY85, with particular focus on the Springbok sandstone and the Macalister coal seam including relevant Walloon Coal Measures (WCM) units. The model was configured to evaluate historical and future changes in groundwater flow directions, and contaminant migration associated with UCG and CSG abstraction. Building on Arrow's most recent PL253 numerical groundwater model (Intera, 2025), the model was updated to incorporate the proposed FDP for the Jammat project, including the Clynes Road wells.

The numerical simulation period was extended to the end of 2225 (200 years predictive period), to enable assessment of long-term groundwater recovery and potential contaminant migration beyond the abstraction period.

History matching groundwater flow and contaminant transport models

History matching (i.e., calibration) of the groundwater flow and contaminant transport models was undertaken using all available groundwater level data, including monitoring data from Arrow's newly installed Hopeland wells (HL34–HL37).

Particle tracking and contaminant transport modelling

Two approaches were considered to assess the impact of Arrow's proposed FDP on migration of contaminants within PL253, in particular around and within Lot 40 DY85. These include particle tracking and contaminant transport modelling.

First, the particle tracking model was developed based on the history-matched groundwater flow model and used to assess potential contaminant flow paths without including natural attenuation processes, effectively simulating the centre of a plume of a conservative tracer. The contaminant transport model was then developed based on the calibrated groundwater flow model. Unlike particle tracking model, the contaminant transport model includes

mechanical dispersion, molecular diffusion, as well as natural attenuation (sorption and biodegradation/decay) and dual domain mass transfer processes continuously occurring within subsurface.

Particle tracking fulfilled the following objectives:

- Assessed the effect of particle tracking starting in wells that have exhibited elevated UCG contaminants.
- Particles included the following locations:
  - All monitoring bores,
  - All model cells intercepting gasifier locations, and
  - All model cells intercepting Lot 40 DY85 boundaries.
- Assessed particle tracks (travel times, distances and trajectories) to evaluate the impact of Arrow's proposed FDP on migration of contaminants from Lot 40 DY85.

The contaminant transport model, developed based on the SCM and groundwater flow model, incorporates:

- the most recent groundwater quality data for model history matching, and
- dual porosity (or dual permeability) capability to better represent contaminant transport into and out of fractures and low permeability pore spaces that may contain residual contaminant sources.

Predictive uncertainty analysis

An uncertainty analysis was undertaken to evaluate the influence of hydrogeological variability on model predictions.

Impact assessment

Predictive impact assessment were undertaken to evaluate potential future contaminant migration from Lot 40 DY85 during the abstraction period and long-term groundwater recovery associated with the former Hopeland UCG site.

1.2 Study objectives

The overarching objective of this study is to provide a comprehensive understanding of the potential impacts of Arrow's proposed FDP on groundwater flow and contaminant migration associated with the former Hopeland UCG site on Lot 40 DY85.

The outcomes of this study are intended to:

- Support Arrow's Environmental Authority application, ongoing groundwater management, and
- Provide confidence that potential impacts to groundwater resources and receptors are appropriately understood and managed.

2. Site conceptualisation model

2.1 Previous studies

Hydrogeological understanding of the former Hopeland UCG site and surrounding PL253 area has evolved through a sequence of investigations, conceptual studies and modelling exercises completed since the start of (and informed by) UCG operations. UCG trial activities conducted on Lot 40 DY85 between 1999 and 2013 established the disturbance setting that subsequent studies sought to characterise, including local depressurisation, potential formation fracturing, and hydrocarbon byproducts in groundwater. Early conceptualisation work documented the site setting and identified the Springbok sandstone and the Macalister coal seams as the principal water-bearing horizons of interest, along with potential recharge mechanisms and the influence of historical operations on pressures and groundwater flow pathways. An SCM of contamination sources, groundwater flow pathways and receptors is shown in Figure 2-1 (from Epic, 2020).

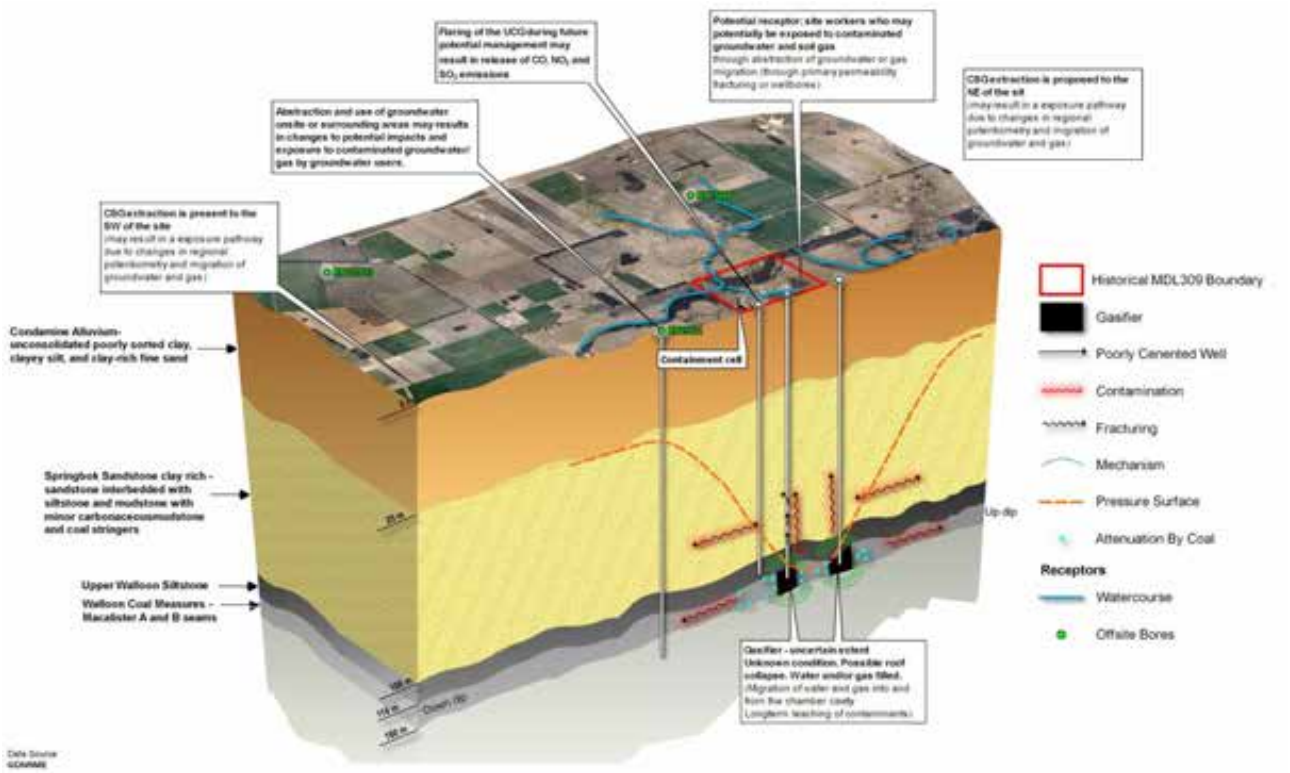

Figure 2-1 Conceptual Site Model of former Hopeland UCG (from Epic, 2020)

Previous hydrogeological studies (GHD, 2019; OGIA, 2021; AGE, 2021, 2023; Intera, 2024, 2025) have progressively integrated regional hydrogeological understanding and datasets, including basin-scale conceptualisation and parameter compilations widely used in the Surat Basin, and groundwater impact assessment studies that represent cumulative CSG influences. These earlier efforts informed the selection of HSUs, parameter ranges and boundary condition approaches used later in numerical groundwater modelling, particularly where regional depressurisation from CSG production governs vertical gradients and flow patterns.

Within PL253 and the immediate Hopeland area, prior groundwater modelling provided the basis for progressively refined representations of stratigraphy, hydraulic properties, and operational stresses. The groundwater modelling studies include earlier models developed by GHD (2019), AGE (2021 and 2023), and Intera (2024 and 2025). These site-focused modelling and assessments aimed to support groundwater monitoring network planning and the evaluation of contaminant mobility under CSG influences. These works collectively established the baseline model domain, local refinement requirements around Lot 40 DY85, and the need to represent UCG-related pressure changes and potential property alterations in and above the gasifier zone.

Detailed hydrogeological conceptualisation of the Surat Basin and PL253 has been reported previously (GHD, 2019; OGIA, 2021a, 2021b; Intera, 2025). The following sections provide a brief overview of the site hydrogeology and summarise relevant updates to date.

2.2 Site setting and geology

The PL253 area is located approximately 20 km south-east of Chinchilla within the Surat Basin. The geological setting comprises Jurassic to Early Cretaceous sedimentary sequences that host multiple aquifers and aquitards relevant to groundwater flow and contaminant transport.

Key HSUs include the Springbok sandstone and the WCM, which are separated by lower-permeability formations that limit vertical groundwater movement. The Macalister coal seam within the WCM was identified as a primary unit of interest due to its association with historical UCG operations and residual contamination. Previous studies (GHD, 2019; AGE, 2021, 2023; Intera, 2024, 2025) used this stratigraphic representation as the basis for numerical model development and conceptualisation.

In these studies, local geological complexity, including heterogeneity within coal seams and interburden units, was incorporated into the groundwater model using pilot point parameterisation. Structural features such as minor faults and fractures were recognised as potential sources of uncertainty but were not considered to form persistent preferential pathways at the site scale.

2.3 Groundwater flow regime

Regional groundwater flow within the Surat Basin is generally directed towards the south to southwest, consistent with basin-scale hydraulic gradients. The localised changes to this regional pattern are influences associated with historical UCG operations and regional CSG production.

Previous modelling works (GHD, 2019; AGE, 2021, 2023; Intera, 2024, 2025) have identified a localised hydraulic depression centred on Lot 40 DY85, reflecting residual effects at the end of UCG activities. Groundwater levels within this area have shown relative stability since the end of UCG activities, with evidence of gradual recovery in some monitoring bores.

Vertical hydraulic gradients are characterised by higher heads in overlying Springbok formation relative to the Macalister coal seam, indicating downward gradients that limit the potential for upward contaminant migration under current conditions.

2.4 Groundwater Monitoring

Groundwater monitoring within and surrounding Lot 40 DY85 has been undertaken over several years to characterise groundwater levels, assess groundwater quality, and track the behaviour of residual contaminants associated with historical UCG activities at Lot 40 DY85. The monitoring network includes bores installed in the Springbok sandstone and WCM, with a particular focus on the Macalister coal seam, reflecting the primary HSUs relevant to contaminant migration risk.

Monitoring data have been collected through a combination of Arrow groundwater monitoring programs, Queensland Government (DETSI/DoR) monitoring, and targeted investigations implemented to satisfy Environmental Authority (EA0001401) requirements. The monitoring framework has been progressively expanded and refined, including installation of additional Springbok sandstone monitoring bores (Hopeland 34 to Hopeland 37), to improve spatial coverage and vertical resolution in the vicinity of the former UCG site and along inferred flow paths.

Groundwater monitoring data has been used to inform groundwater flow directions, assess water quality trends, and support the ongoing history matching of groundwater flow and contaminant transport models, consistent with EA Water Conditions.

2.4.1 Groundwater level

Groundwater level monitoring is undertaken across a network of monitoring bores (including nested bores) screened in the Springbok sandstone and multiple seams within the WCM, including the Macalister coal seam. Regional context indicates that groundwater flow in the Surat Basin is generally towards the south to south-west, with widespread depressurisation of the WCM associated with historical and ongoing CSG production (OGIA, 2021b).

Monitoring data show vertical hydraulic gradients are predominantly directed towards the WCM, indicating downward gradients from the Springbok sandstone and upward gradients from deeper units, consistent with OGIA conceptualisation and reducing the likelihood of vertical contaminant migration out of the coal measures.

Site-specific groundwater level data indicate that, following the end of UCG activities, water levels within the Springbok sandstone and Macalister coal seam have shown partial recovery, with trends stabilising in recent years. Localised variability remains evident near former gasifier locations, reflecting heterogeneity in formation properties and the historical influence of gasifier voids.

Groundwater level observations collected from all monitoring bores up to Q4 2025 were reviewed to remove outlier or non-representative measurements (e.g., data affected by gas interference or incomplete recovery following sampling) prior to use in model history matching. The resulting dataset was used to inform model parameterisation with both absolute head targets and vertical head difference targets, consistent with OGIA (2021a) regional groundwater modelling methodology and Australian Groundwater Modelling Guidelines (Barnett et al., 2012).

To better represent the most recent groundwater flow directions near Lot 40 DY85, groundwater level contours for the Springbok sandstone and Macalister coal seam were generated using Q3 2025 data. Q3 2025 was selected rather than Q4 2025 because it corresponds to the monitoring period with the greatest number of concurrent groundwater level observations across Lot 40 DY85. These contours (shown in Figure 2-2) provide the most recent estimate of potentiometric conditions and were used to inform interpretation of lateral flow directions and hydraulic gradients in the vicinity of the former UCG site.

The Q3 2024 groundwater level indicates that hydraulic gradients in the Springbok sandstone directed inward towards Lot 40 DY85, while for Macalister coal seam it is directed to the west and southwest corner of Lot 40 DY85. These variability of hydraulic gradients reflect the continued influence of historical depressurisation associated with UCG activities and regional WCM drawdown.

Springbok sandstone

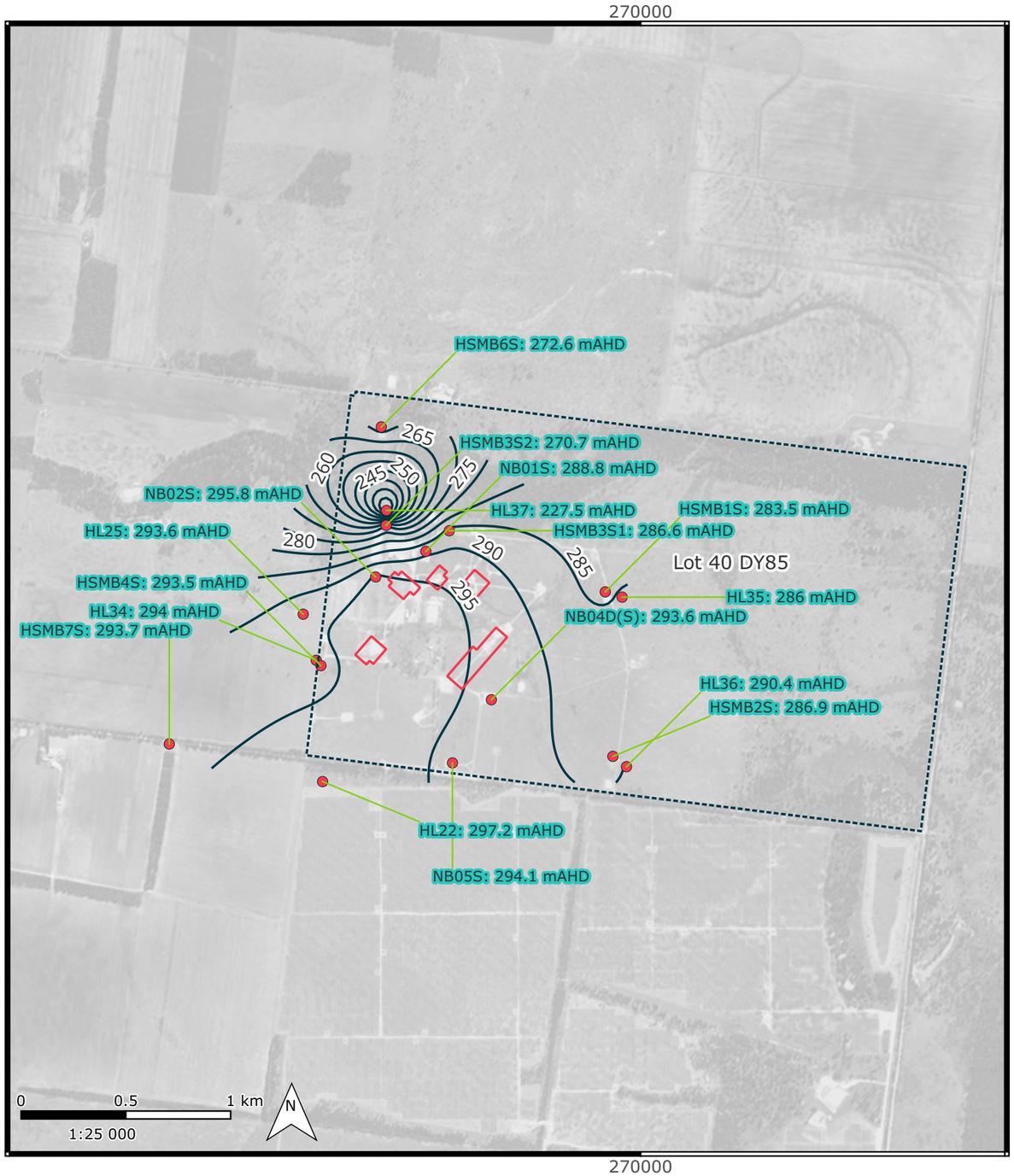

Macalister coal seam

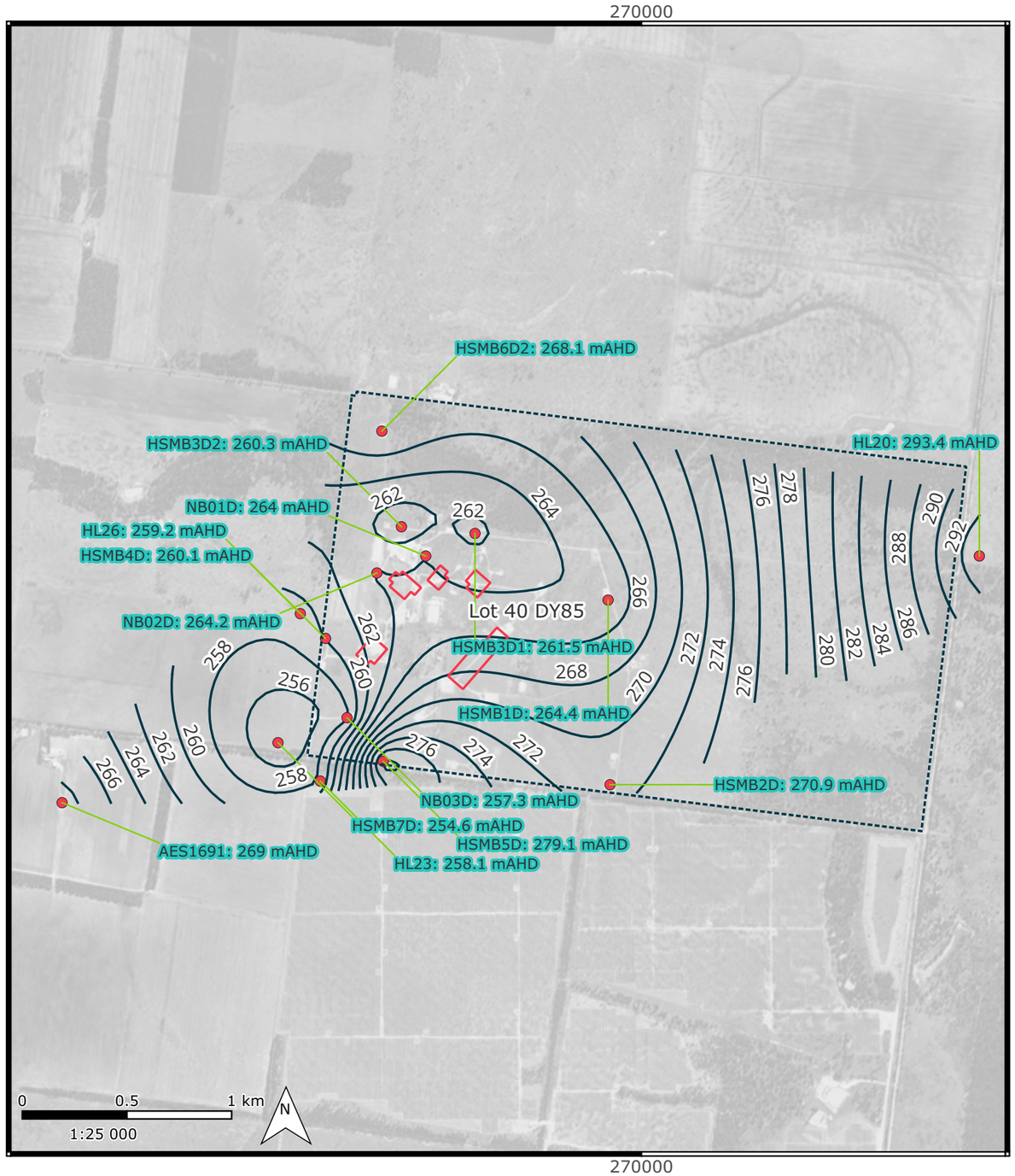

Legend

- Lot 40 DY85
- Gasifiers
- Monitoring bores
- Groundwater contours (mAHD)

Simulated groundwater levels in Springbok sandstone and Macalister coal seam for scenario 3 (end of December 2024)

Project No.	Client	Figure No.
411001-00917	Arrow	2-2

Notes:
Project CRS: GDA94 / MGA zone 56
Last Saved: 15:41 16/04/2026
Filename: Figure_2-2_GWL_contours_2025

Exported by User: Mohsen.Azadi
Project Exported: 15:46 16/04/2026

References:
N/A

File Path: C:\modelling\Arrow\deliverables\Figures_REP-HG-002\Figure_2-2_GWL_contours_2025.qgz

2.4.2 Groundwater quality and contaminants of concern

Similar to previous studies (AGE, 2021, 2023; Intera, 2024, 2025), benzene and naphthalene were selected as representative contaminants of concern (COCs) for the contaminant transport modelling. Benzene, a known carcinogen, is the most mobile of the BTEX (benzene, toluene, ethylbenzene, and xylene) compounds due to its high solubility in water and low adsorption potential (Odermatt, 1994), while naphthalene is the most water-soluble polycyclic aromatic hydrocarbon (PAH) (Bayard et al., 2020). Both compounds exhibited the highest concentrations among their respective groups in the site's chemical dataset. Furthermore, benzene has been shown to degrade more slowly than the other BTEXN compounds (Prommer et al., 2003), making it a reliable indicator of the spatial extent of groundwater contamination.

Elevated concentrations of benzene and naphthalene are generally confined to monitoring bores located on Lot 40 DY85 and in proximity to former gasifier locations. Monitoring data for Springbok sandstone and Macalister coal seam (shown in Figure 2-3 to Figure 2-6) indicate mostly declining concentration trends since 2018, consistent with natural attenuation processes.

Benzene concentrations are generally higher and more persistent than concentrations of other BTEX compounds. Elevated benzene concentrations have been observed onsite in proximity to Gasifiers 1 and 2 (NB01S). In this location, benzene concentrations have shown relative temporal stability or slow decline, consistent with proximity to residual contaminant sources. Offsite monitoring bores generally show low or non-detectable benzene concentrations.

Naphthalene concentrations are typically lower than benzene and are detected less frequently. Monitoring results indicate that naphthalene concentrations have declined over time across most bores, with many locations now recording concentrations below laboratory Limit of Reporting (LOR). This is due to naphthalene's stronger sorption and attenuation characteristics relative to benzene.

Overall, monitoring data demonstrate a general declining trend in benzene and naphthalene concentrations since approximately 2020, attributable to a combination of natural attenuation processes, limited advective transport due to low groundwater velocities, and the persistence of inward hydraulic gradients for Springbok sandstone towards Lot 40 DY85.

The groundwater quality dataset provides no evidence of progressive offsite migration of benzene or naphthalene under current conditions and supports the conclusion that residual contamination remains localised and effectively contained within the former UCG site area under existing and proposed CSG development scenarios.

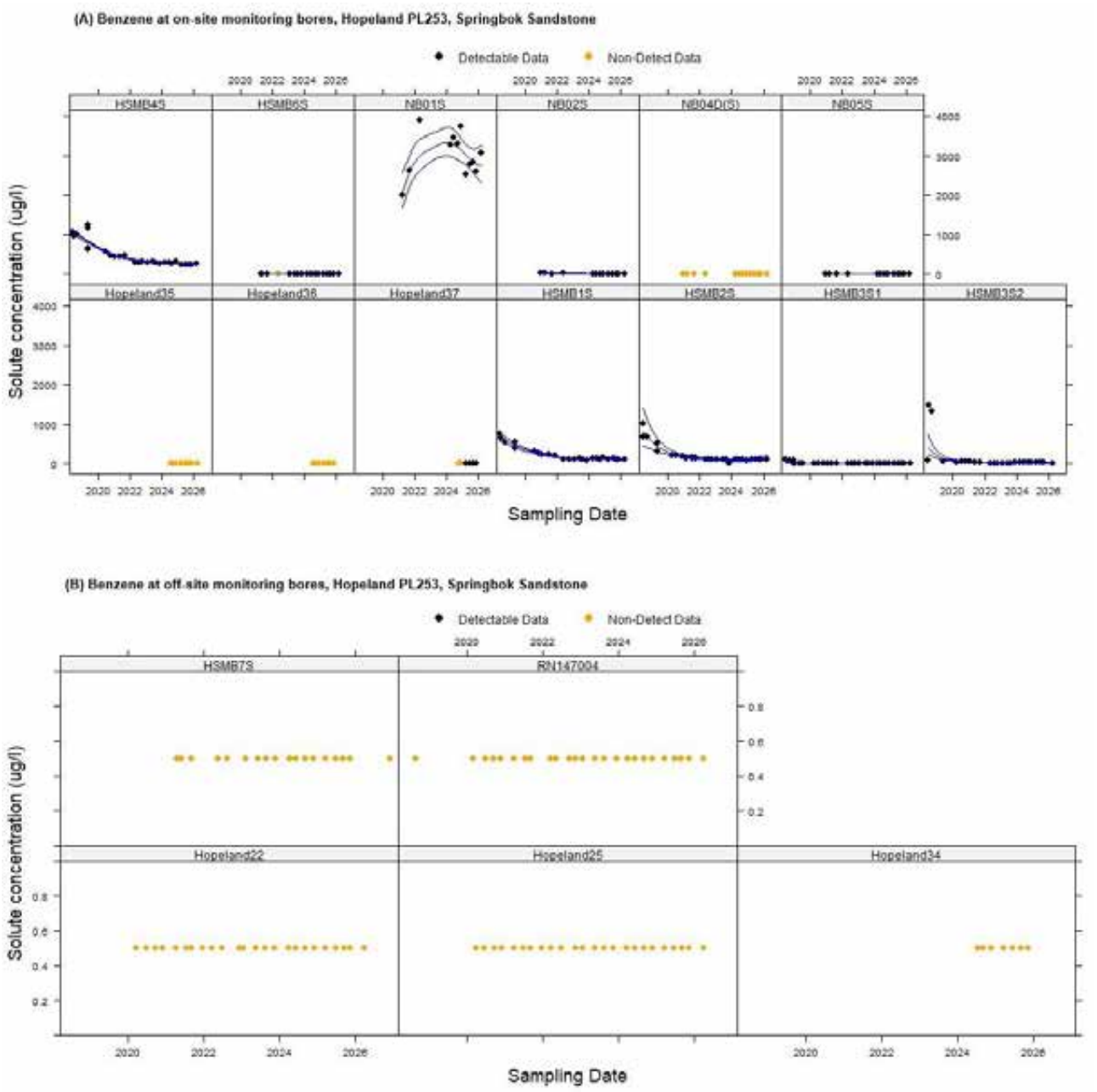

Figure 2-3 Time series benzene concentration for a) on-site and b) off-site bores completed in the Springbok sandstone (provided by Arrow)

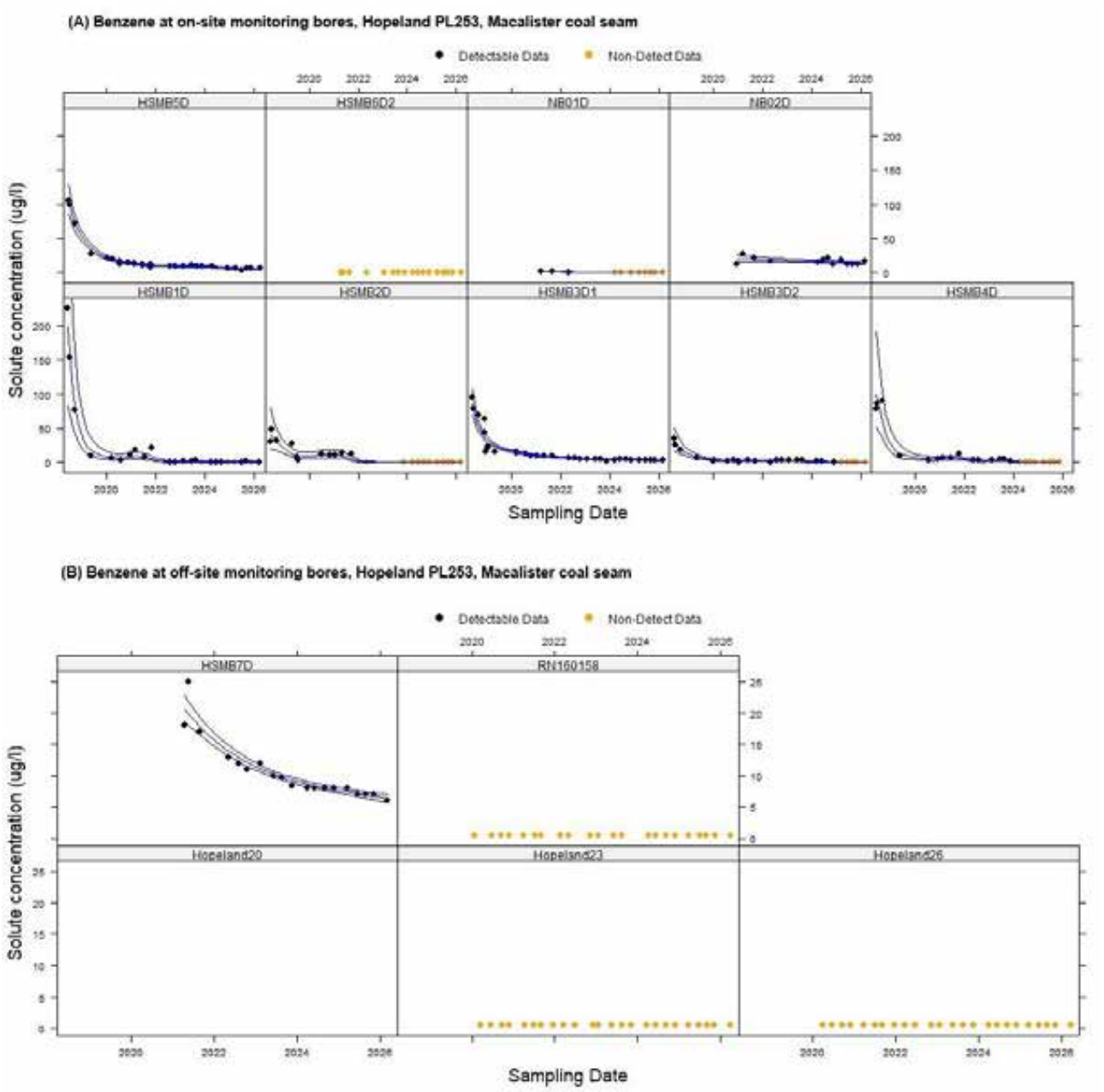

Figure 2-4 Time series benzene concentration for a) on-site and b) off-site bores completed in the Macalister coal seam (provided by Arrow)

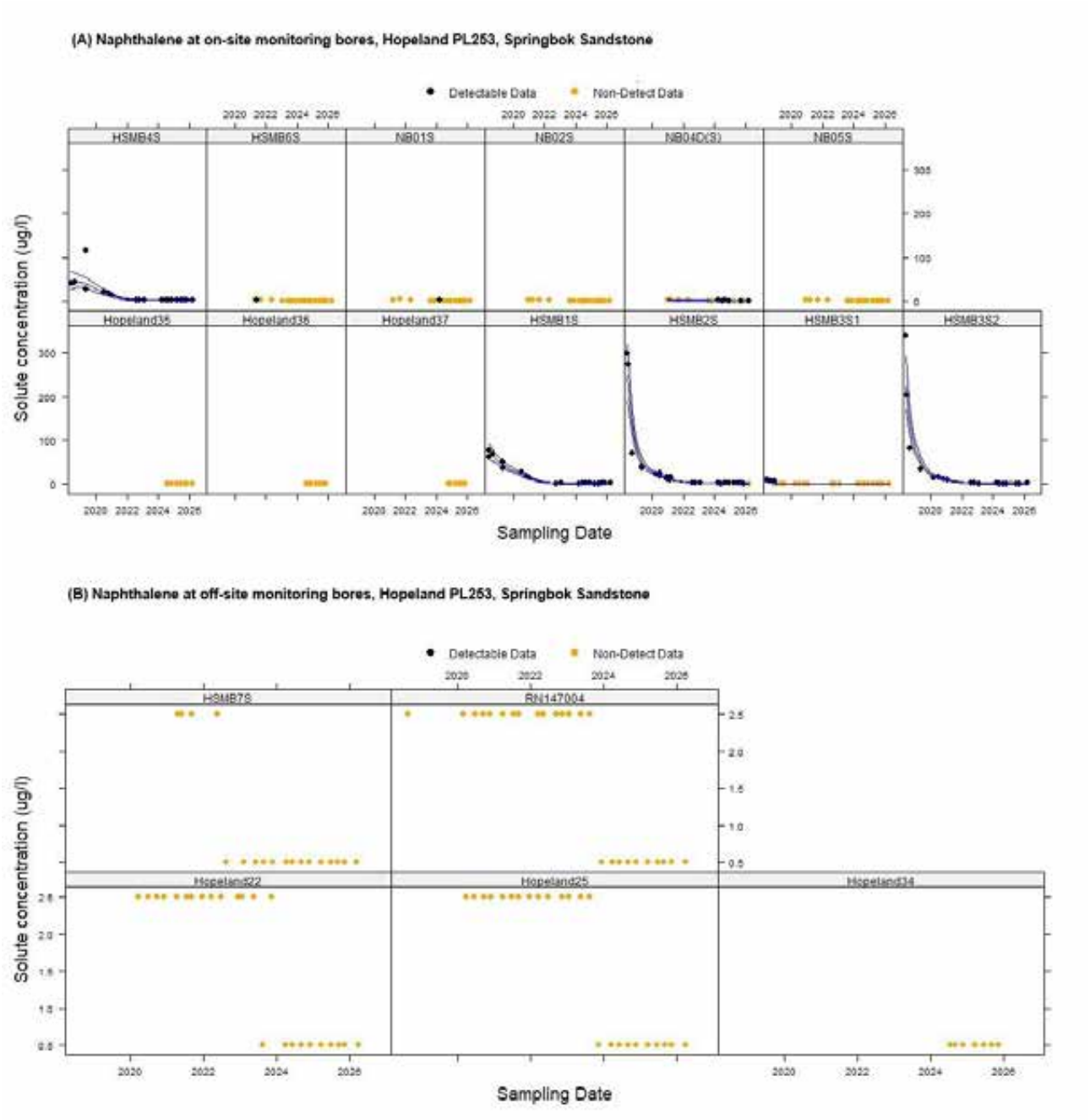

Figure 2-5 Time series naphthalene concentration for a) on-site and b) off-site bores completed in the Springbok sandstone (provided by Arrow)

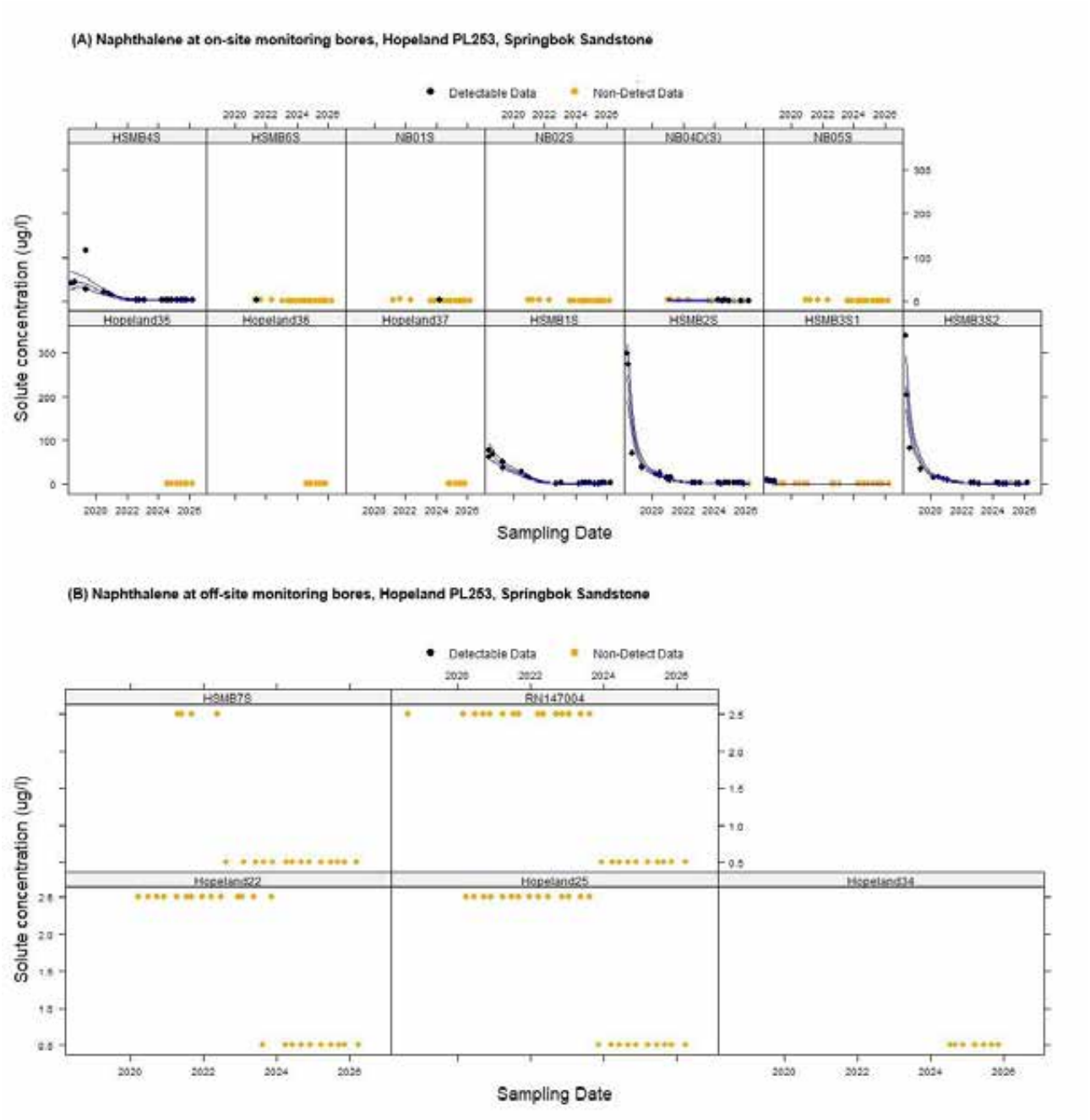

Figure 2-6 Time series naphthalene concentration for a) on-site and b) off-site bores completed in the Macalister coal seam (provided by Arrow)

2.4.2.1 Contaminant source depletion at gasifiers

The contaminant transport model incorporates a time-varying source depletion term to represent the gradual reduction in residual contaminant mass available for dissolution from the gasifiers. Source depletion was implemented to capture long-term declines in contaminant concentrations attributable to natural attenuation processes (i.e., sorption, and degradation). Rather than assuming a constant or infinite source, this approach provides a more realistic

representation of contaminant behaviour, while allowing for the continued release of residual contaminants from dead-end pores.

The source depletion formulation was defined using the most comprehensive available groundwater quality dataset. For each compound and HSU (Springbok sandstone and Macalister coal seam), the highest observed concentration from all monitoring bores at each sampling event was extracted from the full time-series record as shown in Figure 2-7 and Figure 2-8 for benzene and naphthalene, respectively. This upper-envelope dataset was used conservatively to derive an exponential decay relationship describing the temporal reduction in source concentration. The fitted exponential functions were then used to define time-varying source boundary conditions in the contaminant transport model.

For benzene, the extracted maximum concentration time series shows a gradual but persistent decline over time across monitoring bores screened in the Springbok sandstone and Macalister coal seam. An exception is elevated concentrations observed in monitoring bore NB01S within the Springbok sandstone (blue points above the fitted exponential decay curve in Figure 2-7). The elevated benzene concentrations at NB01S, which is proximal to former gasifier areas, are interpreted to represent a localised and spatially confined source. This interpretation is supported by groundwater monitoring data from surrounding bores (HSMB3S1, HSMB3S2, and NB02S), which indicate substantially lower concentrations consistent with the broader monitoring network.

Given the localised nature of the elevated benzene concentrations at NB01S, an ongoing source term with a constant concentration was adopted within a 50 m radius of this bore and assessed separately within the contaminant transport model. This approach allows the broader, data-derived source depletion term to be applied across Lot 40 DY85, while explicitly accounting for localised residual contamination in the vicinity of NB01S.

An exponential decay function was fitted to the upper-envelope benzene dataset for all the remaining monitoring bores, representing the depletion of benzene source as shown in equations (1) and (2) for springbok sandstone and Macalister coal seam, respectively:

$$C(t) = 1750\, e^{-0.00065\, t} \quad (1)$$

$$C(t) = 375\, e^{-0.001\, t} \quad (2)$$

where C(t) is source concentration term in (µg/L), and t is the number of days from the first day of contaminant transport simulation on 1/1/2018.

Naphthalene monitoring data indicate lower maximum concentrations and a more rapid decline relative to benzene, consistent with stronger sorption and attenuation characteristics. The same upper-envelope methodology was applied, with maximum naphthalene concentrations extracted from all monitoring bore records and fitted with an exponential decay function. The resulting relationship was used to define the naphthalene source depletion term in the transport model as shown in equations (3) and (4) for springbok sandstone and Macalister coal seam, respectively:

$$C(t) = 500\, e^{-0.0019\, t} \quad (3)$$

$$C(t) = 75\, e^{-0.0019\, t} \quad (4)$$

Springbok sandstone

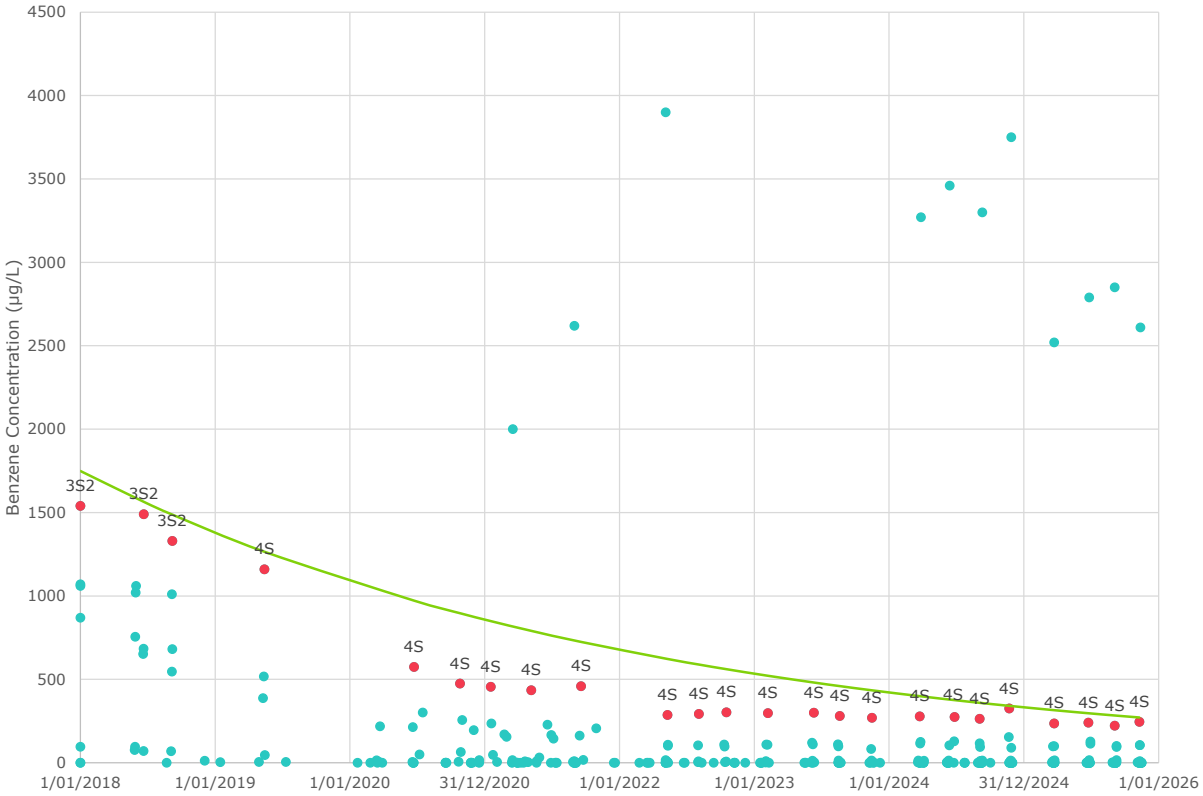

Macalister coal seam

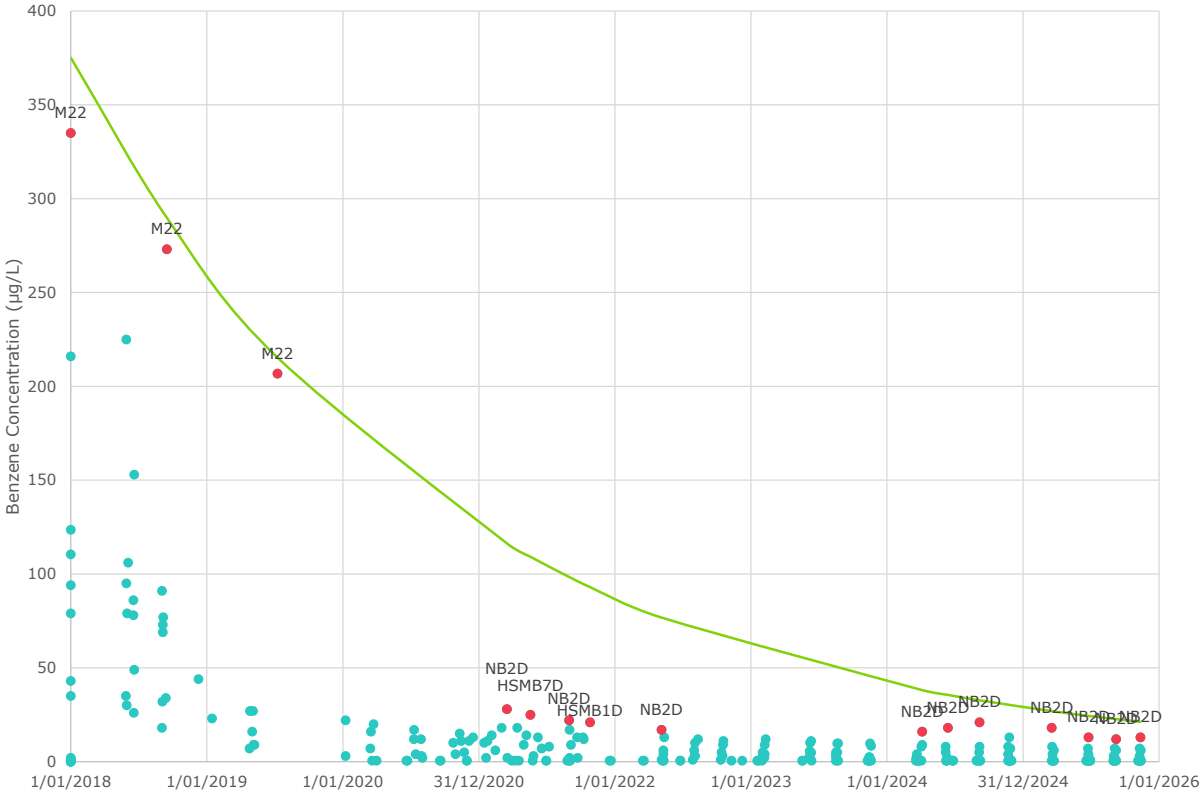

Figure 2-7 Benzene concentration for all monitoring bores compared with exponential curve of source depletion term for a) Springbok sandstone and b) Macalister coal seam

Springbok sandstone

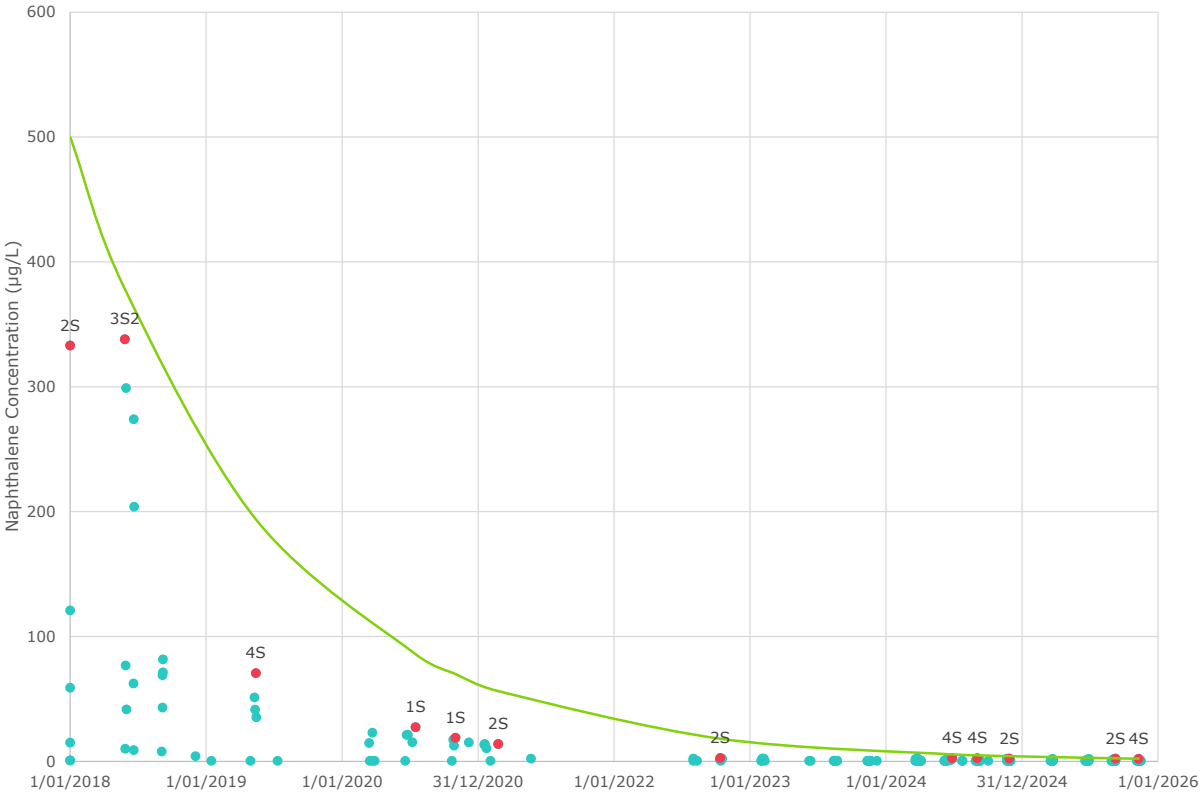

Macalister coal seam

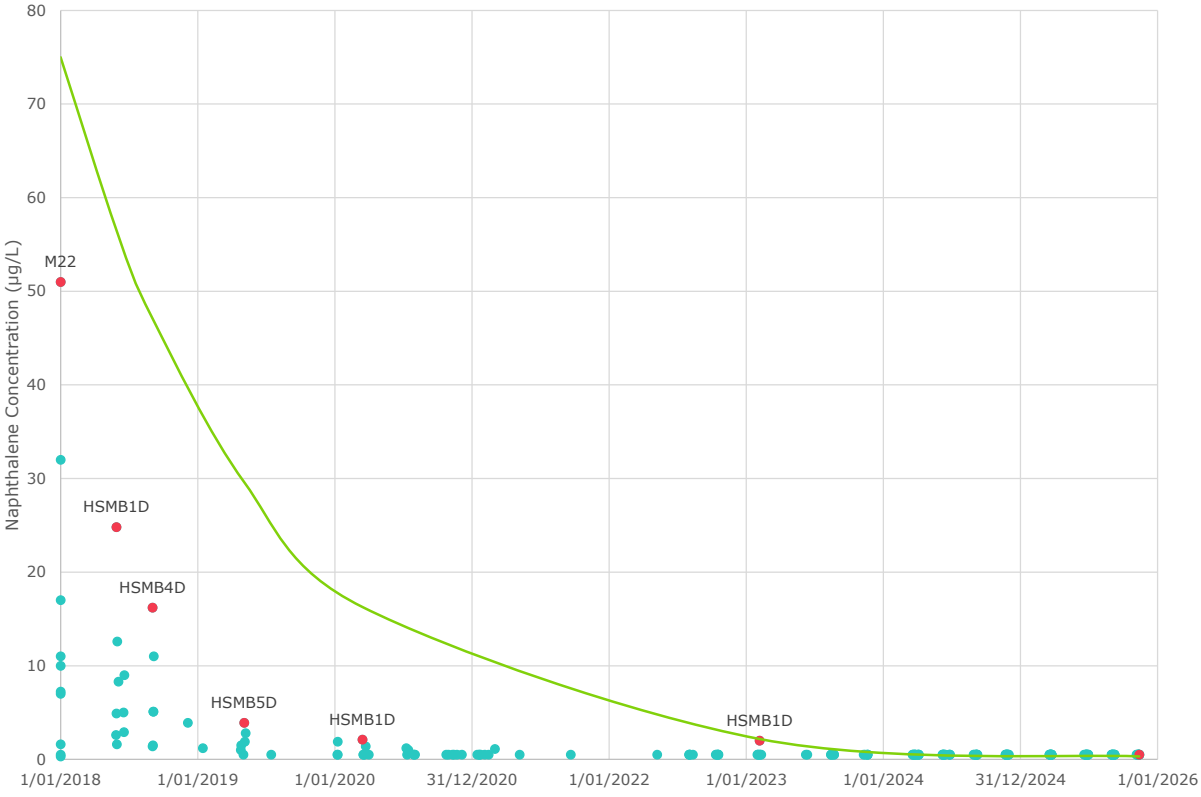

Figure 2-8 Naphthalene concentration for all monitoring bores compared with exponential curve of source depletion term for a) Springbok sandstone and b) Macalister coal seam

3. Groundwater modelling

3.1 Groundwater flow model

Building on Arrow's recent PL253 numerical groundwater model (INTERA, 2025), a numerical groundwater model was developed to assess the impacts of Arrow's proposed FDP for the Clynes Road wells. The model focuses on aquifers on and surrounding Lot 40 DY85, including the Springbok sandstone and the Macalister coal seam and associated aquifers within the WCM. The groundwater model is developed to evaluate and predict potential changes in contaminant transport, groundwater flow directions, and drawdown resulting from development of the Clynes Road wells.

The groundwater model extent (Figure 1-1), is consistent with the area adopted by previous studies (e.g., GHD, 2019, 2020; AGE, 2021, 2023; INTERA, 2024, 2025). It encompasses an approximately 20-km radius around Lot 40 DY85 and includes PLs 253, 493 and 185, as well as adjacent areas, ensuring the model captures key hydrogeological stresses and their zones of influence during past and future activities.

The rectangular model domain (Figure 1-1) was rotated so that the northeastern boundary aligns with the extent of WCM, while the northwest and southeastern boundaries are roughly parallel to the strata dip and regional groundwater flow direction. From a numerical modelling perspective, the boundaries were defined to minimise potential boundary effects and ensure that all relevant flow pathways can be fully simulated within the required timeframes.

Consistent with the most recent groundwater model (INTERA 2025, shown in Figure 3-1), the updated model is developed in MODFLOW 6 incorporating local grid refinement around Lot 40 DY85, with 18 layers representing the key HSUs in the area. The use of MODFLOW 6 introduced improvements in modelling assumptions and boundary condition representation (e.g. incorporation of dual-porosity processes). However, the predictive model remained subject to a wide range of uncertainty in some aspects of the predictions. Accordingly, while maintaining the MODFLOW 6 modelling platform, a comprehensive review of the previous modelling work was undertaken, and key boundary conditions and HSU representation were revised. This approach enabled incorporation of hydrogeological information to revise the model boundary conditions, while retaining the strengths of the MODFLOW 6 platform in the current groundwater model.

Boundary conditions (presented in this chapter) represent regional groundwater influences, historical UCG depressurisation, and CSG abstraction from Arrow and non-Arrow wells. Time-varying hydraulic properties are used to reflect changes associated with UCG operations.

The prediction period extends to the end of 2225 (200 years), well beyond the groundwater abstraction period, when off-site contaminant migration may become possible.

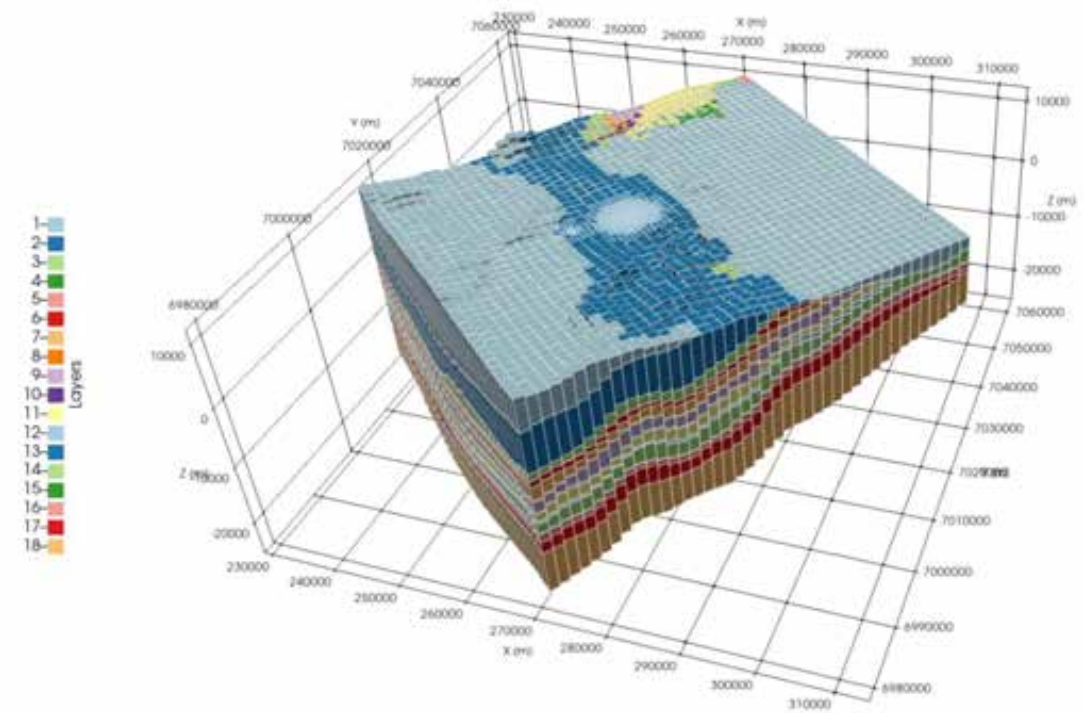

Figure 3-1 3D groundwater model with 30x vertical exaggeration (from Intera, 2025)

Key updates incorporated in the current numerical groundwater flow model include:

- Updated HSUs based on the latest geology model developed by Arrow.
- The General Head Boundary (GHB) conditions were extracted from the OGIA 2021 cumulative groundwater model and assigned to model boundary layers ensuring alignment between the two model layers. Additionally, excessively high conductance values used at the model boundaries in the previous model (INTERA, 2025) were updated based on the individual cells' hydraulic conductivity and thickness.
- The drain (DRN) package elevations were extracted from the OGIA 2021 cumulative groundwater model for simulation of CSG abstraction. The extracted elevation time series were assigned to the groundwater model layers ensuring alignment between the two model layers. Additionally, conductance values were calculated based on the individual cells' hydraulic conductivity, thickness and a multiplier factor informed during history matching.
- Simulation solver settings were updated to ensure the numerical model converges in all the model time steps aligned with Australian Groundwater Modelling Guidelines (Barnett et al 2012). If the model does not converge during a specific time step, the simulation stops and does not proceed further.
- Unlike the previous model (INTERA, 2025), which used the Drain Package to simulate groundwater abstraction under FDP scenarios (with and without the Clynes Road wells), the current model uses the WEL Package. This approach avoids estimation errors associated with converting well flow rates to drain elevations in the drain boundary condition. Model inputs include bore locations, screened intervals, and time-series pumping rates.
- Updated groundwater level datasets to inform both steady-state and transient history matching and incorporated current groundwater flow directions into the calibration targets.
- Refinement of pilot points location to capture spatial heterogeneity in hydraulic parameterisation of the aquifer system based on a conceptual understanding of groundwater flow directions and monitoring bore locations.

- A review and revision of the other modelled boundary conditions (e.g. recharge, and multi-aquifer well boundary conditions) in the previous model (INTERA, 2025) to improve the simulation of groundwater flow regimes consistent with the hydrogeological conceptualisation.
- Model calibration, predictive simulations and uncertainty analysis using the combined Ensemble Space Inversion[1] (PEST-ENSI) and Iterative Ensemble Smoother (PESTPP-IES, White, 2018) methods to replicate historical groundwater flow systems and understand the probability envelope associated with environmental impacts within PL253.

3.1.1 Model layers

Model layers are built based on HSU geometry from Arrow's geological model. The lithological contacts were discretised using Intera's model grid to construct the updated model layers and are aligned with the previous groundwater models as presented in Table 3-1 and shown in Figure 3-2.

Table 3-1 Model layers

Hydrogeological Domain	Average thickness (m)	Model Layer
Condamine alluvium/Gubberamunda sandstone	43.8	1
Westbourne formation	56.7	2
Springbok sandstone	96.3	3
WCM Kogan coal seam	1.2	4
WCM Kogan interburden	11.9	5
WCM Macalister coal seam	9.5	6
WCM Macalister interburden	54.9	7
WCM Wambo coal seam	3.7	8
WCM Wambo interburden	60.3	9
WCM Argyle coal seam	3.5	10
WCM Argyle interburden	50.8	11
WCM Tangalooma sandstone	8.7	12
WCM Upper Taroom coal seam	4.0	13
WCM Upper Taroom interburden	88.5	14
WCM Condamine coal seam	5.5	15
WCM Condamine interburden	43.3	16
Eurombah formation	81.0	17
Hutton sandstone	197.1	18

[1] https://gmdsi.org/blog/ensemble-space-inversion/

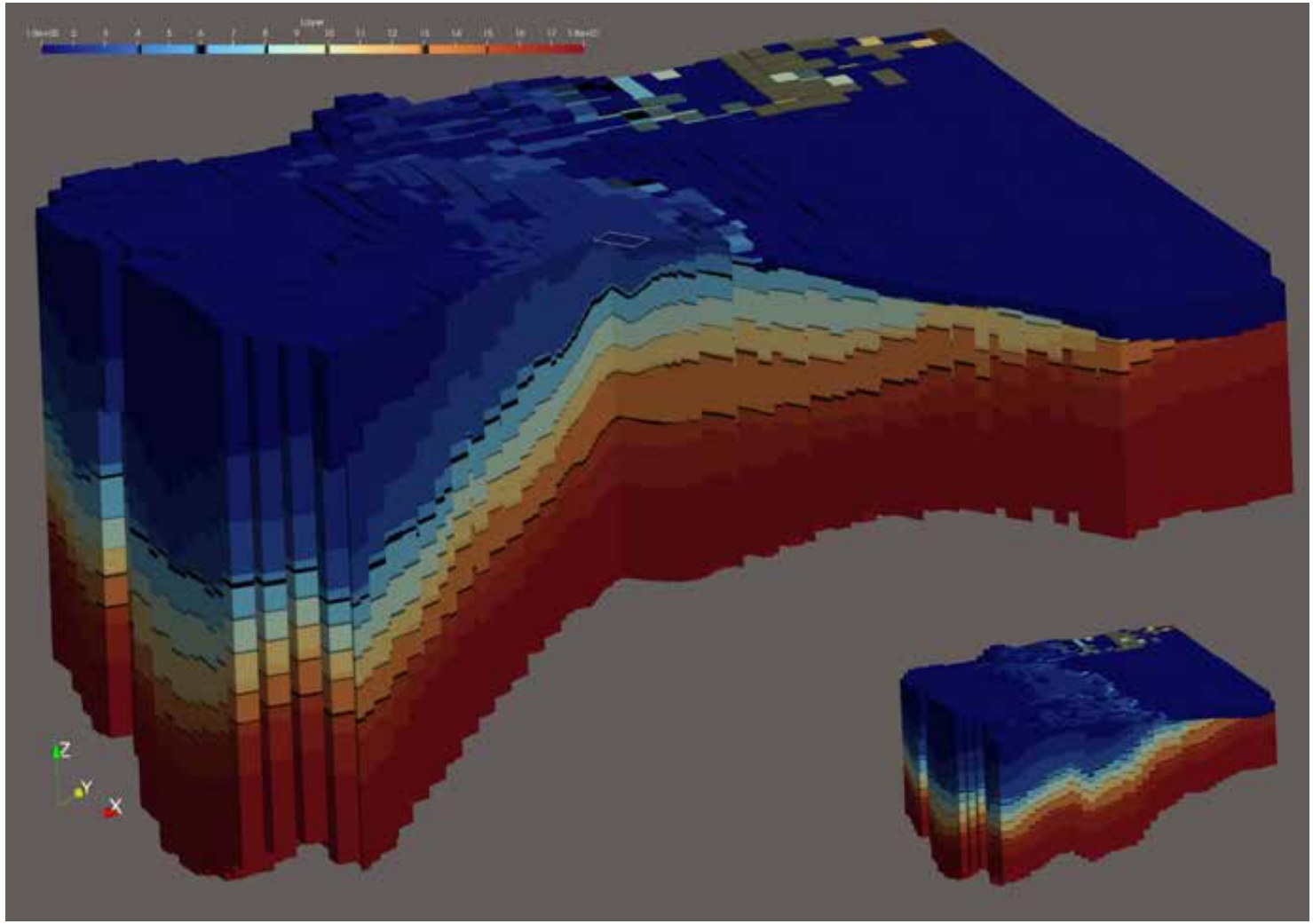

Figure 3-2 PL253 3D groundwater model (with 30x vertical exaggeration of the 3D model and cross-sections)

3.1.2 Hydraulic properties

Initial hydraulic properties were assigned as a single value across each model zone based on the learnings from the previous groundwater model history matching (Intera, 2025 and AGE, 2023). The initial horizontal hydraulic conductivity (k_h), vertical to horizontal hydraulic conductivity ratio (k_v/k_h),specific storage (S_s), and specific yield (S_y) values assigned in each model layer is presented in Table 3-2.

Once the parameter zones were initialised with a hydraulic property value, a 2D distribution of hydraulic properties of each zone was generated using the pilot points with multipliers. This allows for improved data assimilation by extracting information from measured observations in scenarios where the use of a single value for hydraulic properties within a zone is not sufficient to interpret the groundwater level variability or trends in bores located close to each other.

Other details of the parameterisation approach will be discussed further in Section 4.2.

Table 3-2 Summary of initial hydraulic properties

Hydrogeological Domain	Layer	K_h (m/day)	K_v/K_h	S_s (m^{-1})	S_y (%)
Condamine alluvium	1	2.6E+01	1.0E-01	2.3E-05	10
Gubberamunda sandstone	1	1.3E-01	1.0E-02	5.0E-06	2.5
Westbourne formation	2	8.9E-04	1.0E-03	2.3E-05	2.5
Springbok sandstone	3	1.6E-02	5.0E-03	1.0E-05	5
WCM Kogan coal seam	4	6.9E-02	1.0E-01	1.0E-05	1
WCM Kogan interburden	5	2.8E-02	1.0E-03	5.0E-06	1
WCM Macalister coal seam	6	4.0E-02	1.0E-01	5.0E-06	1
WCM Macalister interburden	7	4.9E-03	1.0E-03	5.0E-06	1
WCM Wambo coal seam	8	1.3E-01	1.0E-01	2.3E-05	1
WCM Wambo interburden	9	4.2E-03	1.0E-03	5.0E-06	1
WCM Argyle coal seam	10	1.4E-01	1.0E-01	2.3E-05	1
WCM Argyle interburden	11	5.2E-03	1.0E-03	1.0E-05	1
WCM Tangalooma sandstone	12	9.6E-03	1.0E-03	1.0E-05	1
WCM Upper Taroom coal seam	13	1.7E-01	1.0E-01	5.0E-06	1
WCM Upper Taroom interburden	14	1.7E-02	1.0E-03	5.0E-06	1
WCM Condamine coal seam	15	1.5E-01	1.0E-01	5.0E-06	1
WCM Condamine interburden	16	3.1E-02	1.0E-03	2.3E-05	2.5
Eurombah formation	17	1.8E-04	1.0E-03	5.0E-06	2.5
Hutton sandstone	18	3.4E-02	1.0E-03	2.3E-05	2.5

3.1.3 Boundary conditions

The MODFLOW 6 boundary packages are used to assign the boundary conditions and simulate relevant flow exchange processes. The assigned boundary conditions for PL253 groundwater model are presented in sections 3.1.3.1 to 3.1.3.7.

3.1.3.1 Recharge

Recharge to the groundwater system is represented by setting up three distinct recharge zones (shown in Figure 3-3) including:

- Condamine alluvium,
- Gubberamunda sandstone, and
- Westbourne formation and outcropping layers.

The initial annual recharge rates for each zone, adapted from previous studies (AGE, 2023; INTERA, 2025), are presented in Table 3-3. A recharge factor for each zone was defined and allowed to be adjusted during the model calibration.

Table 3-3 Initial annual recharge rate for each zone

Recharge zone	Initial annual recharge, mm/year
Condamine alluvium	3.5
Gubberamunda sandstone	1.0
Westbourne formation and outcropping layers	0.2

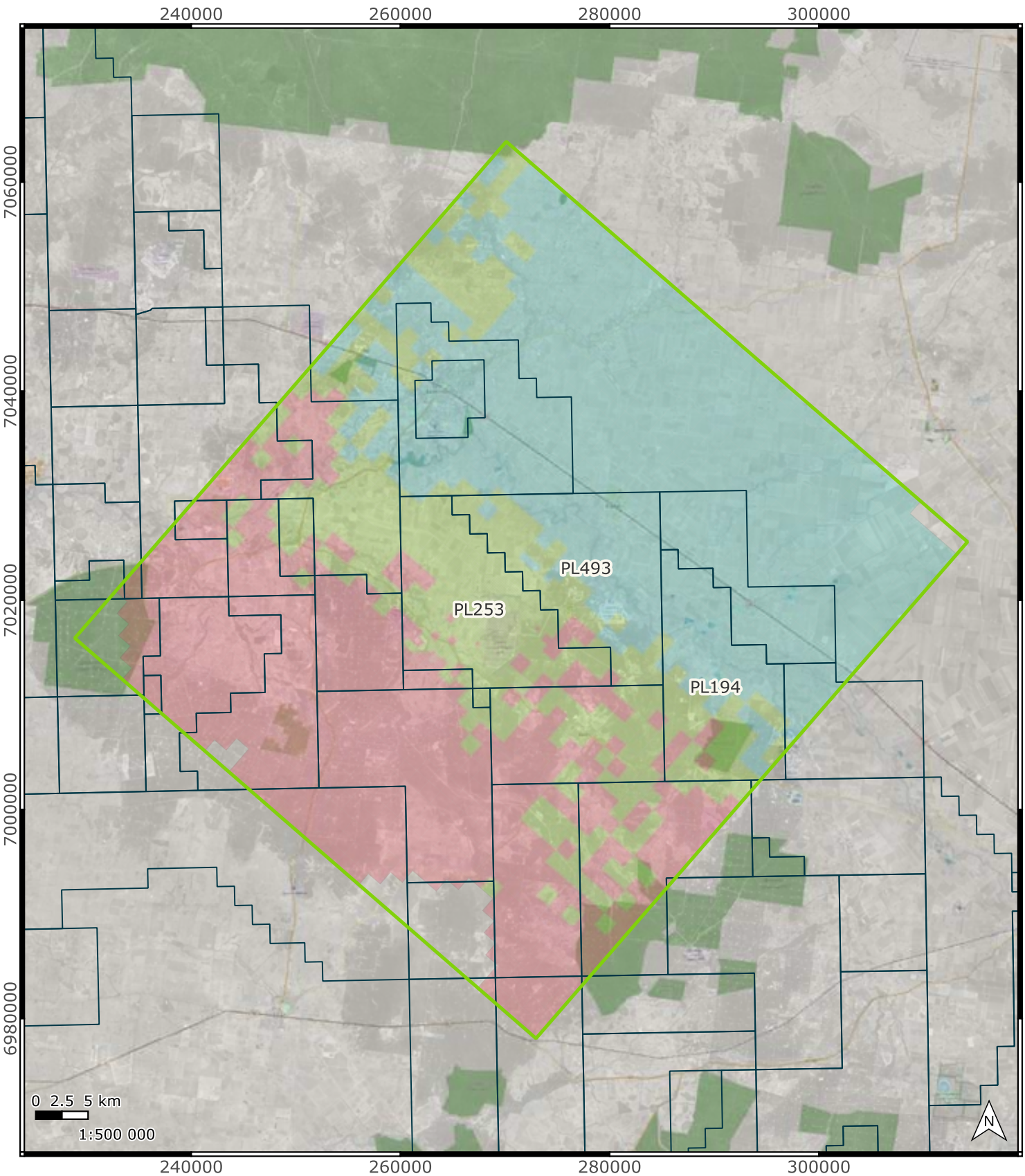

Legend

- Groundwater model extent
- Petroleum Leases

Recharge zones

- Condamine alluvium
- Gubberamunda sandstone
- Westbourne formation and outcropping layers

Simulated recharge zones

Project No.	Client	Figure No.
411001-00917	Arrow	3-3

Notes:
Project CRS: GDA94 / MGA zone 56
Last Saved: 08:35 16/04/2026
Filename: Figure_3-3_recharge
Exported by User: Mohsen.Azadi
Project Exported: 15:17 16/04/2026

References:
N/A

File Path: C:\modelling\Arrow\deliverables\Figures_REP-HG-002\Figure_3-3_recharge.qgz

worley consulting

3.1.3.2 Surface drainage

Surface drainage was simulated using drain (DRN) boundary conditions assigned to the uppermost active model cells, with drain elevations set to the model top (land-surface elevation). This allows groundwater discharge when simulated heads exceed land surface. This head-dependent approach representing surface drainage provides a numerically stable representation of topographically controlled groundwater discharge without imposing fixed hydraulic constraints.

3.1.3.3 General head boundaries

Time series of GHB elevations were extracted from the OGIA (2021) regional groundwater model and assigned to boundary cells in the updated HSUs, with careful alignment of layer elevations between the regional OGIA and PL253 models. Inferred hydraulic heads were obtained for the following units:

- Gubberamunda sandstone,
- Westbourne formation,
- Springbok formation,
- WCM Kogan interburden,
- WCM Macalister coal seam,
- WCM Wambo coal seam,
- WCM Argyle coal seam, and
- WCM Condamine coal seam.

During calibration, GHB head values were allowed to vary through vertical shifting of the prescribed head time series, while boundary conductance was adjusted using multiplier factors. This approach enabled adjustment of the quantitative influence of regional boundary conditions on simulated groundwater flow while preserving the temporal structure of the heads extracted from OGIA (2021) model. All remaining boundary cells, including the northeastern model boundary, were represented as no-flow boundaries.

3.1.3.4 Non-Arrow CSG wells

In the current model, non-Arrow CSG wells included in the OGIA (2021) regional groundwater model were simulated using drain (DRN) boundary conditions. Drain elevation time series were extracted directly from the corresponding OGIA (2021) model layers and assigned to the PL253 model to ensure consistency with the regional depressurisation conceptualisation. Drain conductance for each cell was calculated based on the product of horizontal hydraulic conductivity and individual cell thickness and scaled by a dimensionless multiplier. This multiplier was informed through history matching of observed regional groundwater responses and subsequently assessed during uncertainty analysis. This provides a simplified yet physically consistent representation of non-Arrow CSG extraction impacts while maintaining alignment with OGIA regional groundwater flow directions.

3.1.3.5 FDP abstraction scenarios

In order to quantify the impact of Arrow's proposed FDP (Clynes Road development) on groundwater flow and migration of contaminants, the following groundwater abstraction scenarios were initially considered in the current study:

- **Scenario 1:** this includes all non-Arrow production wells in proximity of PL253 (within the modelled domain).
- **Scenario 2:** this corresponds to the six existing Hopeland pilot wells and the soon to be installed 55 Kogan Creek CSG wells approved under the current EA for PL253 (green points in Figure 1-1), together with approved wells in Arrow's neighbouring tenure. This scenario reflects Arrow's currently authorised Field Development Plan (FDP).
- **Scenario 3:** this includes all wells from Scenario 2, plus the additional 55 Clynes Road wells for which Arrow is seeking approval.

Assessing incremental changes between scenario 2 and scenario 3 will provide insight into understanding impacts from Lot 40 DY85 attributable to Arrow's proposed Clynes Road FDP for the expansion project.

The abstraction rates for Arrow wells scenarios 2 and scenario 3 (simulated using the WEL package), are shown in Figure 3-4.

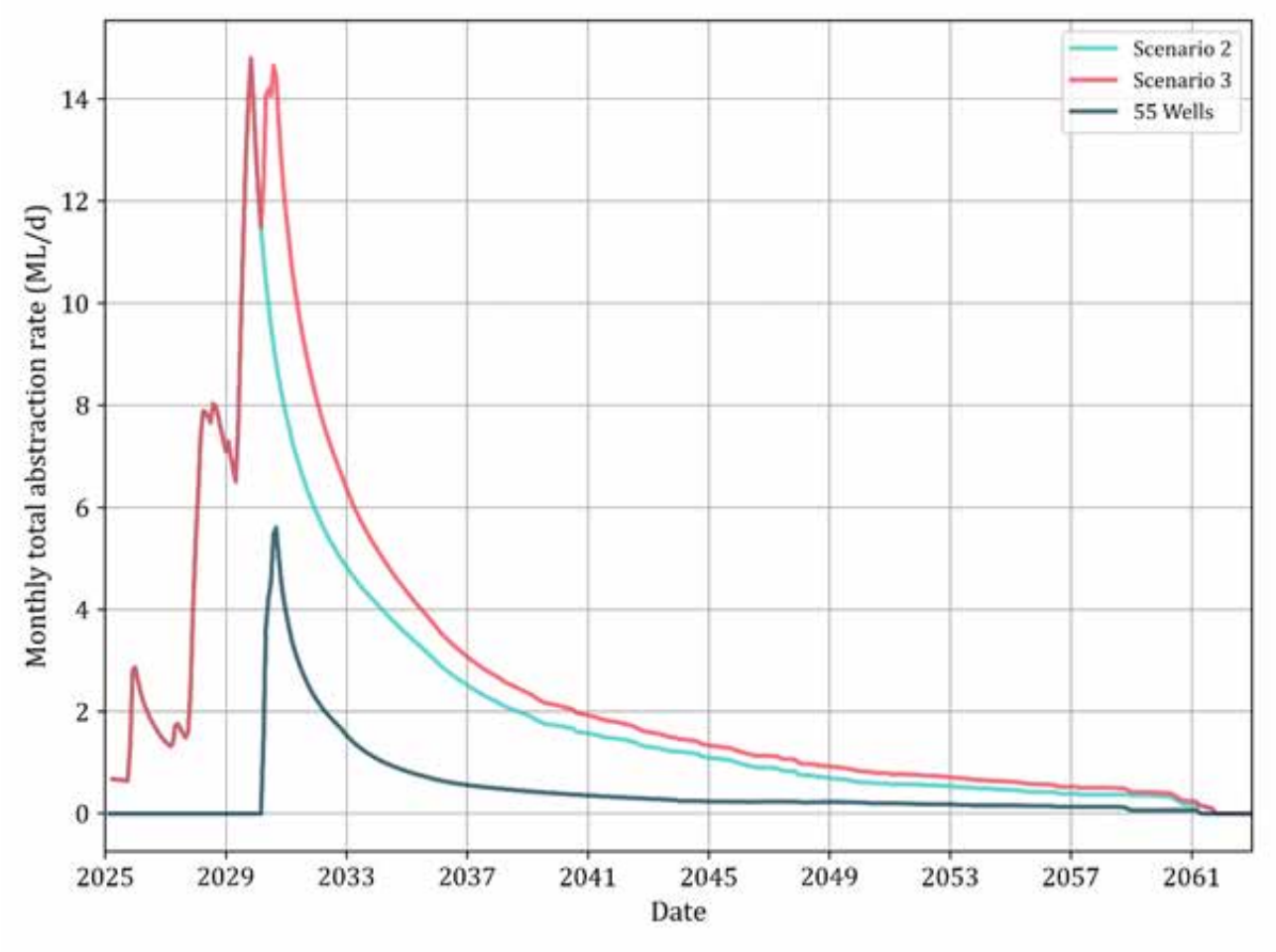

Figure 3-4 Monthly total abstraction rates for FDP scenarios 2 and 3

Extraction from existing and proposed Arrow CSG wells was distributed across multiple WCM layers using a transmissivity-weighted approach. Using this approach, the total abstraction rate from each well is apportioned based on the relative hydraulic conductivity and thickness of the intersected model layers. This ensures that groundwater extraction is preferentially assigned to more transmissive coal seams, consistent with the conceptual understanding of multi-seam CSG production in the Surat Basin.

3.1.3.6 Hopeland pilot wells

Hopeland pilot wells were explicitly simulated in the groundwater flow model to represent multi-seam extraction and to reproduce observed groundwater level responses associated with historical pilot testing at the Hopeland site. The pilot wells are located approximately 8 km southwest of Lot 40 DY85 and comprise six authorised CSG bores completed across several WCM coal seams. Given the vertical extent of well completions and the importance of simulating groundwater level responses to abstraction during pilot tests, these wells were represented using the MODFLOW 6 Multi-Aquifer Well (MAW) package.

Use of the MAW boundary condition allows abstraction to be distributed dynamically along the well as a function of layer transmissivity and simulated hydraulic heads, providing a physically realistic representation of vertical flow within multi-seam CSG wells. The MAW formulation enables interaction between the well and multiple WCM model layers providing improved simulation of observed drawdown behaviour recorded in pilot wells and monitoring bore HL17. Parameters controlling MAW behaviour, including well conductance and scaling height above the pump elevation, were subject to calibration and uncertainty analysis.

3.1.3.7 Historical UCG activities

Historical UCG activities were explicitly simulated over their respective operational periods using drain (DRN) boundary conditions. Combustion processes and subsequent collapse of gasifier voids may have induced broader-scale fracturing beyond the target coal seams, with fractures propagating upward into overlying formations. This secondary fracturing could locally enhance hydraulic connectivity and influence post-UCG groundwater flow and contaminant migration pathways.

The DRN package was used to represent depressurisation and enhanced groundwater discharge associated with gasifier operation. Drain elevations were assigned consistent with the affected HSUs and UCG activities at each gasifier, allowing groundwater discharge to occur. The drain elevation and conductance were allowed to be adjusted during history matching and uncertainty analysis.

To account for changes in hydraulic properties induced by gasification processes, time-varying hydraulic properties were applied to HSUs affected by UCG activities, including the Macalister coal seam, Kogan interburden, and the Springbok sandstone. UCG-related fracturing, material removal, and permeability enhancement were represented by modifying hydraulic conductivity and storage properties during defined gasification periods. Allowing hydraulic property changes in the layers overlying Macalister coal seam provides a conservative representation of the

potential for vertical migration of contaminants into or out of overlying units, including the Springbok sandstone.

Time-varying hydraulic conductivity (TVK) and time-varying storage (TVS) parameters were applied on a gasifier-specific basis, enabling localised impacts to be simulated independently for each gasifier footprint. Spatial variability in fracturing intensity and material alteration was allowed to be adjusted during history matching, uncertainty analysis, and predictive assessment under post-UCG recovery and CSG development scenarios.

3.1.4 Temporal discretisation

The groundwater model simulation starts with a steady state stress period to simulate the "steady-state" groundwater flow regime, reflecting the chosen parameterisation and boundary conditions, before progressing to a transient model.

The combined steady-state and transient model simulations are divided into 215 stress periods for historical matching (calibration) and prediction periods. The number and duration of transient stress periods are tailored based on the dates associated with the recorded groundwater levels, and former UCG activities as follows:

- History-matching period (159 stress periods):
  - 1 steady-state stress period,
  - 14 annual stress periods from 1/1/2000 to 1/1/2014, and
  - 144 quarterly stress periods from 1/1/2014 to 1/1/2026.
- Prediction period (56 stress periods):
  - 40 annual stress periods from 1/1/2026 to 1/1/2066, and
  - 16 10-year stress periods from 1/1/2066 to 1/1/2226.

3.1.5 Metric systems

The groundwater flow model uses units of meters and days. The geographic coordinate system used is the Geographic Datum of Australia 1994 (GDA94), and the projection used is the Map Grid of Australia (MGA) zone 56.

3.2 Particle tracking

Particle tracking was undertaken to assess potential groundwater flow pathways and provide a conservative assessment of advective contaminant migration (compared with contaminant transport model) under approved and proposed coal seam gas (CSG) development scenarios. The particle tracking analysis was designed to evaluate groundwater flow directions, travel distances, and relative changes in migration behaviour, independent of chemical processes such as sorption, decay, or dispersion, thereby providing a conservative representation of potential solute movement.

Particles were released in 2019 at locations representative of residual contaminant source areas (gasifiers), Lot 40 DY85 boundaries, and key monitoring points (shown in Figure 3-5) within the Springbok sandstone and the Macalister coal seam. Release locations were selected

to reflect both the former UCG footprint and bore locations where elevated benzene and naphthalene concentrations have been historically observed. Particle releases were distributed both laterally and vertically within the groundwater model to adequately capture local flow variability. The density and placement of particles were selected to ensure consistent coverage of potential transport pathways and to support interpretation of site-scale flow patterns.

Particle tracking simulations were carried out using groundwater flow fields generated by the calibrated numerical model for both FDP scenarios. The analysis focused on both relative differences between scenarios and absolute travel distance, while recognising uncertainty associated with effective porosity and residual multi-phase effects following UCG operations. Particle tracking simulations were treated as a conservative tool to inform risk assessment rather than a predictive representation of contaminant concentrations.

Porosity values adopted for the particle tracking simulations were derived from the calibrated specific yield values, obtained from the groundwater flow model, with the addition of a layer-wide specific retention component. This approach ensures consistency between the simulated groundwater flow field and particle velocities while accounting for spatially varying storage behaviour within coal seams and interburden lithologies. A range of specific retention between 1% and 10% was explored as part of history matching and uncertainty analysis to assess particle travel distances and trajectories with a plausible variability in porosity.

Legend

- Groundwater model extent
- Lot 40 DY85

Particles released at:

- Monitoring bores
- Gasifiers
- Lot 40 DY 85 boundaries

Particle release locations

Project No.	Client	Figure No.
411001-00917	Arrow	3-5

Notes:
Project CRS: GDA94 / MGA zone 56
Last Saved: 14:45 16/04/2026
Filename: Figure_3-5_prt_locs
Exported by User: Mohsen.Azadi
Project Exported: 15:15 16/04/2026

References:
N/A

File Path: C:\modelling\Arrow\deliverables\Figures_REP-HG-002\Figure_3-5_prt_locs.qgz

worley consulting

3.3 Contaminant transport model

The contaminant transport model was developed to simulate the fate and transport of dissolved benzene and naphthalene within the Springbok sandstone and the Macalister coal seam. The model was configured to represent key processes controlling contaminant migration and attenuation following historic UCG activities, and to assess potential changes under the approved and proposed FDP scenarios.

The transport model focuses on reproducing observed concentration trends and predicting potential future behaviour rather than predicting exact concentrations at individual monitoring locations. Model setup and parameterisation were informed by available monitoring data, previous contaminant transport modelling for PL253, and the Australian Groundwater Modelling Guidelines (Barnett et al., 2012), providing a risk-based impact assessment.

3.3.1 Transport model coupling

In the present study, the contaminant transport model is coupled with the calibrated groundwater flow model, using the transient simulated flow field to represent advective transport processes. The spatial discretisation, layering, and groundwater flow boundary conditions are consistent between the flow and transport models, ensuring internal coherence between groundwater flows and contaminant migration.

Coupling the transport model to the flow model allows changes in hydraulic gradients and groundwater velocities arising from different development scenarios to be directly reflected in simulated contaminant behaviour. This provides a consistent and interconnected basis for assessing migration pathways in both the Springbok sandstone and the Macalister coal seam.

3.3.2 Initial condition

Initial conditions for benzene and naphthalene were defined using groundwater quality monitoring data from Arrow and DoR operated monitoring bores. Similar to the approach used in the previous groundwater modelling studies (AGE, 2023; Intera, 2025), concentrations were spatially assigned to represent residual dissolved contamination associated with former UCG activities, commencing on 1/1/2018.

The initial concentration distributions for benzene and naphthalene within the Springbok sandstone and Macalister coal seam reflect the best available estimate of groundwater quality conditions post-UCG activities and were adjusted to be conservative where uncertainty exists. This approach ensures that subsequent transport simulations evaluate conservative impacts over the assessment period.

Initial contaminant concentration distributions and transient source depletion release at gasifiers (discussed in section 2.4.2.1) were both implemented using the MODFLOW 6 Constant Concentration (CNC) package. Initial concentrations for benzene and naphthalene were defined to represent residual dissolved impacts within Lot 40 DY85 and in the vicinity of former gasifier locations within the Springbok sandstone and Macalister coal seam. Time-varying source boundary conditions at these locations were assigned through compound-specific exponential

depletion equations (1) to (4) derived from the upper-envelope groundwater monitoring datasets within the Springbok sandstone and Macalister coal seam.

3.3.3 Boundary condition

Contaminant transport model was coupled with the calibrated groundwater flow model to ensure that predicted concentrations and plume evolution appropriately reflect the simulated flow regime and contaminant transport parameters. The transport response is therefore governed partially by transport boundary conditions defined by formation physical properties (porosity and bulk density), source representation, and key transport processes such as dispersivity, dual-domain porosity, and natural attenuation (sorption and degradation).

A summary of the parameters used in the transport model with the initial value, lower bound and upper bounds considered in the transport model history matching is summarised in Table 3-4 Contaminant transport parameters. The transport boundary conditions are described in the following sections.

Table 3-4 Contaminant transport parameters

Transport parameter	Unit	Compound	Layer	Initial	Min	Max	Reference
Effective molecular diffusion-coefficient	m^2/d	Benzene	All	1.1E-05	3.9E-06	1.9E-05	Gustafson & Dickhut (1994)
Effective molecular diffusion-coefficient	m^2/d	Naphthalene	All	8.4E-06	3.0E-06	1.4E-05	Gustafson & Dickhut (1994)
Longitudinal dispersivity	m	All	Non-coal	5.0E+00	1.0E+00	1.0E+01	Gelhar et al. (1992), Schulze-Makuch (2005), Bjerg et al. (2025)
Longitudinal dispersivity	m	All	Coal	1.0E+01	5.0E+00	3.0E+01	Gelhar et al. (1992), Schulze-Makuch (2005), Dong et al. (2018)
Transverse horizon-al dispersivity	m	All	Non-coal	5.0E-01	1.0E-01	1.0E+00	Gelhar et al. (1992), Schulze-Makuch (2005), Bjerg et al. (2025)
Transverse horizon-al dispersivity	m	All	Coal	1.0E+00	5.0E-01	3.0E+00	Gelhar et al. (1992), Schulze-Makuch (2005), Dong et al. (2018)
Transverse vertical dispersivity	m	All	Non-coal	5.0E-02	1.0E-02	1.0E-01	Gelhar et al. (1992), Schulze-Makuch (2005), Bjerg et al. (2025)
Transverse vertical dispersivity	m	All	Coal	1.0E-02	1.0E-03	5.0E-02	Gelhar et al. (1992), Grathwohl et al. (2000)
First-Order Decay Rate Coefficients	1/day	Benzene	Non-coal	1.0E-03	1.0E-04	1.0E-02	US EPA (1999), Newell et al. (2002), Zhang et al. (2005)
First-Order Decay Rate Coefficients	1/day	Naphthalene	Non-coal	7.5E-03	5.0E-05	5.0E-02	Anderson & Lovley (1998), Wiedemeier et al. (1999), ATSDR (2022)
First-Order Decay Rate Coefficients	1/day	Benzene	Coal	5.0E-04	1.0E-06	1.0E-03	API (1998), US EPA (1999); Anderson et al. (1998)
First-Order Decay Rate Coefficients	1/day	Naphthalene	Coal	5.0E-03	1.0E-06	1.0E-02	Wiedemeier et al. (1999), Bjerg et al. (1999), Musat et al. (2008)
Immobile First-Order Decay Rate Coefficients	1/day	Benzene	Non-coal	1.0E-04	3.0E-05	1.0E-03	US EPA (1999) Newell et al. (2002); Anderson & Lovley (1998)
Immobile First-Order Decay Rate Coefficients	1/day	Naphthalene	Non-coal	1.0E-03	2.5E-06	1.5E-02	Anderson & Lovley (1998), Wiedemeier et al. (1999), Bjerg et al. (1999), Musat et al. (2008)
Immobile First-Order Decay Rate Coefficients	1/day	Benzene	Coal	5.0E-04	3.0E-07	1.0E-03	US EPA (1999), Newell et al. (2002), Anderson & Lovley (1998)
Immobile First-Order Decay Rate Coefficients	1/day	Naphthalene	Coal	1.0E-04	5.0E-08	3.0E-03	Anderson & Lovley (1998), Wiedemeier et al. (1999), Bjerg et al. (1999), Musat et al. (2008)
Freundlich coefficient	m^3/kg	Benzene	Non-coal	1.0E-04	5.0E-05	3.0E-04	Shi et al. (2020), U.S. EPA (1996), ECETOC (2013)
Freundlich coefficient	m^3/kg	Naphthalene	Non-coal	7.5E-03	2.0E-04	1.0E-02	Osagie & Owabor (2015), Shi et al. (2020), ECETOC (2013)
Freundlich coefficient	m^3/kg	Benzene	Coal	1.0E-03	5.0E-04	3.0E-03	ECETOC (2013), U.S. EPA (1996)
Freundlich coefficient	m^3/kg	Naphthalene	Coal	5.0E-02	2.0E-03	1.0E-01	Ahangar (2010), Ukalska-Jaruga & Smreczak (2020), Osagie & Owabor (2015), ECETOC (2013)
Non-linearity exponent	-	Benzene	Non-coal	9.5E-01	9.0E-01	1.0E+00	Shi et al. (2020), U.S. EPA (1996), ECETOC (2013)
Non-linearity exponent	-	Naphthalene	Non-coal	9.5E-01	9.5E-01	1.0E+00	Osagie & Owabor (2015), Shi et al. (2020), ECETOC (2013)
Non-linearity exponent	-	Benzene	Coal	9.0E-01	8.5E-01	1.0E+00	ECETOC (2013), U.S. EPA (1996)
Non-linearity exponent	-	Naphthalene	Coal	9.5E-01	9.5E-01	1.0E+00	Ahangar (2010), Ukalska-Jaruga & Smreczak (2020), Osagie & Owabor (2015), ECETOC
Immobile non-linearity exponent	-	Benzene	Non-coal	9.0E-01	8.5E-01	9.5E-01	Shi et al. (2020), U.S. EPA (1996), ECETOC (2013)
Immobile non-linearity exponent	-	Naphthalene	Non-coal	8.5E-01	7.5E-01	9.0E-01	Osagie & Owabor (2015), Shi et al. (2020), ECETOC (2013)
Immobile non-linearity exponent	-	Benzene	Coal	8.0E-01	7.0E-01	8.5E-01	ECETOC (2013), U.S. EPA (1996)
Immobile non-linearity exponent	-	Naphthalene	Coal	7.0E-01	5.0E-01	8.5E-01	Ahangar (2010), Ukalska-Jaruga & Smreczak (2020), Osagie & Owabor (2015), ECETOC (2013)
Immobile domain fraction	-	All	Non-coal	2.0E-01	1.0E-02	3.0E-01	Warren & Root (1963), Aguilera (2004), Langevin et al. (2022)
Immobile domain fraction	-	All	Coal	7.0E-01	6.0E-01	8.5E-01	King & Ertekin (1988), Pruess & Narasimhan (1985)
Mass transfer rate coefficient	1/day	All	Non-coal	5.0E-04	1.0E-04	1.0E-03	Warren & Root (1963), Pruess & Narasimhan (1985), Langevin et al. (2022)
Mass transfer rate coefficient	1/day	All	Coal	1.0E-05	1.0E-06	1.0E-04	King & Ertekin (1988)

3.3.3.1 Dispersivity

Dispersivity describes the spreading of dissolved contaminants in groundwater arising from variations in groundwater velocity at different spatial scales and is a key process controlling solute transport behaviour. Contaminant plume dispersion occurs both along the direction of groundwater flow (longitudinal dispersivity) and perpendicular to flow in the horizontal and vertical directions (transverse horizontal and transverse vertical dispersivity), reflecting aquifer heterogeneity, pore-scale velocity differences, and preferential flow pathways. In addition to mechanical dispersion, solute spreading is influenced by molecular diffusion, which governs mass transfer driven by concentration gradients, particularly in low-velocity or low-permeability zones. Together, these processes control plume shape, extent, and dilution over time. MODFLOW 6 Dispersion (DSP) package was used in the contaminant transport model to simulate mechanical dispersion and molecular diffusion. The input parameters included longitudinal, transverse horizontal, and transverse vertical dispersivity (Table 3-4) defined on a layer-specific basis and effective molecular diffusion-coefficient defined on a compound-specific basis. All these input parameters were adjusted during history matching of the transport model.

3.3.3.2 Natural attenuation

Natural attenuation processes were incorporated in the contaminant transport model to represent the reduction in contaminant mobility and mass through physicochemical and biological mechanisms occurring within the subsurface. For benzene and naphthalene, natural attenuation was represented through equilibrium-controlled sorption and first-order degradation processes, which together influence plume migration, and long-term concentration trends.

MODFLOW 6 Mobile Storage and Transfer (MST) package was used in the contaminant transport model to simulate natural attenuation processes. This included both first-order degradation processes, as outlined above, and equilibrium-controlled sorption described using a Freundlich isotherm formulation. These processes were applied to simulate reduction in contaminant mass and mobility for benzene and naphthalene within the mobile groundwater domain. The input parameters included porosity, bulk density of the layer, first-order decay rate coefficient, Freundlich coefficient and mobile non-linearity exponent (Table 3-4) defined on a layer-specific basis and adjusted during history matching of the transport model.

3.3.3.3 Dual-Domain Porosity

Dual-porosity behaviour was simulated in the contaminant transport model to represent mass exchange between mobile groundwater flowing through fracture-dominated pathways and immobile pore water stored within low-permeability micropore domains. Solute mass can transfer from the fracture-scale flow system into the rock matrix and micro-porosity, and subsequently diffuse back into the mobile domain over time. This bidirectional mass transfer mechanism allows contaminant mass to be temporarily retained or released depending on concentration gradients, influencing plume persistence and long-term concentration trends.

Representation of immobile-mobile mass transfer is particularly relevant for coal seams and fine-grained sandstone units, where pore structure heterogeneity and sorptive surfaces can result in delayed contaminant breakthrough. MODFLOW 6 Immobile Storage and Transfer (IST) package was used in the transport model to simulate dual-domain porosity and associated mass exchange processes. This boundary condition allows for diffusion-controlled mass transfer between micro-pores and fracture-scale flow. The input parameters included porosity, bulk density of the layer, immobile domain fraction, mass transfer rate coefficient, first-order decay rate coefficient, Freundlich coefficient and immobile non-linearity exponent (Table 3-4) defined on a layer-specific basis and adjusted during history matching of the transport model.

4. History matching

4.1 Calibration approach

This section details the approach used for history matching the historical groundwater flow regime, UCG activities, and contaminant transport migration within Lot 40 DY85, PL253 and the model domain.

In this study, "history matching" refers to the process of assimilating observed transient groundwater data into the model, its calibration and its outputs. The purpose of history-matching in this context is to constrain model parameters and allowable ranges, based on what we know from field testing, conceptual ideas and observed system behaviour (ideally of direct relevance to the model predictions of interest), using a range of observation data.

This in turn constrains the suite of parameter fields that are used to make model predictions and to assess their uncertainty. This approach provides a sound basis for enhanced use and understanding of model outputs, including their limitations, in decision-making.

PEST, the tool providing the basis for calibration, represents a family of optimisation and uncertainty analysis tools. PEST also represents a suite of workflows for highly parameterised environmental model optimisation (inversion), uncertainty analysis and associated tasks.

ENSI (Ensemble Space Inversion) is a relatively new method for fast history-matching. It attains its speed through estimation of "super parameters" instead of parameters themselves. These super parameters are factors applied to random parameter vectors which, ideally, should be samples of the prior parameter probability distribution. The number of realisations required for achieving a high level of model-to-measurement fit can be far fewer than the number of parameters that are used by a model (Doherty, 2024).

In contrast to other calibration methods such as SVD-assist (which also estimates super parameters), it is not necessary to calculate a Jacobian matrix in order to formulate super parameters prior to implementing ENSI inversion. What it gets is an ensemble of random samples of the prior parameter probability distribution.

The combined steady-state and history-matching transient model is calibrated by adjusting aquifer parameters and other boundary condition parameters for the groundwater flow and transport models to develop a suitable match between the observed and simulated groundwater levels and concentrations across the model domain.

4.2 Parameterisation

This section discusses additional details with respect to the PESTPP-ENSI model parameterisation. Once a good model-to-measurement fit was achieved using PESTPP-ENSI, the model parameterisation was used to inform the PESTPP-IES workflow of uncertainty quantification.

Use of PEST-ENSI for history-matching suggests that its model run efficiency is greater than that of PEST_HP in highly parameterised cases, and its model-to-measurement fit is better than that of PESTPP-IES (Doherty, 2024). However, PEST-ENSI associates no uncertainty with the parameter field that it calculates, and with model predictions that are calculated using this field. The complementary PESTPP-IES methodology is therefore deployed for predictive uncertainty analysis.

Both PEST-ENSI and PESTPP-IES PPP-IES approaches allow for large numbers of pilot points as in practice they sample a subset of pilot points (ensemble) during each iteration. This does not charge parameterisation approach with any further computational penalties.

The parameterisation scheme uses pilot points in the proximity of monitoring sites, acknowledging the need for spatial interpolation and extraction of information from observed data. All pilot points are assigned spatial covariance structures to encourage the history matching process to honour the initial (prior) parameters and their spatial differences as closely as possible. Departures from this would occur where necessary to significantly improve the simulation of historical system behaviour as measured by PESTPP-ENSI against the strategically weighted observation data.

These covariances are computed using PEST utilities MKPPSTAT and PPCOV_SVA. Covariances are computed using a variogram with the range based on the mean distance from each pilot point and its ten nearest neighbours. No nugget is applied.

For parameters that are not spatially correlated, standard deviations are defined in the same way (one quarter of the allowable parameter range). These standard deviations and covariance matrices are provided to PESTPP-IES via a PEST parameter uncertainty file.

The parameterisation scheme was reviewed and revised during history matching with learnings from each iteration feeding to the next round. A total of seven rounds of history matching (each running for several iterations) were conducted.

Pilot point interpolation across the model zones using the PLPROC kriging and Python scripting were applied to parameterise successive model runs and adjust model boundary conditions discussed in section 3.1.3.

Overall, the numerical groundwater model has 26,032 adjustable parameters. PEST-ENSI/PESTPP-IES randomly samples parameter fields based on prior parameter ranges where each parameter field is referred to as a “realisation”. An initial ensemble size of 800 realisations was defined for PEST-ENSI/PESTPP-IES automated history matching which was reduced to 364 realisations after seven rounds of calibration iterations removing realisations that did not converge for all the time steps or did not satisfy history matching metrics for the groundwater flow and contaminant transport model. The prior and posterior ranges of parameters were compared ensuring that the posterior parameters fields are not over-constrained.

Pilot point application is described below:

- A total of 578 pilot points is used across the model domain as shown in Figure 4-1.
- Pilot points allow for perturbations in:
  - hydraulic conductivity (horizontal and vertical),
  - specific storage, and
  - specific yield.
- Pilot points are spread out based on their proximity to monitoring sites and potential parameterisation of structures and geological zones within each layer with the following spacings:
  - 250 m within Lot 40 DY85,
  - 1,500 m within areas with groundwater level records, and
  - 5,000 m in areas with no groundwater level data.

A pilot point is placed between each pair of monitoring sites to allow for capturing different groundwater trends in bores caused by heterogeneity in hydraulic properties of HSUs.

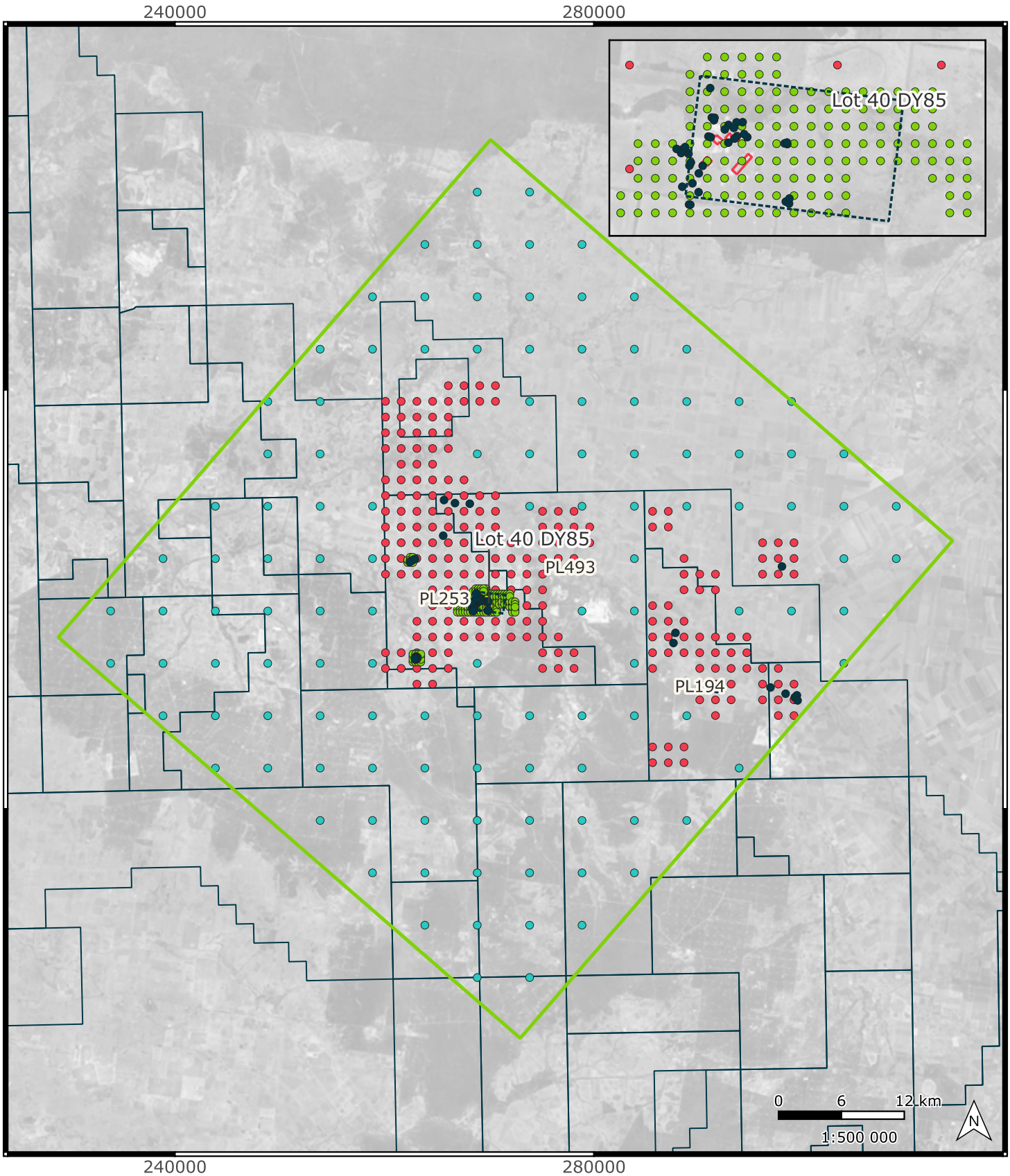

Legend

- Groundwater model extent
- Lot 40 DY85

Pilot points with:

- 250 m
- 1500 m
- 5000 m
- Additional PP near monitoring sites

Pilot point locations

Project No.	Client	Figure No.
411001-00917	Arrow	4-1

Notes:
Project CRS: GDA94 / MGA zone 56
Last Saved: 14:49 16/04/2026
Filename: Figure_4-1_pilot_points
Exported by User: Mohsen.Azadi
Project Exported: 15:11 16/04/2026

References:
N/A

File Path: C:\modelling\Arrow\deliverables\Figures_REP-HG-002\Figure_4-1_pilot_points.qgz

worley consulting

4.3 Observation data assimilation

PEST is designed to progressively minimise its objective function (phi) by adjusting model parameters in an iterative fashion within prescribed bounds. Phi is calculated internally by PEST as the sum of squared weighted residuals between observations and their modelled counterparts.

PEST allows the user to group different observation data types and apply different weights (and individual observations within each group). This facilitates strategic weighing of different observation types and locations according to the objectives of the modelling and accuracy of various data sources.

For example, strategic weighting may be used to account for the fact that some bores can have far more data than others; those with fewer observation data may be less "visible" to PEST during inversion, unless their weighting is increased relative to those sites with more data.

Other reasons for different weightings may include less reliable versus more reliable data. Or bores in a particular area are more important to the project objectives than those in other areas. In the current model, weight adjustment is focused on monitoring bores within PL253 and Lot 40 DY85.

The performance of the model is tested against the measured groundwater levels and concentrations (for benzene and naphthalene) as well as pumping data for Hopeland pilot wells. Observation data used for history matching of the groundwater flow model and the weights assigned to them are defined so that the total calculated phi is distributed among various calibration targets (shown in Figure 4-2):

- Starting water levels in 115 monitoring sites - representing background (pre-abstraction) groundwater level in each monitoring site (10%),
- Transient water levels recorded between 2008 and 2025 in 115 monitoring sites (30%),
- Temporal changes in the transient water levels for 115 monitoring sites (5%),
- Vertical head differences in 18 pairs of monitoring sites (10%),
- Inferred water levels based on Q3 2025 contours in Macalister coal seam shown in Figure 2-2 to replicate current hydraulic gradients within Lot 40 DY85 – water levels in 1,683 model cells across the contoured areas were sampled for a refined per cell history matching (15%),
- Monitoring bores within Springbok sandstone for Q3 2025 (5%), and
- Transient water levels, recorded in the Hopeland pilot wells and HL17 (25%).

For the contaminant transport model, the total calculated phi is distributed among various calibration targets:

- Benzene concentration in 18 monitoring sites located in the Springbok sandstone (50%),
- Benzene concentration in 12 monitoring sites located in the Macalister coal seam (30%),
- Naphthalene concentration in 19 monitoring sites located in the Springbok sandstone (15%), and
- Naphthalene concentration in 12 monitoring sites located in the Macalister coal seam (5%).

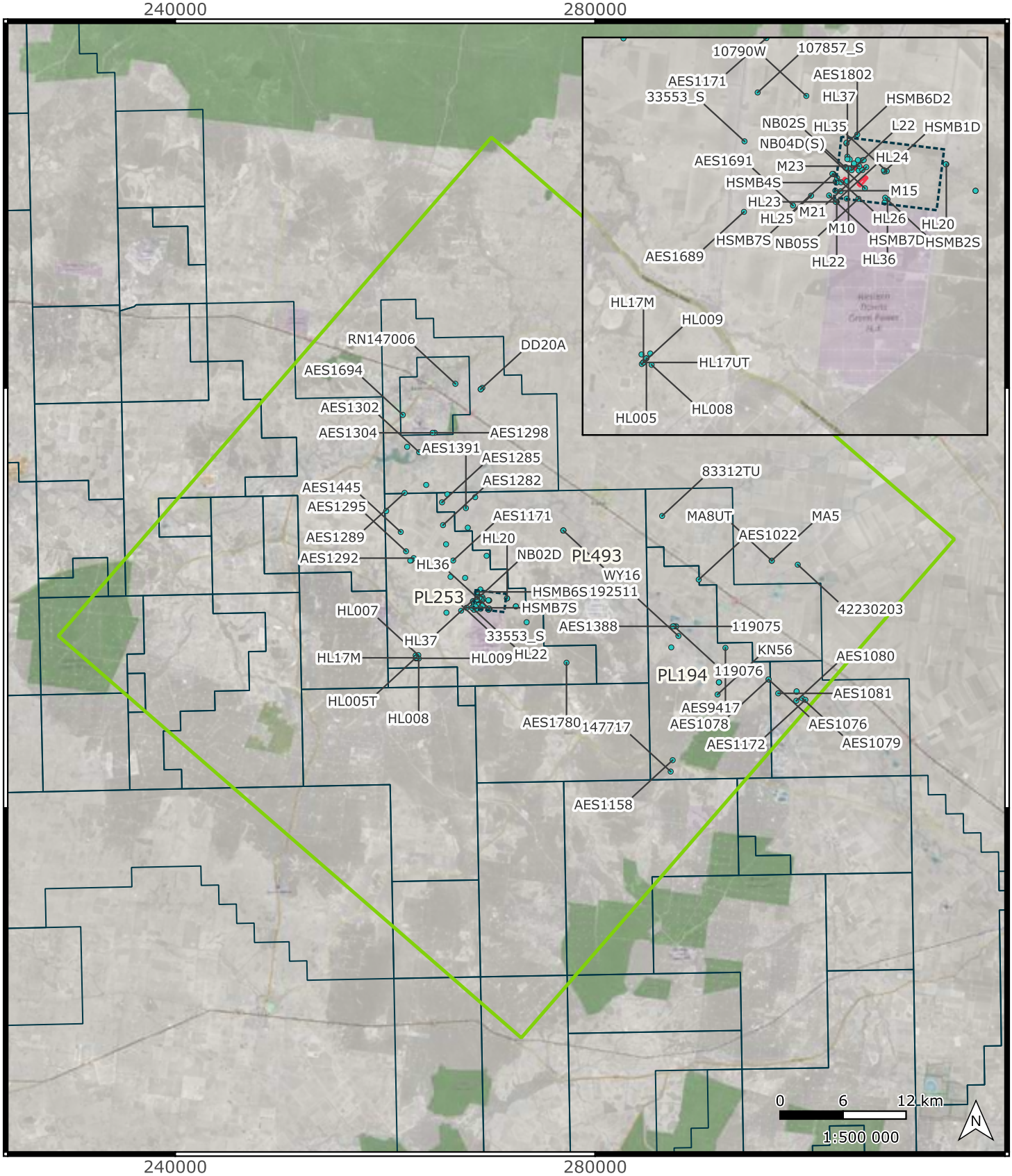

Legend

- Groundwater model extent
- Lot 40 DY85
- Monitoring bores

Bore locations with transient groundwater level data

Project No.	Client	Figure No.
411001-00917	Arrow	4-2

Notes:
Project CRS: GDA94 / MGA zone 56
Last Saved: 17:17 16/04/2026
Filename: Figure_4-3_bore_loc
Exported by User: Mohsen.Azadi
Project Exported: 17:22 16/04/2026

References:
N/A

File Path: C:\modelling\Arrow\deliverables\Figures_REP-HG-002\Figure_4-3_bore_loc.qgz

4.4 Groundwater flow model

4.4.1 History matching metrics

Model performance acceptance is evaluated based on Australian Groundwater Modelling Guidelines (Barnett et al., 2012) using a number of measures that are not necessarily related to model history matching. The following aspects of the model performance are considered:

- Model convergence: the head change tolerance of 0.001 m between iterations is set in the solver setting,
- Water balance: A value of less than 1% should be achieved at any time step and cumulatively,
- Qualitative measures: robustness/plausibility of model parameters, groundwater flow directions, and temporal groundwater level trends must be consistent with the conceptual model, and
- Quantitative measures such as root mean square error (RMS) and scaled root mean square error (SRMS).

The performance of the 364 model realisations was analysed to ensure the models used during predictive uncertainty analysis are calibrated. A maximum SRMS of 10% was considered as the criterion to assess the model calibration with all 364 models deemed calibrated as shown in Figure 4-3.

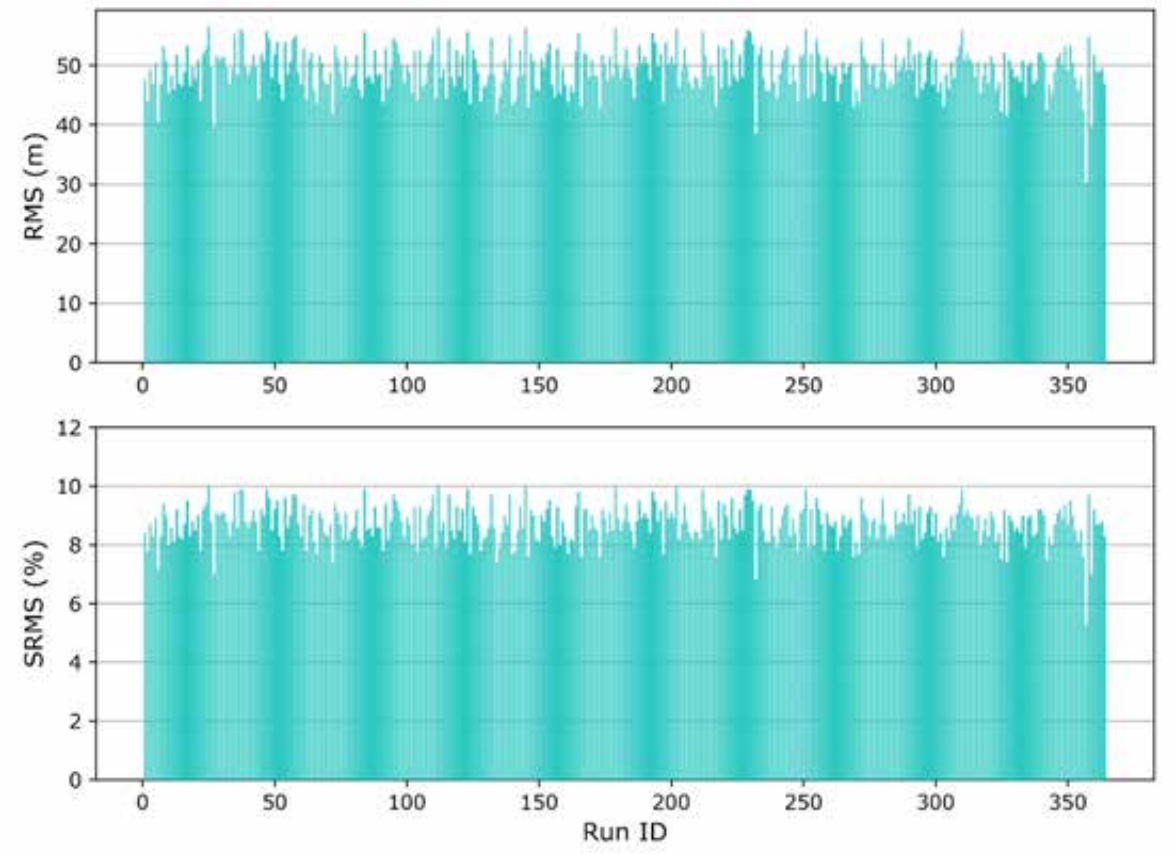

Figure 4-3 Calculated RMS and SRMS for converged model realisations

The results presented in the remainder of this section are extracted from the realisation that yields the best statistical fit with the observed groundwater levels, referred to as reference case.

The matches between individual water level measurements are presented as a scatter plot in Figure 4-4. The calibration statistics are expressed by RMS and the scaled RMS values of 30.2 m and 5.4%, respectively. Barnett et al. (2012) propose that groundwater models should aim to minimise the SRMS (RMS divided by the range of observed data) error to below 10%. Therefore, a value of 5.4% is deemed a satisfactory level of calibration.

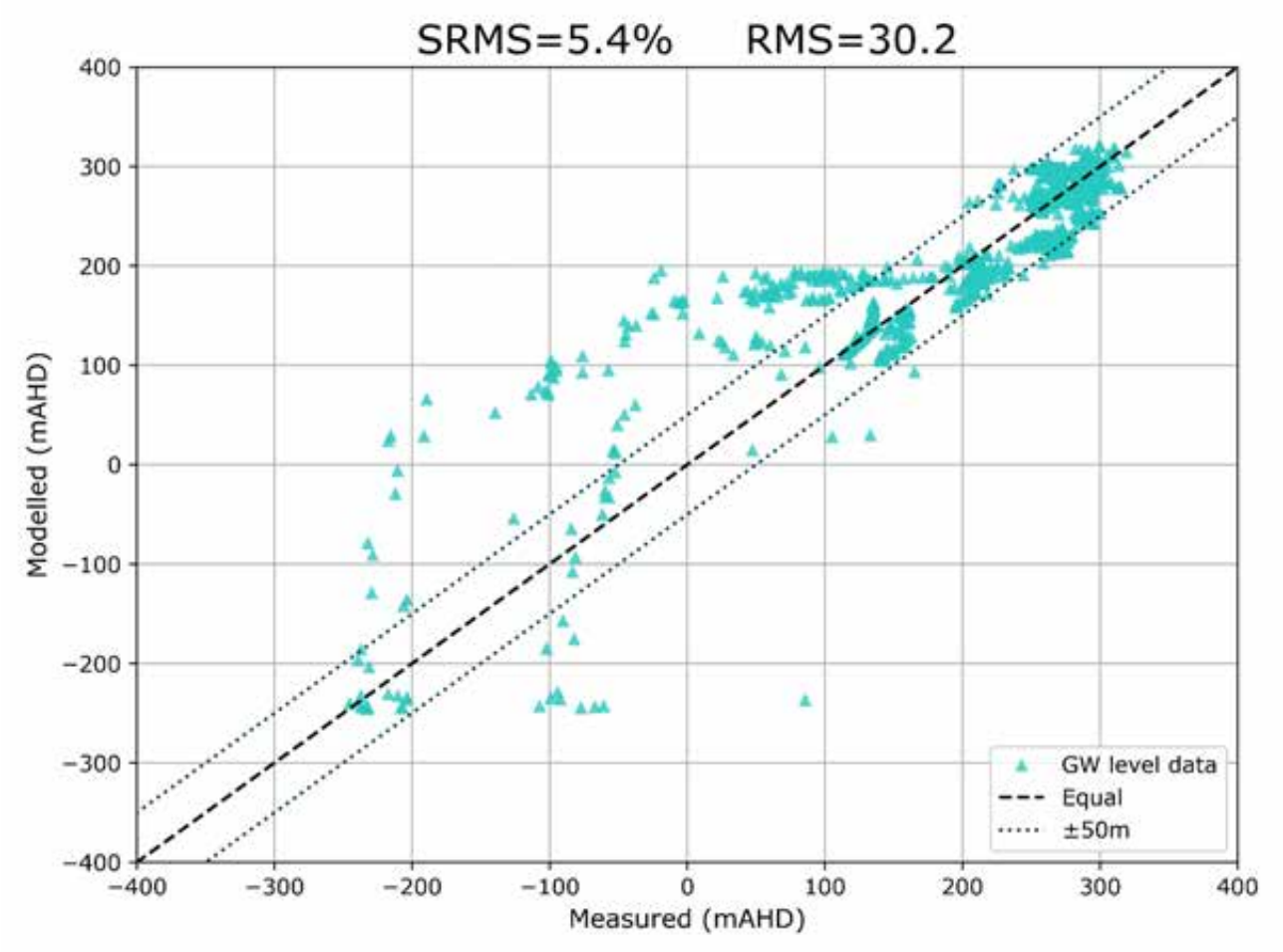

Figure 4-4 Calibration fit of reference case

One of the metrics to evaluate groundwater model performance is by quantifying the match between the observed and modelled groundwater levels and by assessing the consistency of their trends.

A reasonable match for groundwater level trends was achieved (shown in Figure 4-5) as noted in the observed groundwater levels showing recovering trends or declining trends due to groundwater abstraction.

All hydrographs for simulated groundwater levels are presented in Appendix A.

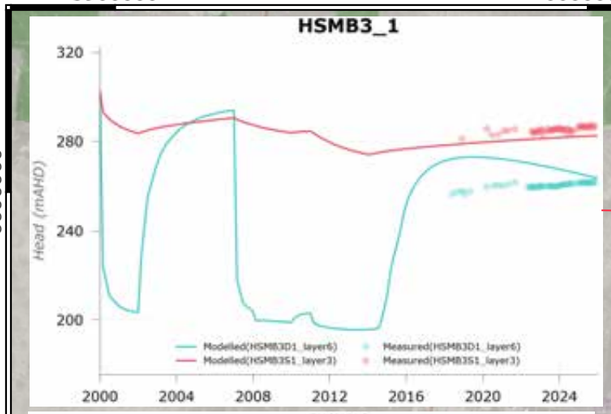

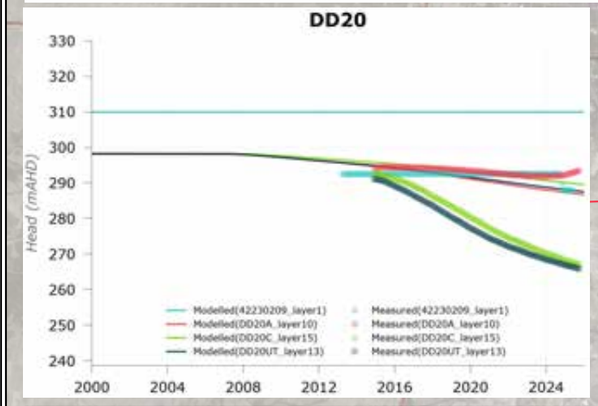

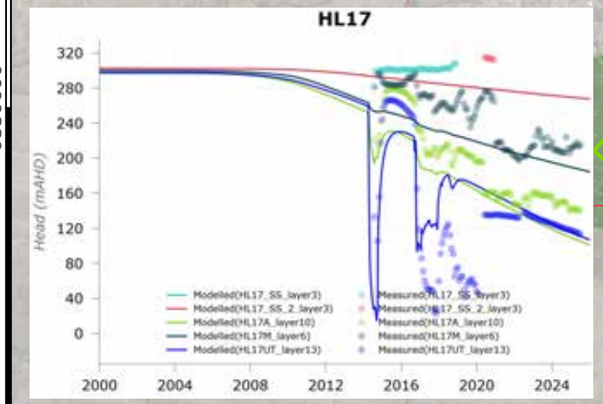

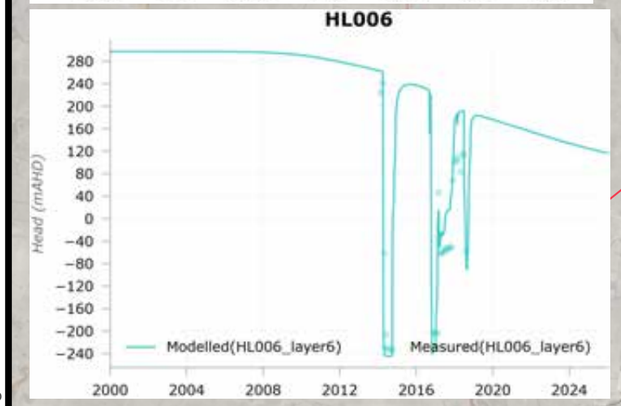

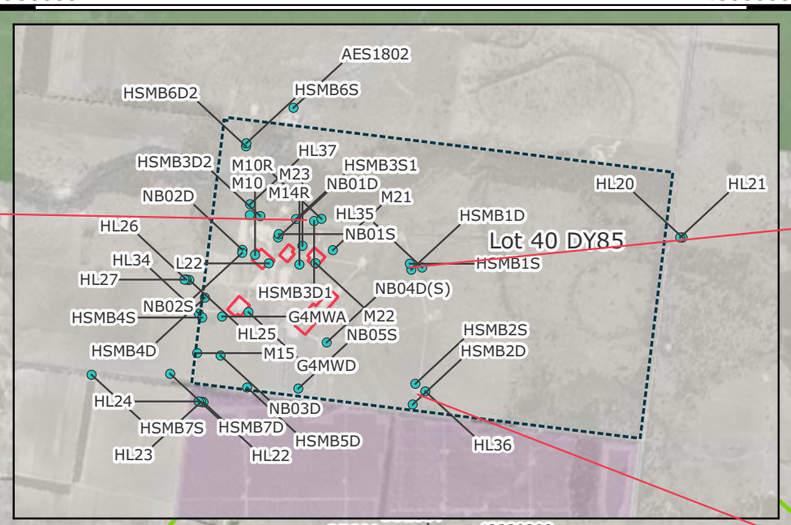

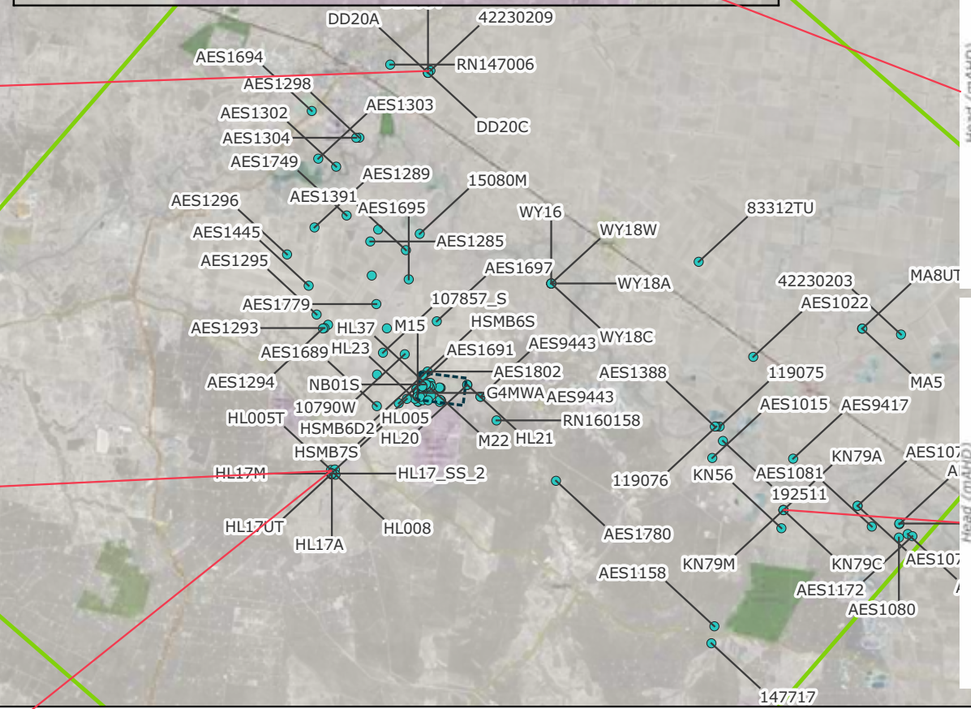

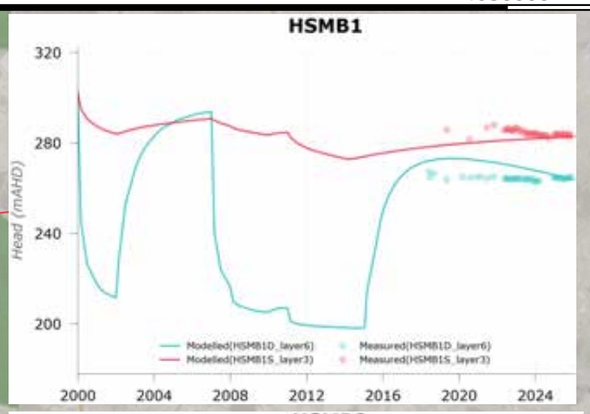

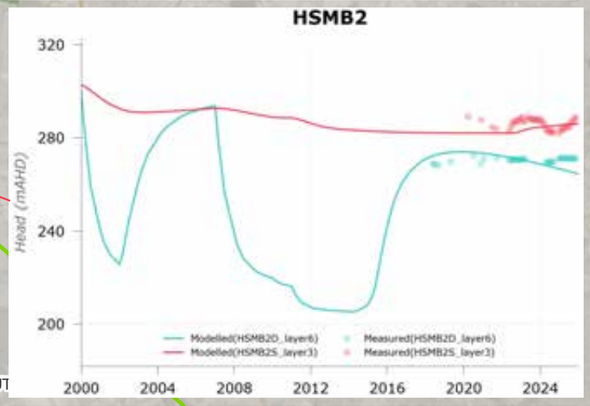

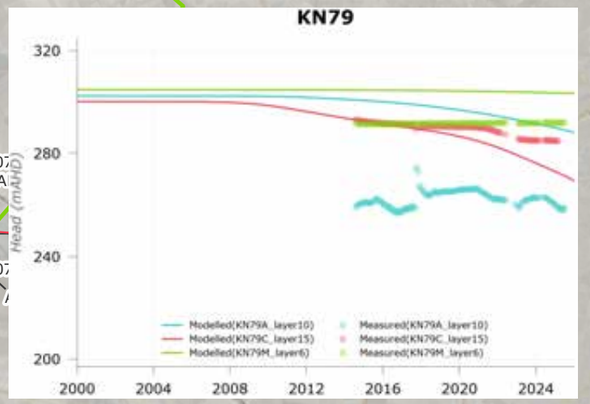

Legend

- Groundwater model extent
- Gasifiers
- Monitoring bores
- Lot 40 DY85

Observed vs modelled groundwater levels in monitoring bores

Project No.	Client	Figure No.
411001-00917	Arrow	4-5

Notes:
Project CRS: GDA94 / MGA zone 56
Last Saved: 20:27 16/04/2026
Exported by User: Mohsen.Azadi
Project Exported: 21:59 16/04/2026

References:
N/A

File Path: C:\modelling\Arrow\deliverables\Figures_REP-HG-002\Figure_4-5_GW_trends.qgz

0 4 8 12 16 km
1:391,516

N

3900000 3950000 4000000 4050000
6600000 6550000 6500000 6450000

4.4.2 Groundwater levels and flow directions

Figure 4-6 shows the simulated groundwater levels (reference case) at the end of the history matching period. As discussed in section 4.3, Q3 2025 groundwater levels were used as a calibration target to ensure the current simulated groundwater flow directions are largely aligned with the interpreted groundwater contours within Lot 40 DY85 (discussed in section 2.4.1). The calibration results indicate this approach achieves a reasonable spatial match between simulated and inferred (from bore measurements) groundwater levels and flow directions.

Modelled groundwater flow gradients within the Springbok sandstone indicate inward flow towards Lot 40 DY85. In the Macalister coal seam, hydraulic gradients are directed towards the gasifiers from the east, north, and parts of the west boundary, with groundwater continuing to flow towards the southwest corner of Lot 40 DY85. This flow direction potentially reflects partial groundwater recovery near the gasifiers and regional south to southwest groundwater flow associated with the current CSG abstraction beyond the PL253 area.

Springbok sandstone

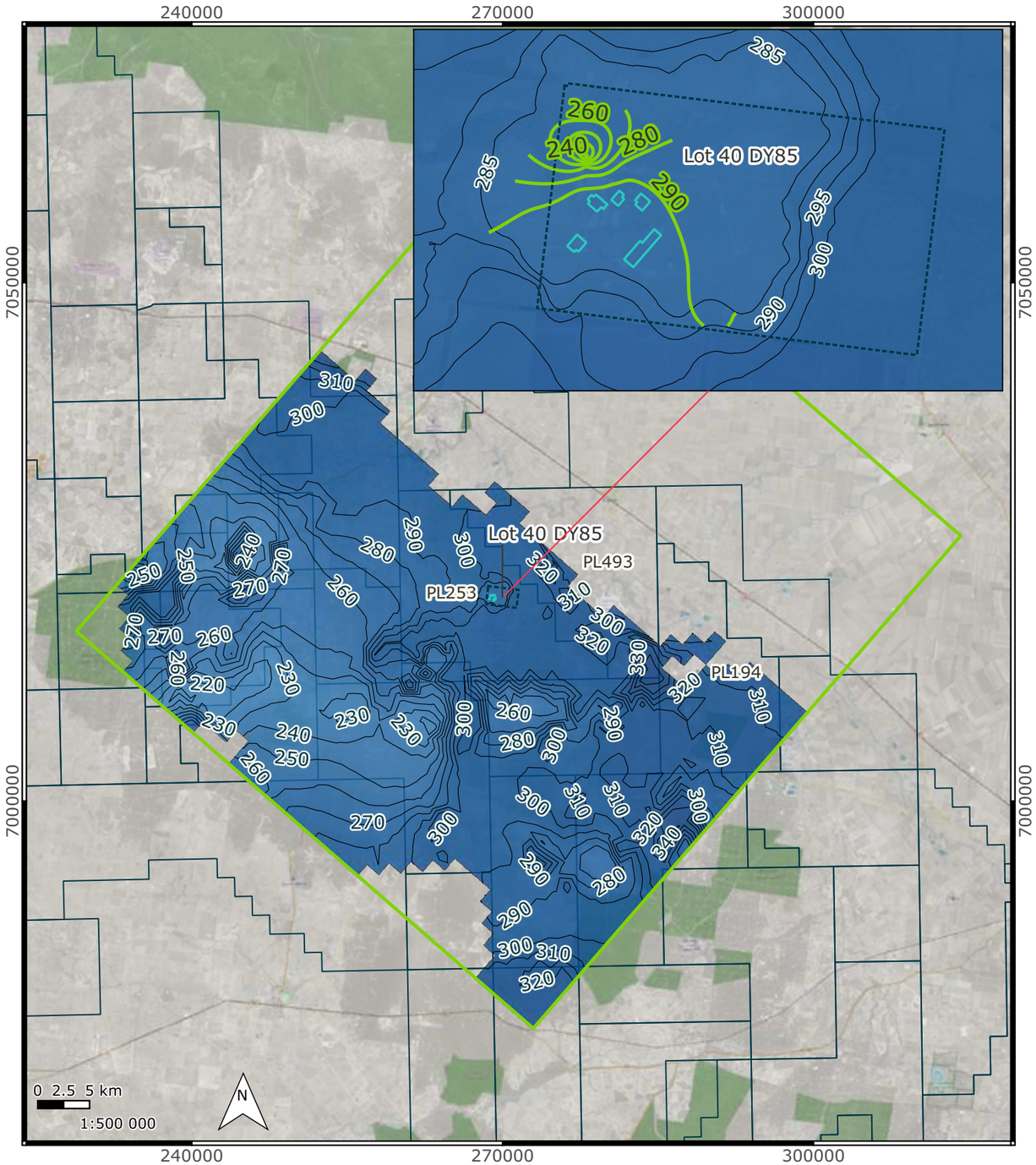

Macalister coal seam

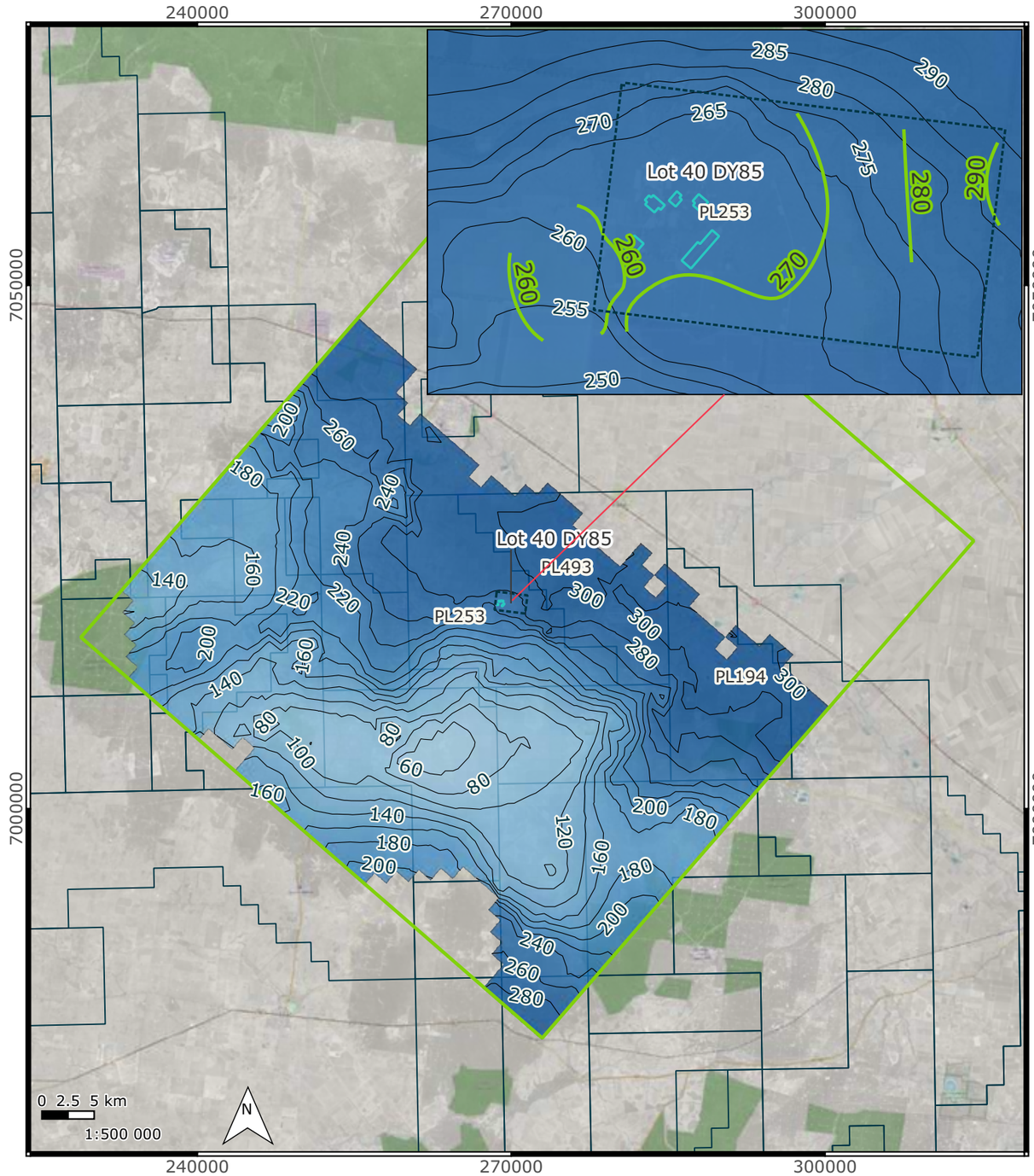

Legend

- Groundwater model extent
- Lot 40 DY85
- Petroleum leases
- Groundwater contours - Q3 2025

Groundwater level (mAHD)

- -200
- -100
- 0
- 100
- 200
- 300
- 400

Simulated groundwater levels in Springbok sandstone and Macalister coal seam (end of December 2025)

Project No.	Client	Figure No.
411001-00917	Arrow	4-6

Notes:
Project CRS: GDA94 / MGA zone 56
Last Saved: 11:48 17/04/2026
Filename: Figure_4-6_GW_cal_end

Exported by User: Mohsen.Azadi
Project Exported: 11:15 28/04/2026

References:
N/A

File Path: C:\modelling\Arrow\deliverables\Figures_REP-HG-002\Figure_4-6_GW_cal_end.qgz

4.4.3 Calibrated hydraulic parameters

The ranges of calibrated hydraulic properties derived from the calibration ensemble (reference case realisation) are summarised by respective box and whiskers (BAW) plots shown in Figure 4-7. The BAW plot characterises:

- a median value with the line inside the box
- the range between the 25th and 75th percentiles - box extent
- the minimum and maximum values as whiskers
- an area-averaged value for the cells in each zone (the red line shows) which is discussed below for comparison of hydraulic properties across different zones.

The calibrated hydraulic property ranges indicate that:

- Condamine alluvium has the highest horizontal conductivity with a median value of 14.9 m/day.
- The remaining mode layers are calibrated to a median range of horizontal conductivity between 0.001 m/day and 0.1 m/day with the following exceptions:
  - Kogan interburden, Macalister interburden, and Eurombah formation are calibrated to median values between 0.001 m/day to 0.00001 m/day, and
  - Koan coal seam and Condamine coal seam is calibrated to median values slightly over 0.1 m/day.
- Vertical hydraulic conductivity is calibrated to lower values compared to horizontal hydraulic properties with similar trend among various layers with Condamine alluvium and Eurombah formation having the highest and lowest values, respectively.
- The specific storage and specific yield values are calibrated within the plausible bounds, with a general trend of higher storage values for coal seams and lower values for interburden units and deeper HSUs as the storativity values reduce with depth.

Prior and posterior distribution of median value for each HSU across the full ensemble is presented in Appendix B.

Figure 4-7 Calibrated hydraulic property ranges

4.5 Contaminant transport model

Contaminant transport history matching was undertaken to replicate observed groundwater quality trends for benzene and naphthalene and to provide confidence in subsequent predictive uncertainty analysis. The process focused on assessing whether the combined representation of groundwater flow fluxes, source term characterisation, transport parameters, and natural attenuation processes could reasonably replicate the magnitude, spatial extent, and temporal evolution of measured concentrations.

4.5.1 History-matching metrics

The performance of the 364 model realisations was analysed to ensure the transport models used during predictive uncertainty analysis are calibrated. A maximum SRMS of 10% was adopted as the criterion to assess history matching fit for benzene and naphthalene, with all 364 realisations meeting the history matching criterion, as shown in Figure 4-8 and Figure 4-9.

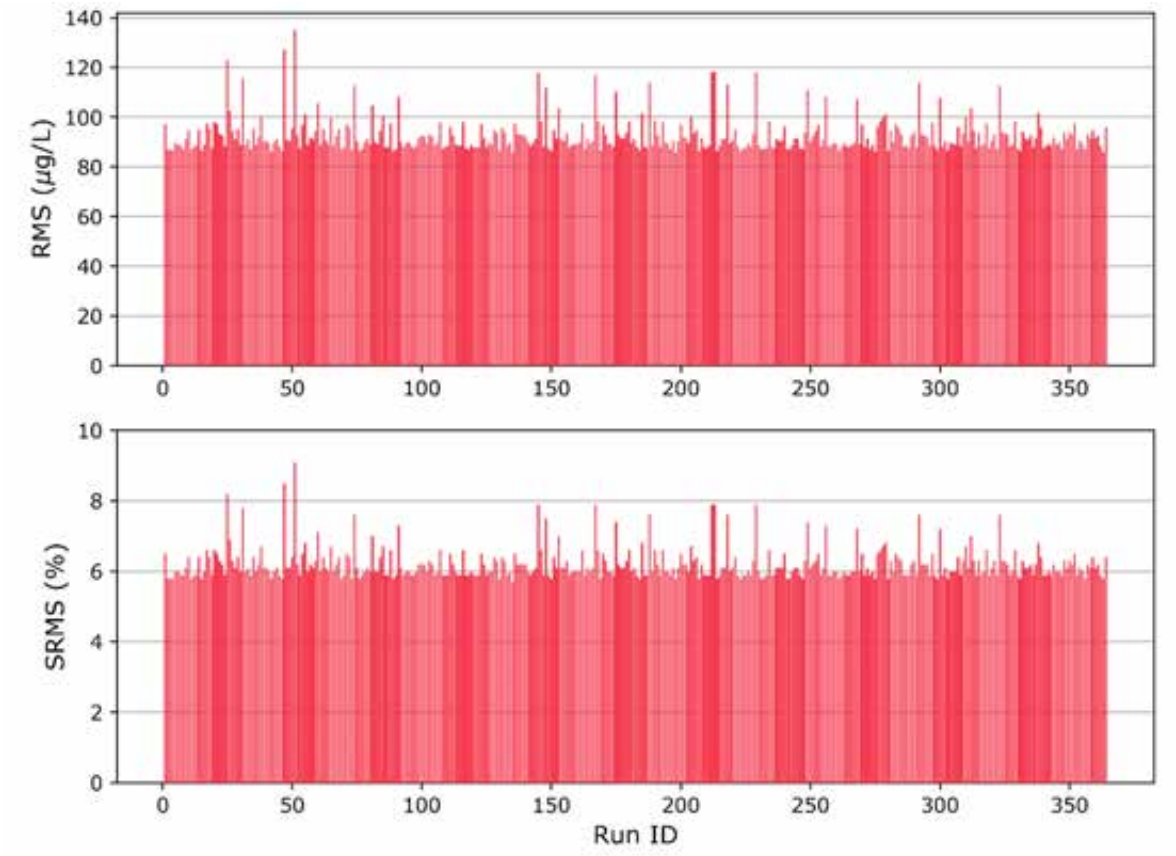

Figure 4-8 Calculated RMS and SRSM for benzene concentration across the posterior ensemble

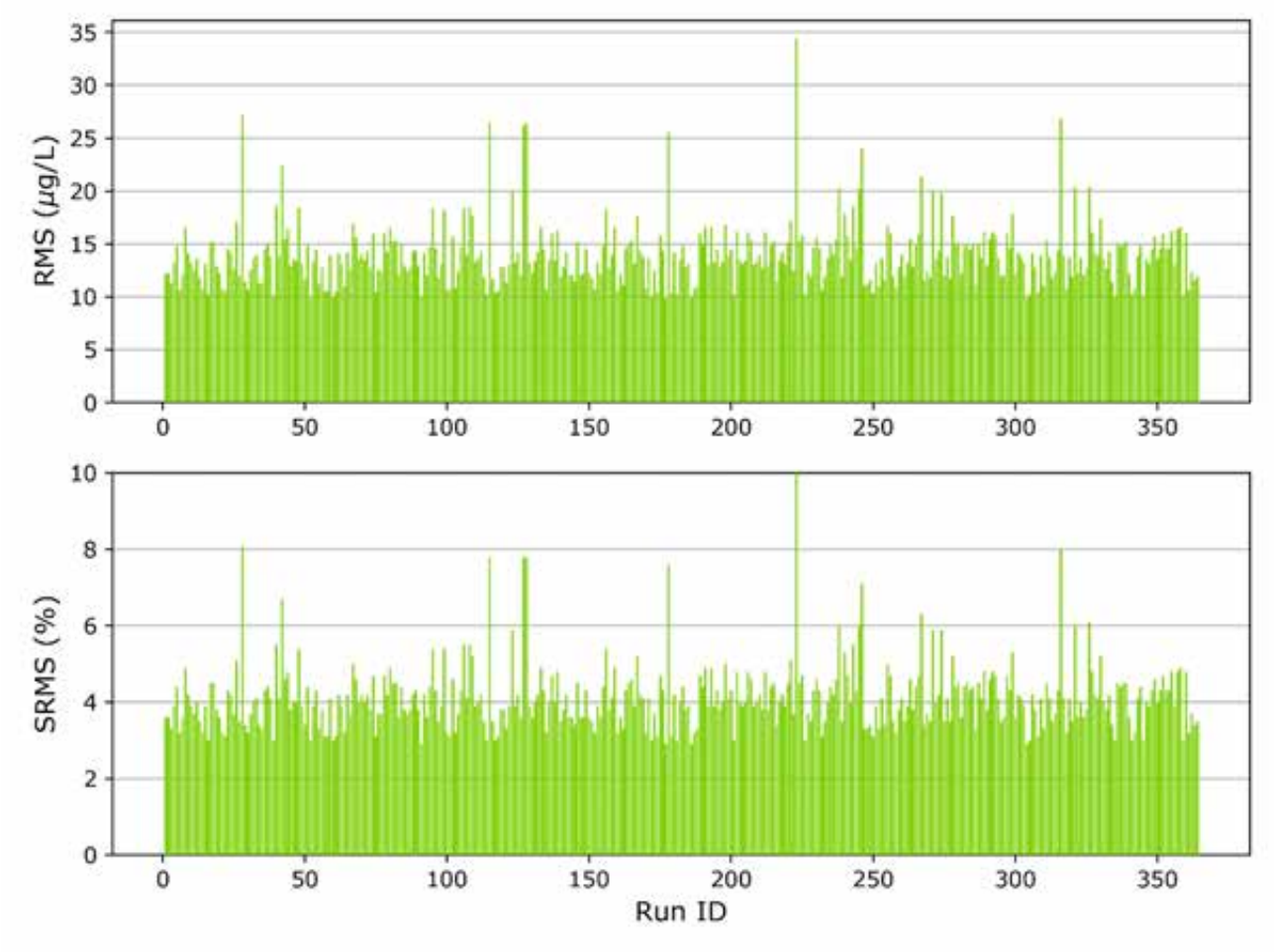

Figure 4-9 Calculated RMS and SRSM for naphthalene concentration across the posterior ensemble

The results presented in the remainder of this section are extracted from the realisation that yields the best statistical fit with the observed groundwater concentrations, referred to as reference case.

The matches between individual water concentration measurements are presented as a scatter plot in Figure 4-10 and Figure 4-11. The history matching results indicate that a good calibration fit is achieved for the magnitude of benzene and naphthalene concentrations in the contaminant transport model.

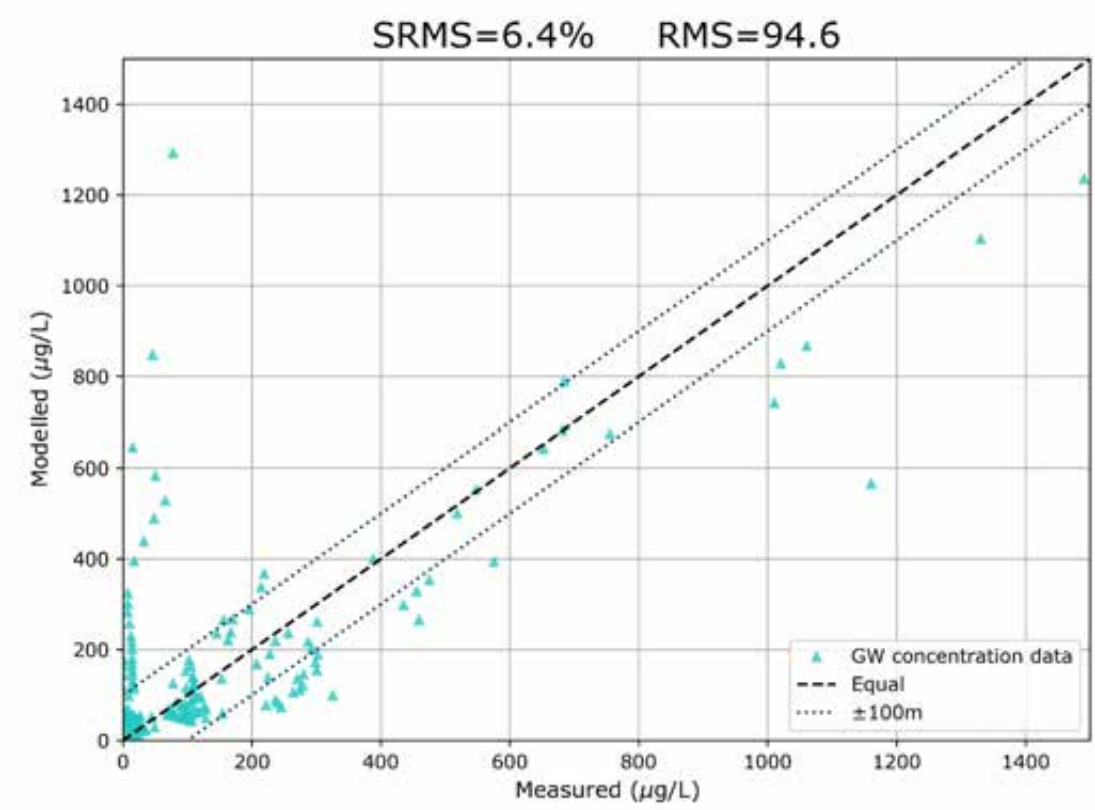

Figure 4-10 Benzene history matching fit for the reference case

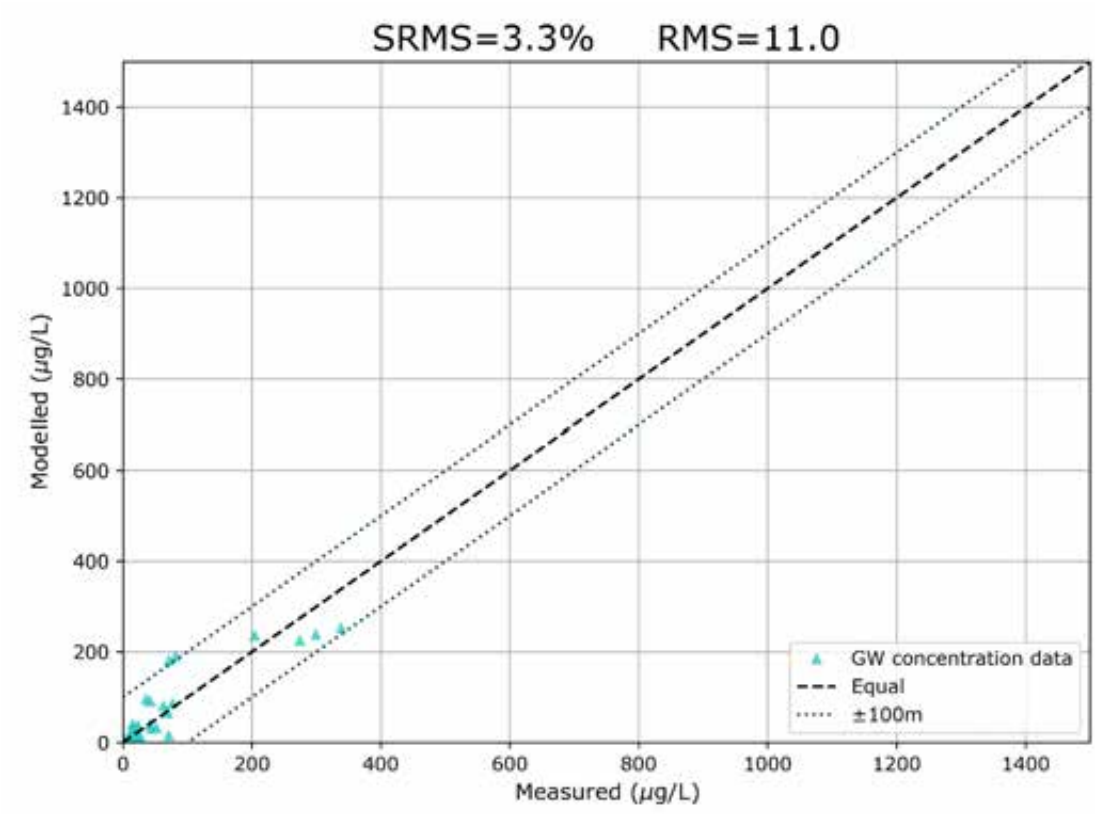

Figure 4-11 Naphthalene history matching fit for the reference case

One of the metrics used to evaluate the transport model performance is by quantifying the match between the observed and modelled groundwater concentrations and by assessing the consistency of their trends.

A reasonable match for groundwater concentration trends was achieved for both benzene and naphthalene (example shown in Figure 4-12) as noted in the observed groundwater concentrations showing below LOR values or declining trends due to groundwater dilution and natural attenuation.

The simulated benzene and naphthalene concentration trends for remaining monitoring bores are presented in Appendix C and D, respectively.

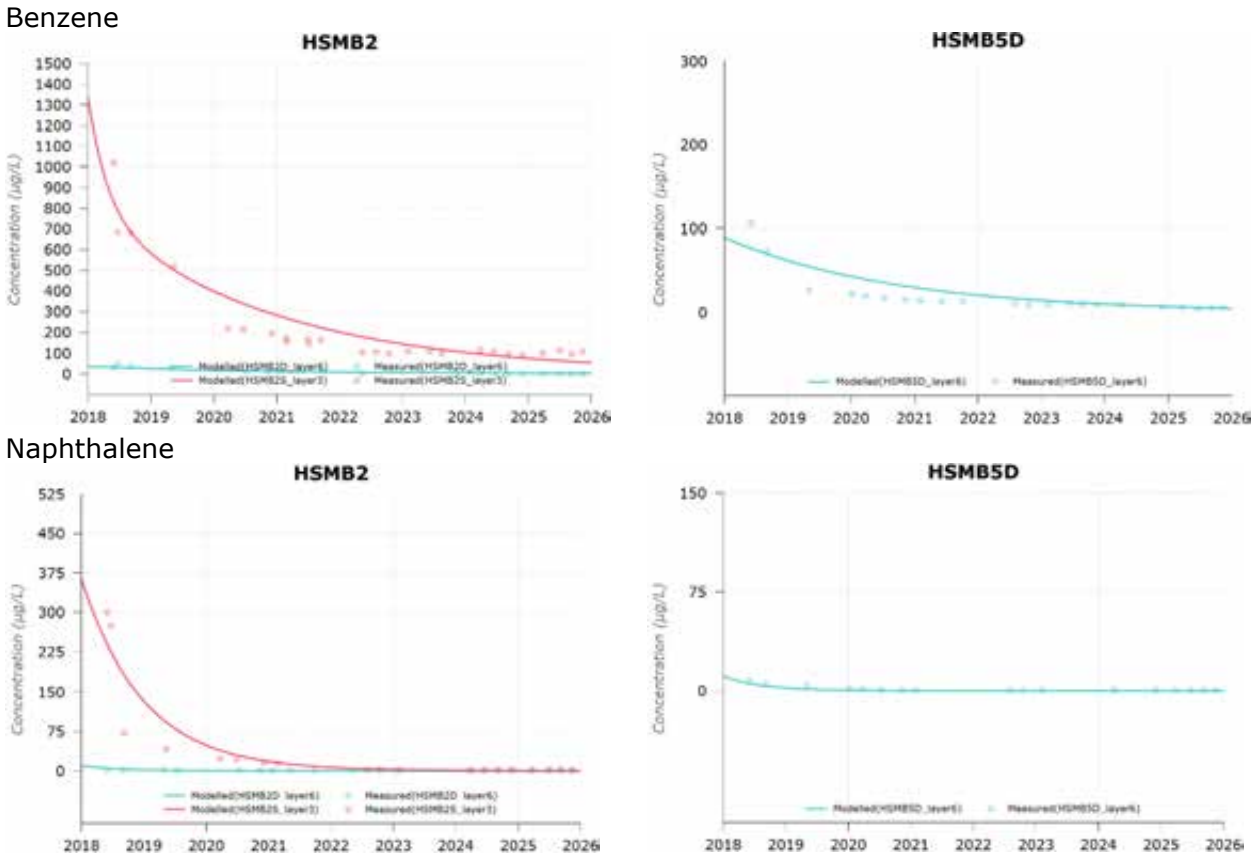

Figure 4-12 Simulated benzene and naphthalene concentration trends for representative monitoring bores screened in the Springbok sandstone and Macalister coal seam

4.5.2 Simulated benzene and naphthalene concentrations

Figure 4-13 shows the simulated benzene concentration (reference case) at the end of the history matching period in the Springbok sandstone and Macalister coal seam. The simulation results indicate that, for both formations, the benzene plume with concentrations exceeding 10 µg/L is largely contained within Lot 40 DY85. This is consistent with groundwater quality monitoring data from bores located outside the Lot 40 DY85 boundary (HL22, HL23, HL25, HL26, HSMB7D, and HL34), where benzene concentrations have remained below the LOR.

While monitoring bore HSMB4S is located within the Lot 40 DY85 boundary and indicates the potential for limited migration of benzene at concentrations above 10 µg/L beyond the boundary, monitoring results from downstream bores HSMB7S and HL22 have consistently reported below LOR concentrations for several years. This indicates that elevated benzene concentrations observed at HSMB4S are localised, with limited plume migration beyond the Lot 40 DY85 boundary.

The simulated benzene plume shows a zone of elevated concentrations (approximately 50–100 µg/L) within the central part of Lot 40 DY85, extending east of gasifier 5. This zone reflects history matching of the coupled groundwater flow and contaminant transport model to monitoring data that include both below LOR and elevated concentrations, spanning several orders of magnitude. Monitoring data from bores NB04D(S), HL36, HSMB1S, and HL35 (with concentrations below LOR), together with data from bore HSMB2S, define the extent, magnitude, and orientation of the simulated plume in this area.

These monitoring data are reflected with spatial variations in calibrated hydraulic conductivity, which indicate the potential presence of a locally enhanced permeability zone near gasifier 5. This feature is interpreted to reflect hydrogeological alteration associated with historical UCG activities, including fracturing of the formation in this direction.

Simulation results at the end of history matching period for naphthalene indicate concentrations below the LOR within the Macalister coal seam across the model domain. In the Springbok sandstone, simulated naphthalene concentrations remain spatially confined within the former gasifier locations. These results reflect the conservative source depletion formulation adopted in the transport model, where the maximum source concentration was defined as 2.2 µg/Lat the end of 2025. The results indicate limited migration potential for naphthalene beyond localised source zones, consistent with groundwater monitoring data.

Springbok sandstone

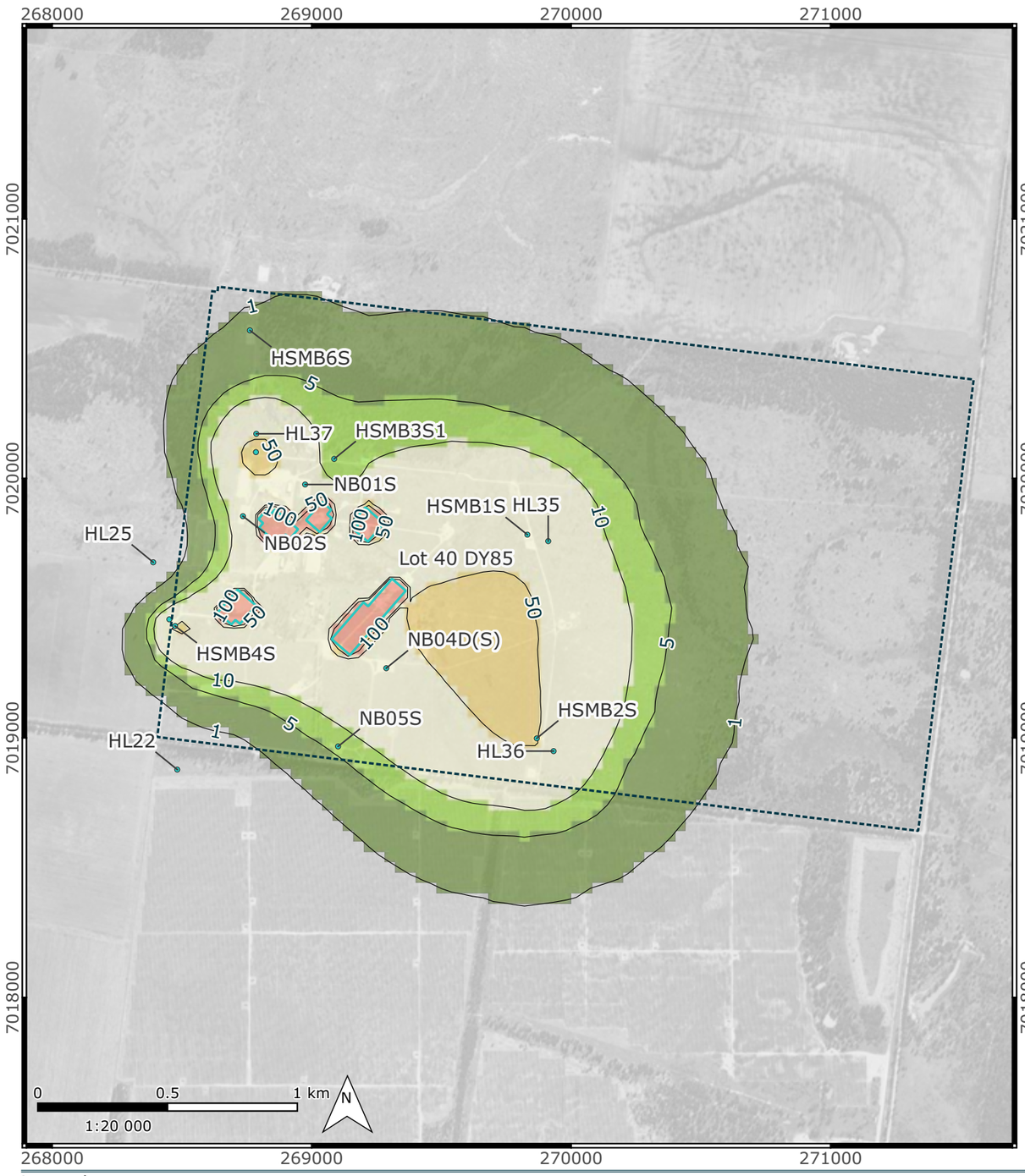

Macalister coal seam

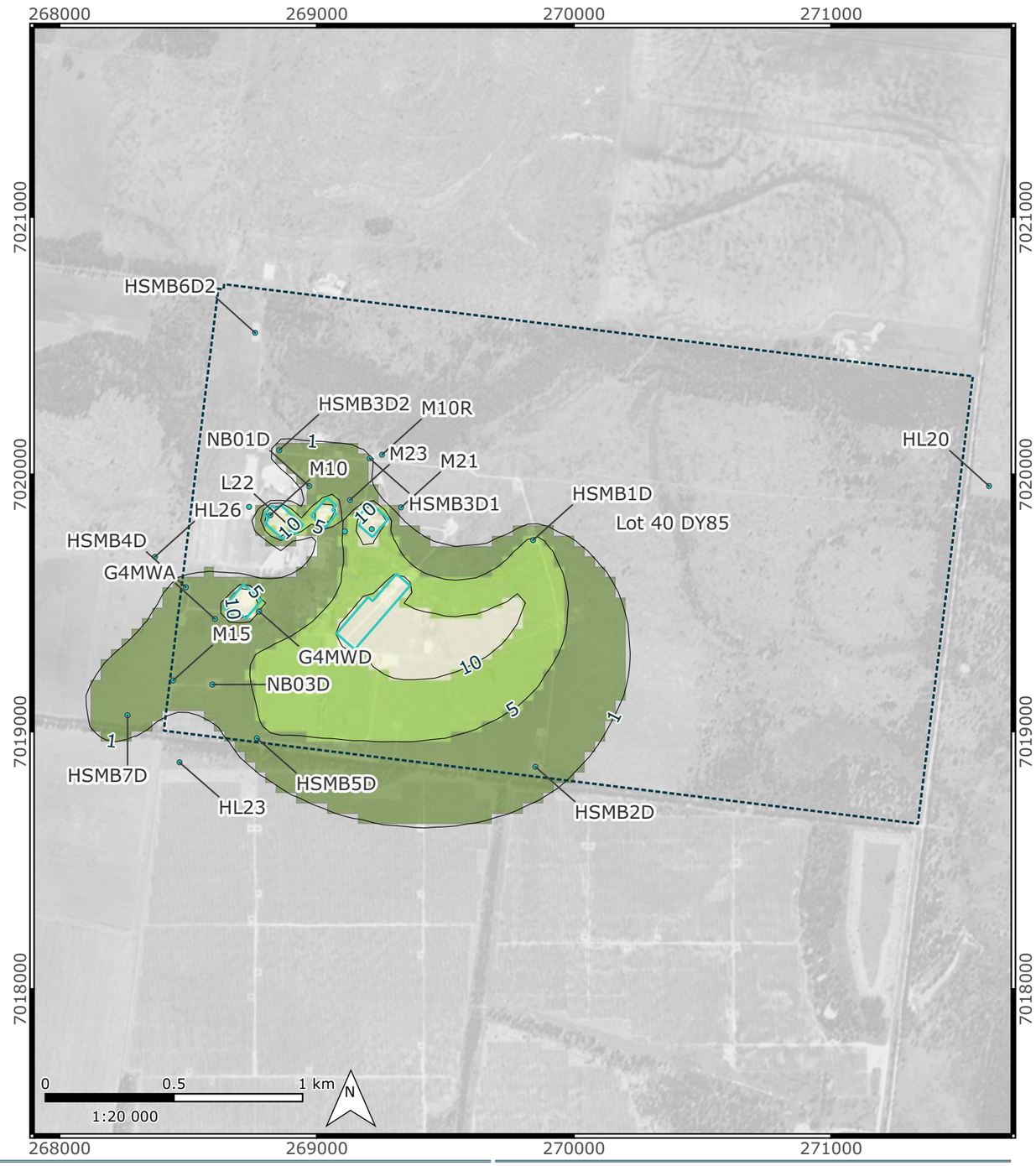

Legend

- Lot 40 DY85
- Gasifier
- Monitoring bores

Concentration (ug/L)

- 1 - 5
- 5 - 10
- 10 - 50
- 50 - 100
- 100 - 500
- 500 - 1000
- 1000 - 5000

Simulated benzene concentrations in Springbok sandstone and Macalister coal seam (end of December 2025)

Project No.	Client	Figure No.
411001-00917	Arrow	4-13

Notes:
Project CRS: GDA94 / MGA zone 56
Last Saved: 16:48 17/04/2026
Filename: Figure_4-13_benzene_cal_end

Exported by User: Mohsen.Azadi
Project Exported: 17:49 21/04/2026

References:
N/A

File Path: C:\modelling\Arrow\deliverables\Figures_REP-HG-002\Figure_4-13_benzene_cal_end.qgz

5. Predictive groundwater flow modelling

5.1 Predictive model setup

Predictive groundwater modelling was undertaken to assess the potential impacts of current and proposed CSG FDP scenarios on groundwater flow and contaminant transport and fate within the Springbok sandstone and the Macalister coal seam. The predictive assessment was based on an ensemble of 364 calibrated realisations, generated through history matching and uncertainty analysis, to quantify the range of potential future outcomes and provide a basis for risk-based impact assessment and decision-making. Model predictions are presented using the P5, P50, and P95 percentiles, representing different likelihoods of predictive outcomes.

Predictive simulations were completed for scenario 2 (existing approved development, including Hopeland pilot wells and authorised Arrow CSG wells) and scenario 3 (maximum proposed development incorporating additional Clynes Road wells). For each scenario, predicted impacts were evaluated separately for the Springbok sandstone and Macalister coal seam. Comparison of percentile-based outcomes between scenarios enabled assessment of incremental impacts attributable to proposed development while explicitly accounting for uncertainty in model parameters and boundary conditions.

All simulations incorporated the full simulation period starting from year 2000, with predictive model starting in 2026, groundwater abstraction ceasing in 2061, and followed by extended recovery simulations through to the end of year 2225. This long-term simulation period allowed assessment of post-abstraction recovery trajectories, potential long-term drawdown or concentration changes.The results of the uncertainty are presented using the risk-based terminology outlined in Peeters & Middlemis (2023) as presented in Table 5-1.

Table 5-1 Probabilistic terminology used (from Peeters & Middlemis, 2023)

Percentile	Probability	Description
<10%	>90%	It is **very likely** that the outcome is **larger** than this value
10–33%	67–90%	It is **likely** that the outcome is **larger** than this value
33–67%	33–67%	It is **as likely as not** that the outcome is **larger** than this value
67–90%	10–33%	It is **unlikely** that the outcome is **larger** than this value
>90%	<10%	It is **very unlikely** that the outcome is **larger** than this value

5.2 Groundwater level and flow directions

Cumulative groundwater abstraction progressively lowers groundwater levels. The extent of the zone affected by abstraction is dependent on the properties of the hydrogeologic units, pumping rates and locations, cumulative production rates, schedule and target aquifer(s) relative to the water table.

Predicted median groundwater levels in the Springbok sandstone and Macalister coal seam at the end of the abstraction period (December 2061), and at the end of the recovery period (December 2225), for non-Arrow wells and Arrow wells in scenario 3, are shown in Figure 5-1 to Figure 5-2.

Model results indicate the development of a cone of depression around abstraction wells because of cumulative groundwater extraction, with regional groundwater flow directed predominantly toward the south and southwest of the model domain.

Within Lot 40 DY85, simulated groundwater flow directions vary by formation. In the Springbok sandstone, predicted groundwater flow is directed toward the gasifiers, with inflow from the north, east, and south boundaries of Lot 40 DY85 and a relatively flat hydraulic gradient along the western boundary. Groundwater flow in the Macalister coal seam is directed toward the southwest. Comparison with groundwater level contours at the end of 2025 (Figure 4-6), indicates partial groundwater recovery in the Springbok sandstone, while groundwater levels in the Macalister coal seam is lowered due to ongoing CSG abstraction from the WCM.

By the end of the recovery period, simulated regional groundwater levels increase relative to those at the end of abstraction period. However, groundwater levels are not predicted to fully return to pre-abstraction conditions. Long-term water balance recovery simulations indicate that total groundwater outflows, including evaporative losses and boundary fluxes, continue to exceed rainfall recharge, limiting full recovery to pre-development groundwater levels.

Differences between the predicted median groundwater levels at the end of abstraction period for scenarios 2 and 3 were evaluated across the ensemble for both the Springbok sandstone and the Macalister coal seam, as shown in Figure 5-3. The predictions indicate a limited area of difference, with up to 1 m change in median groundwater levels occurring at the southwest corner of PL253 within the Springbok sandstone. In the Macalister coal seam, a localised zone with predicted differences of approximately 1–2 m occurs in the vicinity of the proposed Clynes Road wells. These results indicate that the additional abstraction associated with the proposed Clynes Road development results in only minor incremental changes to groundwater levels when compared with the approved development scenario.

Predicted differences in median groundwater levels at the end of the recovery period between scenarios 2 and 3 are less than 1 m, indicating that inclusion of the proposed Clynes Road wells is not expected to result in a material change to groundwater level recovery relative to the currently approved development.

Predicted groundwater level trends at monitoring bores across the ensemble, showing declining trend during the abstraction period and subsequent recovery following the end of abstraction, are presented in Appendix E.

Springbok sandstone

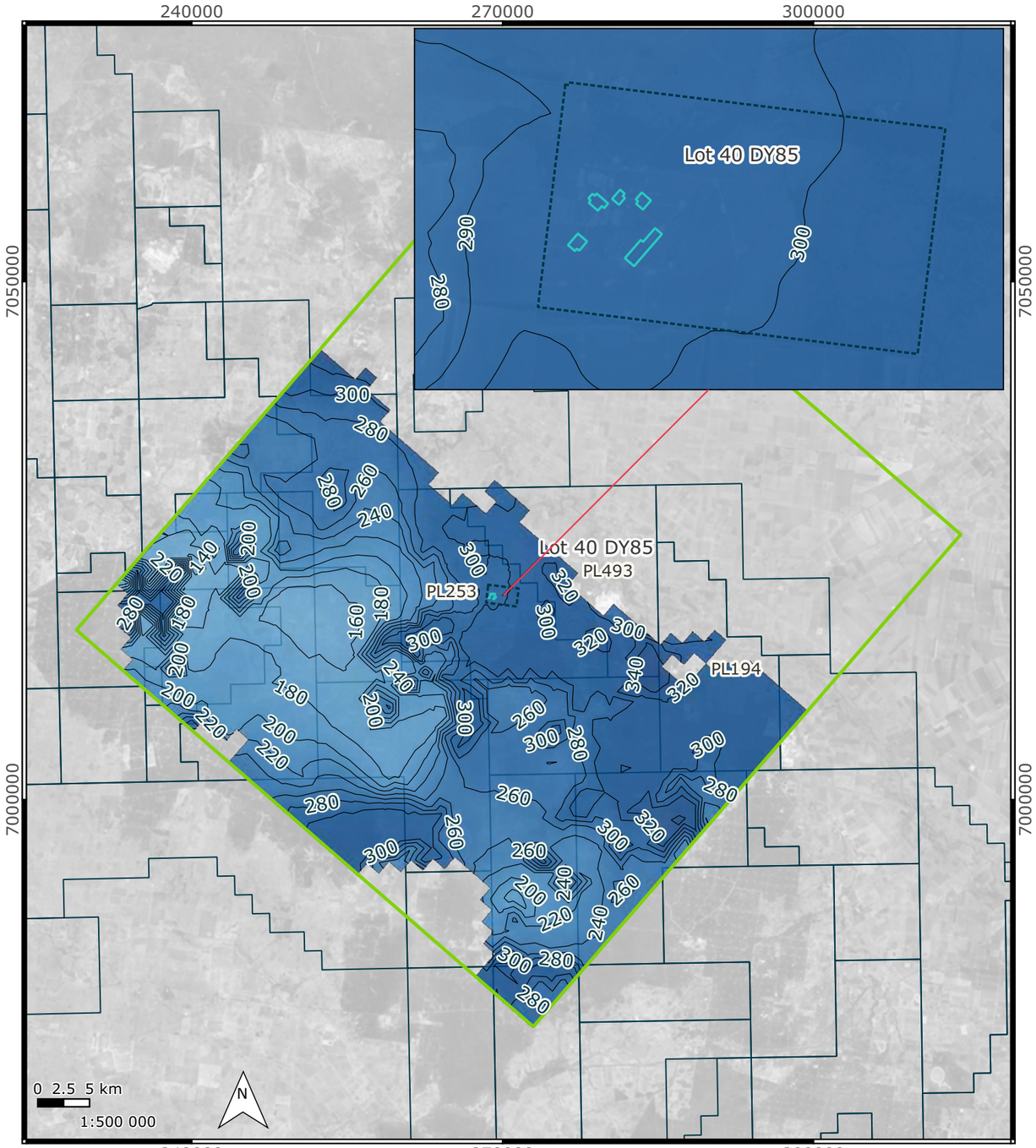

Macalister coal seam

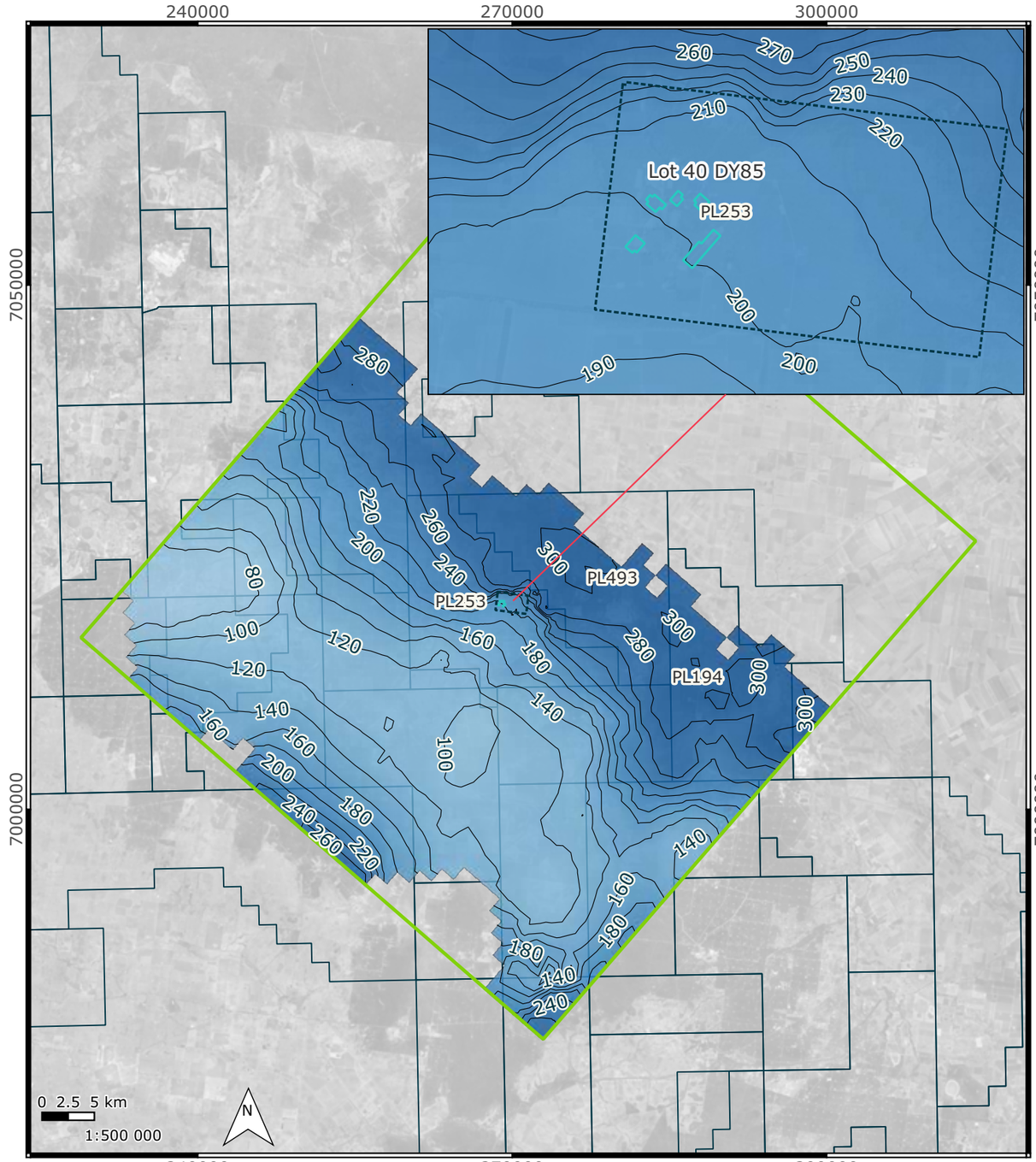

Legend

- Groundwater model extent
- Lot 40 DY85
- Petroleum leases
- Gasifiers

Groundwater level (mAHD)

- -200
- -100
- 0
- 100
- 200
- 300
- 400

Predicted median groundwater levels in Springbok sandstone and Macalister coal seam for scenario 3 (end of December 2061)

Project No.	Client	Figure No.
411001-00917	Arrow	5-1

Notes:
Project CRS: GDA94 / MGA zone 56
Last Saved: 17:08 17/04/2026
Filename: Figure_5-1_GW_abs_end

Exported by User: Mohsen.Azadi
Project Exported: 18:28 17/04/2026

References:
N/A

File Path: C:\modelling\Arrow\deliverables\Figures_REP-HG-002\Figure_5-1_GW_abs_end.qgz

Springbok sandstone

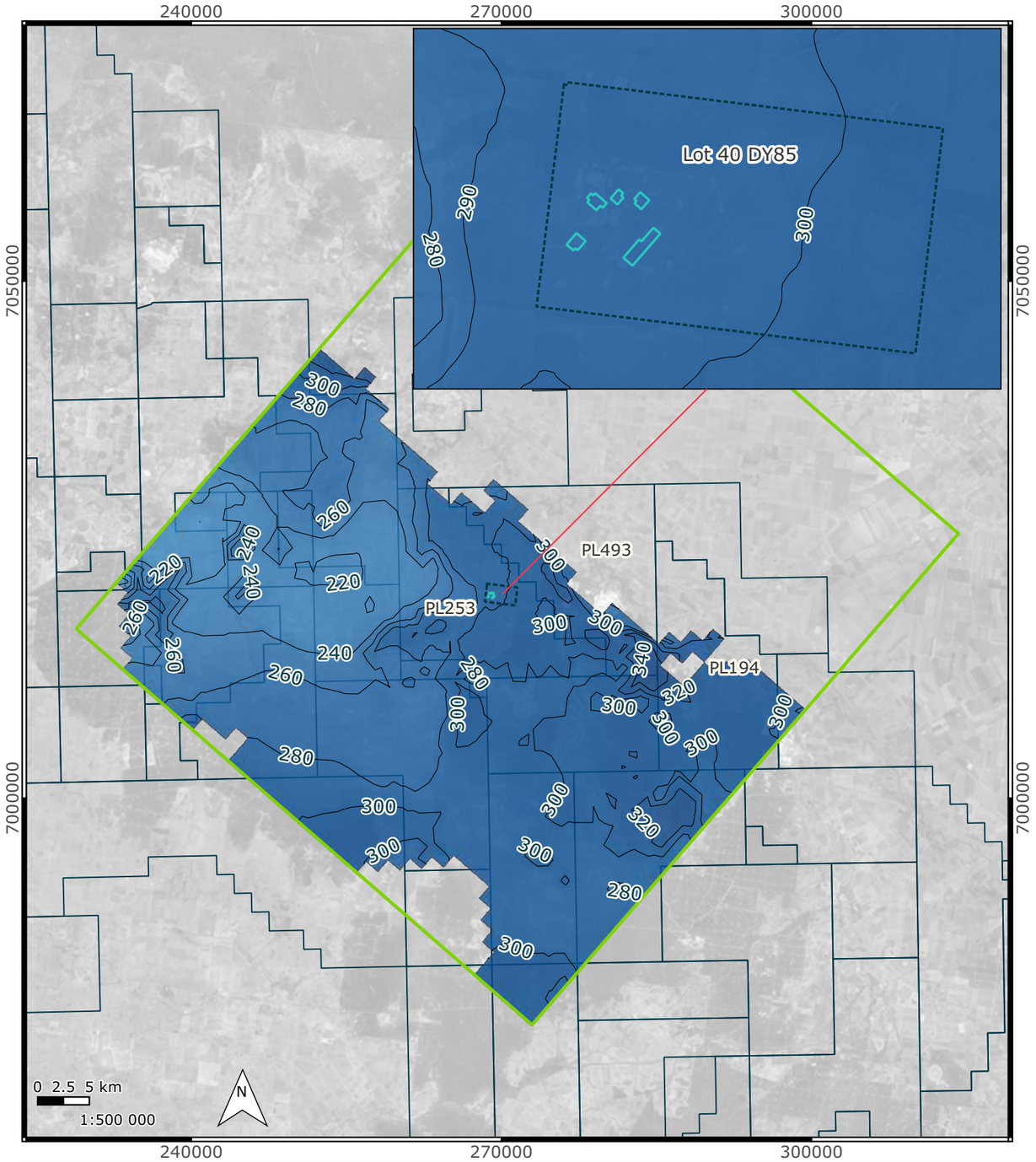

Macalister coal seam

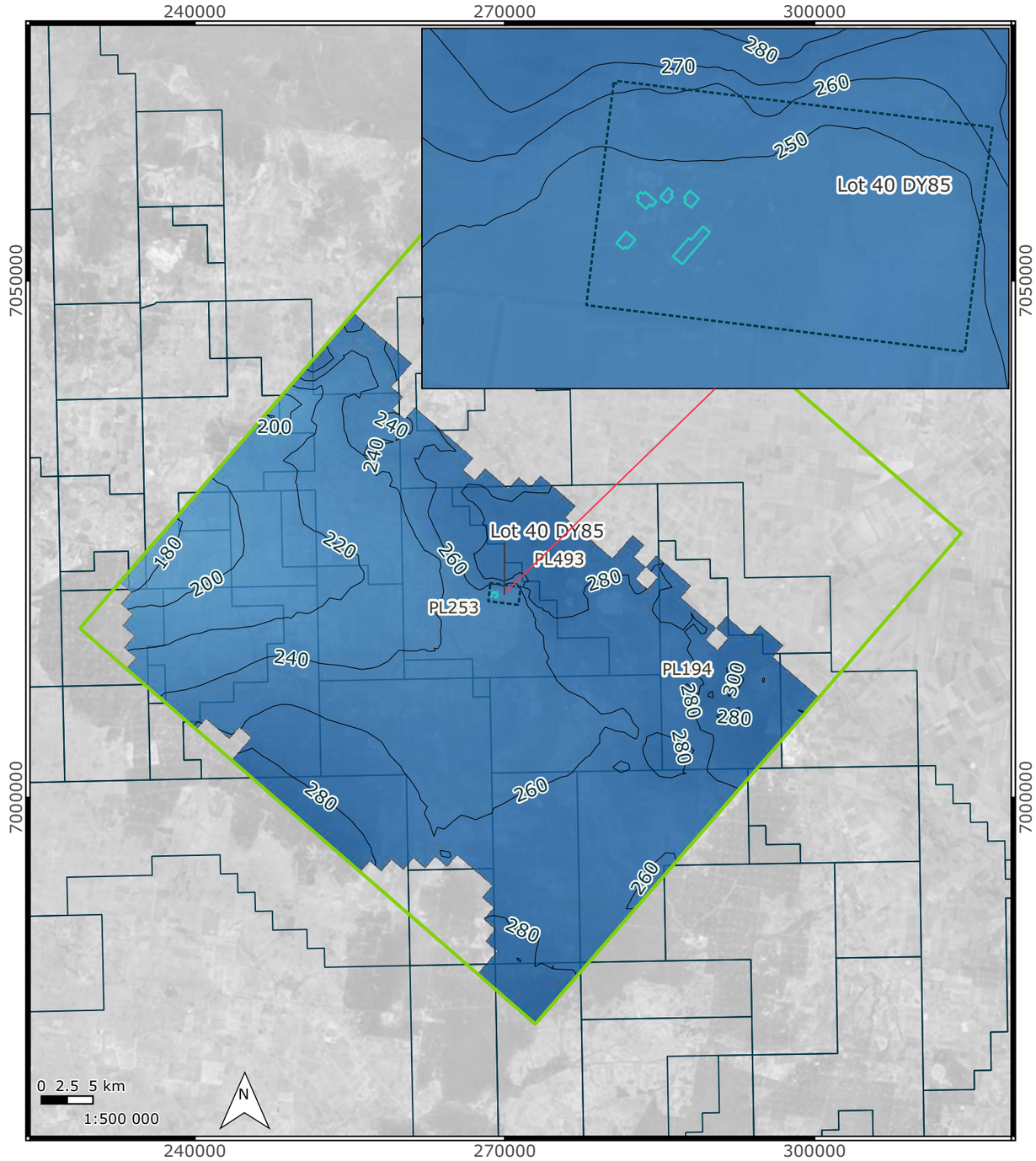

Legend

- Groundwater model extent
- Lot 40 DY85
- Petroleum leases
- Gasifiers

Groundwater level (mAHD)

- -200
- -100
- 0
- 100
- 200
- 300
- 400

Predicted median groundwater levels in Springbok sandstone and Macalister coal seam for scenario 3 (end of December 2225)

Project No.	Client	Figure No.
411001-00917	Arrow	5-2

Notes:
Project CRS: GDA94 / MGA zone 56
Last Saved: 18:37 17/04/2026
Filename: Figure_5-2_GW_rec_end

Exported by User: Mohsen.Azadi
Project Exported: 18:38 17/04/2026

References:
N/A

File Path: C:\modelling\Arrow\deliverables\Figures_REP-HG-002\Figure_5-2_GW_rec_end.qgz

Springbok sandstone

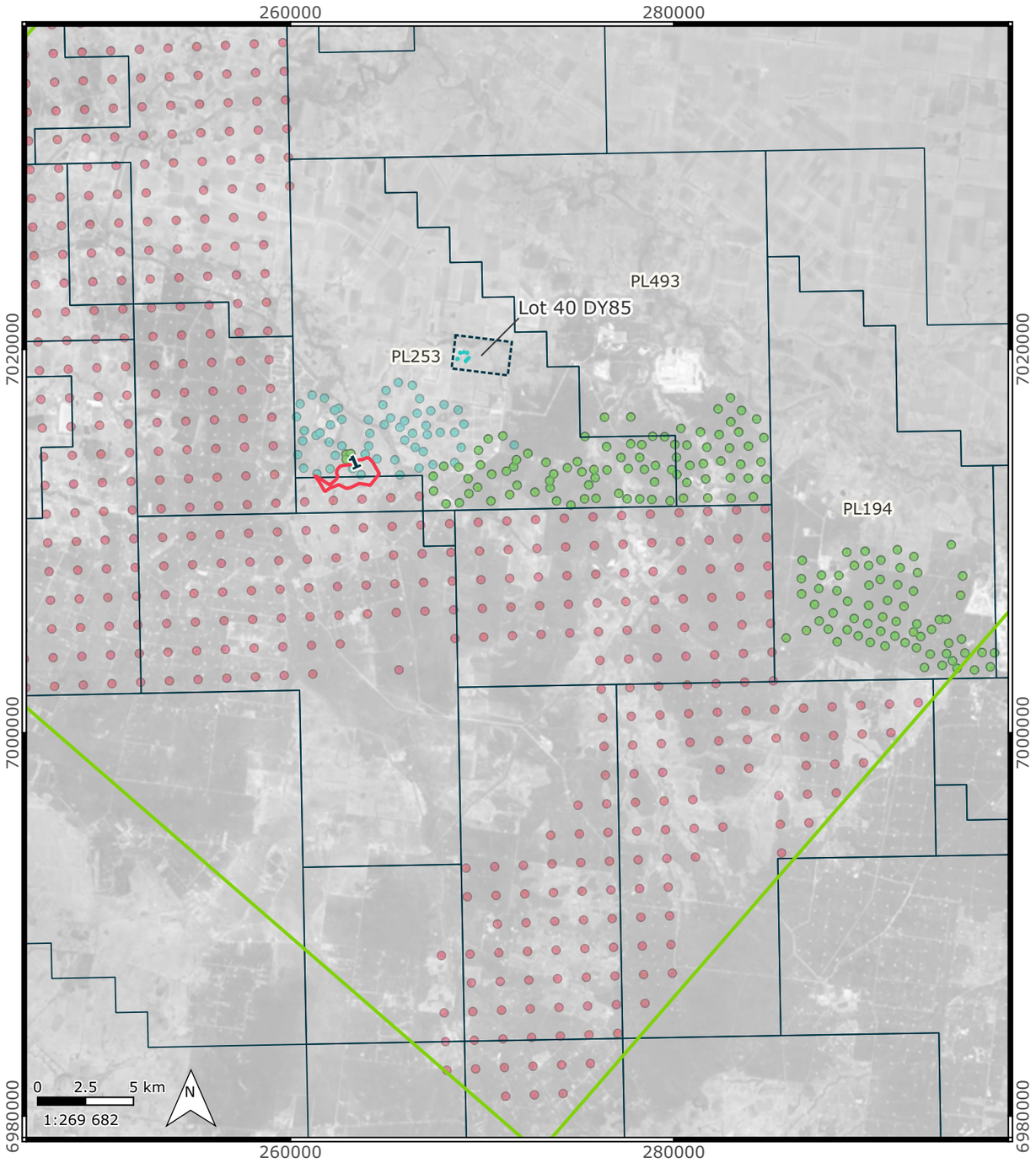

Macalister coal seam

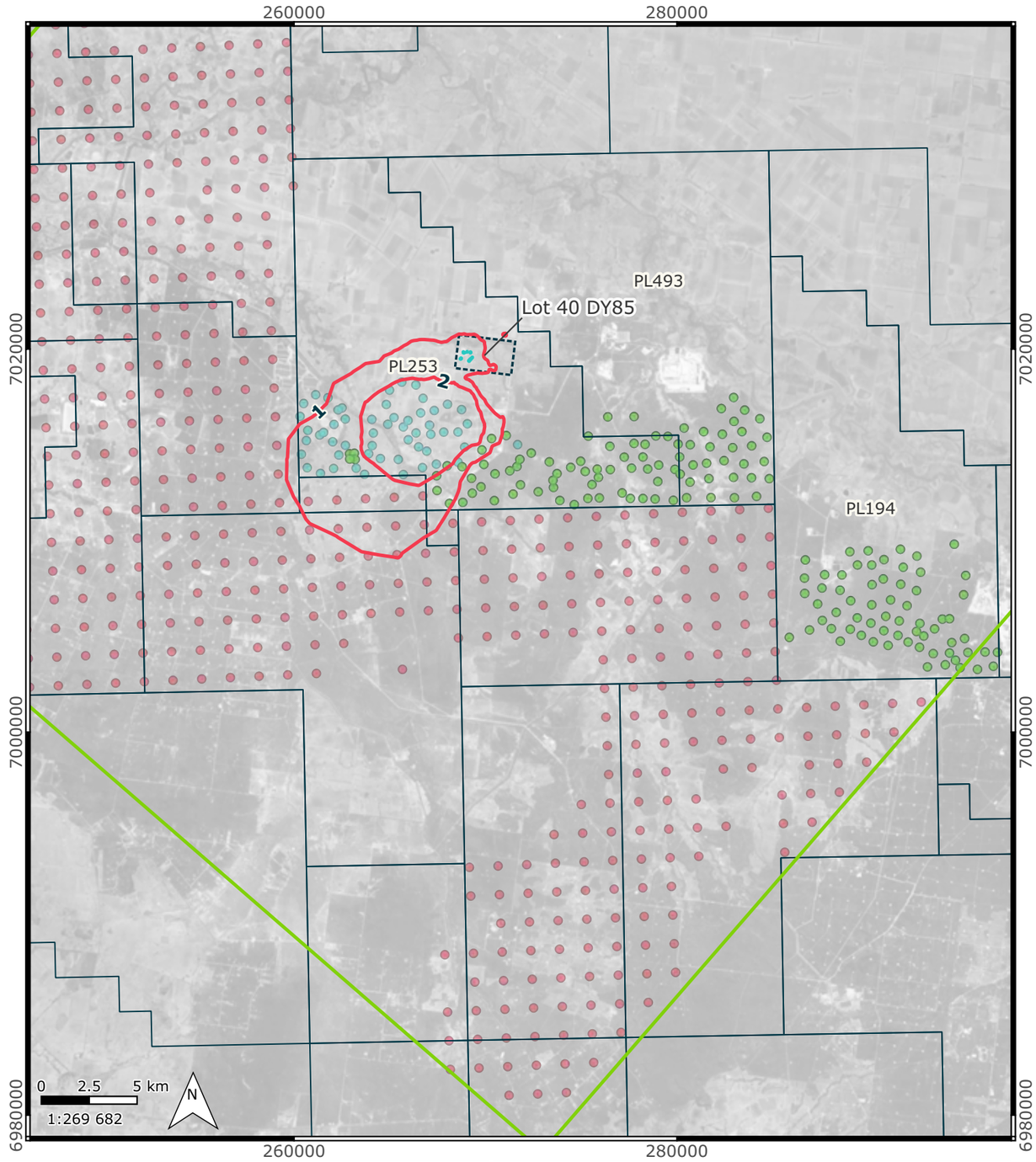

Legend

- Groundwater model extent
- Lot 40 DY85
- Gasifiers
- Petroleum Leases

Well groups

- Approved Arrow wells
- Arrow Clynes Rd wells
- Non-Arrow abstraction points (from UWIR 2021)
- Contours of groundwater level difference (m)

Predicted median difference in groundwater levels between scenario 2 and 3 in Springbok sandstone and Macalister coal seam (end of December 2061)

Project No.	Client	Figure No.
411001-00917	Arrow	5-3

Notes:
Project CRS: GDA94 / MGA zone 56
Last Saved: 10:02 20/04/2026
Filename: Figure_5-3_GW_Sc2m3

Exported by User: Mohsen.Azadi
Project Exported: 10:52 20/04/2026

References:
N/A

File Path: C:\modelling\Arrow\deliverables\Figures_REP-HG-002\Figure_5-3_GW_Sc2m3.qgz

As discussed in section 2.4.1, historical UCG activities altered local hydraulic gradients within Lot 40 DY85. One of the key QOIs assessed in this study is the incremental change in horizontal hydraulic gradients across the site under the two FDP scenarios. Intera (2025), previously assessed hydraulic gradients using the full extent of Lot 40 DY85.

In the current impact assessment, and in consideration of gasifier locations, regional flow directions, and the need to evaluate the potential for contaminant migration beyond the site boundary, the analysis focused on 1,500 m sections along the southern and western boundaries of Lot 40 DY85 (shown in Figure 5-4). Groundwater level differences were calculated between model cells along these boundary sections and corresponding cells located within a 100 m buffer inside the site boundary. The proportion of boundary cells with higher groundwater levels than interior cells was used as an indicator of groundwater flow direction from locations beyond Lot 40 DY85 toward zones within Lot 40 DY85 (in the vicinity of gasifiers). Comparison of results between scenarios 2 and 3 provides a quantitative basis for assessing the extent to which the proposed Clynes Road wells may influence these hydraulic gradients and associated flow directions.

Summary statistics of predicted horizontal hydraulic gradients toward Lot 40 DY85 along 1,500 m sections of the southern and western boundaries are presented in Table 5-2. The simulation results indicate stronger inward hydraulic gradients in the Springbok sandstone compared to the Macalister coal seam, consistent with the groundwater contour patterns discussed previously. This is considered to reflect potential vertical hydraulic connectivity (near historical UCG activities) between the Springbok sandstone and the underlying Macalister coal seam, together with a downward vertical gradient driven by CSG abstraction within the WCM.

Comparison of summary statistics between the two FDP scenarios indicates that incremental changes in hydraulic gradients across these boundary sections are negligible, with differences generally within 1%. These results suggest that it is unlikely that the proposed Clynes Road wells materially alter regional groundwater flow directions or hydraulic gradients at the boundaries of Lot 40 DY85.

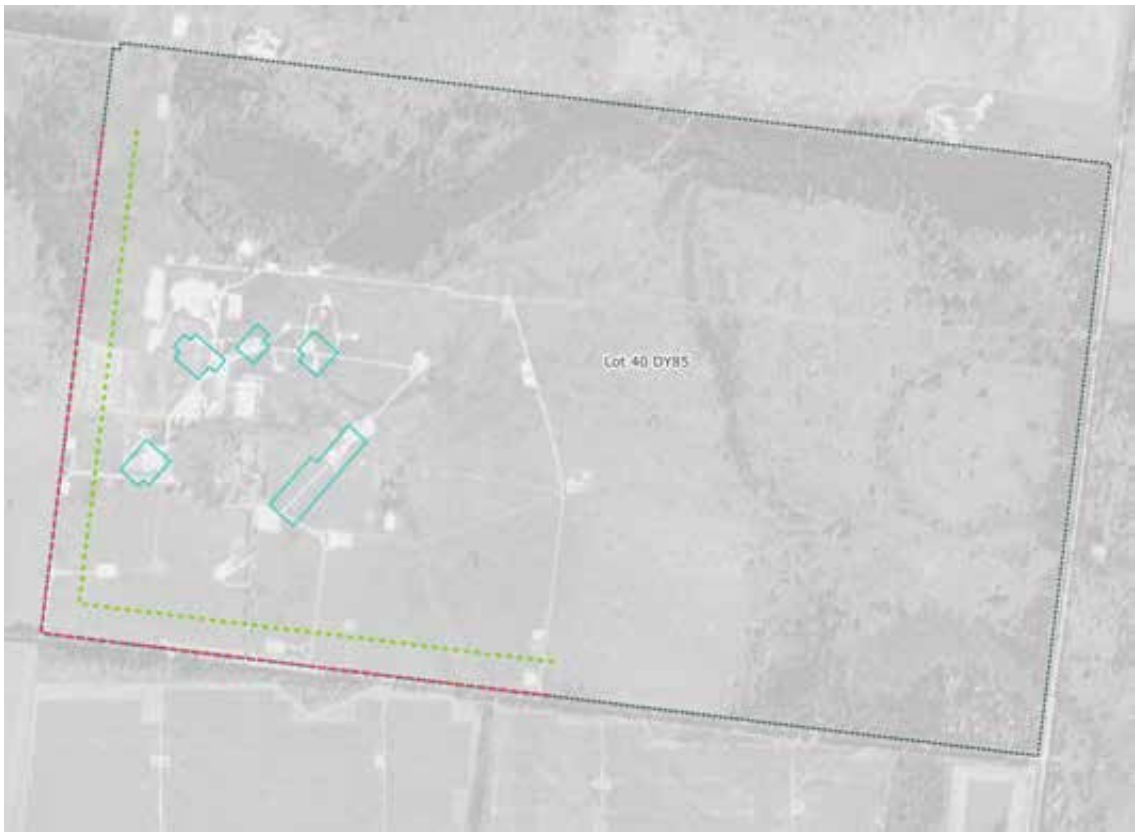

Figure 5-4 Lot 40 DY85 boundary sections (red dashed lines, 1500 m each) and 100 m buffer lines within the boundary (green dashed lines) used for calculation of horizontal hydraulic gradient

Table 5-2 Summary statistics of predicted percentage of cells along 1,500 m sections of the southern and western boundaries with horizontal hydraulic gradients toward Lot 40 DY85

Modelling scenario	Percentile	Springbok sandstone			Macalister coal		
		2025	2040	2061	2025	2040	2061
Scenario 2 (approved)	P5	45%	52%	53%	9%	6%	5%
	P50	74%	75%	78%	20%	13%	13%
	P95	92%	92%	92%	44%	23%	22%
Scenario 3 (Clynes Rd)	P5	45%	52%	52%	9%	5%	6%
	P50	74%	76%	78%	20%	13%	13%
	P95	92%	91%	92%	44%	22%	22%
Predicted impact	P5	<1%	<1%	1%	<1%	1%	-1%
	P50	<1%	-1%	1%	<1%	<1%	<1%
	P95	<1%	1%	<1%	<1%	1%	<1%

5.3 Vertical hydraulic gradient

Assessment of the vertical hydraulic gradient between the Springbok sandstone and the underlying Macalister coal seam was undertaken to confirm the direction of vertical groundwater flow under scenario 3, representing the maximum proposed development. This assessment was intended to evaluate whether vertical gradients are upward or downward under abstraction and recovery conditions. Understanding the direction of vertical flow is important for interpreting potential vertical migration pathways under a conservative development scenario.

The assessment was carried out using 10 pairs of monitoring locations where groundwater level monitoring data was available in both the Springbok sandstone and the Macalister coal seam. For each pair, the groundwater level difference between the two formations was calculated across the ensemble of model realisations. Positive and negative values indicate the direction of the vertical hydraulic gradient, to evaluate whether groundwater flow is directed downward from the Springbok sandstone to the Macalister coal seam (for positive values), or upward in the opposite direction (for negative values).

As shown in Figure 5-5, the predicted groundwater level differences under scenario 3 are positive from 2026 through to 2226, indicating a continuous downward vertical hydraulic gradient from the Springbok sandstone to the Macalister coal seam. This is consistent across all realisations and through both the abstraction and recovery periods.

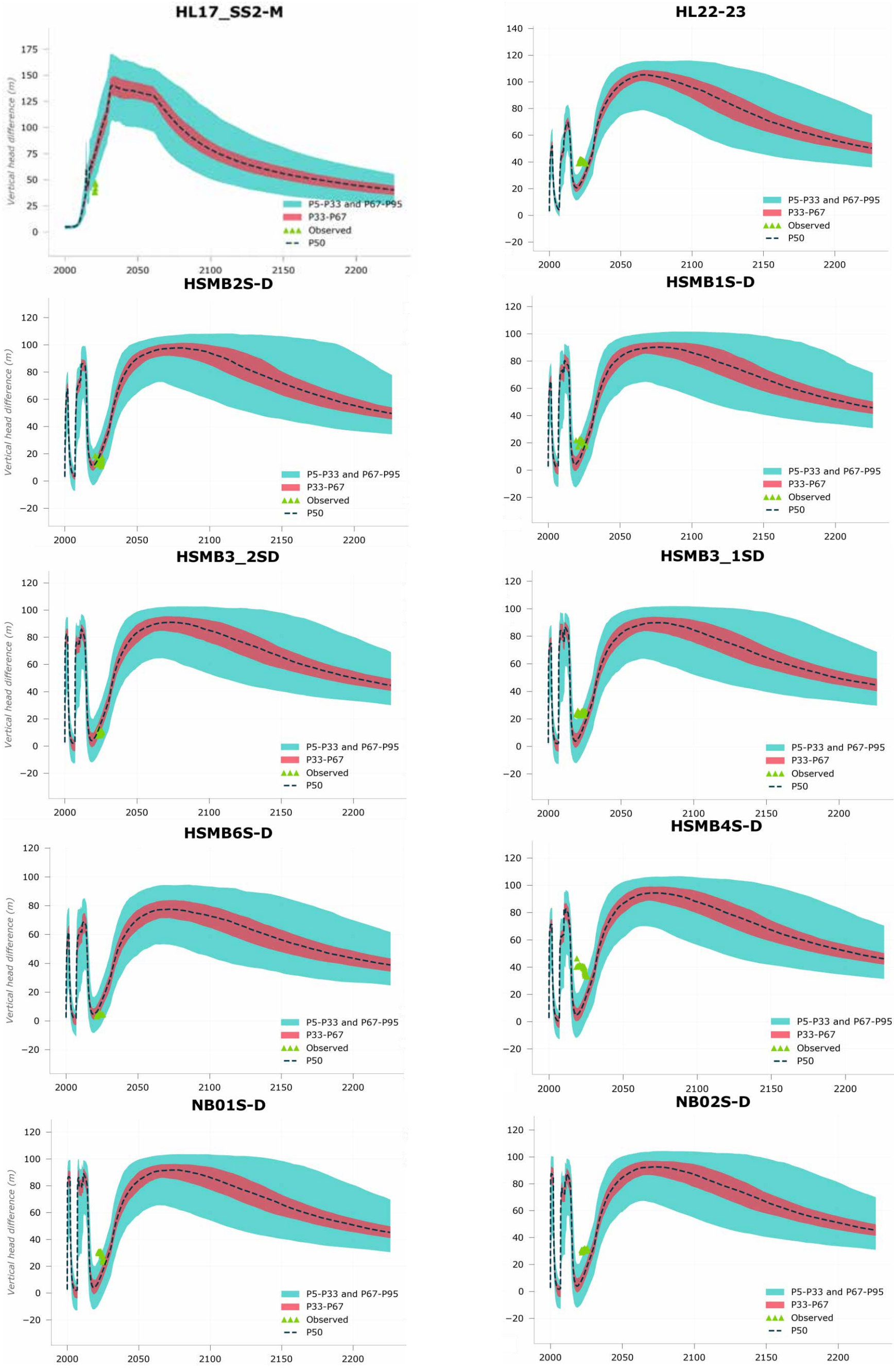

Figure 5-5 Predicted vertical hydraulic gradient between the Springbok sandstone and Macalister coal seam at paired monitoring locations

5.4 Particle tracking

Particle tracking was undertaken as a conservative approach to assess the maximum potential extent of contaminant movement under simulated groundwater flow conditions. Unlike solute transport modelling, particle tracking does not account for attenuation processes such as sorption, degradation, or dilution, and therefore represents an upper-bound estimate of advective contaminant migration. Particles were released in 2019 from the following locations:

- Monitoring bores,
- Gasifier locations, and
- Lot 40 DY85 boundaries.

Particle movement was simulated under transient conditions from January 2019 through to the end of December 2225 for both scenario 2 and scenario 3.

For scenario 3, the probability of particle pathlines intersecting each model cell within the Springbok sandstone and Macalister coal seam is presented in Figure 5-6 to Figure 5-8, for particles released from monitoring bores, gasifier locations, and the Lot 40 DY85 boundaries. These figures also show representative particle pathlines extracted from the realisation simulating the maximum particle displacement for particles released at gasifier locations within the Springbok sandstone. The results indicate that:

- Particles released in the Springbok sandstone generally travel shorter distances than those released in the Macalister coal seam, reflecting lower hydraulic conductivity, reduced transmissivity, and weaker advective flow conditions in the Springbok Sandstone compared to the more transmissive and regionally depressurised Macalister coal seam.
- Groundwater flow within the Macalister coal seam is predominantly directed toward the south-southwest, consistent with regional groundwater flow patterns, whereas flow directions within the Springbok sandstone vary at a more localised scale and are mostly directed inward toward Lot 40 DY85, reflecting the influence of historical depressurisation associated with former UCG activities.
- It is very unlikely (probability of less than 5%) that, by the end of the recovery period in 2225, particles released at or near the gasifier locations will travel beyond:
  - Lot 40 DY85 boundary within the Springbok sandstone, and
  - Approximately 1,250 m beyond the Lot 40 DY85 boundary within the Macalister coal seam.
- Most particle movement occurs during the post-abstraction recovery period (year 2062 to 2225), reflecting longer travel times associated with this phase of the simulation. Given the considerable natural attenuation of contaminants observed in groundwater monitoring data (discussed in section 2.4.2), by the year 2062 these predictions represent a conservative estimate of the likelihood and extent of contaminant movement from Lot 40 DY85.

Springbok sandstone

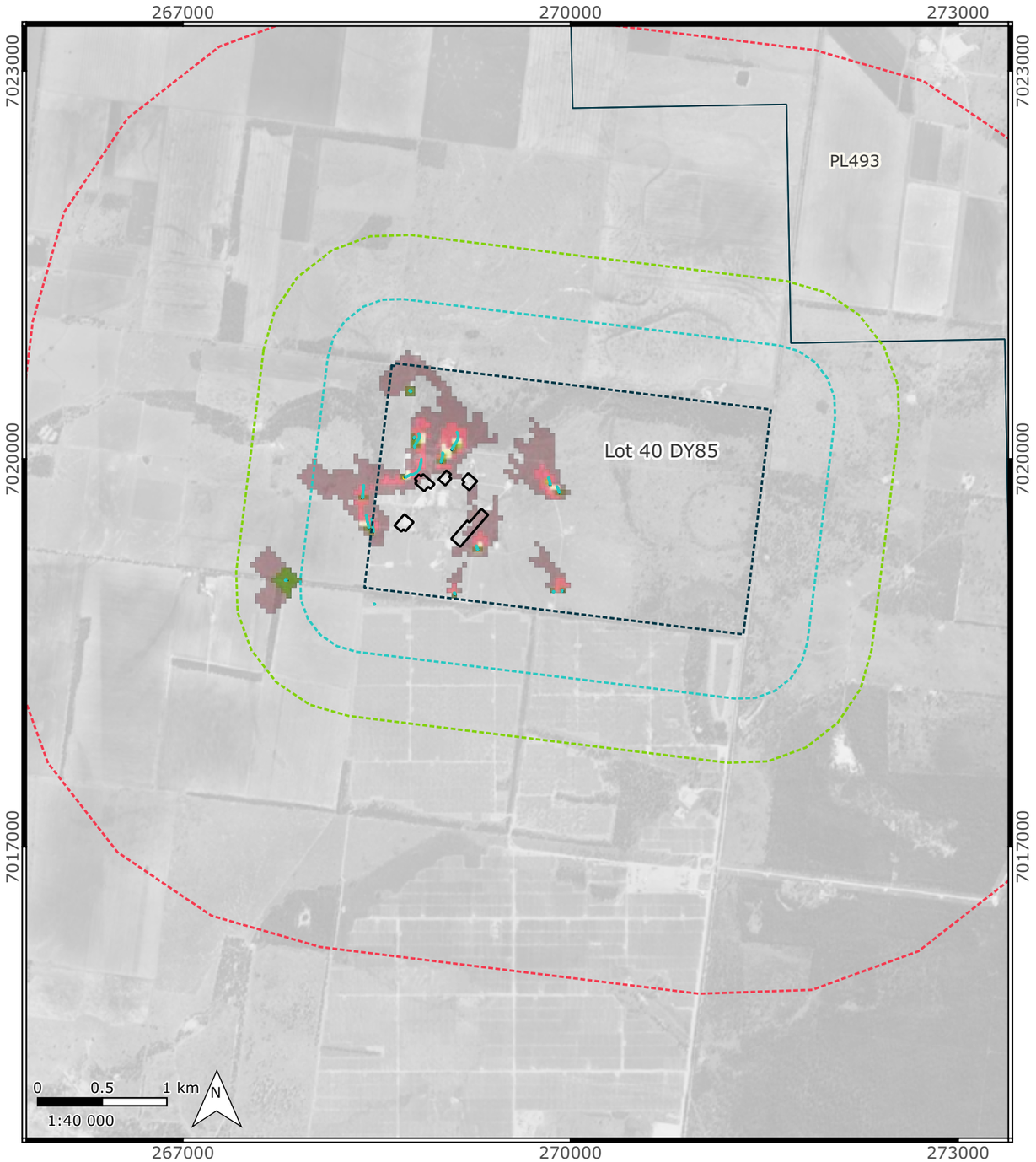

Macalister coal seam

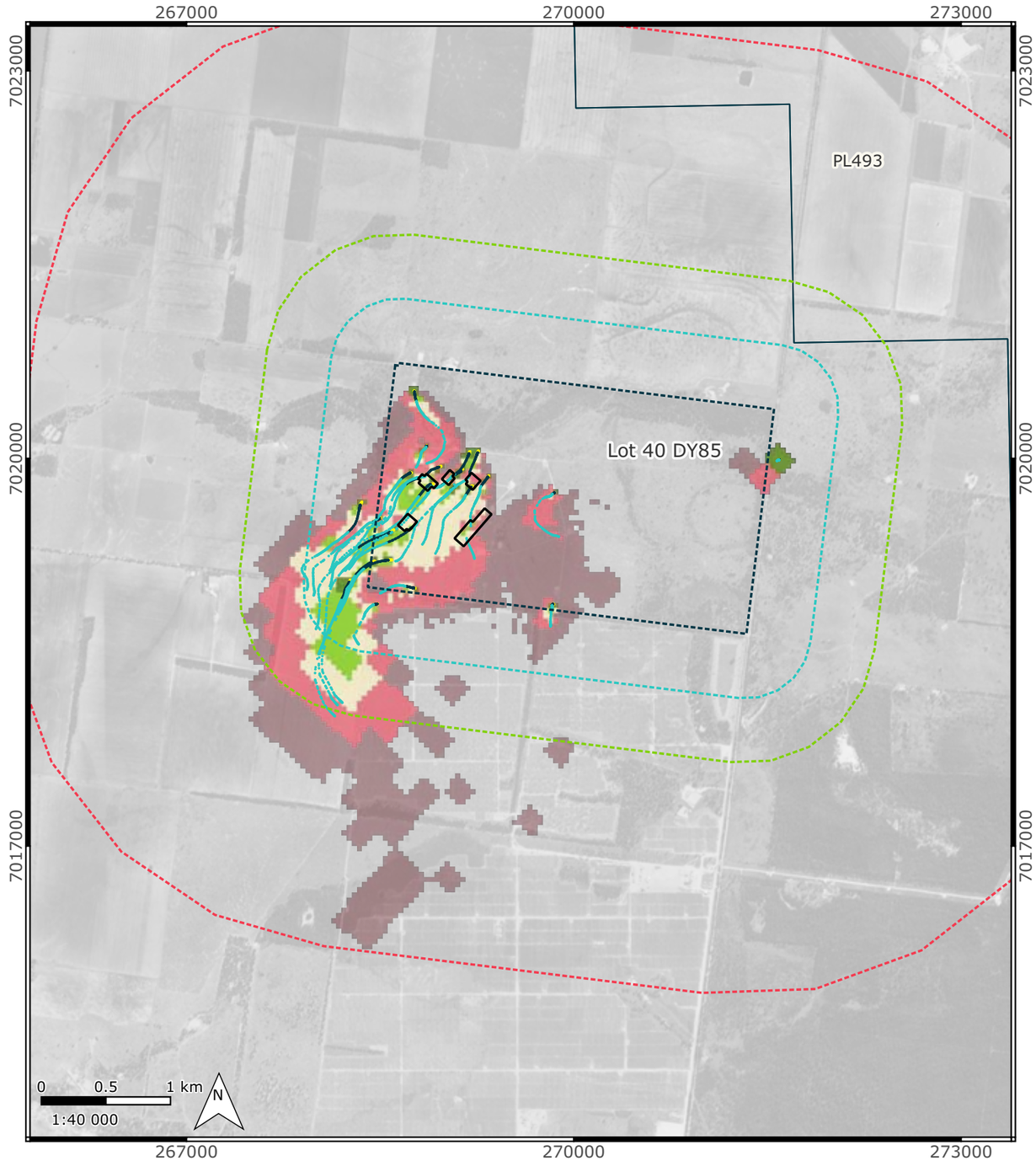

Legend

- Groundwater model extent
- Lot 40 DY85
- Gasifiers
- Petroleum Leases

Lot 40 DY85 buffer zones:
- 500 m
- 1000 m
- 2800 m

Particle travel period:
- 2019-2025
- 2026-2061
- 2062-2225

Pathline probability
- Very unlikely (<5%)
- Unlikely (5-33%)
- As likely as not (33-67%)
- Likely (67-95%)
- Very likely (>95%)

Probability of particle tracking pathlines in Springbok sandstone and Macalister coal seam for scenario 3 (particles released at monitoring bores)

Project No.	Client	Figure No.
411001-00917	Arrow	5-6

Notes:
Project CRS: GDA94 / MGA zone 56
Last Saved: 16:53 28/04/2026
Filename: Figure_5-6_PT_probability_bores

Exported by User: Mohsen.Azadi
Project Exported: 16:54 28/04/2026

References:
N/A

File Path: C:\modelling\Arrow\deliverables\Figures_REP-HG-002\Figure_5-6_PT_probability_bores.qgz

worley consulting

Springbok sandstone

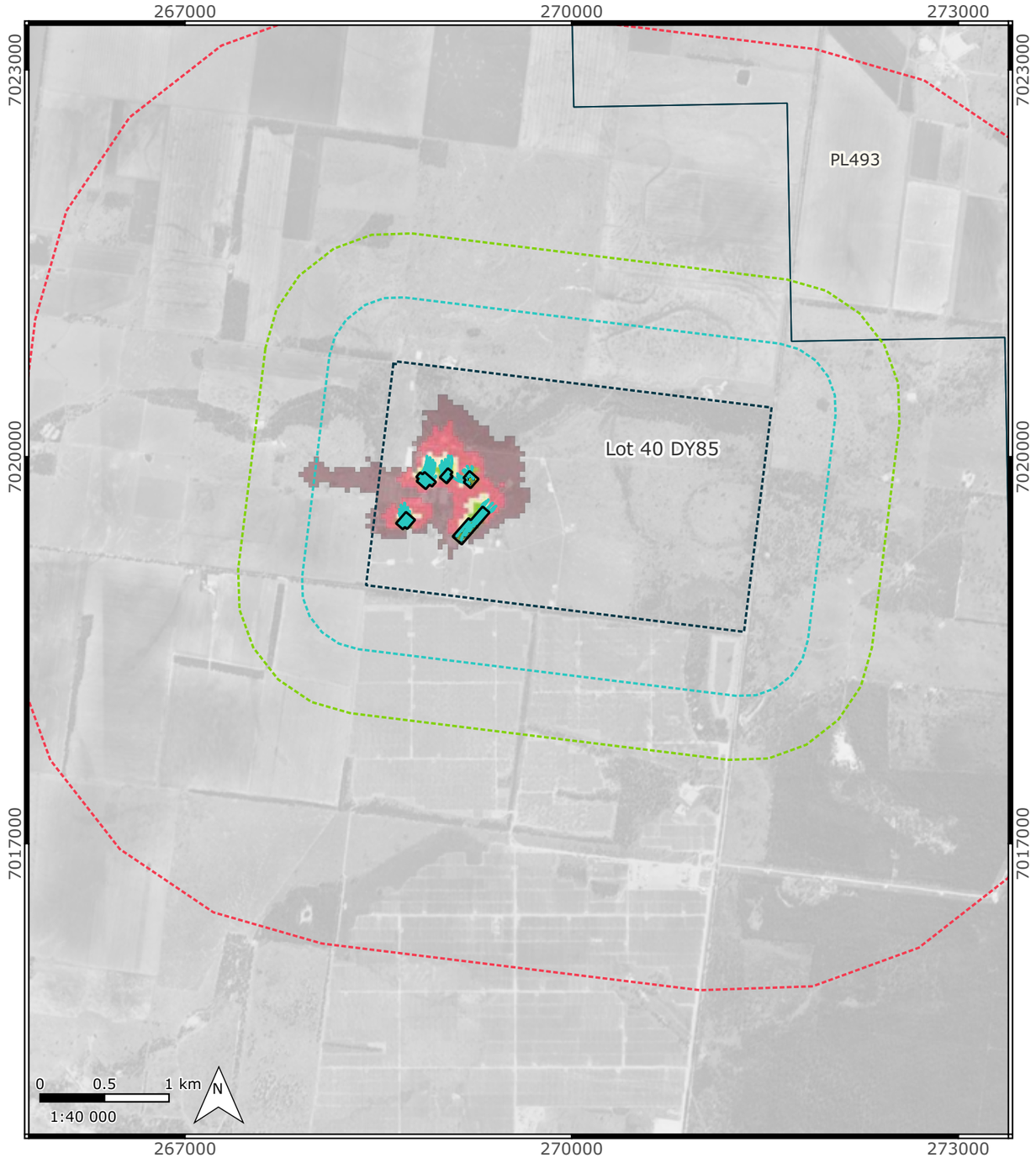

Macalister coal seam

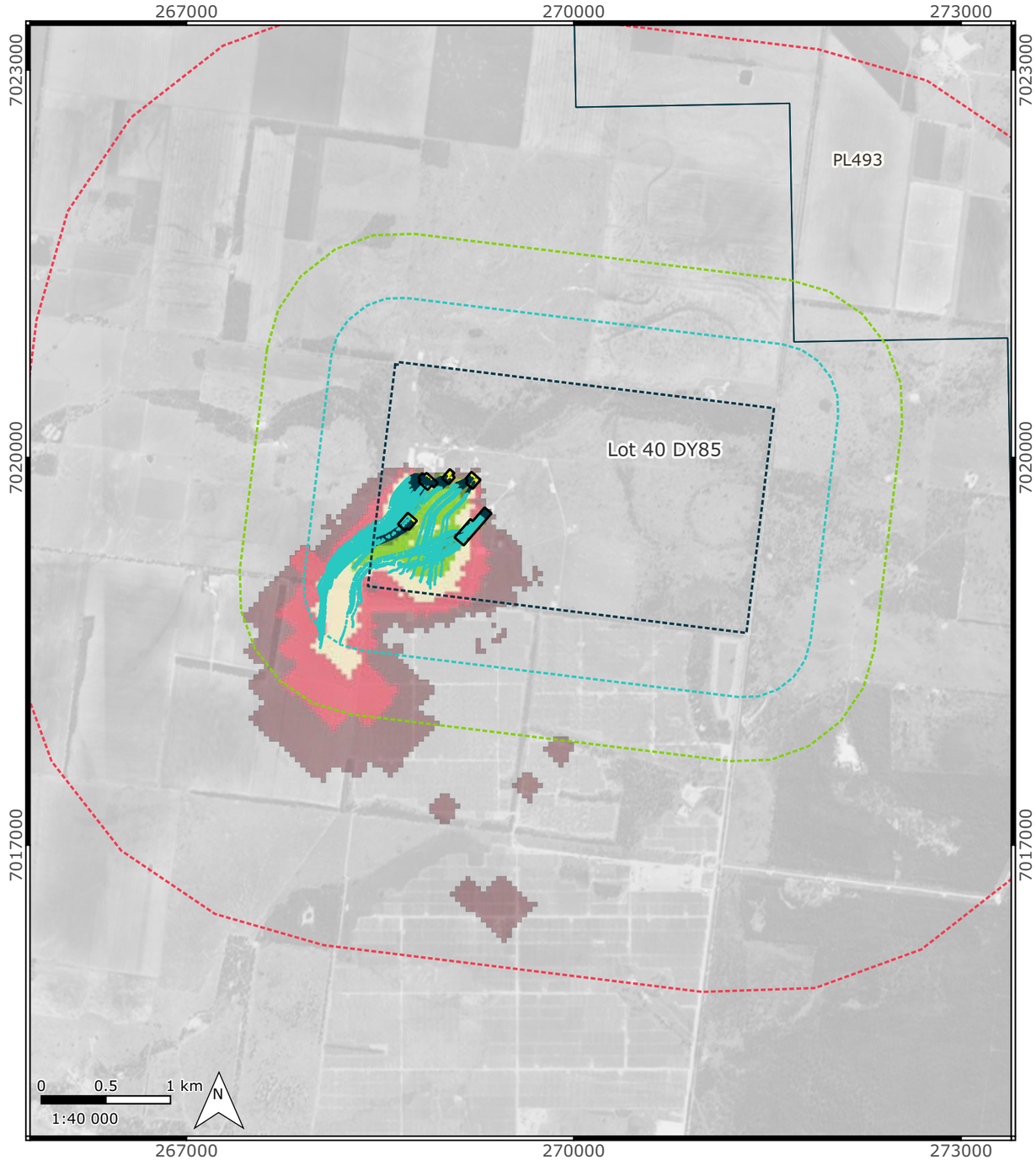

Legend

- Groundwater model extent
- Lot 40 DY85
- Gasifiers
- Petroleum Leases

Lot 40 DY85 buffer zones:

- 500 m
- 1000 m
- 2800 m

Particle travel period:

- 2019-2025
- 2026-2061
- 2062-2225

Pathline probability

- Very unlikely (<5%)
- Unlikely (5-33%)
- As likely as not (33-67%)
- Likely (67-95%)
- Very likely (>95%)

Probability of particle tracking pathlines in Springbok sandstone and Macalister coal seam for scenario 3 (particles released at gasifiers)

Project No.	Client	Figure No.
411001-00917	Arrow	5-7

Notes:
Project CRS: GDA94 / MGA zone 56
Last Saved: 16:55 28/04/2026
Filename: Figure_5-6_PT_probability_bores

Exported by User: Mohsen.Azadi
Project Exported: 17:04 28/04/2026

References:
N/A

File Path: C:\modelling\Arrow\deliverables\Figures_REP-HG-002\Figure_5-6_PT_probability_bores.qgz

Springbok sandstone

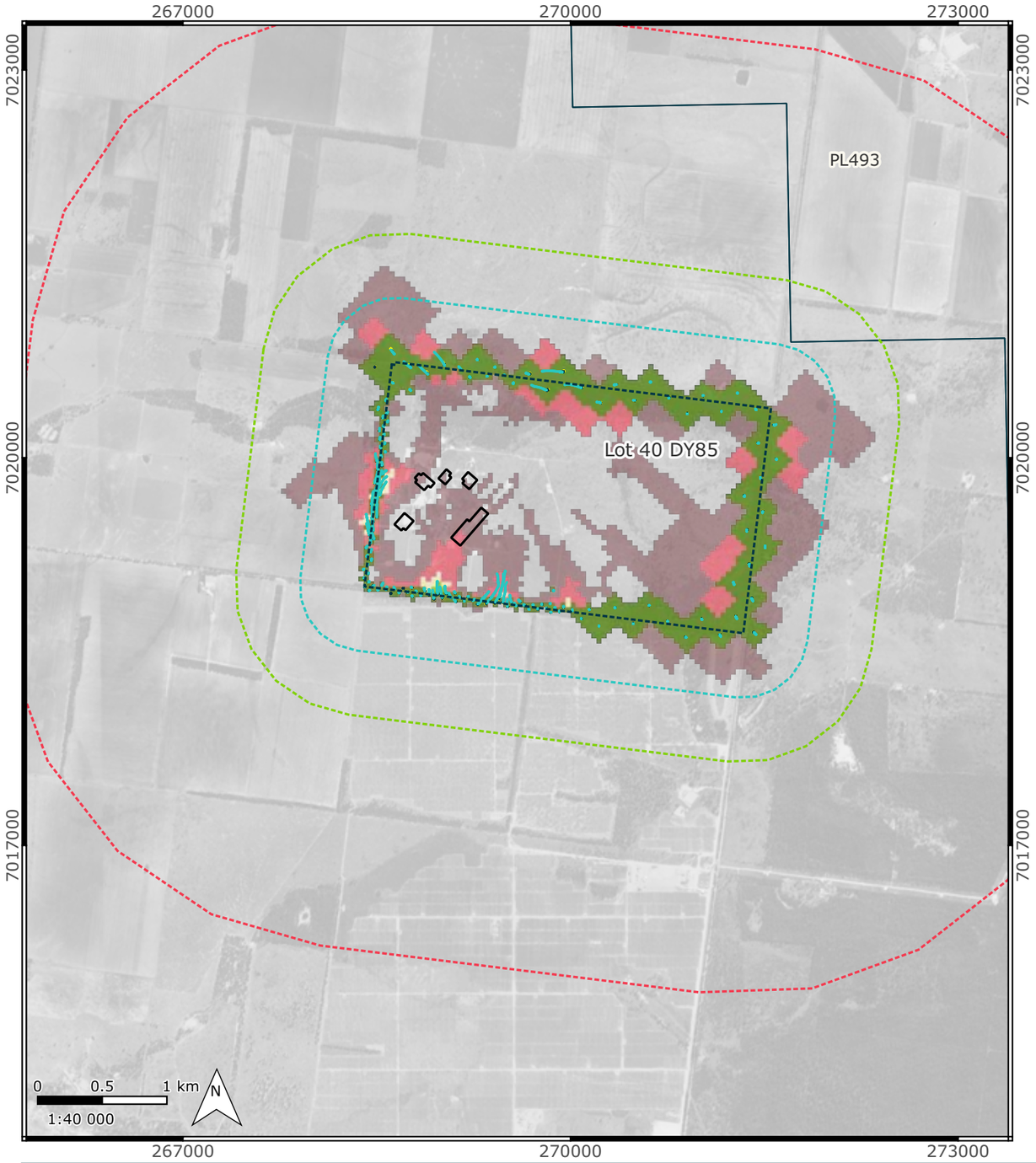

Macalister coal seam

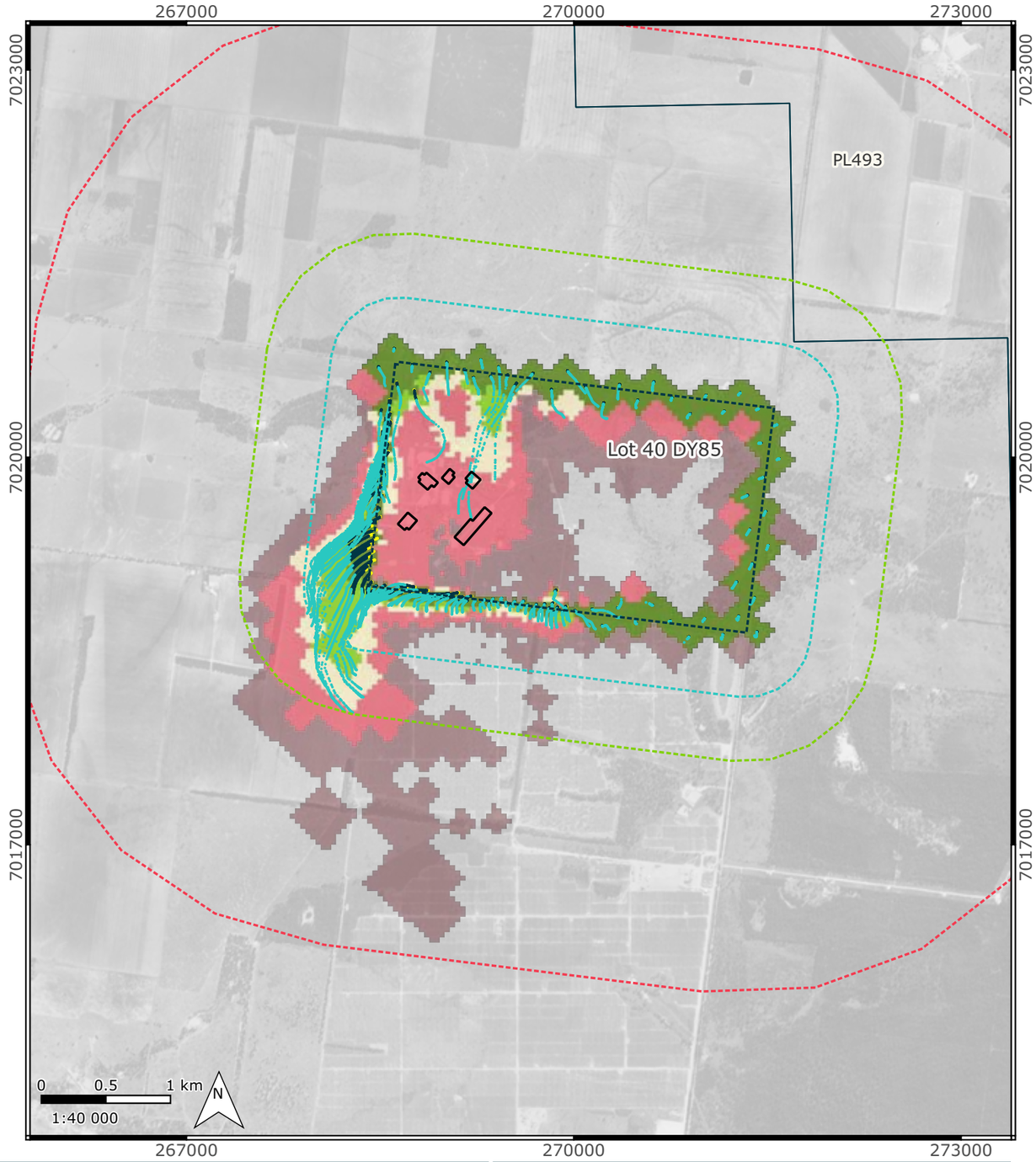

Legend

- Groundwater model extent
- Lot 40 DY85
- Gasifiers
- Petroleum Leases

Lot 40 DY85 buffer zones:
- 500 m
- 1000 m
- 2800 m

Particle travel period:
- 2019-2025
- 2026-2061
- 2062-2225

Pathline probability
- Very unlikely (<5%)
- Unlikely (5-33%)
- As likely as not (33-67%)
- Likely (67-95%)
- Very likely (>95%)

Probability of particle tracking pathlines in Springbok sandstone and Macalister coal seam for scenario 3 (particles released at Lot 40 DY85 boundaries)

Project No.	Client	Figure No.
411001-00917	Arrow	5-8

Notes:
Project CRS: GDA94 / MGA zone 56
Last Saved: 17:05 28/04/2026
Filename: Figure_5-6_PT_probability_bores

Exported by User: Mohsen.Azadi
Project Exported: 17:12 28/04/2026

References:
N/A

File Path: C:\modelling\Arrow\deliverables\Figures_REP-HG-002\Figure_5-6_PT_probability_bores.qgz

To assess the potential influence of the proposed Clynes Road wells, particle travel distances were compared across the ensemble of model realisations for scenario 2 (approved development) and scenario 3 (approved plus proposed wells). The assessment focused on differences in particle travel distances (simulated to the end of the recovery period) to evaluate whether abstraction from the proposed wells materially modifies advective transport behaviour of the residual contaminants in Lot 40 DY85. This scenario-based comparison allows the potential effect of the Clynes Road wells on maximum contaminant migration to be evaluated independently of attenuation processes, while accounting for parameter uncertainty.

Summary statistics of particle travel distances (from 2019 to 2225) for particles released within the Springbok sandstone and Macalister coal seam under scenario 2, scenario 3, and their incremental differences are presented in Table 5-3. The particle tracking predictions indicate that, by the end of the recovery period in 2225:

- Particle travel distances are consistently greater within the Macalister coal seam than within the Springbok Sandstone, as discussed previously.
- For the ensemble median results:
  - A maximum particle travel distance of approximately 139 m was predicted within the Springbok sandstone,
  - A maximum particle travel distance of approximately 1,092 m was predicted within the Macalister coal seam,
  - A maximum incremental particle travel distance increase of approximately 2 m was predicted in the Springbok sandstone associated with the proposed Clynes Road wells, and
  - A maximum incremental particle travel distance increase of approximately 55 m was predicted in the Macalister coal seam associated with the proposed Clynes Road wells.
- It is very unlikely (based on P95 percentile results) that addition of the proposed Clynes Road wells would result in an increase in particle travel distance exceeding of approximately 24 m in the Springbok sandstone and 92 m in the Macalister coal seam.

Table 5-3 Summary statistics of particle travel distances (from 2019 and 2225) for particles released within Springbok sandstone and Macalister coal seam

Modelling scenario	Layer	Particle location	P5			P50			P95		
			Min	Mean	Max	Min	Mean	Max	Min	Mean	Max
Scenario 2 (approved)	Springbok	Bores	<1	6	24	1	38	103	7	191	910
		Gasifiers	4	15	28	27	80	138	132	280	407
		Boundaries	<1	3	42	<1	18	112	7	114	676
	Macalister	Bores	7	216	526	41	625	963	125	1369	1862
		Gasifiers	99	313	500	516	718	848	1000	1531	1826
		Boundaries	2	72	302	10	288	1038	40	760	1797
Scenario 3 (Clynes Rd)	Springbok	Bores	<1	6	24	1	39	105	7	194	934
		Gasifiers	4	15	28	27	81	139	134	282	409
		Boundaries	<1	3	42	<1	18	112	7	115	682
	Macalister	Bores	8	224	523	41	652	973	126	1419	1943
		Gasifiers	132	321	504	544	749	892	1092	1606	1876
		Boundaries	3	76	336	11	304	1092	46	783	1834
Predicted impacted	Springbok	Bores	<1	<1	<1	<1	<1	2	<1	3	24
		Gasifiers	<1	<1	<1	<1	1	1	2	3	2
		Boundaries	<1	<1	1	<1	<1	1	<1	1	5
	Macalister	Bores	1	8	-3	<1	27	9	1	50	81
		Gasifiers	33	9	4	28	31	45	92	76	50
		Boundaries	<1	4	35	<1	16	55	6	22	37

5.5 Contaminant transport and fate

The contaminant transport and fate were evaluated based on long-term evolution of benzene and naphthalene concentrations under simulated groundwater flow, source depletion, and natural attenuation processes (discussed in section 3.3). Predictions are based on the ensemble of calibrated model realisations and are interpreted using percentile statistics (P5, P50, and P95) to characterise uncertainty and provide a risk-based assessment of contaminant attenuation and migration within the Springbok sandstone and Macalister coal seam. The assessment focuses on concentration trends at monitoring locations, the timing of concentration depletion below LOR, and the spatial distribution of residual concentrations.

Ensemble predictions indicate a consistent decline in benzene and naphthalene concentrations at monitoring locations across both formations, reflecting the combined effects of source dilution and natural attenuation (shown in Appendices F and G). For benzene, concentration trends show progressive reductions over time, with variability between monitoring locations diminishing as source contributions decrease. Naphthalene concentrations decline more rapidly across the ensemble, consistent with its lower source strength and stronger attenuation characteristics. Overall, the ensemble results demonstrate convergence toward declining concentrations at monitoring bores.

The year in which contaminant concentrations are predicted to decline below the LOR was evaluated across the ensemble of model realisations for both HSUs and contaminants, as summarised in in Table 5-4. Ensemble results indicate that the median (P50) predictions are as follows:

- Benzene concentrations are predicted to fall below the LOR in:
  - 2049 for the Springbok sandstone, and
  - 2035 for the Macalister coal seam.
- Naphthalene concentrations are predicted to fall below the LOR in:
  - January 2027 for the Springbok sandstone, and
  - April 2024 for the Macalister coal seam.

Upper-bound ensemble predictions (P95) further indicate that it is very unlikely that the year of depletion below the LOR will exceed the following:

- For benzene:
  - 2053 for the Springbok sandstone, and
  - 2042 for the Macalister coal seam.
- For naphthalene:
  - 2037 for the Springbok sandstone, and
  - June 2024 for the Macalister coal seam, consistent with current groundwater monitoring observations.

Comparison of predicted depletion timing between scenarios 2 and 3 indicates no change in the year at which concentrations are predicted to fall below the LOR for either contaminant or formation. This outcome indicates that inclusion of the proposed Clynes Road wells is not expected to materially influence natural attenuation or long-term depletion of benzene or naphthalene concentrations.

Based on the ensemble depletion timing, median (P50) benzene concentration distributions were examined for future years, including year 2030 in the Macalister coal seam and year 2040 in the Springbok sandstone (Figure 5-9). These years were chosen based on the median years discussed above to better understand the plume distribution before reaching below LOR. The benzene distribution in the final years before reaching below the LOR are predominantly present within or near gasifier releasing source depletion term. This also indicates that removal of the source terms will likely result in earlier timing when the contaminants concentrations reach below the LOR.

Table 5-4 Predicted year of contaminant concentration reaching below the LOR

Modelling scenario	Compound	Springbok sandstone			Macalister coal		
		P5	P50	P95	P5	P50	P95
Scenario 2 (approved)	Benzene	Jan 2049	Jan 2049	Jan 2053	Jan 2033	Jan 2035	Jan 2042
	Naphthalene	Jan 2026	Jan 2027	Jan 2037	Jan 2024	Apr 2024	Jun 2024
Scenario 3 (Clynes Rd)	Benzene	Jan 2049	Jan 2049	Jan 2053	Jan 2033	Jan 2035	Jan 2042
	Naphthalene	Jan 2026	Jan 2027	Jan 2037	Jan 2024	Apr 2024	Jun 2024

Springbok sandstone (end of 2040)

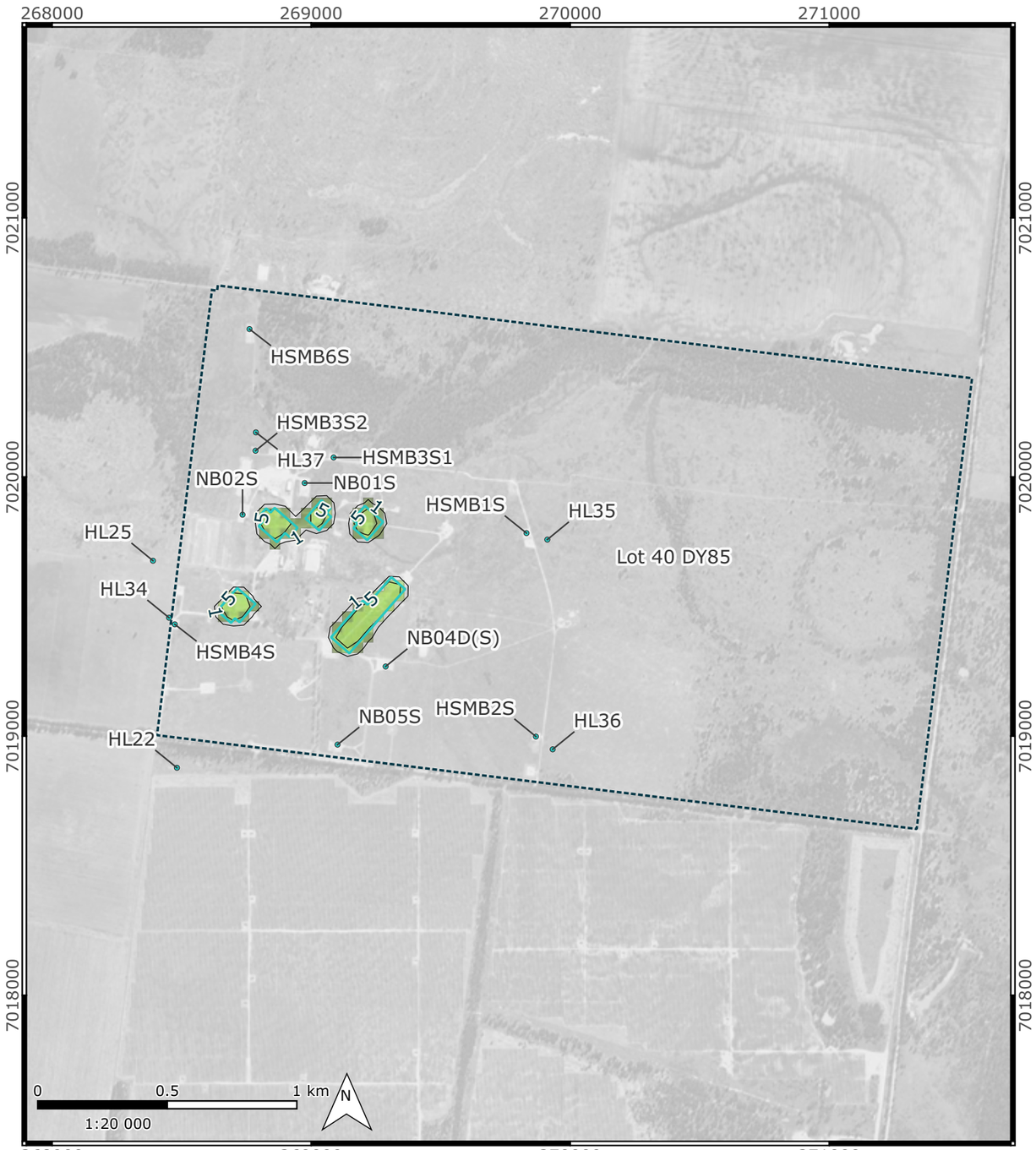

Macalister coal seam (end of 2030)

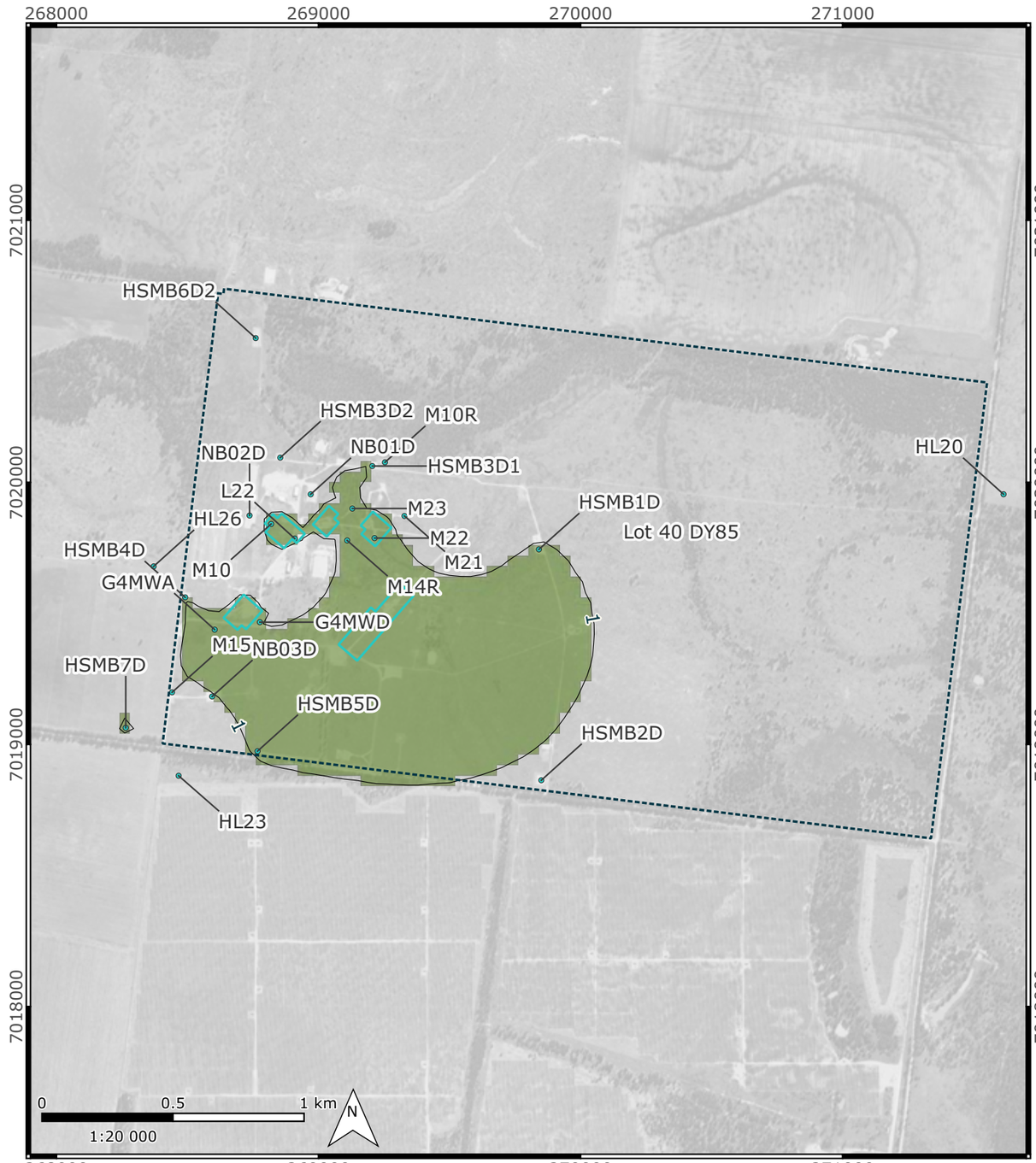

Legend

- Lot 40 DY85
- Gasifier
- Monitoring bores

Concentration (ug/L)

- 1 - 5
- 5 - 10
- 10 - 50
- 50 - 100
- 100 - 500
- 500 - 1000
- 1000 - 5000

Predicted median benzene concentrations in the Springbok sandstone (end of December 2040) and Macalister coal seam (end of December 2030)

Project No.	Client	Figure No.
411001-00917	Arrow	5-9

Notes:
Project CRS: GDA94 / MGA zone 56
Last Saved: 17:36 21/04/2026
Filename: Figure_5-9_benzene_pred

Exported by User: Mohsen.Azadi
Project Exported: 17:48 21/04/2026

References:
N/A

File Path: C:\modelling\Arrow\deliverables\Figures_REP-HG-002\Figure_5-9_benzene_pred.qgz

5.6 Impact assessment

This impact assessment evaluates the incremental effects of the proposed Clynes Road wells (scenario 3) relative to the currently approved FDP (scenario 2) on groundwater flow, hydraulic gradients, contaminant transport and fate within the Springbok sandstone and Macalister coal seam. The assessment is based on the predictive ensemble modelling results presented in sections 5.2 to 5.5, using uncertainty analysis results (for P5, P50, and P95 percentiles) to provide a conservative, risk-based assessment.

Groundwater levels and flow directions

Predictive groundwater level simulations indicate that cumulative abstraction under both scenarios results in drawdown centered on abstraction areas, with groundwater flow directed predominantly toward the south to southwest at the regional scale. At the end of 2025, groundwater flow shows inward gradients toward Lot 40 DY85 in the Springbok sandstone, while flow in the Macalister coal seam converges toward the gasifiers and continues toward the southwest of the site.

Comparison of median groundwater levels between scenarios 2 and 3 demonstrates that the incremental drawdown attributable to the proposed Clynes Road wells is small and spatially limited. At the end of the abstraction period (2061), predicted median differences are generally less than 1 m, with a localised zone of approximately 1–2 m difference in the Macalister coal seam near the proposed wells. By the end of the recovery period (2225), differences in median groundwater levels between scenarios are less than 1 m across both formations, indicating that inclusion of the Clynes Road wells is not expected to result in a material change to long-term groundwater level recovery relative to the approved development.

Assessment of horizontal hydraulic gradients across 1,500 m sections of the southern and western boundaries of Lot 40 DY85 shows stronger inward gradients in the Springbok sandstone compared to partially-inward gradients in the Macalister coal seam. Comparison between scenarios indicates that incremental changes in these gradients are negligible, with differences generally within ±1% across all percentiles. These results demonstrate that it is unlikely that the proposed Clynes Road wells will materially alter regional or site-scale groundwater flow directions relevant to contaminant migration beyond Lot 40 DY85.

Vertical hydraulic gradient

Evaluation of vertical hydraulic gradients between the Springbok sandstone and the Macalister coal seam was undertaken under scenario 3 to confirm the direction of vertical groundwater flow under the maximum proposed development. Analysis of groundwater level differences at 10 pairs of monitoring locations indicates continuous positive head differences from 2026 through to 2225, corresponding to a constant downward vertical gradient from the Springbok sandstone into the Macalister coal seam.

This outcome is consistent across the ensemble and throughout both abstraction and recovery phases, indicating that vertical groundwater flow remains directed downward under scenario 3. These results predict that the proposed Clynes Road wells do not cause upward vertical flow from the Macalister coal seam into the overlying Springbok sandstone, supporting a very low likelihood of upward contaminant migration under the maximum development scenario.

Particle tracking – conservative assessment of contaminants

Particle tracking was undertaken as a conservative assessment of maximum potential contaminant movement, independent of attenuation processes such as sorption, degradation, and dilution. Comparison of ensemble particle travel distances between scenarios 2 and 3 provides a measure of the incremental impact of the proposed Clynes Road wells on potential migration pathways.

Results indicate that particle travel distances are consistently greater in the Macalister coal seam than in the Springbok sandstone, reflecting higher formation transmissivity and CSG abstraction within WCM. For ensemble median (P50) results, maximum particle travel distances of approximately 139 m were predicted in the Springbok sandstone and approximately 1,092 m in the Macalister coal seam. The incremental impact associated with the proposed Clynes Road wells is small, with maximum increases in median particle travel distance of approximately 2 m in the Springbok sandstone and approximately 55 m in the Macalister coal seam.

Upper-bound (P95) results further indicate that it is very unlikely that inclusion of the proposed Clynes Road wells would result in an increase in particle travel distance exceeding of approximately 24 m in the Springbok sandstone or approximately 92 m in the Macalister coal seam. These incremental changes are small relative to overall travel distances (between 2019 and 2225) and do not materially change particle migration pathways beyond those predicted under the approved scenario.

Contaminant transport and fate

Contaminant transport modelling indicates continued long-term decline in benzene and naphthalene concentrations across both formations due to dilution and natural attenuation. Ensemble results show consistent depletion trends at monitoring locations, with naphthalene attenuating more rapidly than benzene and reaching below the laboratory limit of reporting (LOR) earlier across all percentiles.

Predicted depletion timing indicates that, at the ensemble median (P50), benzene concentrations fall below the LOR by approximately 2049 in the Springbok sandstone and approximately 2035 in the Macalister coal seam, while naphthalene concentrations fall below the LOR by approximately January 2027 and April 2024, respectively. Upper-bound (P95) predictions indicate that it is very unlikely for benzene depletion to extend beyond approximately 2053 for Springbok sandstone or 2042 for Macalister coal seam, and for naphthalene beyond approximately 2037 and mid-2024, respectively.

Comparison of depletion timing between scenarios 2 and 3 indicates no change in predicted years at which concentrations fall below the LOR for either contaminant or formation. This outcome indicates that inclusion of the proposed Clynes Road wells is not expected to materially influence natural attenuation or long-term depletion of benzene or naphthalene concentrations.

Overall impact assessment

Collectively, results from groundwater level predictions, hydraulic gradient assessments, particle tracking, and contaminant transport modelling demonstrate that the proposed Clynes

Road wells (scenario 3) result in minor localised incremental changes relative to the approved development (scenario 2). No material changes are predicted in groundwater flow directions, vertical gradients, contaminant migration, or contaminant depletion timing. The assessment indicates that the proposed development is unlikely to increase the risk of off-site contaminant migration or compromise long-term groundwater recovery and containment of residual contamination associated with the former Hopeland UCG site.

6. Conclusions and recommendations

This groundwater impact assessment presents the results of an updated numerical groundwater flow and contaminant transport modelling study undertaken to support Arrow Energy's proposed Field Development Plan (FDP) for Clynes Road (scenario 3) within PL253. The study builds on a sequence of previous investigations and modelling studies (AGE, 2021; AGE, 2023; Intera, 2024; Intera, 2025), incorporating updated monitoring data, revised conceptual model and hydrostratigraphic interpretation, and improved representation of boundary conditions and modelling assumptions The modelling has been undertaken in accordance with Environmental Authority EA0001401, OGIA (2021a) regional groundwater modelling approach, Australian Groundwater Modelling Guidelines (Barnett et al., 2012), and using the risk-based terminology outlined in Peeters & Middlemis (2023) with a focus on groundwater flow behaviour, contaminant migration, uncertainty analysis, and long term recovery associated with the former Hopeland UCG site on Lot 40 DY85.

Hydrogeological conceptualisation of the PL253 area and the former Hopeland UCG site was updated building upon, and refining, the conceptual understanding established in earlier studies (including AGE and Intera investigations). The updated conceptualisation incorporates the latest groundwater level and groundwater quality monitoring data, revised hydrostratigraphic interpretation, and updated regional groundwater incorporation to better represent current groundwater conditions. The Springbok sandstone and the Walloon Coal Measures (WCM), particularly the Macalister coal seam, remain the key hydrostratigraphic units governing groundwater flow and contaminant behaviour, with monitoring data confirming persistent downward vertical hydraulic gradients from the Springbok sandstone toward the WCM. Updated groundwater level and quality datasets indicate that residual effects of historical UCG activities remain localised within Lot 40 DY85, with declining benzene and naphthalene concentrations. Regionally, groundwater flow is expected to be directed predominantly toward the south to southwest, consistent with OGIA (2021) conceptualisation, while local scale variability reflects historical UCG depressurisation and formation heterogeneity near gasifier locations.

The groundwater flow and contaminant transport model, consistent with recent studies (Intera, 2024 and 2025), were developed in MODFLOW 6 to better replicate the groundwater flow regime and contaminant transport processes, while targeted refinements were introduced to improve representation of hydrostratigraphic units, boundary conditions, and historical UCG related activities. Key improvements include alignment of General Head Boundary (GHB) and drain boundary conditions with OGIA (2021) regional model datasets for non-Arrow CSG extraction, updated boundary condition for simulation of Arrow CSG extraction, adjusted simulation of Hopeland pilot wells using the Multi Aquifer Well package, and incorporation of time varying hydraulic properties to represent UCG related fracturing and material alteration. For contaminant transport, the model implements data driven source depletion terms, dual domain porosity, mechanical dispersion, molecular diffusion, sorption, and degradation processes using MODFLOW 6 transport packages and aligned with the conceptual understanding of concentration distributions.

The updated groundwater flow and contaminant transport models achieved a good history matching fit with the observed groundwater levels and contaminant concentrations. A total of

364 model realisations satisfied convergence and history matching performance criteria, with scaled root mean square errors less than 10% consistent with Australian Groundwater Modelling Guidelines threshold. History matching successfully reproduced observed temporal trends, spatial groundwater level patterns, vertical hydraulic gradients, and benzene and naphthalene concentration behaviour in both the Springbok sandstone and the Macalister coal seam. History matching also reasonably replicated the current groundwater flow regimes and contaminant transport processes aligned with the conceptual understanding of the study area utilised as history matching targets.

Predictive modelling indicates that inclusion of the proposed Clynes Road wells results in minor and localised incremental impacts relative to the approved development (scenario 2). Differences in predicted median groundwater levels between scenarios 2 and 3 are generally less than 1 m at the end of abstraction and recovery, with localised differences (of approximately 1–2 m) confined to areas near the proposed wells in the Macalister coal seam. Horizontal hydraulic gradient assessments along the southern and western boundaries of Lot 40 DY85 show incremental changes generally within ±1%, indicating no material alteration to Lot 40 DY85 flow directions relevant to contaminant migration beyond the site boundary.

Predictive modelling indicates that inclusion of the proposed Clynes Road wells results in minor and localised incremental impacts relative to the approved development (scenario 2). Differences in predicted median groundwater levels between scenarios 2 and 3 are generally less than 1 m at the end of abstraction and recovery, with localised differences of up to approximately 1-2 m confined to areas near the proposed wells in the Macalister coal seam. Assessment of horizontal hydraulic gradients along the southern and western boundaries of Lot 40 DY85 indicates incremental changes generally within ±1%, demonstrating no material alteration to site-scale flow directions relevant to contaminant migration beyond the site boundary. In addition, predictive results indicate that a downward vertical hydraulic gradient from the Springbok sandstone to the Macalister coal seam is maintained throughout both the abstraction and recovery periods.

Particle tracking and contaminant transport simulations further demonstrate that the proposed Clynes Road wells is unlikely to materially alter contaminant transport pathways, travel distances or contaminant depletion timing. Incremental increases in particle travel distance are small relative to total travel distances and remain spatially limited for the simulation period between 2019 and 2225. Ensemble contaminant transport predictions indicate continued decline in benzene and naphthalene concentrations across both formations, with no change in the predicted year of depletion below the laboratory limit of reporting between scenarios 2 and 3. Residual concentrations predicted during the abstraction period remain confined to areas proximal to former gasifier locations, consistent with the observed monitoring data.

While the current modelling reasonably replicates the magnitude and trends in the observed groundwater level and contaminants' concentrations, continued model update is recommended to further reduce prediction uncertainty over time. Ongoing groundwater level and groundwater quality monitoring should be maintained within the Springbok sandstone and Macalister coal seam, with particular focus on groundwater flow directions, vertical gradients, and any areas of persistent elevated concentrations near former gasifier locations or beyond Lot 40 DY 85. Periodic review and incorporation of new monitoring data into the numerical model would allow reassessment of predictions and confirmation of long-term trends.

It is also recommended that future updates to the groundwater model consider refinement of source representation as additional data becomes available regarding the persistence or removal of residual contamination zones. Should any site-scale alterations occur to the current declining trends across monitoring bores within and around Lot 40 DY85, updated groundwater flow and contaminant transport modelling is recommended to be undertaken to reassess contaminant movement and depletion timing. Continued alignment with OGIA regional model updates is recommended to ensure future modelling remains consistent with updated basin-scale conceptualisation and regional flow directions.

7. References

AGE, (2021). Production Licensing Modelling Support prepared for Arrow Energy by Australasian Groundwater and Environmental Consultants Pty Ltd. June 2021.

AGE, (2023). PL 253 Environmental Approval Amendment Support – Contaminant transport validation – Addendum to AGE (2022) by Australasian Groundwater and Environmental Consultants Pty Ltd. 19th January 2023.

Ahangar, A.G. (2010). Sorption of PAHs in the soil environment with emphasis on the role of soil organic matter: A review. World Applied Sciences Journal, 11(7), 759–765.

Aguilera, R. (2004). A triple porosity model for petrophysical analysis of naturally fractured reservoirs. Petrophysics (SPWLA Journal), 45(2).

Anderson, R.T., Rooney-Varga, J.N., Gaw, C.V. & Lovley, D.R. (1998). Anaerobic benzene oxidation in the Fe(III) reduction zone of petroleum-contaminated aquifers. Environmental Science & Technology, 32(9), 1222–1229.

American Petroleum Institute (API). (1998). Delineation and characterization of the Borden MTBE plume: An evaluation of eight years of natural attenuation processes. Health and Environmental Sciences Department, Publication No. 4668.

Agency for Toxic Substances and Disease Registry (ATSDR). (2024). Toxicological profile for benzene (Draft for public comment). Atlanta, GA: U.S. Department of Health and Human Services, Public Health Service.

Barnett, B., Townley, L., Post, V., Evans, R., Hunt, R., Peeters, L., Richardson, S., Werner, A., Knapton, A., & Boronkay, A. (2012). Australian groundwater modelling guidelines. National Water Commission.

Bayard, R., Barna, L., Mahjoub, B., and Gourdon, R., (2020). Influence of the presence of PAHs and coal tar on naphthalene sorption in soils. Journal of Contaminant Hydrology, Volume 46, Issues 1–2, pp. 61-80. https://doi.org/10.1016/S0169-7722(00)00125-X.

Bjerg, P.L., Rügge, K., Cortsen, J., Nielsen, P.H. & Christensen, T.H. (1999). Degradation of aromatic and chlorinated aliphatic hydrocarbons in the anaerobic part of the Grindsted landfill leachate plume: In situ microcosm and laboratory batch experiments. Ground Water, 37, 113–121.

Bjerg, P.L., Bøllingtoft, A. & Mosthaf, K. (2025). Lecture Note: Dispersion in Aquifers. DTU Sustain.

Doherty, J., (2024). Tutorial: Ensemble Space Inversion. GMDSI. https://gmdsi.org/blog/ensemble-space-inversion/.

Dong, S., Dai, Z., Li, J. & Zhou, W. (2018). The scale dependence of dispersivity in multi-facies heterogeneous formations. Carbonates and Evaporites, 33, 161–165.

ECETOC (European Centre for Ecotoxicology and Toxicology of Chemicals). (2013). Environmental Exposure Assessment of Ionisable Organic Compounds. Technical Report No. 123, Brussels: ECETOC.

Epic, (2020). Former Underground Coal Gasification Plant, Hopeland - Updated Conceptual Site Model. 17 December 2020.

Gelhar, L.W., Welty, C. & Rehfeldt, K.R. (1992). A critical review of data on field-scale dispersion in aquifers. Water Resources Research, 28(7), 1955–1974.

GHD, (2019). Arrow Hopeland Groundwater Study Groundwater Modelling Report – PL253.

Grathwohl, P., Eberhardt, C., Klenk, I., Rügner, H. & Maier, U. (2000). Transverse vertical dispersivity in aquifer materials: Implications on mass transfer across the capillary fringe and the length of steady state plumes. In: Bjerg, P.L. (ed.), Groundwater 2000: Proceedings of the International Conference on Groundwater Research, Copenhagen, Denmark, 6–8 June 2000. Rotterdam: A.A. Balkema.

Gustafson, K.E. & Dickhut, R.M. (1994). Molecular diffusivity of polycyclic aromatic hydrocarbons in air. Journal of Chemical & Engineering Data, 39(2), 286–289.

Intera (2024). PL253 –Site Conceptual Model, and Groundwater Flow, Contaminant Transport and Predictive Modelling.

Intera (2025). PL253 Groundwater Flow and Contaminant Transport Modelling Report. Prepared for Arrow Energy Pty Ltd.

King, G.R., Ertekin, T. & Schwerer, F.C. (1986). Numerical simulation of the transient behavior of coal-seam degasification wells. SPE Formation Evaluation, 1(2), 165–183.

Langevin, C.D., Provost, A.M., Panday, S. & Hughes, J.D. (2022). Documentation for the MODFLOW 6 Groundwater Transport Model. U.S. Geological Survey, Techniques and Methods, Book 6, Chap. A61.

Musat, F., Galushko, A., Jacob, J., Widdel, F., Kube, M., Reinhardt, R., Wilkes, H., Schink, B. & Rabus, R. (2009). Anaerobic degradation of naphthalene and 2-methylnaphthalene by strains of marine sulfate-reducing bacteria. Environmental Microbiology, 11(1), 209–219.

Newell, C.J., Rifai, H.S., Wilson, J.T., Connor, J.A., Aziz, J.A. & Suarez, M.P. (2002). Calculation and use of first-order rate constants for monitored natural attenuation studies. U.S. Environmental Protection Agency, Ground Water Issue.

Odermatt, J.R., (1994). Natural chromatographic separation of benzene, toluene, ethylbenzene and xylenes (BTEX compounds) in a gasoline contaminated ground water aquifer. Organic Chemistry v. 21, 10-11; p 1141-1150.

OGIA, (2021a). Modelling of Cumulative Groundwater Impacts in the Surat CMA: Approach and Methods. Version 1.0.

OGIA, (2021b). Regional Flow Systems and Potentiometry in Queensland's Surat and Southern Bowen Basins. Version 1.0.

Osagie, E.I. & Owabor, C.N. (2015a). Adsorption of benzene in batch system in natural clay and sandy soil. Advances in Chemical Engineering and Science, 5, 352–361.

Osagie, E.I. & Owabor, C.N. (2015b). Adsorption of naphthalene on clay and sandy soil from aqueous solution. Advances in Chemical Engineering and Science, 5, 345–351.

Peeters, L.J.M. and Middlemis, H. (2023). Information Guidelines Explanatory Note: Uncertainty analysis for groundwater modelling. Independent Expert Scientific Committee on Coal Seam Gas and Large Coal Mining Development, Commonwealth of Australia.

Prommer, H., Davis G.B., Barry D.A., Miller C.T., (2003). Modelling the Fate of Petroleum Hydrocarbons in Groundwater. Proceedings of the Fifth National Workshop on the Assessment of Site Contamination.

Pruess, K. & Narasimhan, T.N. (1985). A practical method for modeling fluid and heat flow in fractured porous media. Society of Petroleum Engineers Journal, 25(1), 14–26.

Schulze-Makuch, D. (2005). Longitudinal dispersivity data and implications for scaling behavior. Ground Water, 43(3), 443–456.

Shi, B., Ngueleu, S.K., Rezanezhad, F., Slowinski, S., Pronk, G.J., Smeaton, C.M., Stevenson, K., Al-Raoush, R.I. & Van Cappellen, P. (2020). Sorption and desorption of the model aromatic hydrocarbons naphthalene and benzene: Effects of temperature and soil composition. Frontiers in Environmental Chemistry, 1, 581103.

Ukalska-Jaruga, A. & Smreczak, B. (2020). The impact of organic matter on polycyclic aromatic hydrocarbon (PAH) availability and persistence in soils. Molecules, 25(11), 2470.

U.S. Environmental Protection Agency (U.S. EPA). (1996). A citizen's guide to natural attenuation. EPA 542-F-96-015, Office of Solid Waste and Emergency Response.

U.S. Environmental Protection Agency (US EPA). (1999). Monitored natural attenuation of petroleum hydrocarbons. EPA 600/F-98/021.

Warren, J.E. & Root, P.J. (1963). The behavior of naturally fractured reservoirs. Society of Petroleum Engineers Journal, 3(3), 245–255.

White, J.T., (2018). A model-independent iterative ensemble smoother for efficient history-matching and uncertainty quantification in very high dimensions. Environmental Modelling & Software, vol. 109.

Wiedemeier, T.H., Rifai, H.S., Newell, C.J., and Wilson, J.T. (1999). Natural Attenuation of Fuels and Chlorinated Solvents in the Subsurface. John Wiley & Sons, New York, 617 pp.

Zhang, T., [et al.] (2005). Hydroxylation and carboxylation—two crucial steps of anaerobic benzene degradation by Dechloromonas strain RCB. Applied and Environmental Microbiology, 71(9), 5427–5432.

Appendix A. Modelled versus observed hydrographs

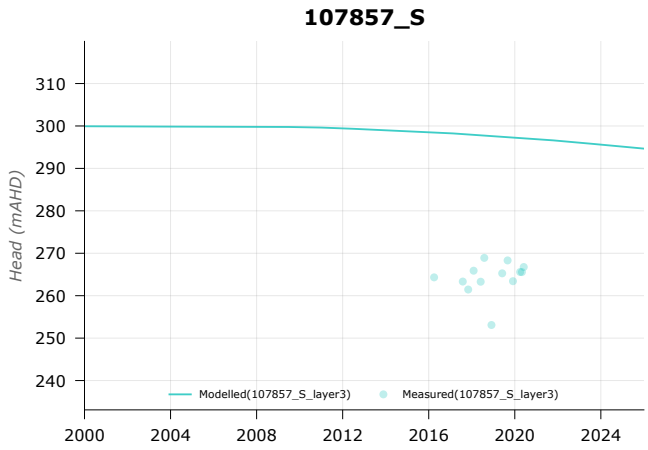
107857_S
Head (mAHD)
Modelled(107857_S_layer3)
Measured(107857_S_layer3)

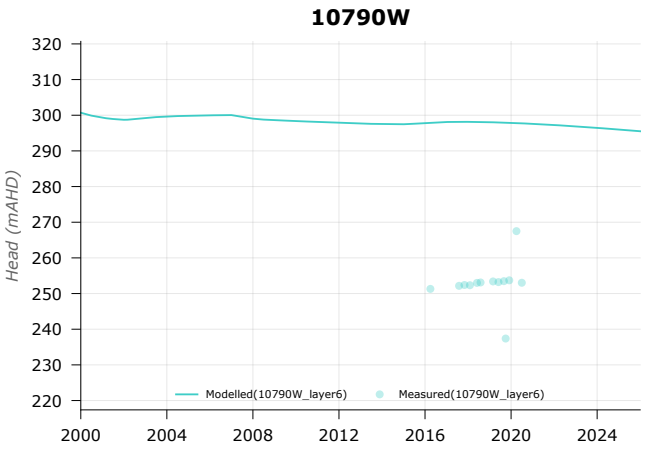
10790W
Head (mAHD)
Modelled(10790W_layer6)
Measured(10790W_layer6)

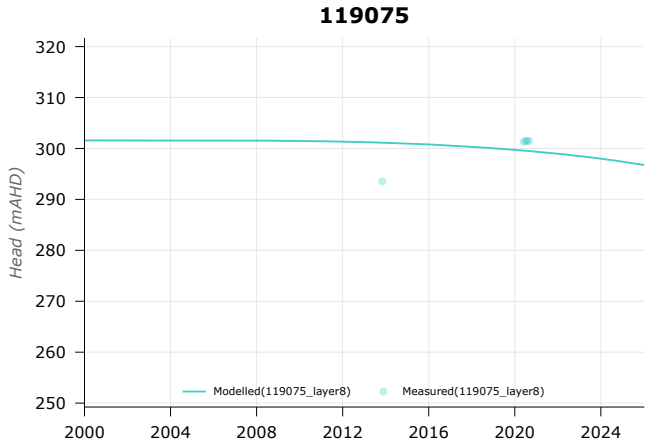
119075
Head (mAHD)
Modelled(119075_layer8)
Measured(119075_layer8)

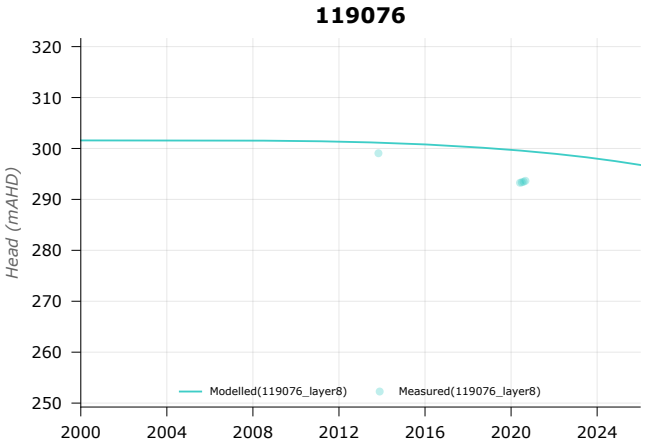
119076
Head (mAHD)
Modelled(119076_layer8)
Measured(119076_layer8)

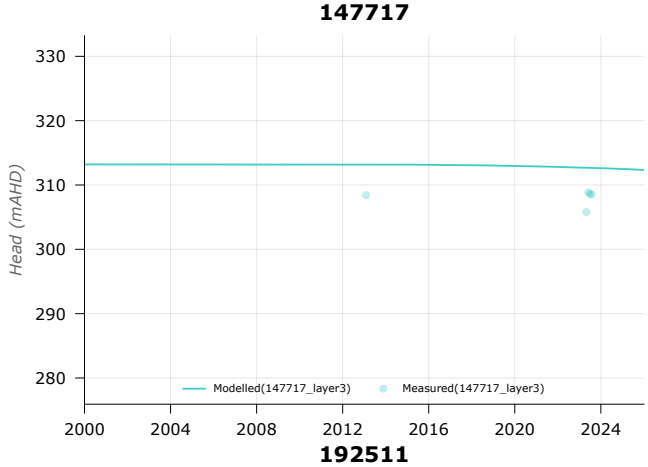
147717
Head (mAHD)
Modelled(147717_layer3)
Measured(147717_layer3)

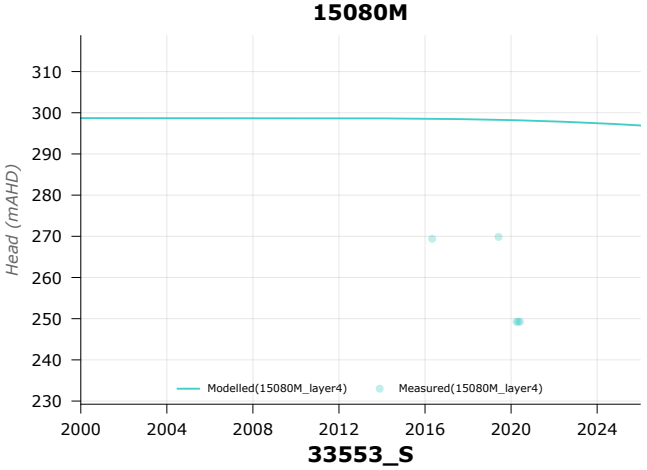
15080M
Head (mAHD)
Modelled(15080M_layer4)
Measured(15080M_layer4)

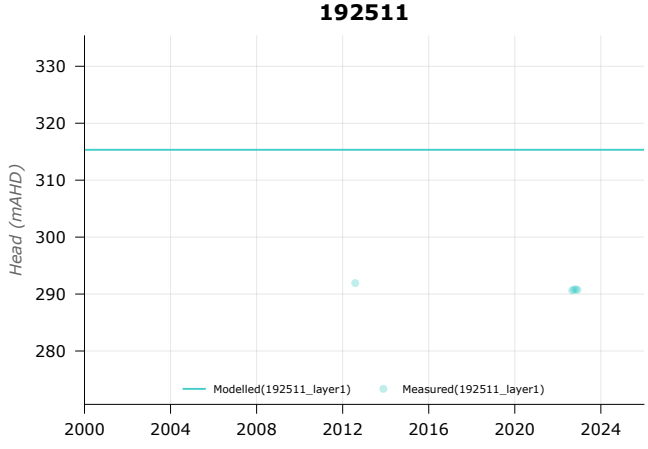
192511
Head (mAHD)
Modelled(192511_layer1)
Measured(192511_layer1)

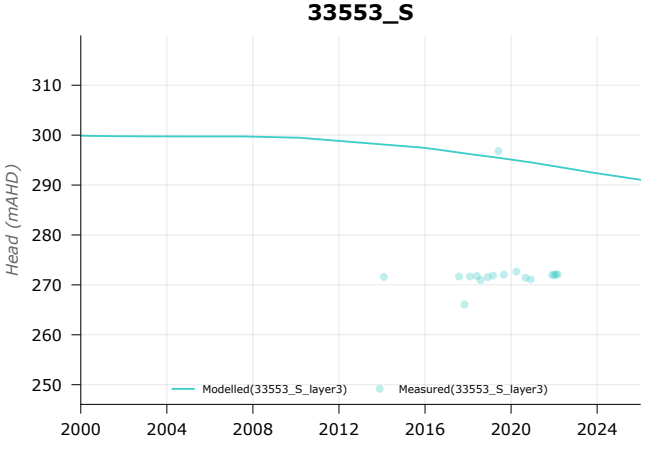
33553_S
Head (mAHD)
Modelled(33553_S_layer3)
Measured(33553_S_layer3)

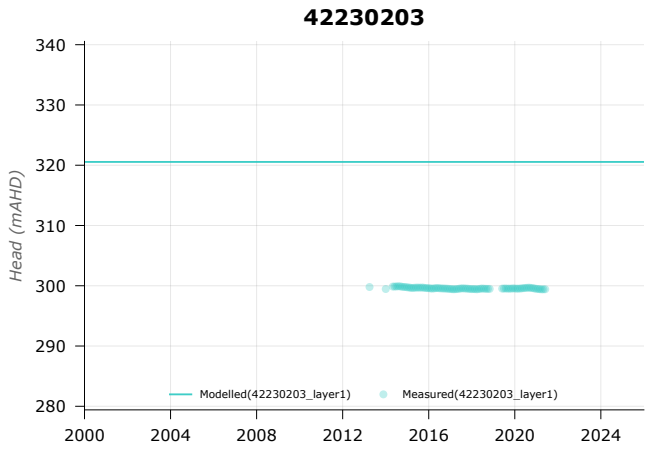
42230203
Head (mAHD)
340
330
320
310
300
290
280
2000
2004
2008
2012
2016
2020
2024
Modelled(42230203_layer1)
Measured(42230203_layer1)

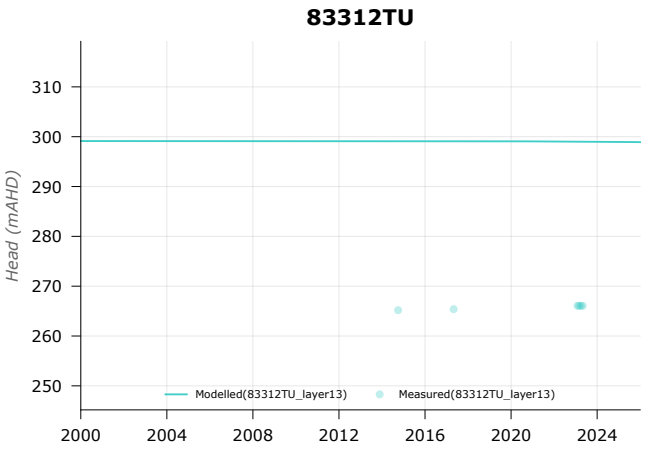
83312TU
Head (mAHD)
310
300
290
280
270
260
250
2000
2004
2008
2012
2016
2020
2024
Modelled(83312TU_layer13)
Measured(83312TU_layer13)

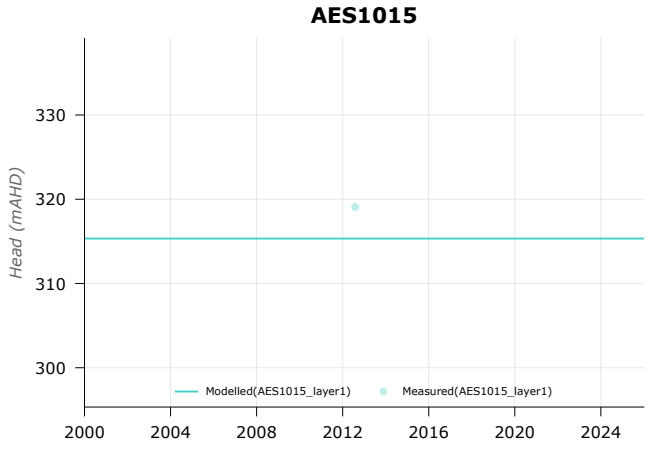
AES1015
Head (mAHD)
330
320
310
300
2000
2004
2008
2012
2016
2020
2024
Modelled(AES1015_layer1)
Measured(AES1015_layer1)

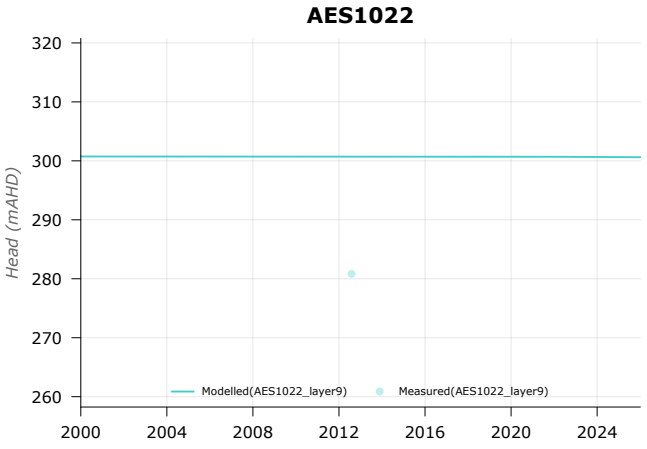
AES1022
Head (mAHD)
320
310
300
290
280
270
260
2000
2004
2008
2012
2016
2020
2024
Modelled(AES1022_layer9)
Measured(AES1022_layer9)

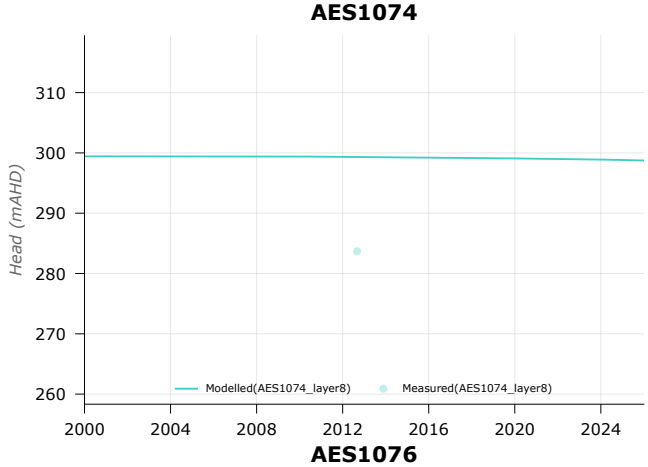
AES1074
Head (mAHD)
310
300
290
280
270
260
2000
2004
2008
2012
2016
2020
2024
Modelled(AES1074_layer8)
Measured(AES1074_layer8)

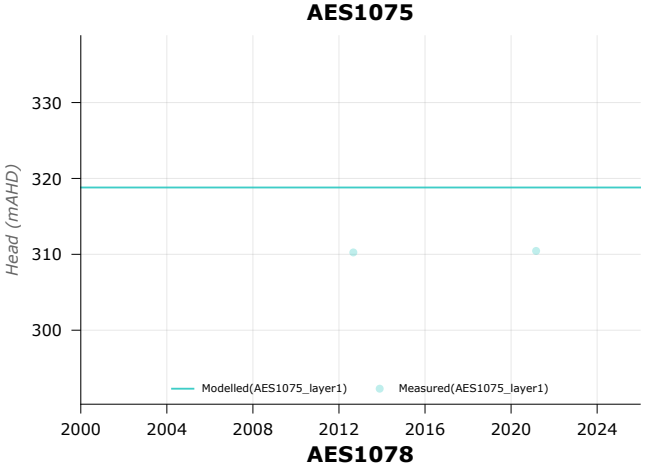
AES1075
Head (mAHD)
330
320
310
300
2000
2004
2008
2012
2016
2020
2024
Modelled(AES1075_layer1)
Measured(AES1075_layer1)

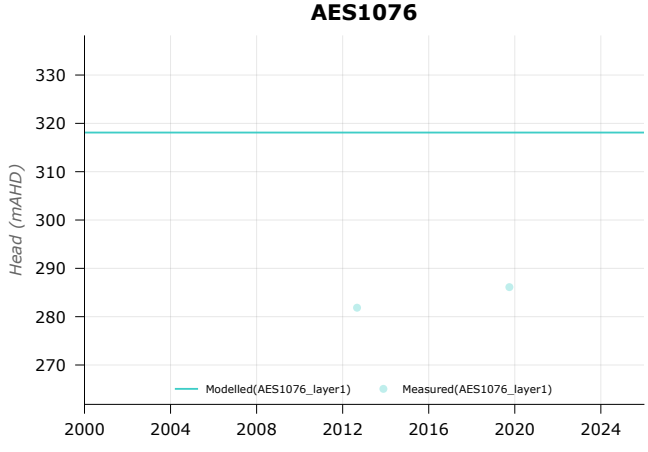
AES1076
Head (mAHD)
330
320
310
300
290
280
270
2000
2004
2008
2012
2016
2020
2024
Modelled(AES1076_layer1)
Measured(AES1076_layer1)

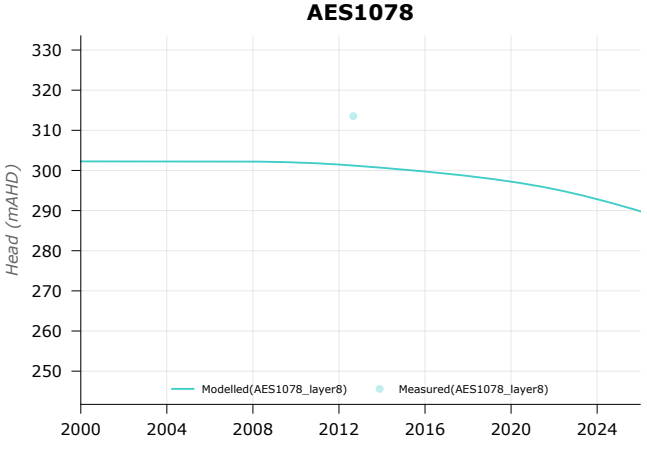
AES1078
Head (mAHD)
330
320
310
300
290
280
270
260
250
2000
2004
2008
2012
2016
2020
2024
Modelled(AES1078_layer8)
Measured(AES1078_layer8)

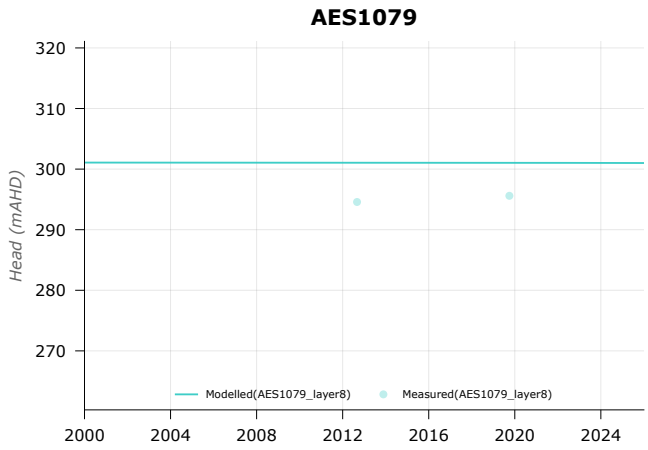
AES1079
Head (mAHD)
320
310
300
290
280
270
2000
2004
2008
2012
2016
2020
2024
Modelled(AES1079_layer8)
Measured(AES1079_layer8)

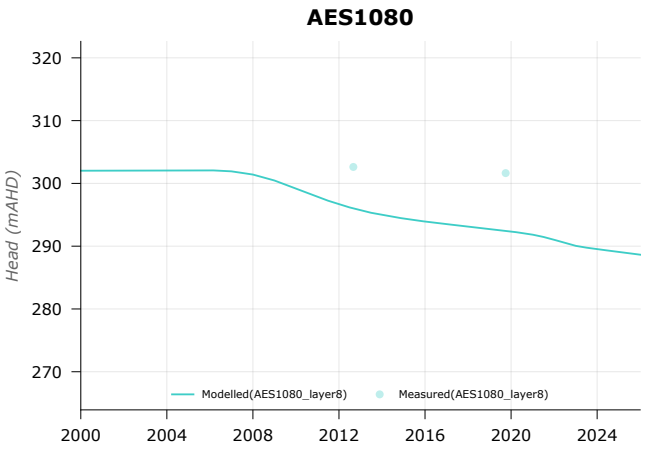
AES1080
Head (mAHD)
320
310
300
290
280
270
2000
2004
2008
2012
2016
2020
2024
Modelled(AES1080_layer8)
Measured(AES1080_layer8)

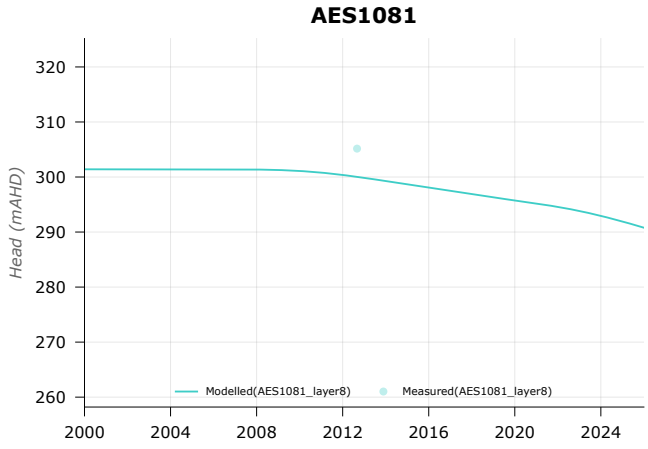
AES1081
Head (mAHD)
320
310
300
290
280
270
260
2000
2004
2008
2012
2016
2020
2024
Modelled(AES1081_layer8)
Measured(AES1081_layer8)

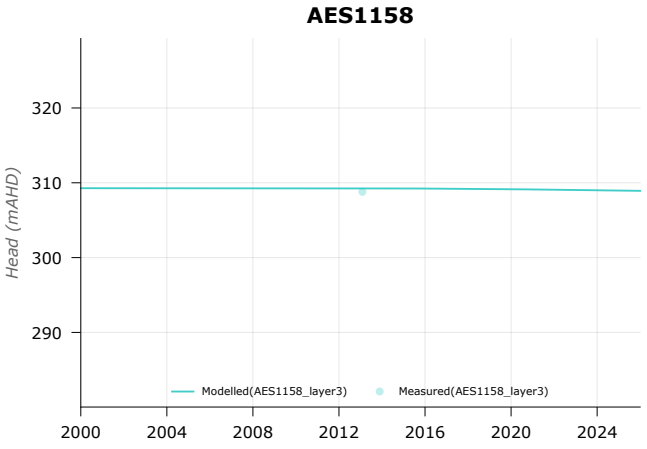
AES1158
Head (mAHD)
320
310
300
290
2000
2004
2008
2012
2016
2020
2024
Modelled(AES1158_layer3)
Measured(AES1158_layer3)

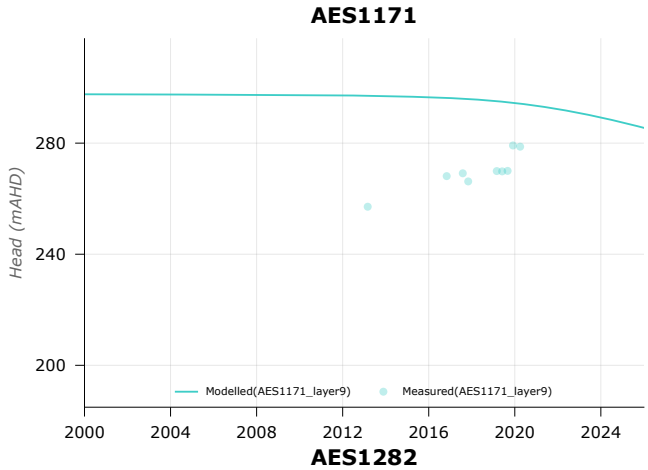
AES1171
Head (mAHD)
280
240
200
2000
2004
2008
2012
2016
2020
2024
Modelled(AES1171_layer9)
Measured(AES1171_layer9)

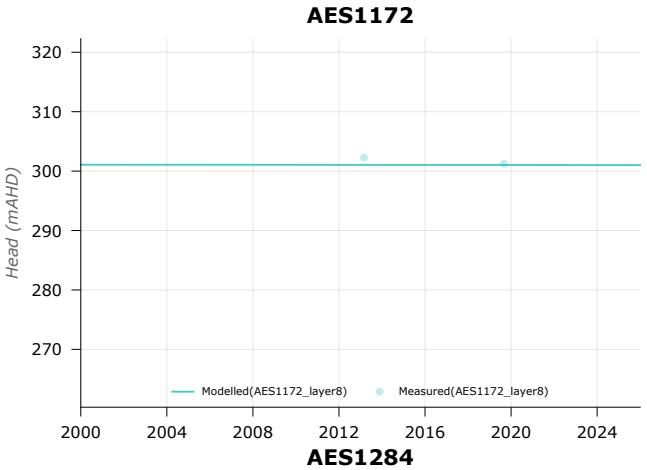
AES1172
Head (mAHD)
320
310
300
290
280
270
2000
2004
2008
2012
2016
2020
2024
Modelled(AES1172_layer8)
Measured(AES1172_layer8)

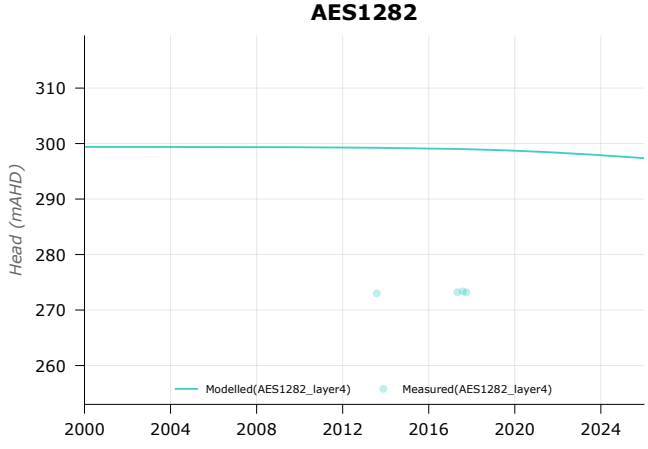
AES1282
Head (mAHD)
310
300
290
280
270
260
2000
2004
2008
2012
2016
2020
2024
Modelled(AES1282_layer4)
Measured(AES1282_layer4)

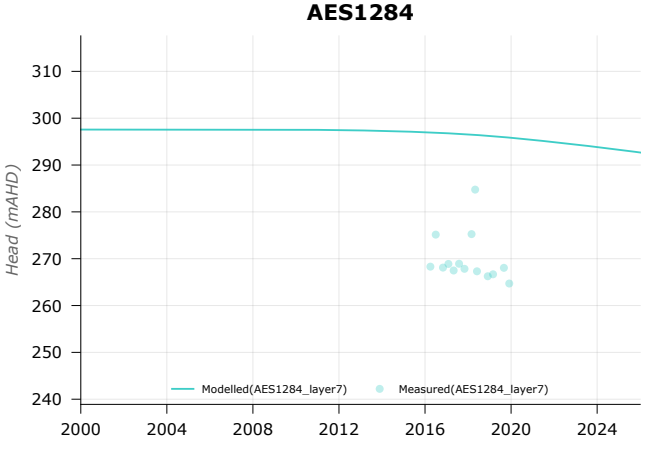
AES1284
Head (mAHD)
310
300
290
280
270
260
250
240
2000
2004
2008
2012
2016
2020
2024
Modelled(AES1284_layer7)
Measured(AES1284_layer7)

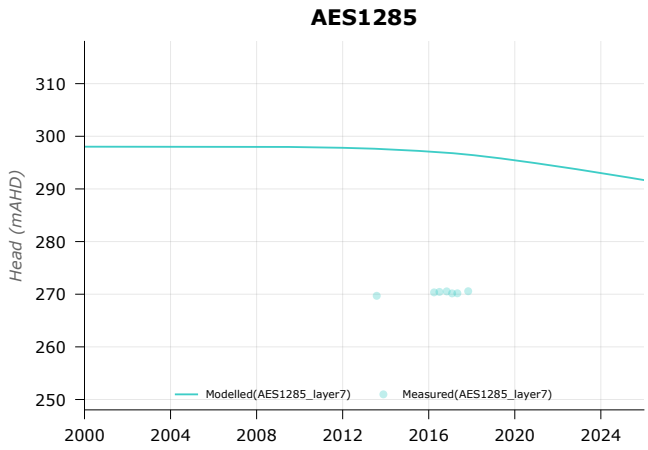
AES1285
Head (mAHD)
Modelled(AES1285_layer7)
Measured(AES1285_layer7)

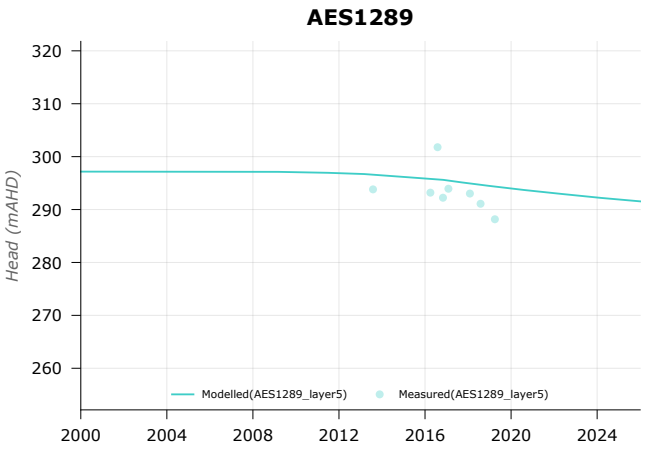
AES1289
Head (mAHD)
Modelled(AES1289_layer5)
Measured(AES1289_layer5)

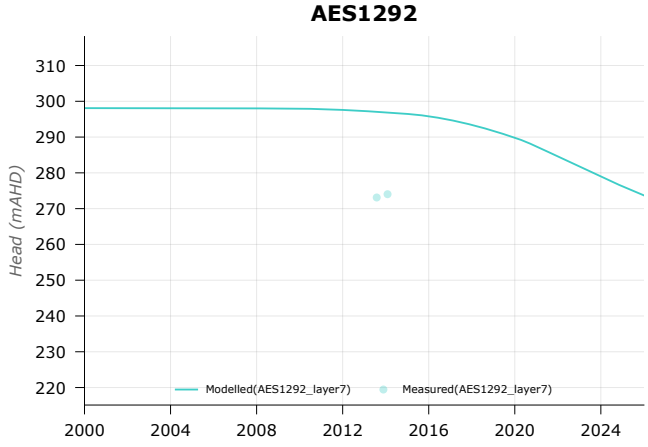
AES1292
Head (mAHD)
Modelled(AES1292_layer7)
Measured(AES1292_layer7)

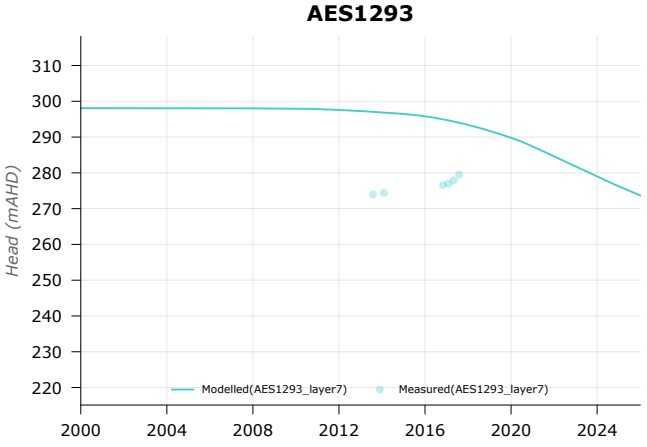
AES1293
Head (mAHD)
Modelled(AES1293_layer7)
Measured(AES1293_layer7)

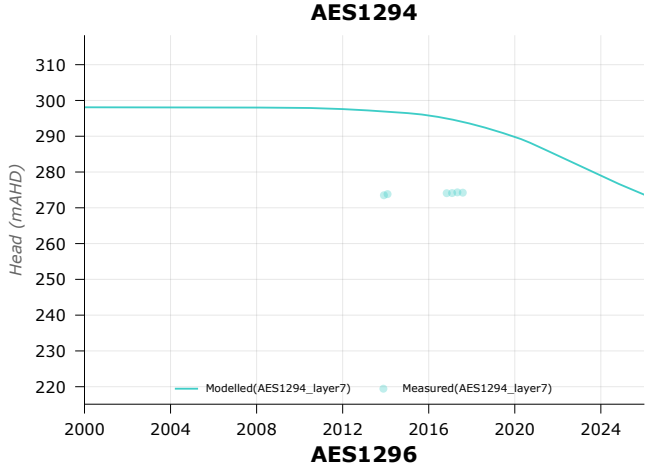
AES1294
Head (mAHD)
Modelled(AES1294_layer7)
Measured(AES1294_layer7)

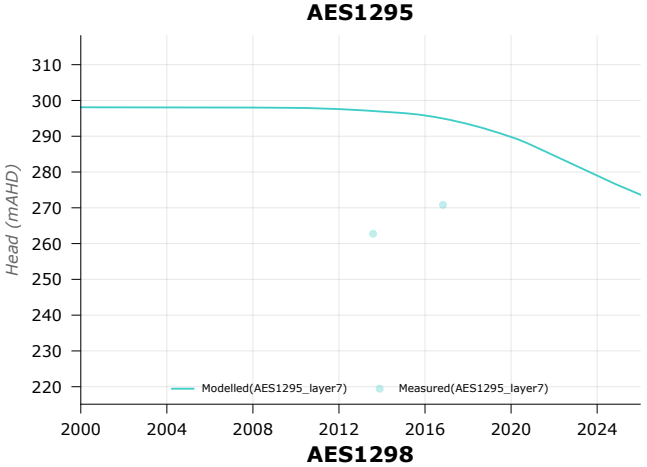
AES1295
Head (mAHD)
Modelled(AES1295_layer7)
Measured(AES1295_layer7)

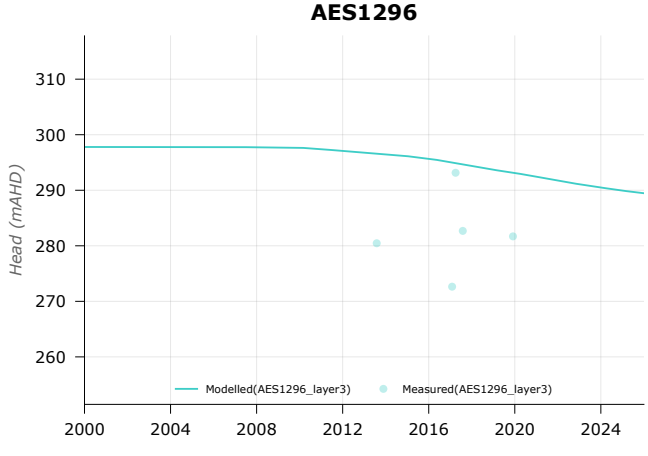
AES1296
Head (mAHD)
Modelled(AES1296_layer3)
Measured(AES1296_layer3)

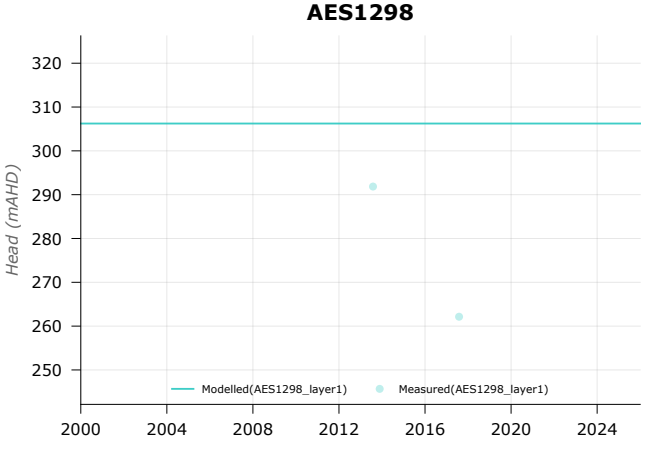
AES1298
Head (mAHD)
Modelled(AES1298_layer1)
Measured(AES1298_layer1)

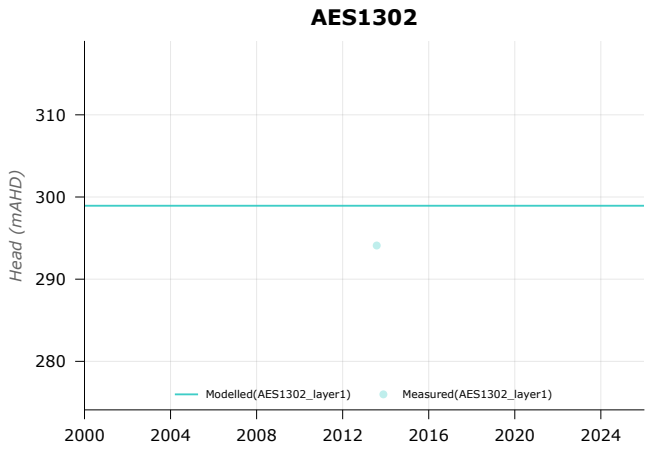
AES1302
Head (mAHD)
310
300
290
280
2000
2004
2008
2012
2016
2020
2024
Modelled(AES1302_layer1)
Measured(AES1302_layer1)

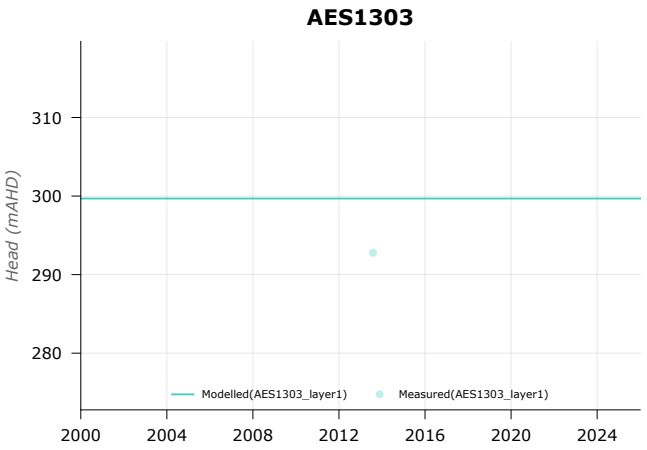
AES1303
Head (mAHD)
310
300
290
280
2000
2004
2008
2012
2016
2020
2024
Modelled(AES1303_layer1)
Measured(AES1303_layer1)

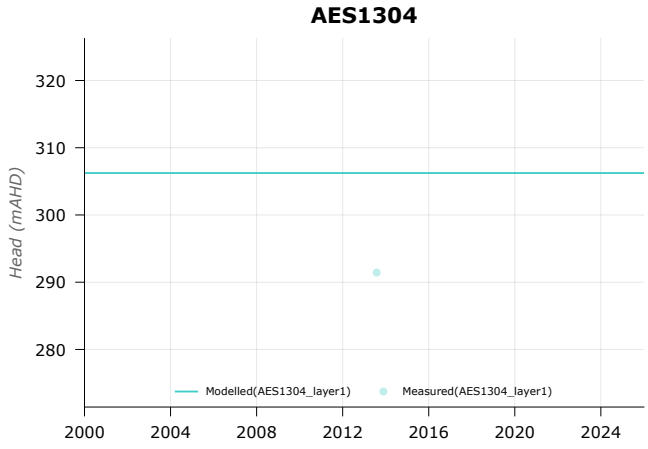
AES1304
Head (mAHD)
320
310
300
290
280
2000
2004
2008
2012
2016
2020
2024
Modelled(AES1304_layer1)
Measured(AES1304_layer1)

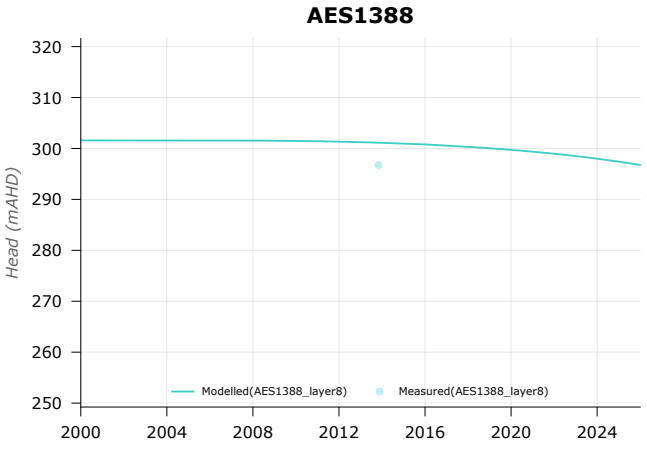
AES1388
Head (mAHD)
320
310
300
290
280
270
260
250
2000
2004
2008
2012
2016
2020
2024
Modelled(AES1388_layer8)
Measured(AES1388_layer8)

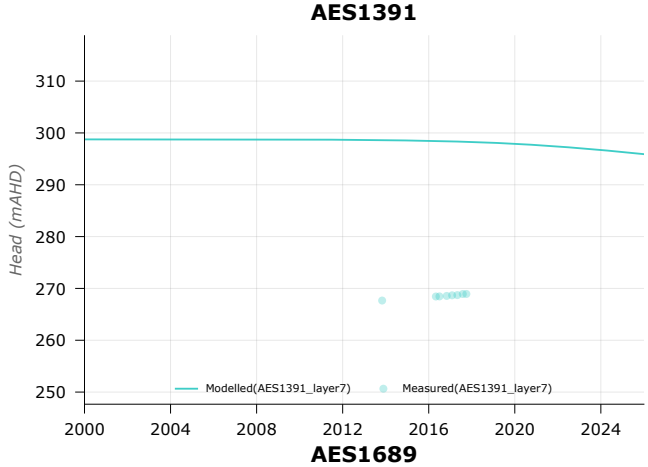
AES1391
Head (mAHD)
310
300
290
280
270
260
250
2000
2004
2008
2012
2016
2020
2024
Modelled(AES1391_layer7)
Measured(AES1391_layer7)

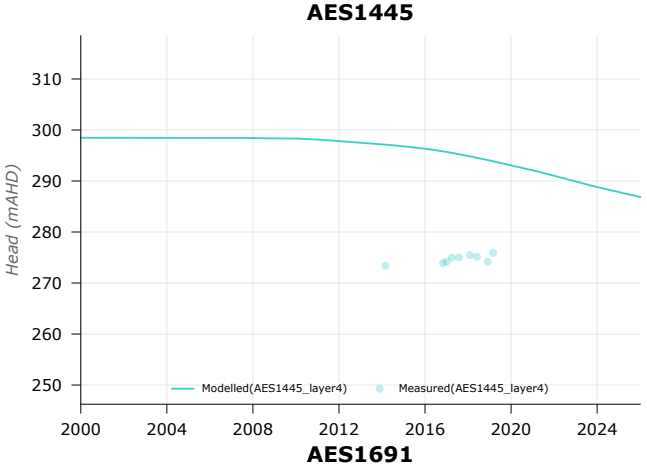
AES1445
Head (mAHD)
310
300
290
280
270
260
250
2000
2004
2008
2012
2016
2020
2024
Modelled(AES1445_layer4)
Measured(AES1445_layer4)

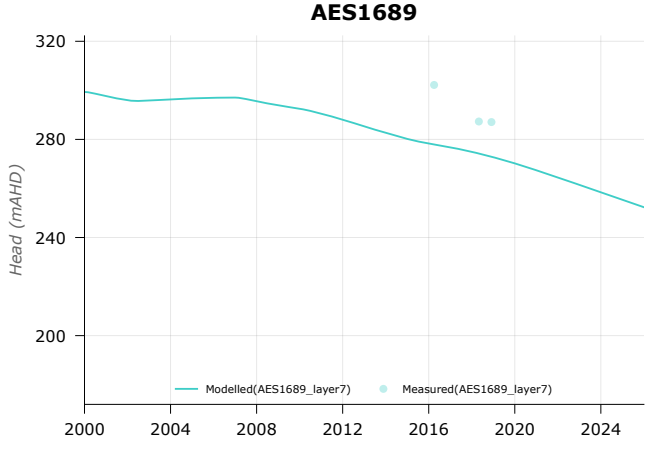
AES1689
Head (mAHD)
320
280
240
200
2000
2004
2008
2012
2016
2020
2024
Modelled(AES1689_layer7)
Measured(AES1689_layer7)

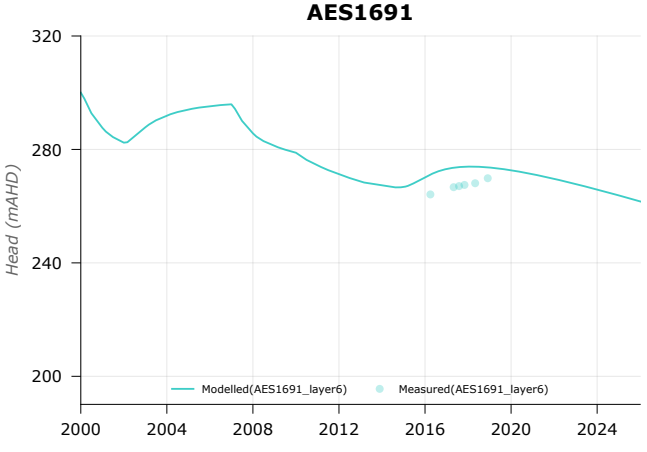
AES1691
Head (mAHD)
320
280
240
200
2000
2004
2008
2012
2016
2020
2024
Modelled(AES1691_layer6)
Measured(AES1691_layer6)

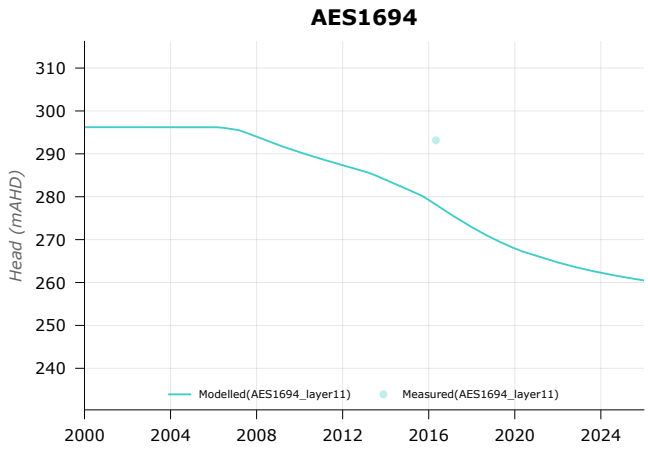
AES1694
Head (mAHD)
Modelled(AES1694_layer11)
Measured(AES1694_layer11)

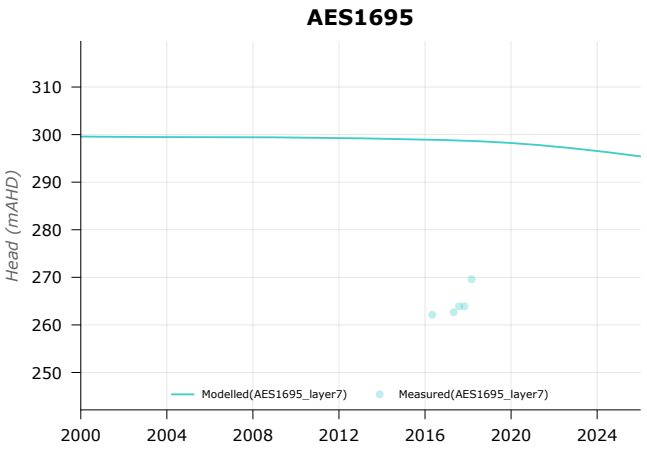
AES1695
Head (mAHD)
Modelled(AES1695_layer7)
Measured(AES1695_layer7)

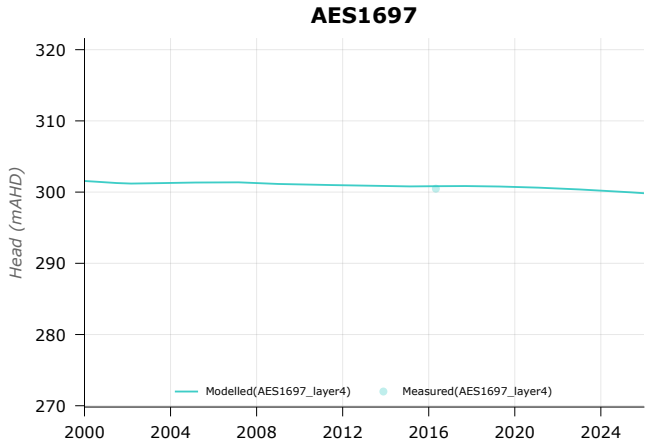
AES1697
Head (mAHD)
Modelled(AES1697_layer4)
Measured(AES1697_layer4)

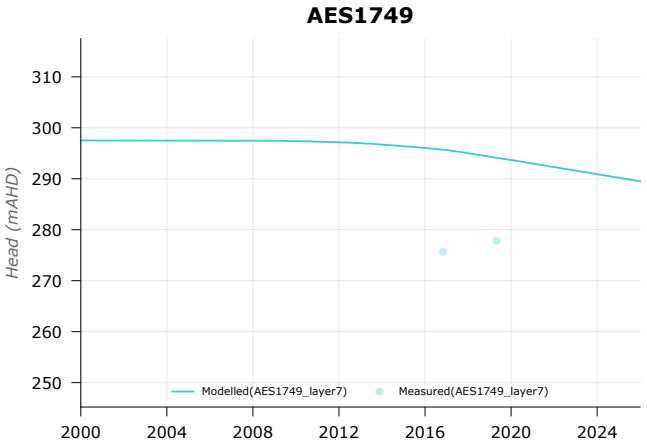
AES1749
Head (mAHD)
Modelled(AES1749_layer7)
Measured(AES1749_layer7)

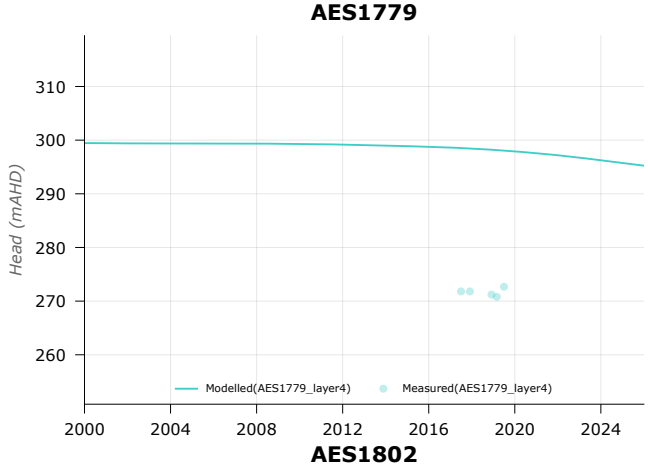
AES1779
Head (mAHD)
Modelled(AES1779_layer4)
Measured(AES1779_layer4)

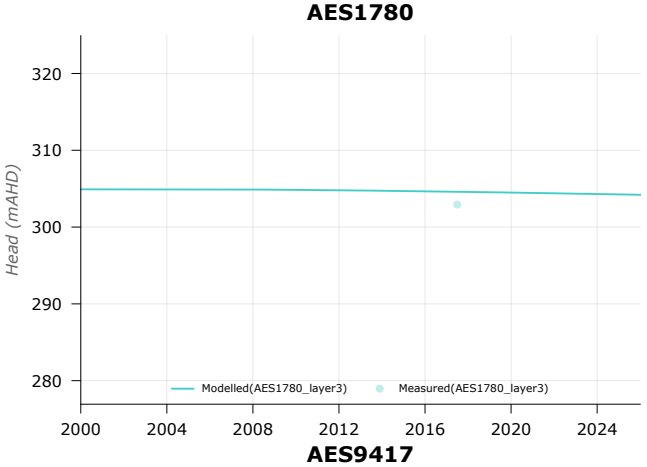
AES1780
Head (mAHD)
Modelled(AES1780_layer3)
Measured(AES1780_layer3)

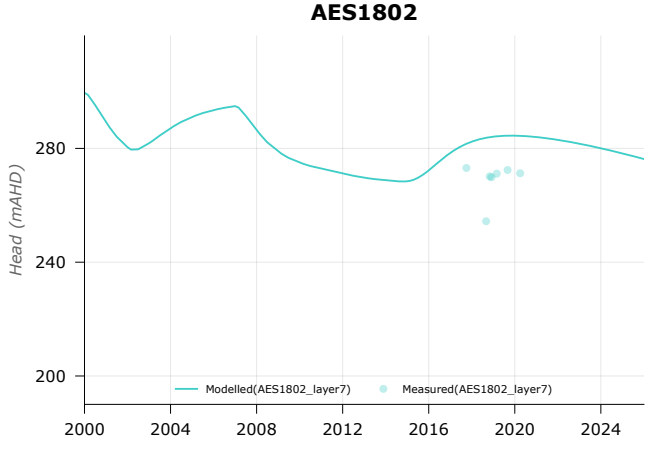
AES1802
Head (mAHD)
Modelled(AES1802_layer7)
Measured(AES1802_layer7)

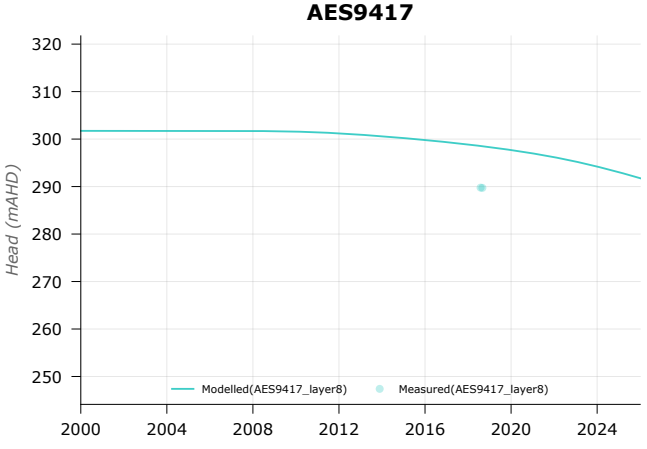
AES9417
Head (mAHD)
Modelled(AES9417_layer8)
Measured(AES9417_layer8)

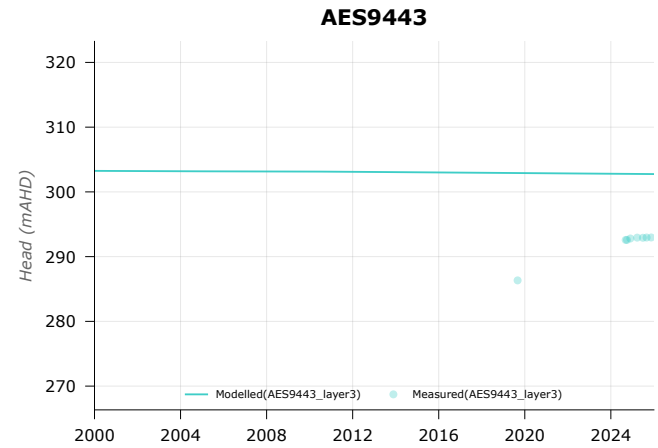
AES9443
Head (mAHD)
Modelled(AES9443_layer3)
Measured(AES9443_layer3)

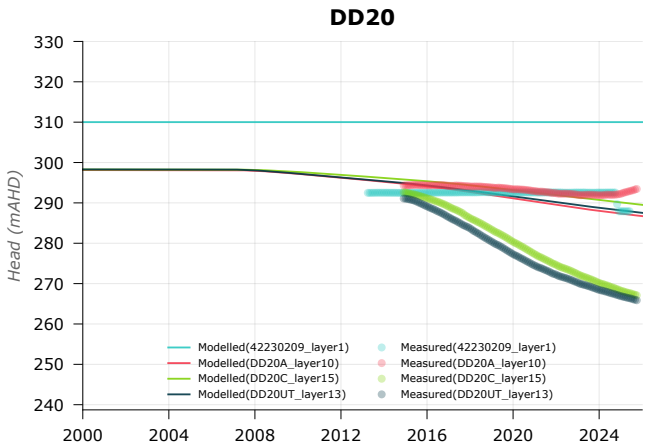
DD20
Head (mAHD)
Modelled(42230209_layer1)
Measured(42230209_layer1)
Modelled(DD20A_layer10)
Measured(DD20A_layer10)
Modelled(DD20C_layer15)
Measured(DD20C_layer15)
Modelled(DD20UT_layer13)
Measured(DD20UT_layer13)

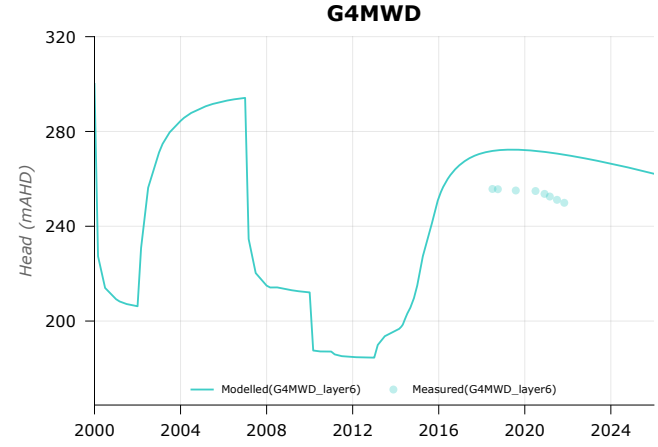
G4MWD
Head (mAHD)
Modelled(G4MWD_layer6)
Measured(G4MWD_layer6)

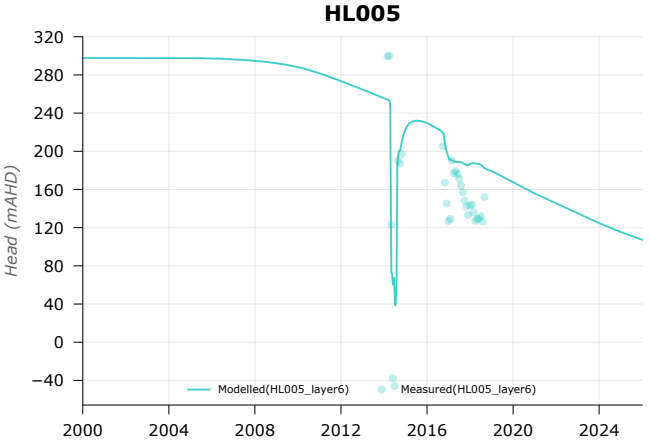
HL005
Head (mAHD)
Modelled(HL005_layer6)
Measured(HL005_layer6)

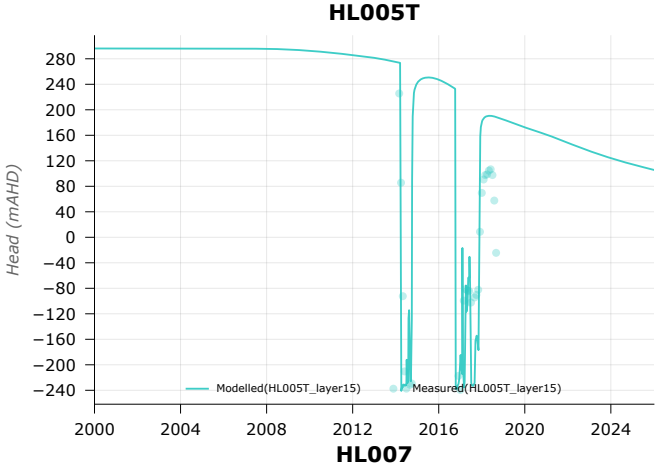
HL005T
Head (mAHD)
Modelled(HL005T_layer15)
Measured(HL005T_layer15)

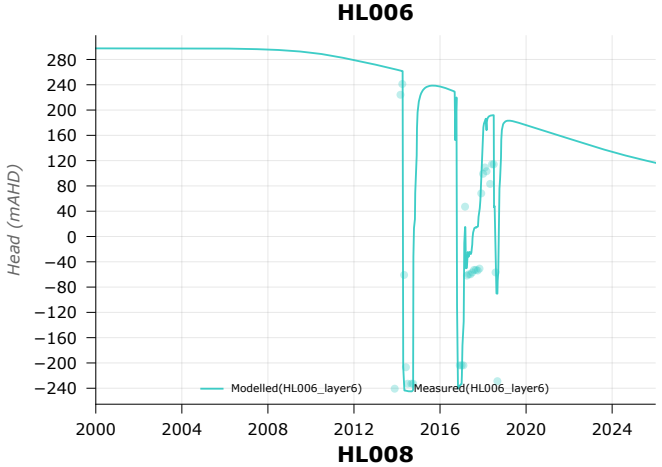
HL006
Head (mAHD)
Modelled(HL006_layer6)
Measured(HL006_layer6)

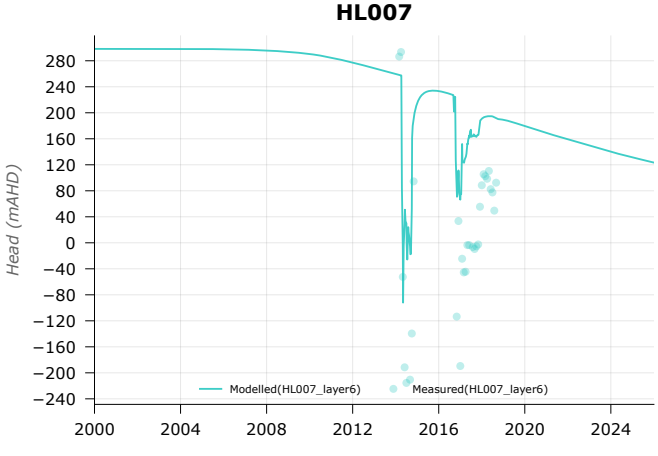
HL007
Head (mAHD)
Modelled(HL007_layer6)
Measured(HL007_layer6)

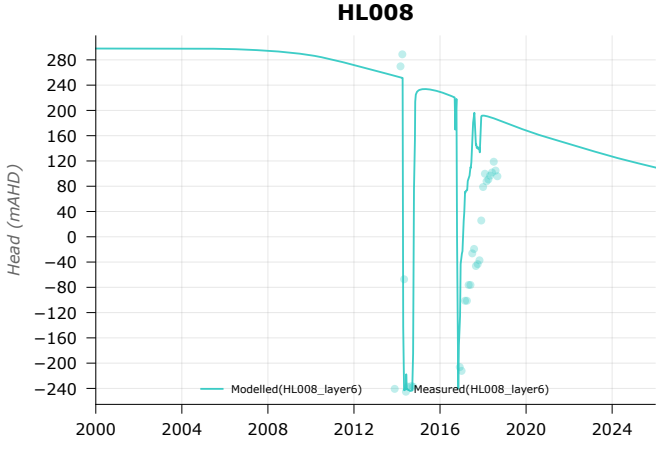
HL008
Head (mAHD)
Modelled(HL008_layer6)
Measured(HL008_layer6)

HL009

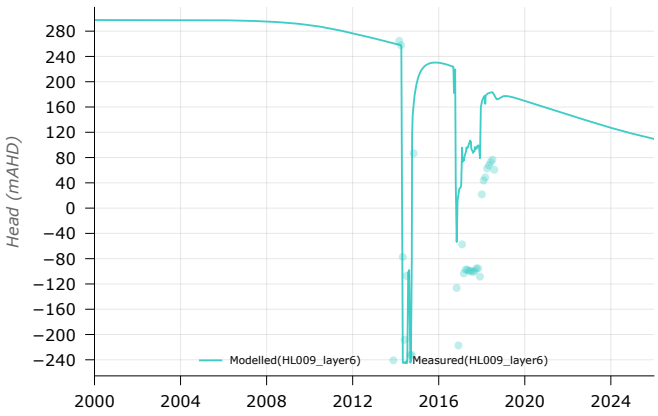

HL17

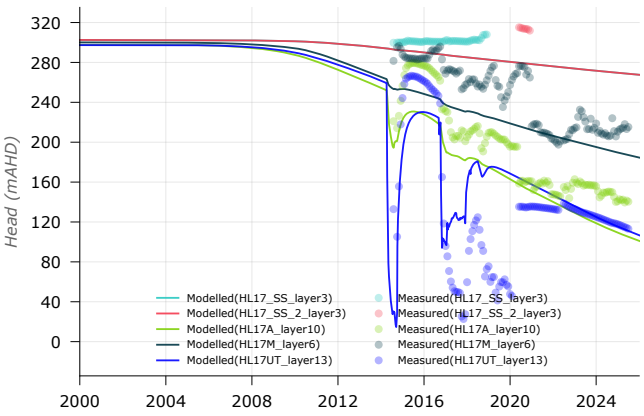

HL20-21

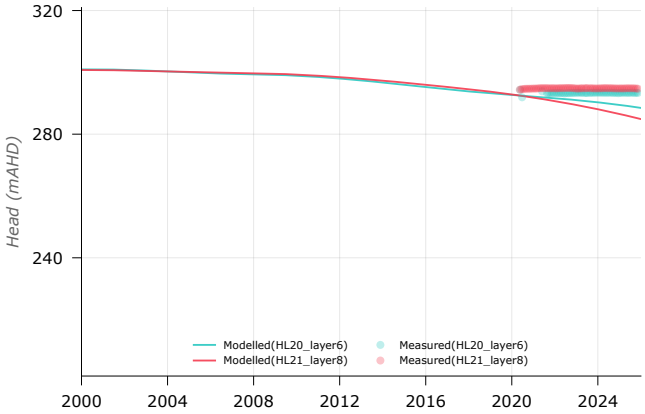

HL22-24

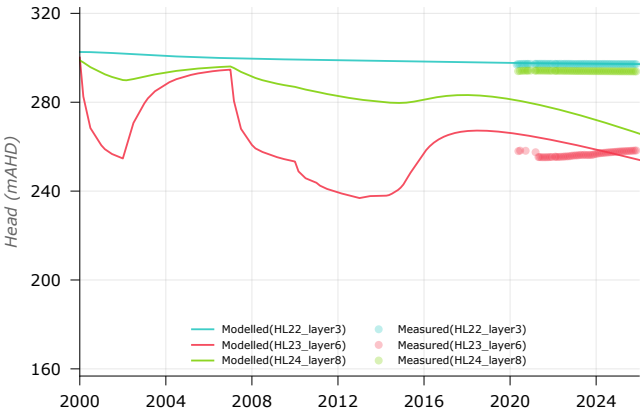

HL25-27

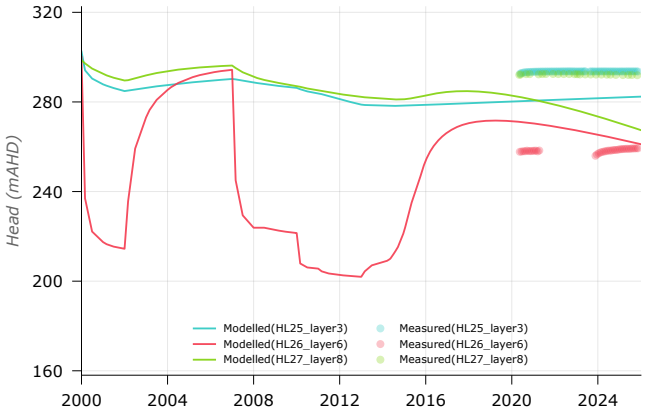

HL34

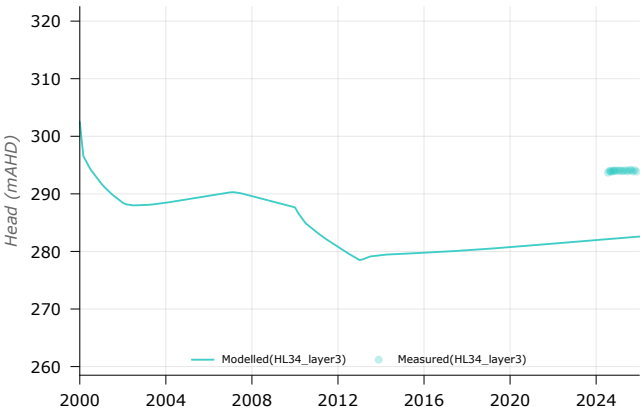

HL35

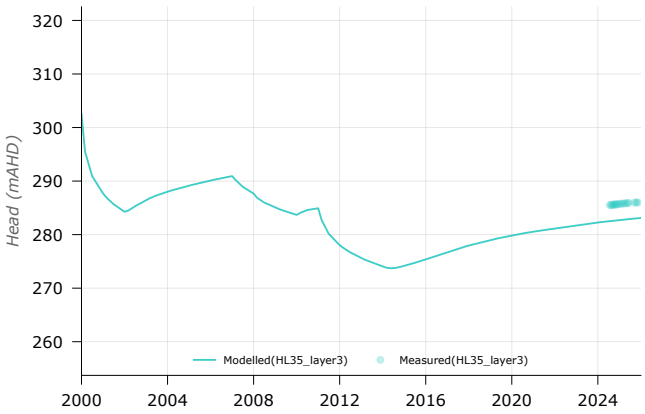

HL36

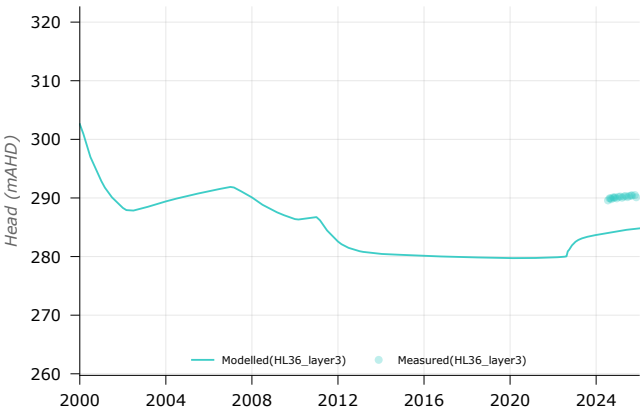

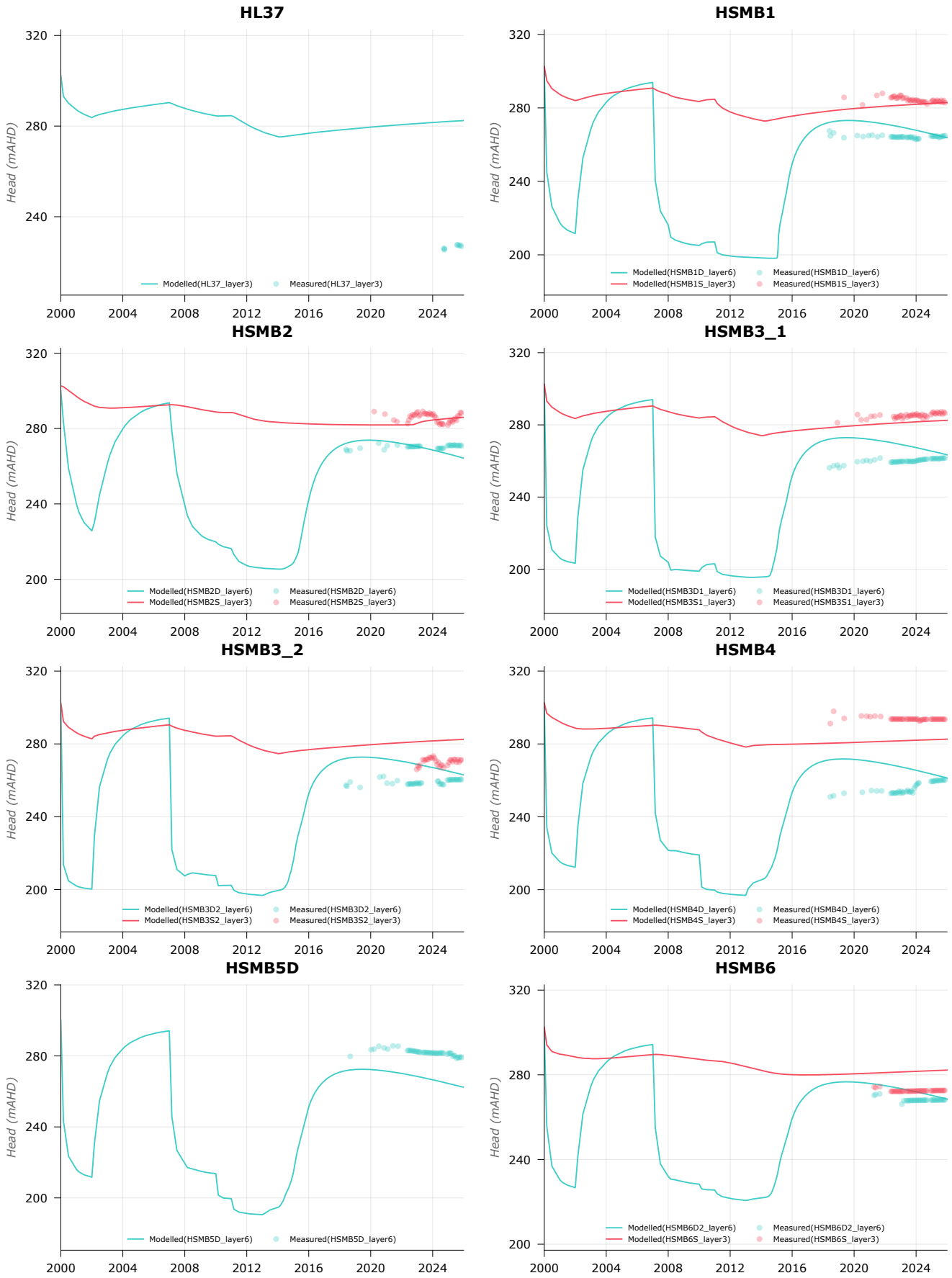
HL37
Head (mAHD)
320
280
240
2000
2004
2008
2012
2016
2020
2024
Modelled(HL37_layer3)
Measured(HL37_layer3)
HSMB1
200
Modelled(HSMB1D_layer6)
Measured(HSMB1D_layer6)
Modelled(HSMB1S_layer3)
Measured(HSMB1S_layer3)
HSMB2
Modelled(HSMB2D_layer6)
Measured(HSMB2D_layer6)
Modelled(HSMB2S_layer3)
Measured(HSMB2S_layer3)
HSMB3_1
Modelled(HSMB3D1_layer6)
Measured(HSMB3D1_layer6)
Modelled(HSMB3S1_layer3)
Measured(HSMB3S1_layer3)
HSMB3_2
Modelled(HSMB3D2_layer6)
Measured(HSMB3D2_layer6)
Modelled(HSMB3S2_layer3)
Measured(HSMB3S2_layer3)
HSMB4
Modelled(HSMB4D_layer6)
Measured(HSMB4D_layer6)
Modelled(HSMB4S_layer3)
Measured(HSMB4S_layer3)
HSMB5D
Modelled(HSMB5D_layer6)
Measured(HSMB5D_layer6)
HSMB6
Modelled(HSMB6D2_layer6)
Measured(HSMB6D2_layer6)
Modelled(HSMB6S_layer3)
Measured(HSMB6S_layer3)

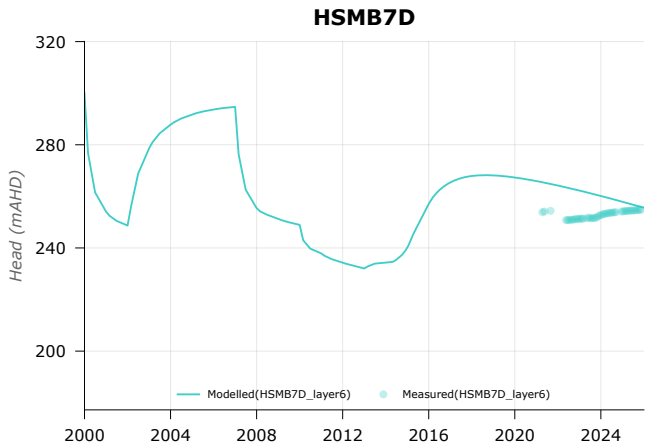
HSMB7D
Head (mAHD)
320
280
240
200
2000
2004
2008
2012
2016
2020
2024
Modelled(HSMB7D_layer6)
Measured(HSMB7D_layer6)

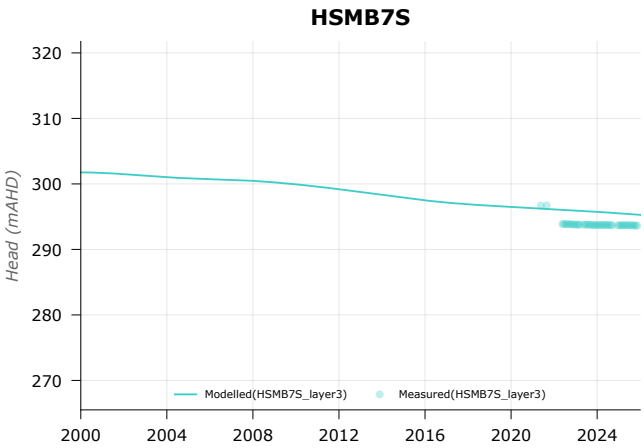
HSMB7S
Head (mAHD)
320
310
300
290
280
270
2000
2004
2008
2012
2016
2020
2024
Modelled(HSMB7S_layer3)
Measured(HSMB7S_layer3)

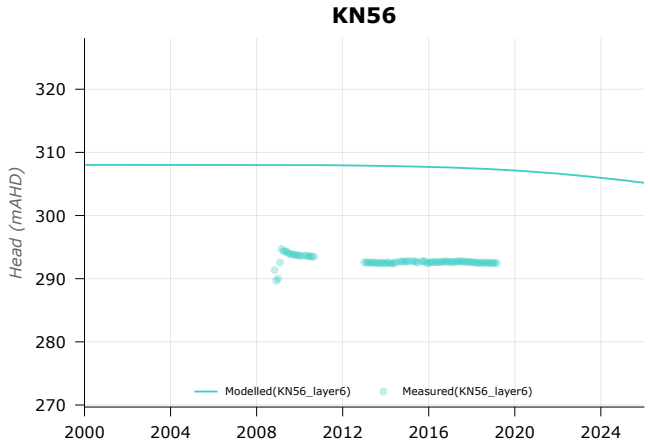
KN56
Head (mAHD)
320
310
300
290
280
270
2000
2004
2008
2012
2016
2020
2024
Modelled(KN56_layer6)
Measured(KN56_layer6)

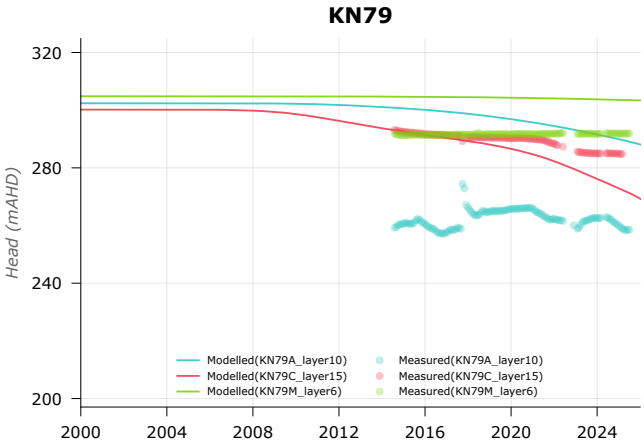
KN79
Head (mAHD)
320
280
240
200
2000
2004
2008
2012
2016
2020
2024
Modelled(KN79A_layer10)
Measured(KN79A_layer10)
Modelled(KN79C_layer15)
Measured(KN79C_layer15)
Modelled(KN79M_layer6)
Measured(KN79M_layer6)

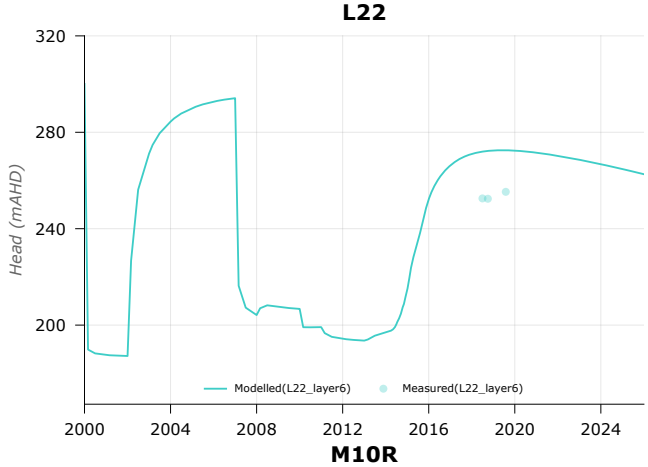
L22
Head (mAHD)
320
280
240
200
2000
2004
2008
2012
2016
2020
2024
Modelled(L22_layer6)
Measured(L22_layer6)

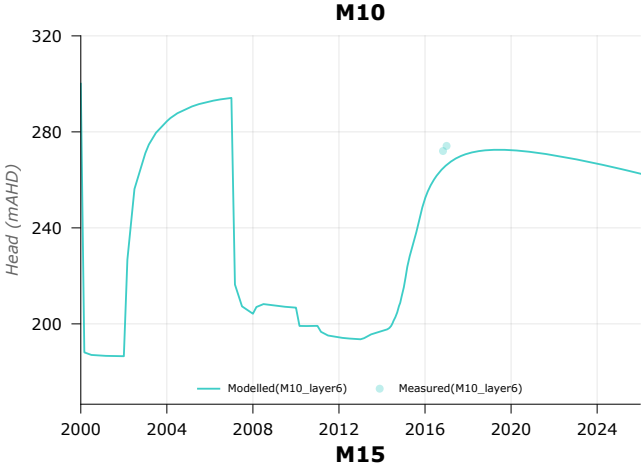
M10
Head (mAHD)
320
280
240
200
2000
2004
2008
2012
2016
2020
2024
Modelled(M10_layer6)
Measured(M10_layer6)


M10R
Head (mAHD)
320
280
240
200
2000
2004
2008
2012
2016
2020
2024
Modelled(M10R_layer6)
Measured(M10R_layer6)

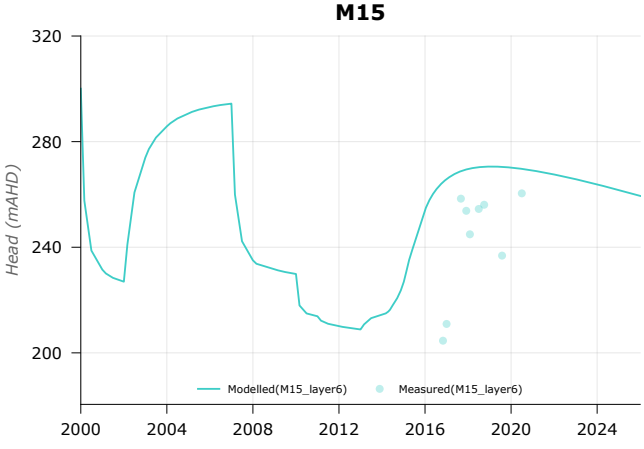
M15
Head (mAHD)
320
280
240
200
2000
2004
2008
2012
2016
2020
2024
Modelled(M15_layer6)
Measured(M15_layer6)

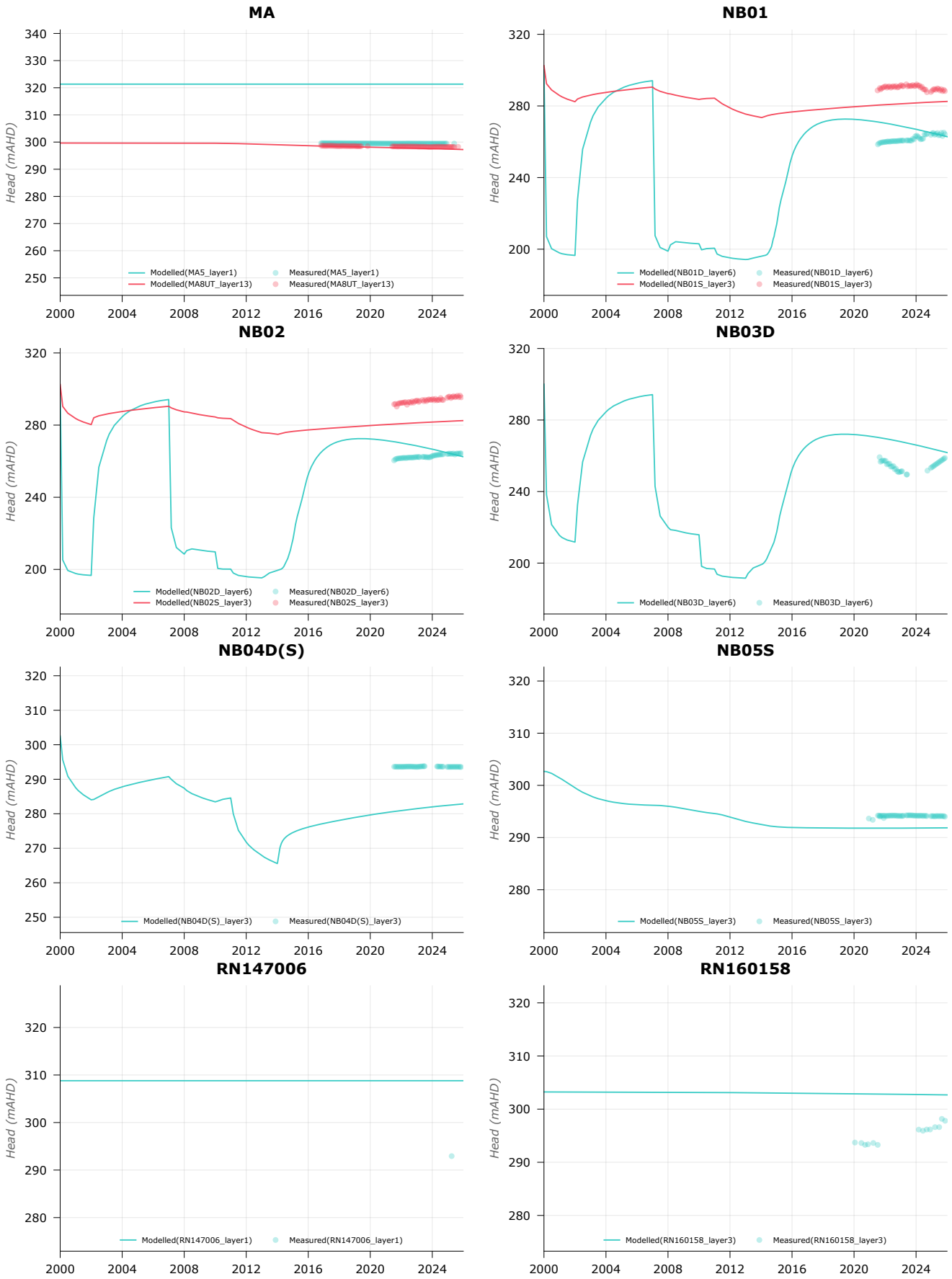
MA
Head (mAHD)
Modelled(MA5_layer1)
Measured(MA5_layer1)
Modelled(MA8UT_layer13)
Measured(MA8UT_layer13)
NB01
Modelled(NB01D_layer6)
Measured(NB01D_layer6)
Modelled(NB01S_layer3)
Measured(NB01S_layer3)
NB02
Modelled(NB02D_layer6)
Measured(NB02D_layer6)
Modelled(NB02S_layer3)
Measured(NB02S_layer3)
NB03D
Modelled(NB03D_layer6)
Measured(NB03D_layer6)
NB04D(S)
Modelled(NB04D(S)_layer3)
Measured(NB04D(S)_layer3)
NB05S
Modelled(NB05S_layer3)
Measured(NB05S_layer3)
RN147006
Modelled(RN147006_layer1)
Measured(RN147006_layer1)
RN160158
Modelled(RN160158_layer3)
Measured(RN160158_layer3)

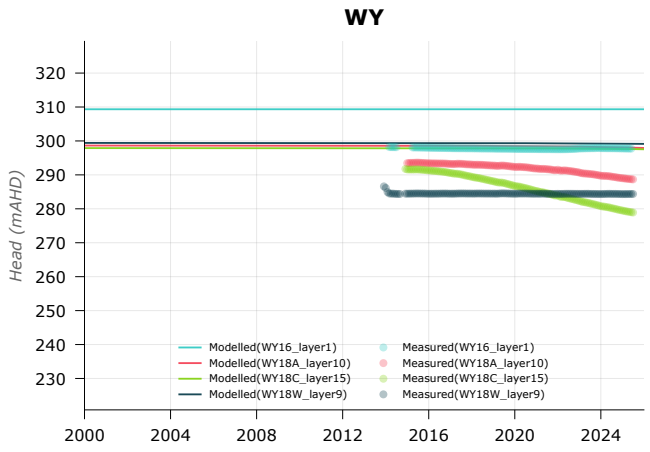
WY
Head (mAHD)
320
310
300
290
280
270
260
250
240
230
2000
2004
2008
2012
2016
2020
2024
Modelled(WY16_layer1)
Modelled(WY18A_layer10)
Modelled(WY18C_layer15)
Modelled(WY18W_layer9)
Measured(WY16_layer1)
Measured(WY18A_layer10)
Measured(WY18C_layer15)
Measured(WY18W_layer9)

Appendix B. Median prior and posterior parameter distributions

Kh:CondamineAlv

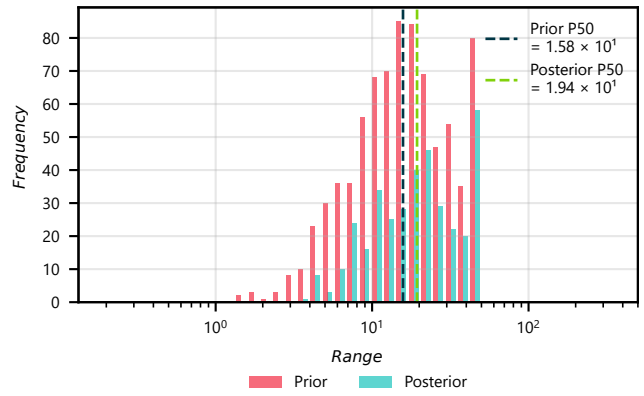

Kh:Gubb.Sst

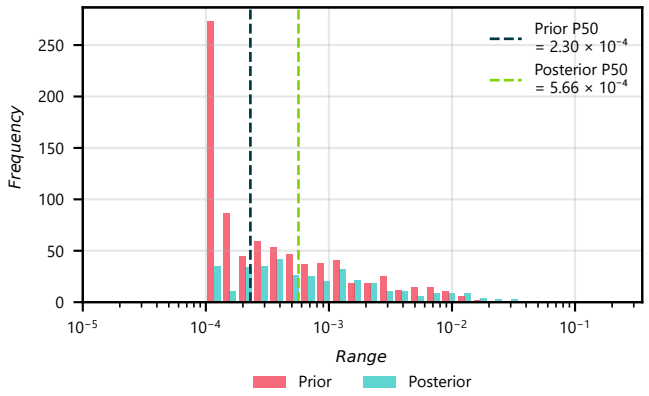

Kh:WestbourneFm

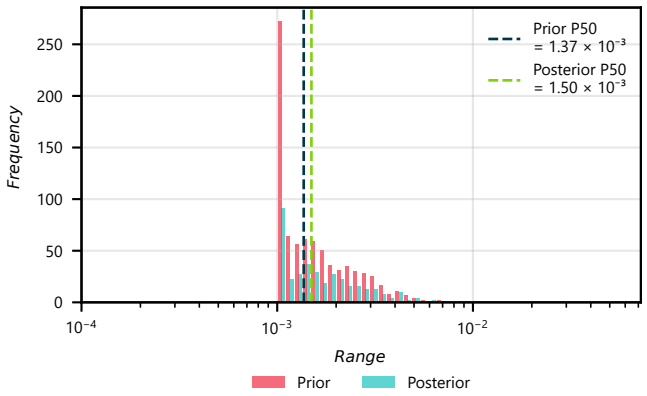

Kh:SpringbokSst

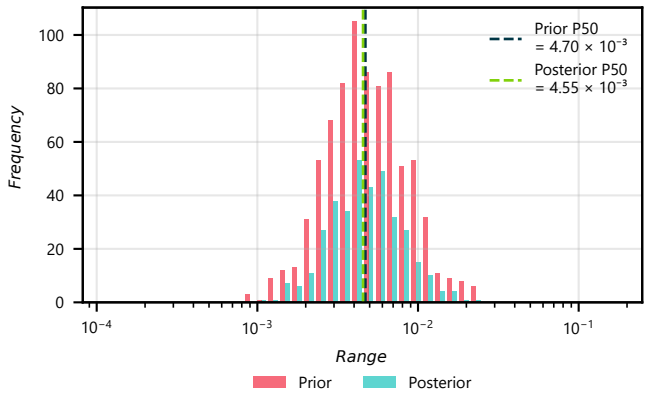

Kh:KoganC

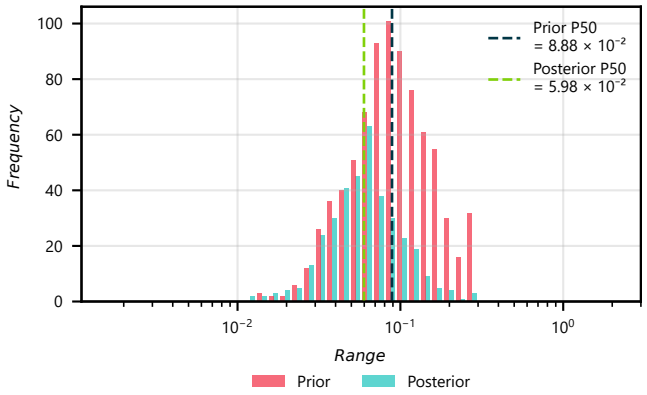

Kh:KoganIB

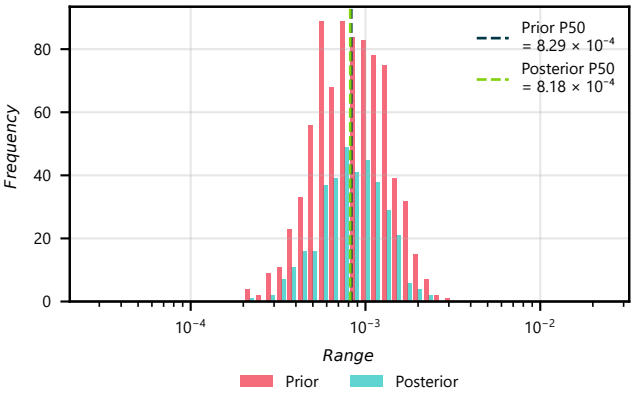

Kh:MacalisterC

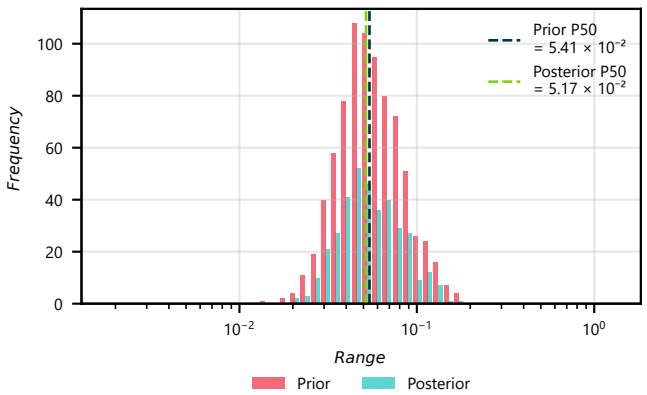

Kh:MacalisterIB

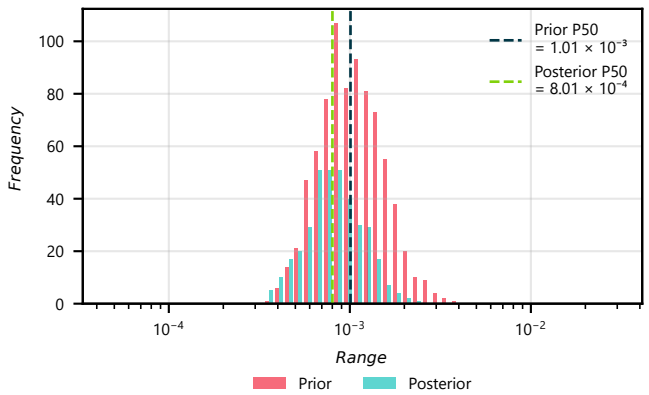

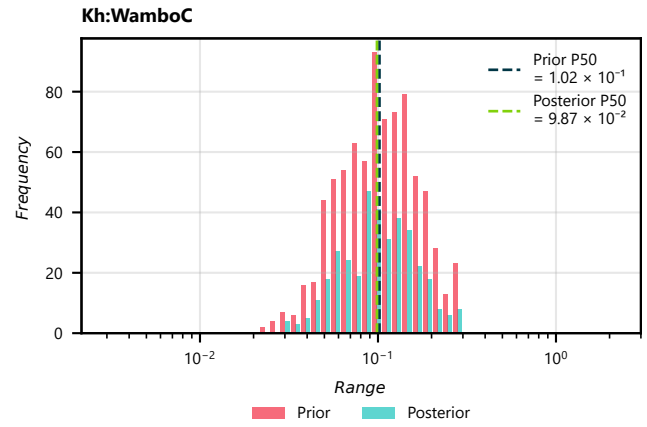
Kh:WamboC
Prior P50
= 1.02 × 10⁻¹
Posterior P50
= 9.87 × 10⁻²
Frequency
Range
Prior
Posterior

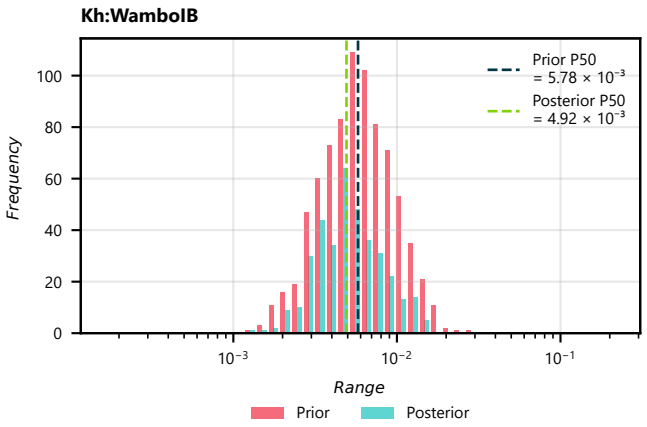
Kh:WamboIB
Prior P50
= 5.78 × 10⁻³
Posterior P50
= 4.92 × 10⁻³
Frequency
Range
Prior
Posterior

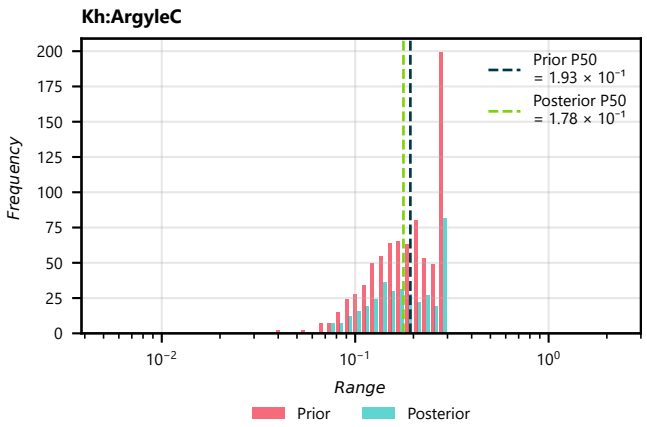
Kh:ArgyleC
Prior P50
= 1.93 × 10⁻¹
Posterior P50
= 1.78 × 10⁻¹
Frequency
Range
Prior
Posterior

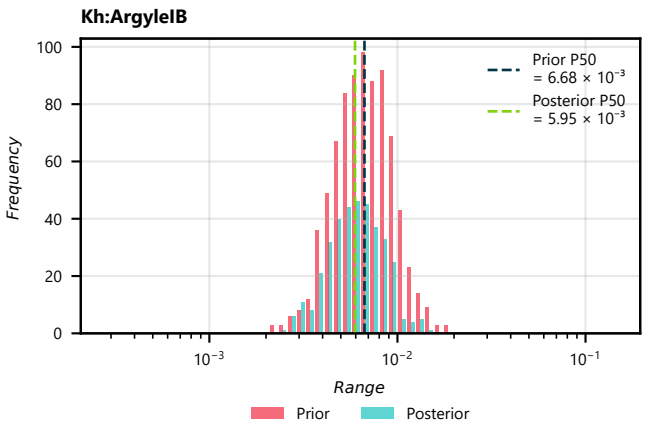
Kh:ArgyleIB
Prior P50
= 6.68 × 10⁻³
Posterior P50
= 5.95 × 10⁻³
Frequency
Range
Prior
Posterior

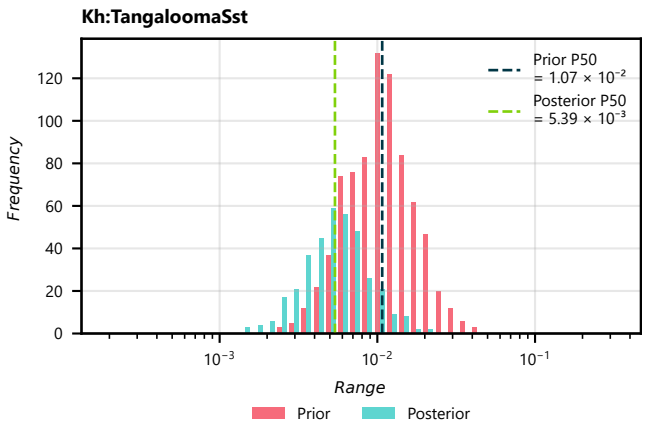
Kh:TangaloomaSst
Prior P50
= 1.07 × 10⁻²
Posterior P50
= 5.39 × 10⁻³
Frequency
Range
Prior
Posterior

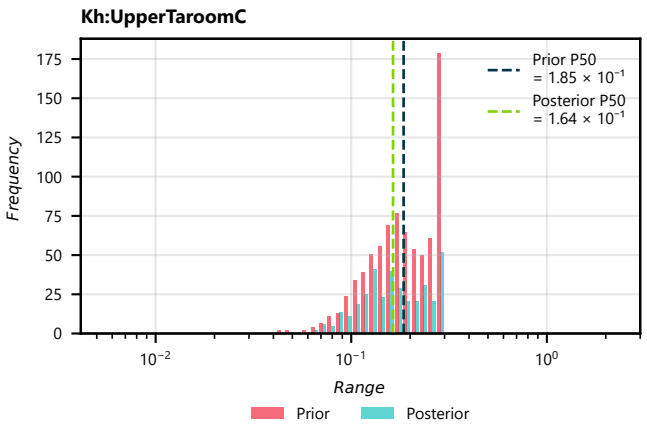
Kh:UpperTaroomC
Prior P50
= 1.85 × 10⁻¹
Posterior P50
= 1.64 × 10⁻¹
Frequency
Range
Prior
Posterior

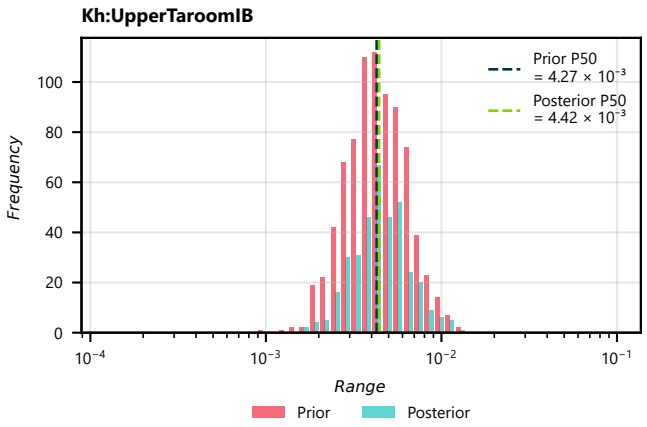
Kh:UpperTaroomIB
Prior P50
= 4.27 × 10⁻³
Posterior P50
= 4.42 × 10⁻³
Frequency
Range
Prior
Posterior

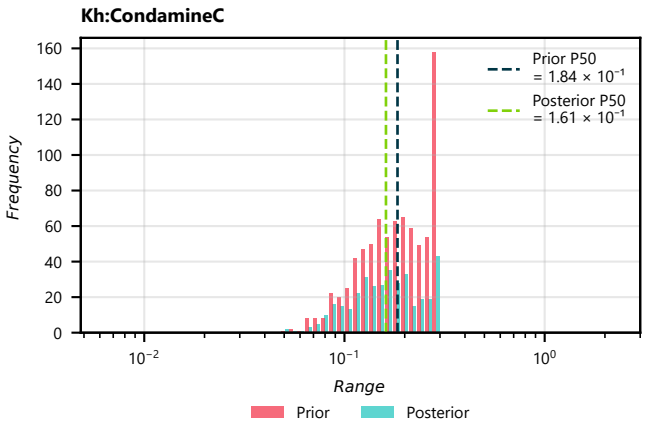
Kh:CondamineC
Prior P50
= 1.84 × 10⁻¹
Posterior P50
= 1.61 × 10⁻¹
Frequency
Range
Prior
Posterior

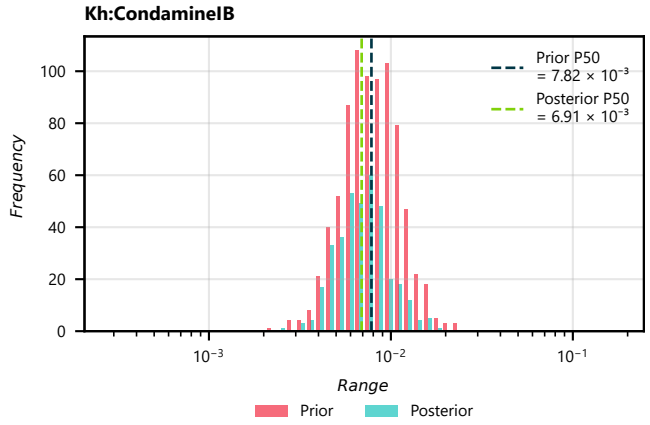
Kh:CondamineIB
Prior P50
= 7.82 × 10⁻³
Posterior P50
= 6.91 × 10⁻³
Frequency
Range
Prior
Posterior

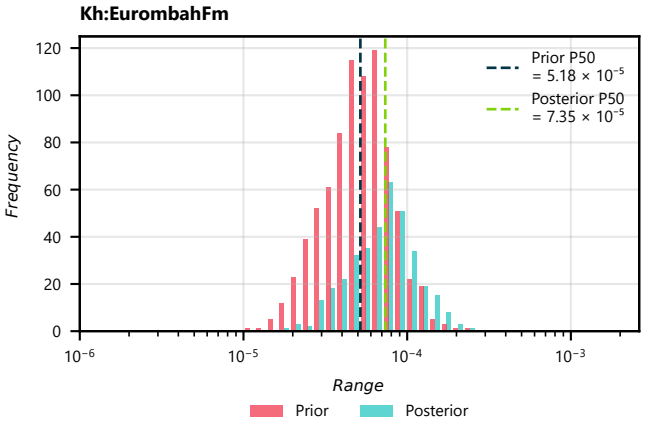
Kh:EurombahFm
Prior P50
= 5.18 × 10⁻⁵
Posterior P50
= 7.35 × 10⁻⁵
Frequency
Range
Prior
Posterior

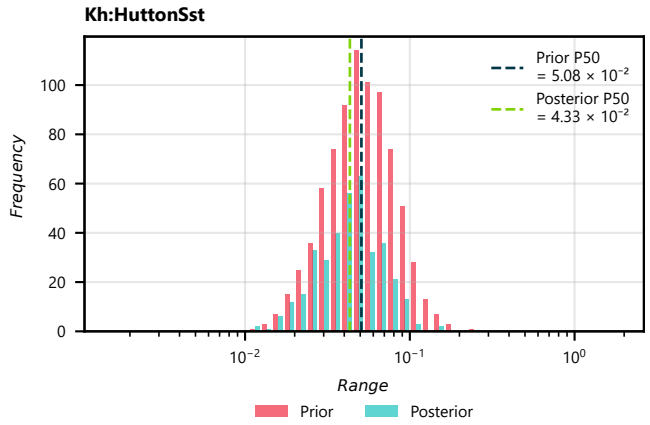
Kh:HuttonSst
Prior P50
= 5.08 × 10⁻²
Posterior P50
= 4.33 × 10⁻²
Frequency
Range
Prior
Posterior

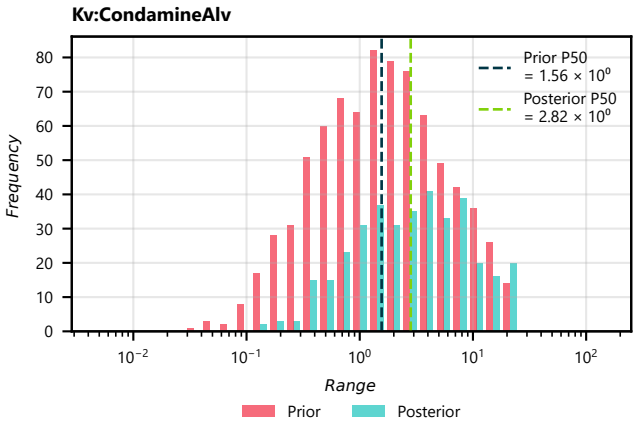
Kv:CondamineAlv
Prior P50
= 1.56 × 10⁰
Posterior P50
= 2.82 × 10⁰
Frequency
Range
Prior
Posterior

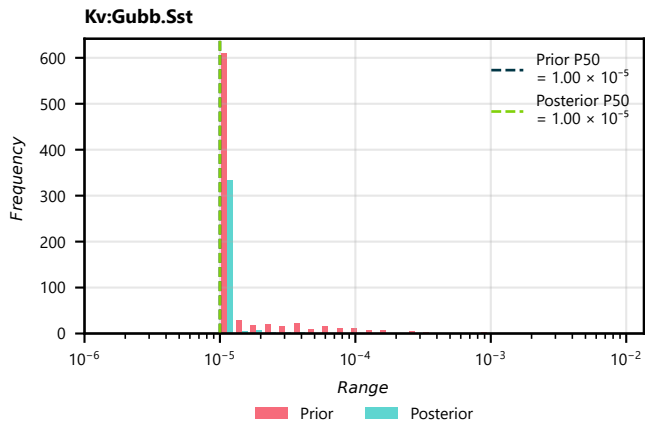
Kv:Gubb.Sst
Prior P50
= 1.00 × 10⁻⁵
Posterior P50
= 1.00 × 10⁻⁵
Frequency
Range
Prior
Posterior

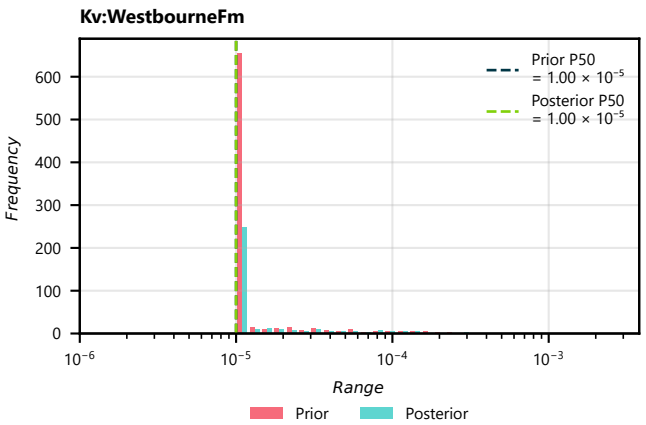
Kv:WestbourneFm
Prior P50
= 1.00 × 10⁻⁵
Posterior P50
= 1.00 × 10⁻⁵
Frequency
Range
Prior
Posterior

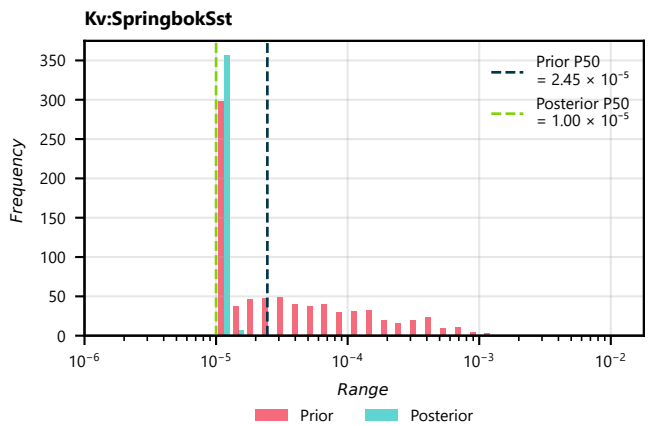
Kv:SpringbokSst
Prior P50
= 2.45 × 10⁻⁵
Posterior P50
= 1.00 × 10⁻⁵
Frequency
Range
Prior
Posterior

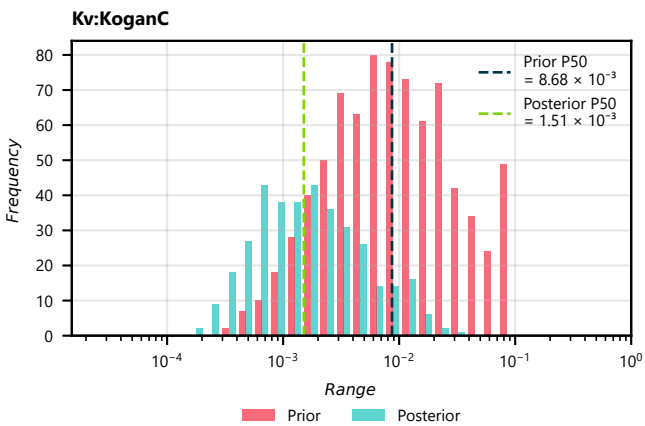
Kv:KoganC
Prior P50
= 8.68 × 10⁻³
Posterior P50
= 1.51 × 10⁻³
Frequency
Range
Prior
Posterior

Kv:KoganIB

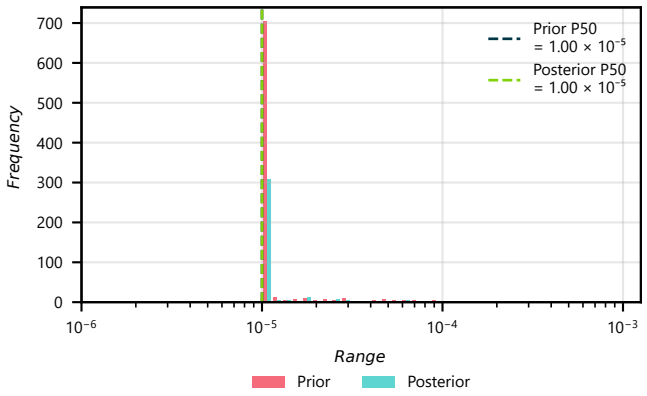

Kv:MacalisterC

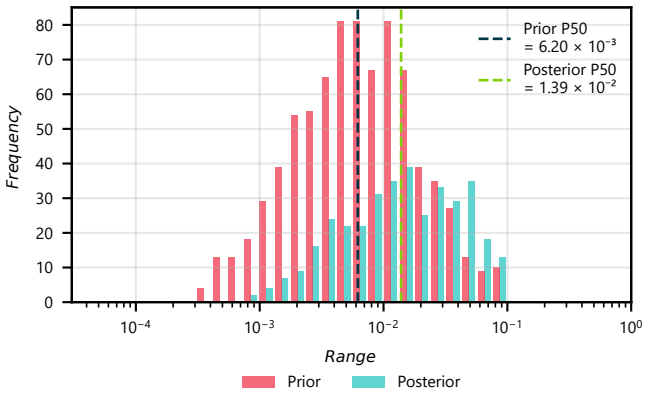

Kv:MacalisterIB

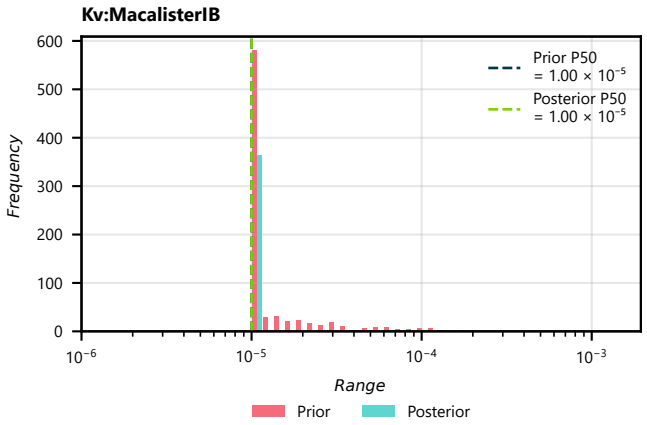

Kv:WamboC

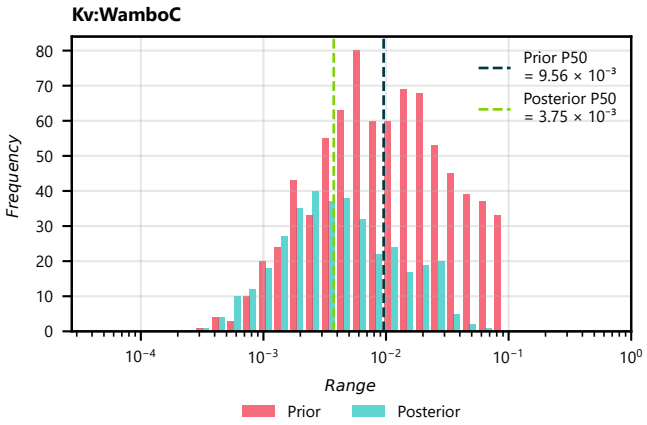

Kv:WamboIB

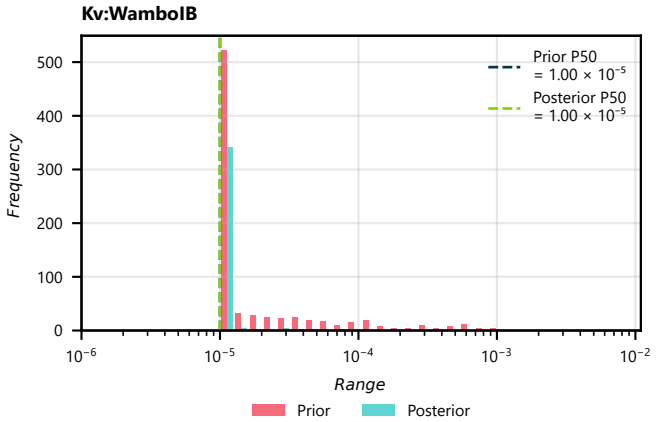

Kv:ArgyleC

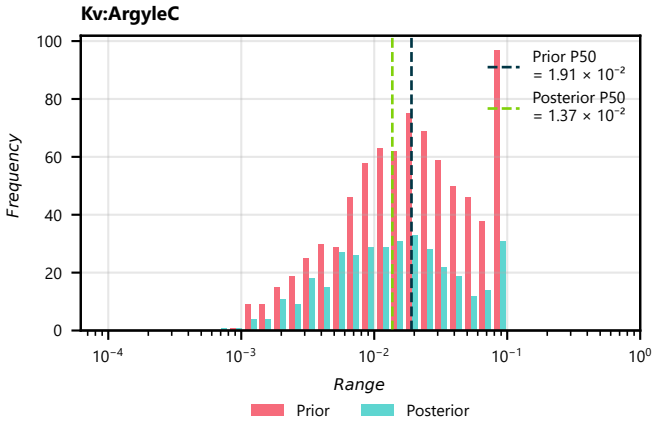

Kv:ArgyleIB

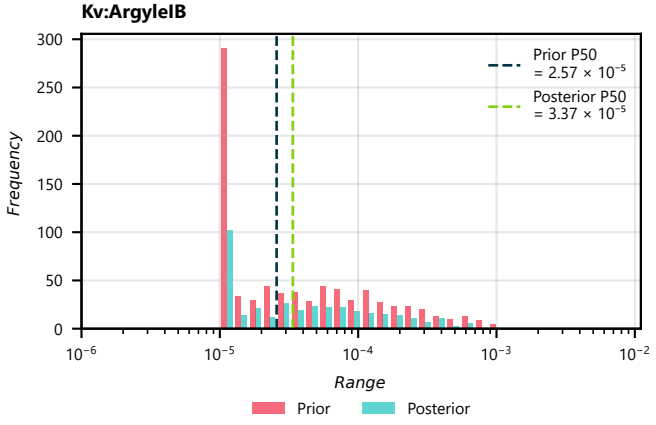

Kv:TangaloomaSst

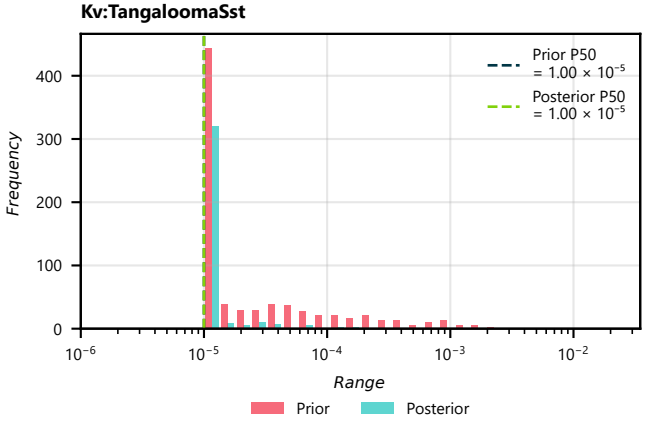

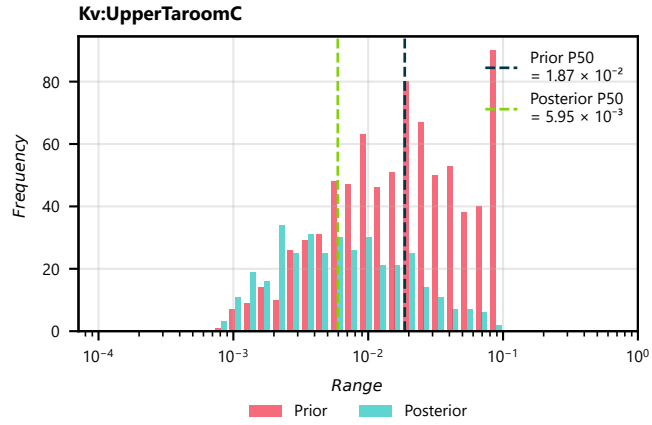
Kv:UpperTaroomC
Prior P50
= 1.87 × 10⁻²
Posterior P50
= 5.95 × 10⁻³
Frequency
Range
Prior
Posterior

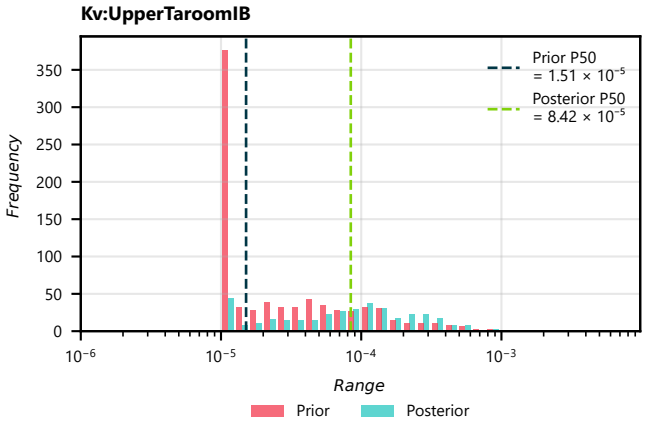
Kv:UpperTaroomIB
Prior P50
= 1.51 × 10⁻⁵
Posterior P50
= 8.42 × 10⁻⁵
Frequency
Range
Prior
Posterior

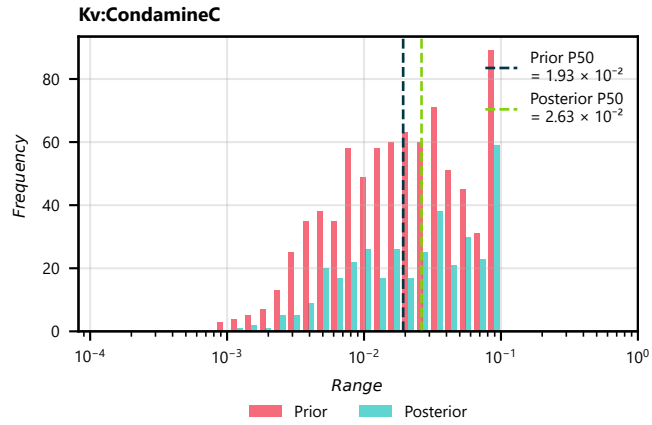
Kv:CondamineC
Prior P50
= 1.93 × 10⁻²
Posterior P50
= 2.63 × 10⁻²
Frequency
Range
Prior
Posterior

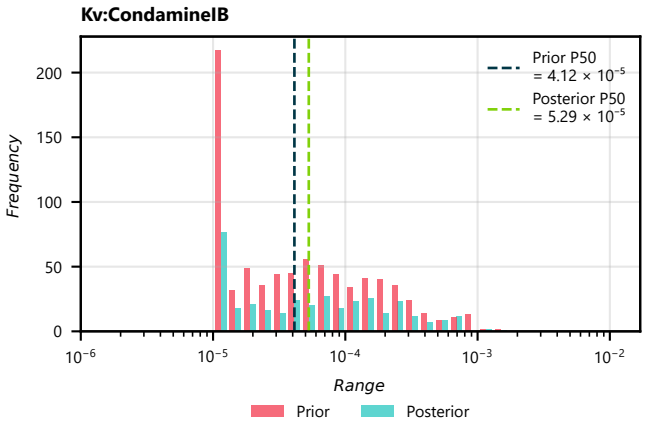
Kv:CondamineIB
Prior P50
= 4.12 × 10⁻⁵
Posterior P50
= 5.29 × 10⁻⁵
Frequency
Range
Prior
Posterior

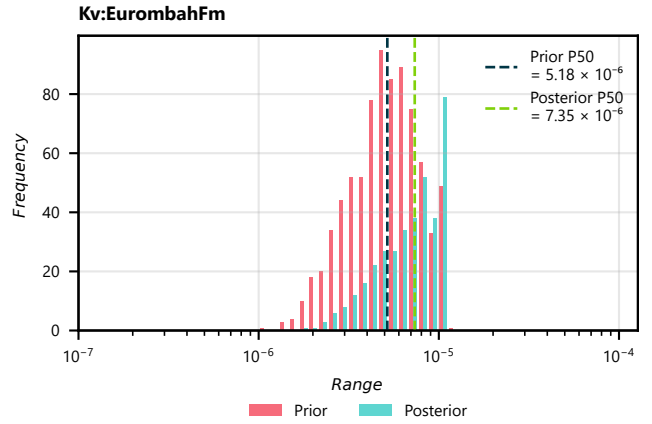
Kv:EurombahFm
Prior P50
= 5.18 × 10⁻⁶
Posterior P50
= 7.35 × 10⁻⁶
Frequency
Range
Prior
Posterior

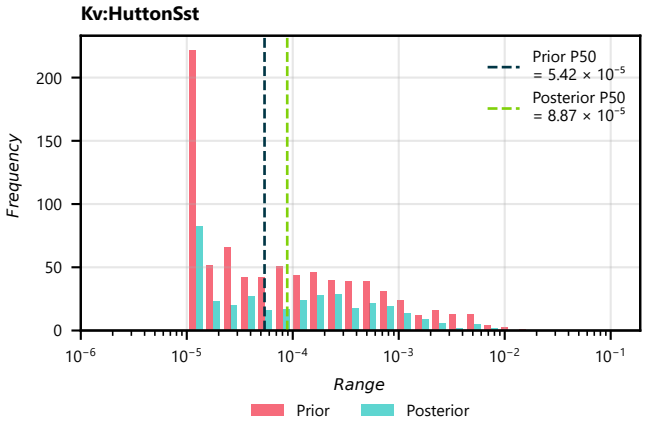
Kv:HuttonSst
Prior P50
= 5.42 × 10⁻⁵
Posterior P50
= 8.87 × 10⁻⁵
Frequency
Range
Prior
Posterior

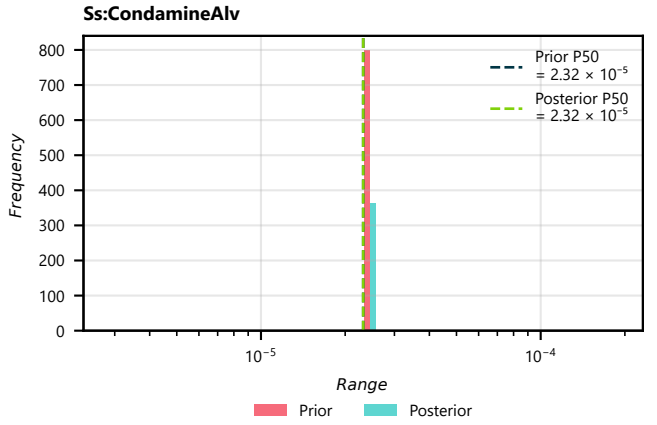
Ss:CondamineAlv
Prior P50
= 2.32 × 10⁻⁵
Posterior P50
= 2.32 × 10⁻⁵
Frequency
Range
Prior
Posterior

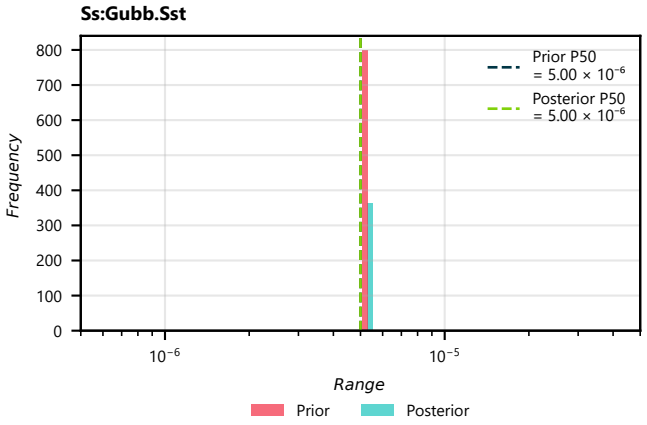
Ss:Gubb.Sst
Prior P50
= 5.00 × 10⁻⁶
Posterior P50
= 5.00 × 10⁻⁶
Frequency
Range
Prior
Posterior

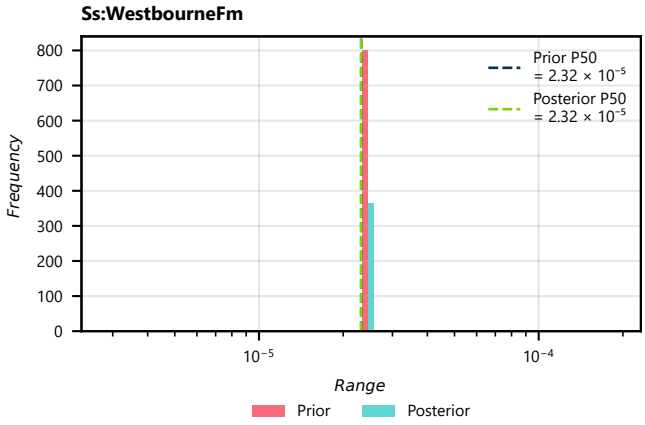
Ss:WestbourneFm
Prior P50
= 2.32 × 10⁻⁵
Posterior P50
= 2.32 × 10⁻⁵
Frequency
Range
Prior
Posterior

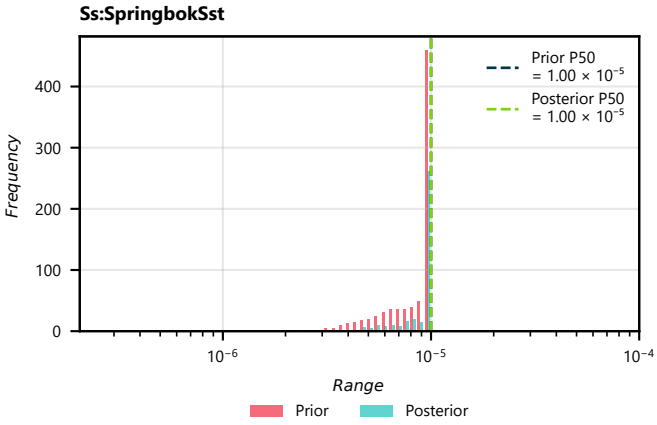
Ss:SpringbokSst
Prior P50
= 1.00 × 10⁻⁵
Posterior P50
= 1.00 × 10⁻⁵
Frequency
Range
Prior
Posterior

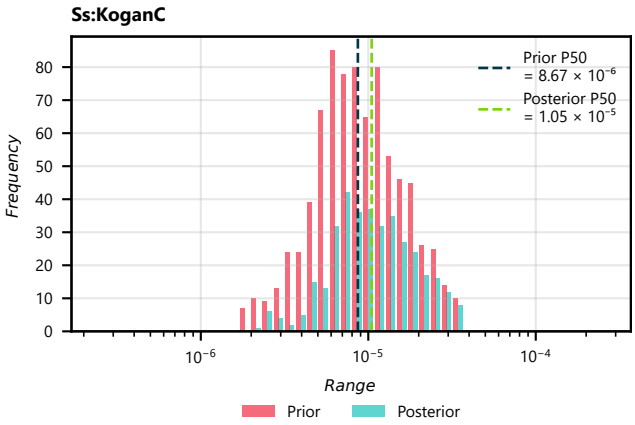
Ss:KoganC
Prior P50
= 8.67 × 10⁻⁶
Posterior P50
= 1.05 × 10⁻⁵
Frequency
Range
Prior
Posterior

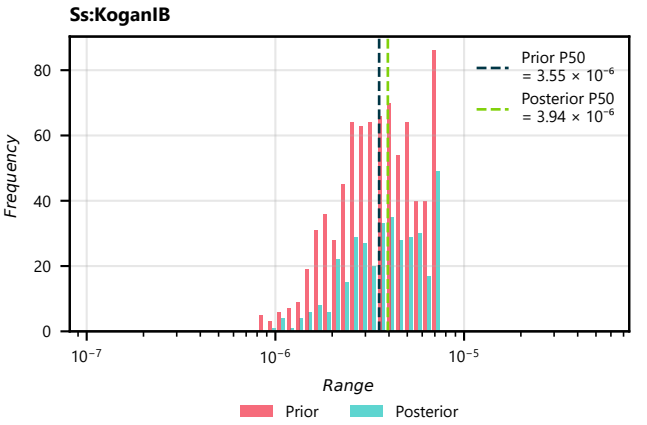
Ss:KoganIB
Prior P50
= 3.55 × 10⁻⁶
Posterior P50
= 3.94 × 10⁻⁶
Frequency
Range
Prior
Posterior

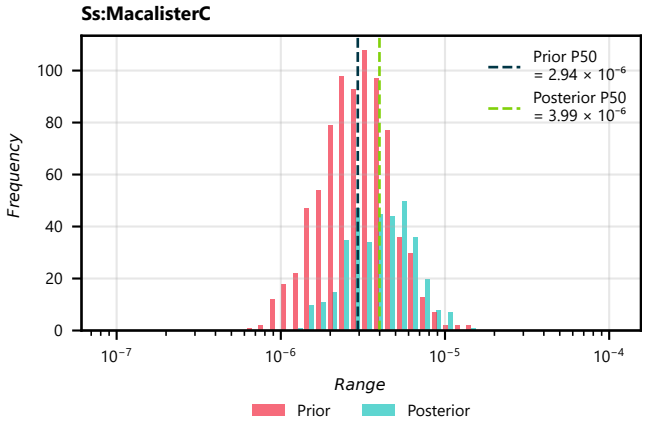
Ss:MacalisterC
Prior P50
= 2.94 × 10⁻⁶
Posterior P50
= 3.99 × 10⁻⁶
Frequency
Range
Prior
Posterior

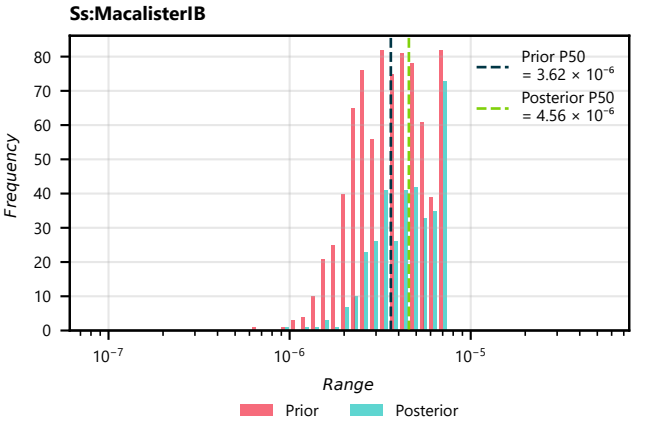
Ss:MacalisterIB
Prior P50
= 3.62 × 10⁻⁶
Posterior P50
= 4.56 × 10⁻⁶
Frequency
Range
Prior
Posterior

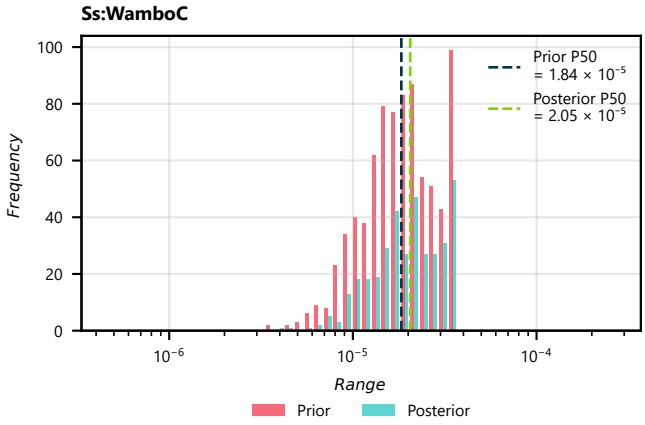
Ss:WamboC
Prior P50
= 1.84 × 10⁻⁵
Posterior P50
= 2.05 × 10⁻⁵
Frequency
Range
Prior
Posterior

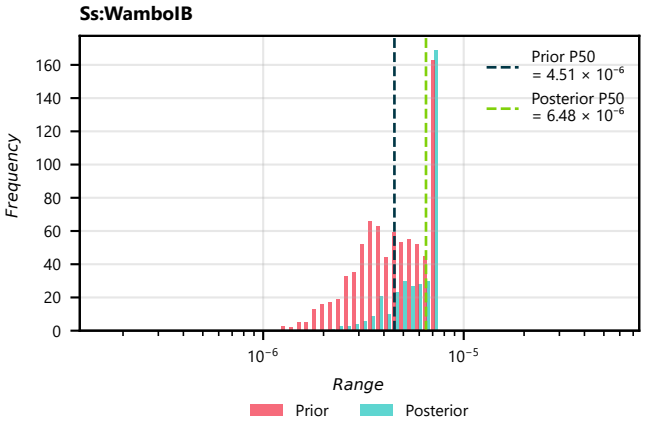
Ss:WamboIB
Prior P50
= 4.51 × 10⁻⁶
Posterior P50
= 6.48 × 10⁻⁶
Frequency
Range
Prior
Posterior

Ss:ArgyleC

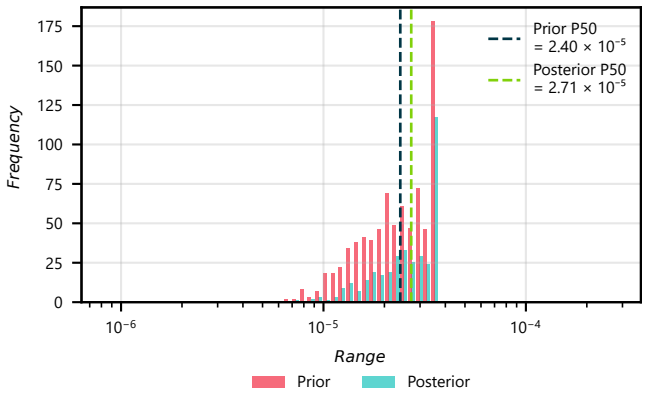

Ss:ArgyleIB

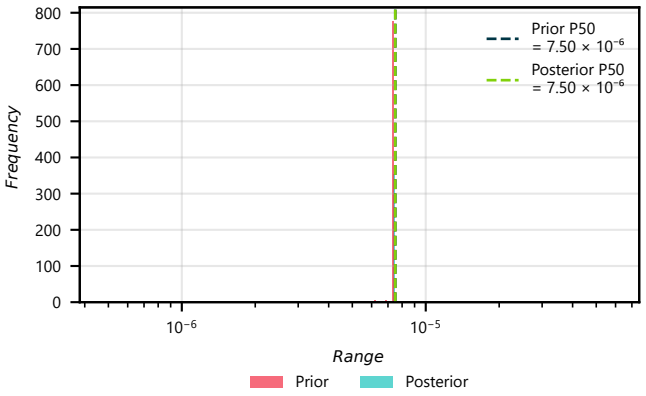

Ss:TangaloomaSst

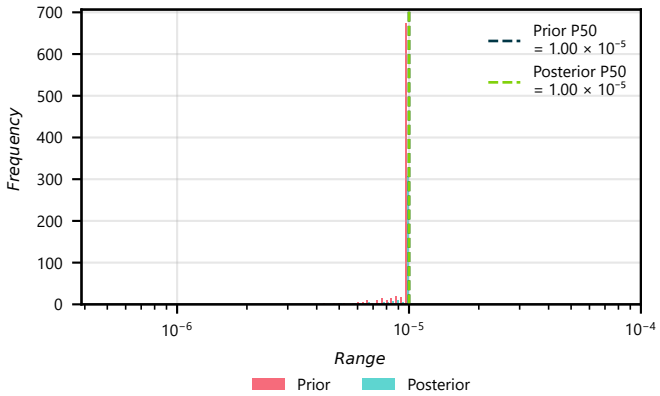

Ss:UpperTaroomC

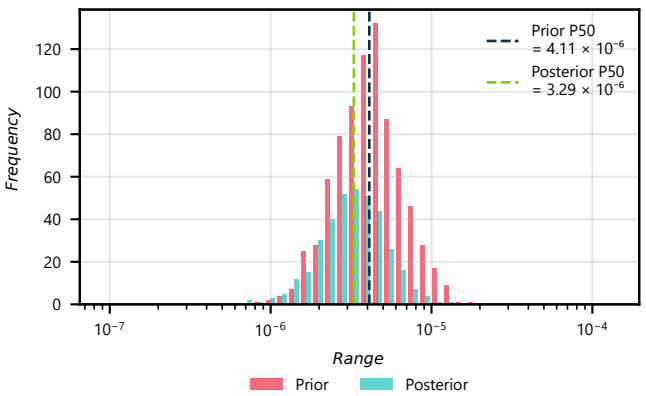

Ss:UpperTaroomIB

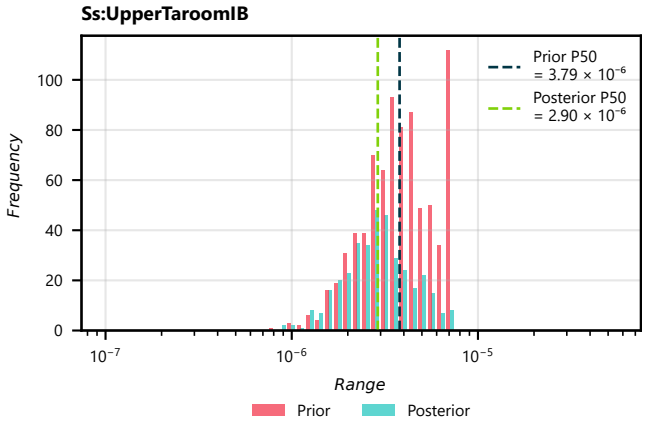

Ss:CondamineC

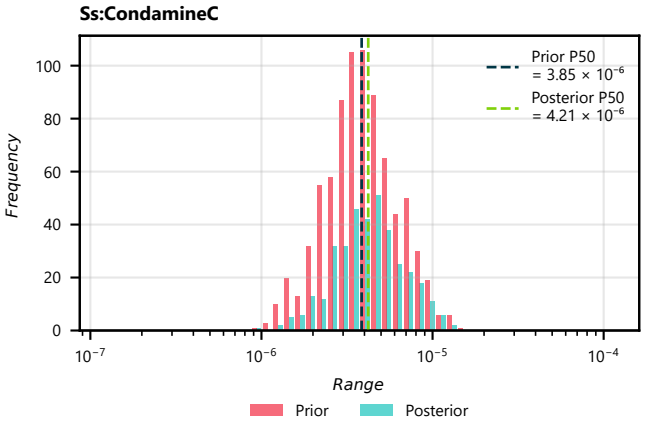

Ss:CondamineIB

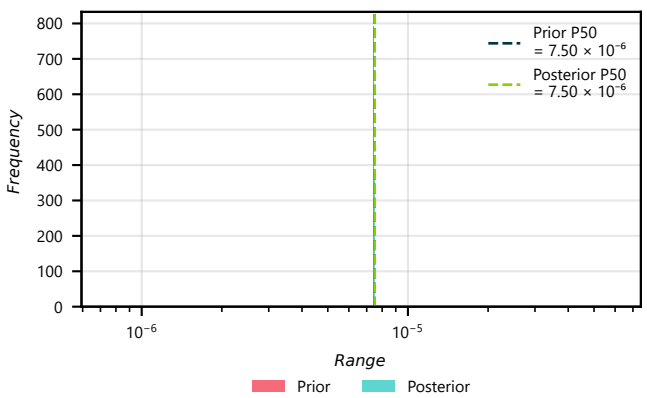

Ss:EurombahFm

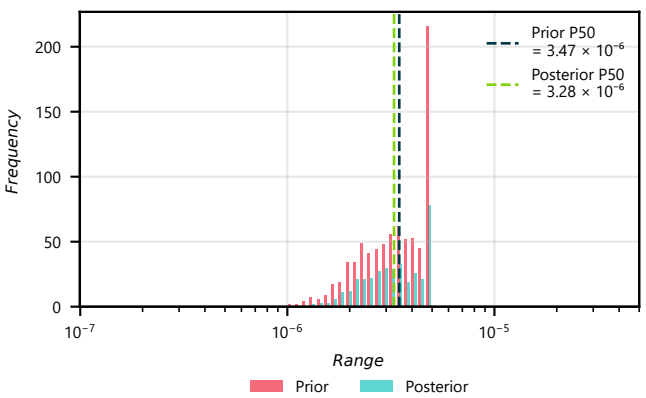

Ss:HuttonSst

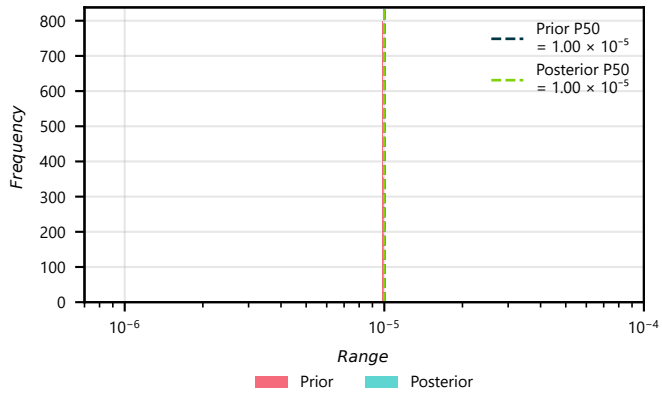

Sy:CondamineAlv

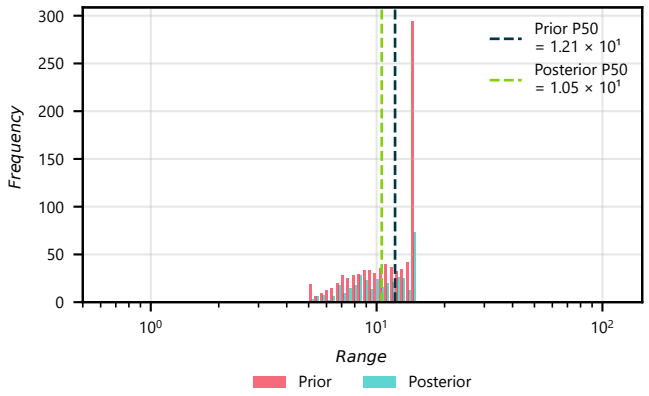

Sy:Gubb.Sst

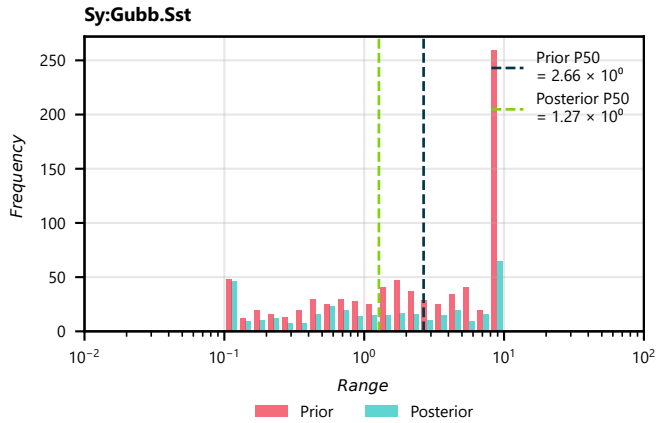

Sy:WestbourneFm

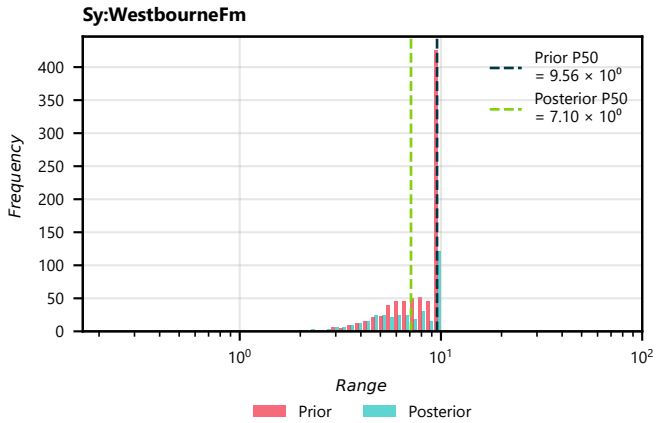

Sy:SpringbokSst

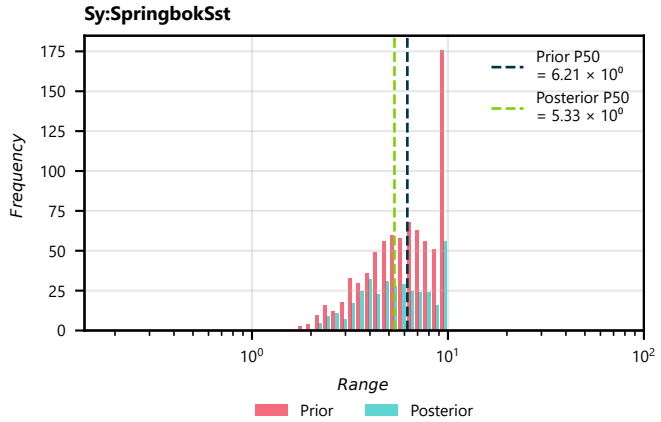

Sy:KoganC

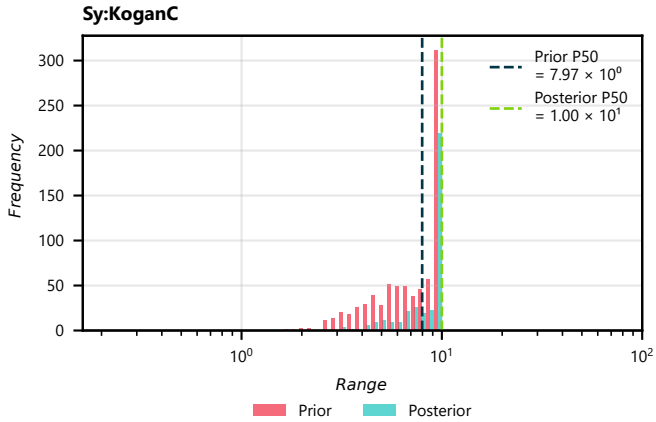

Sy:KoganIB

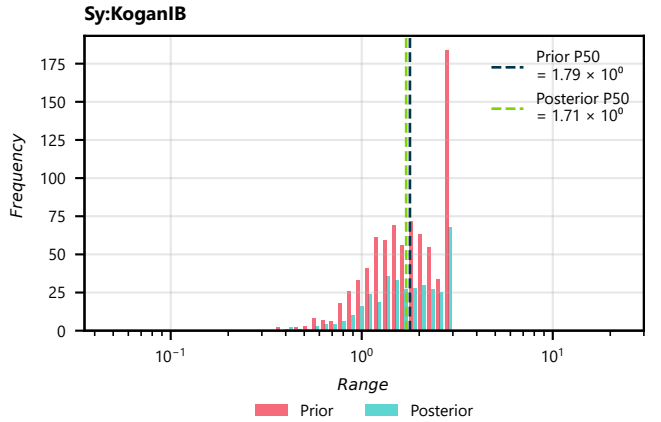

Sy:MacalisterC

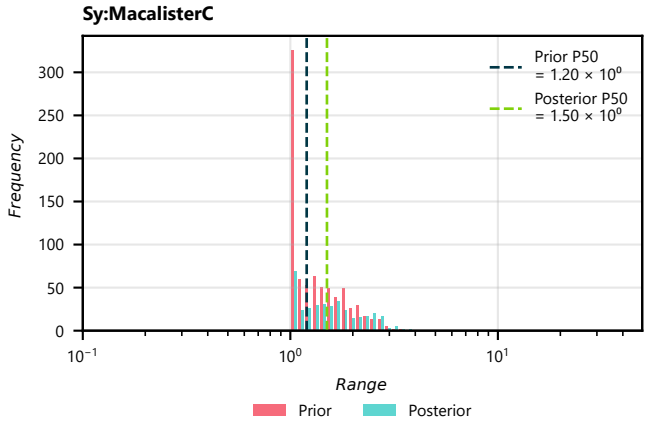

Sy:MacalisterIB

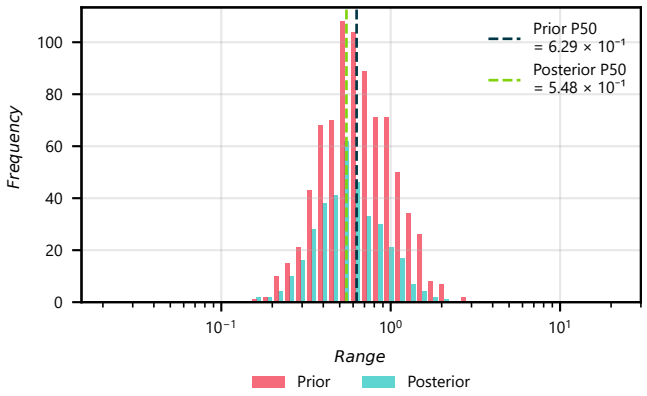

Sy:WamboC

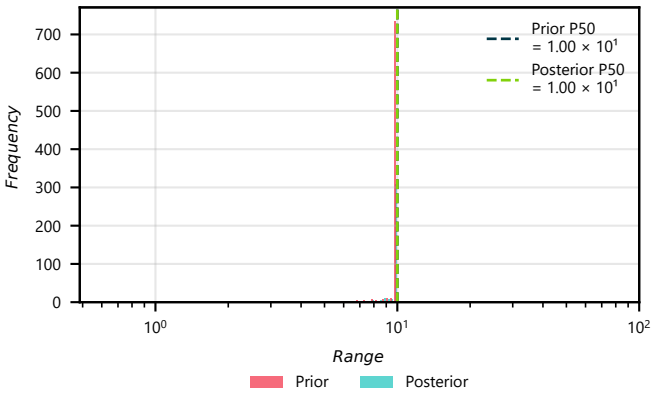

Sy:WamboIB

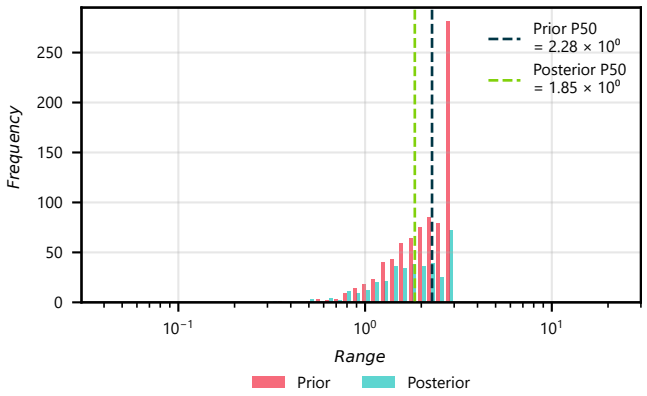

Sy:ArgyleC

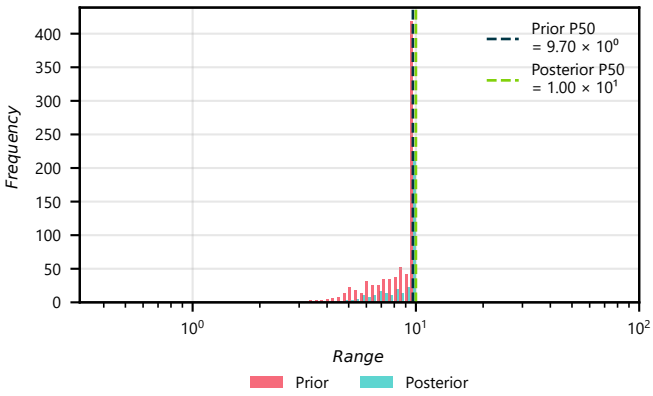

Sy:ArgyleIB

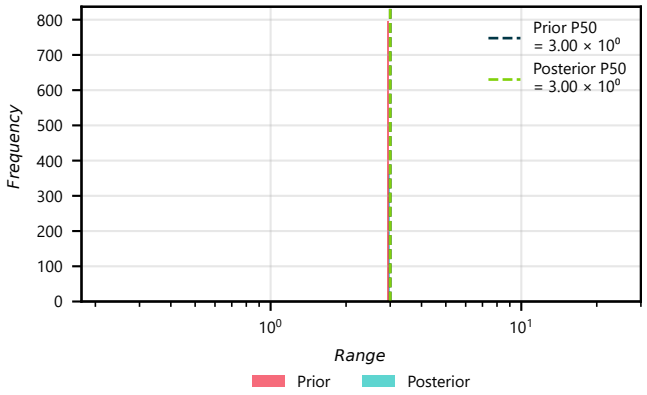

Sy:TangaloomaSst

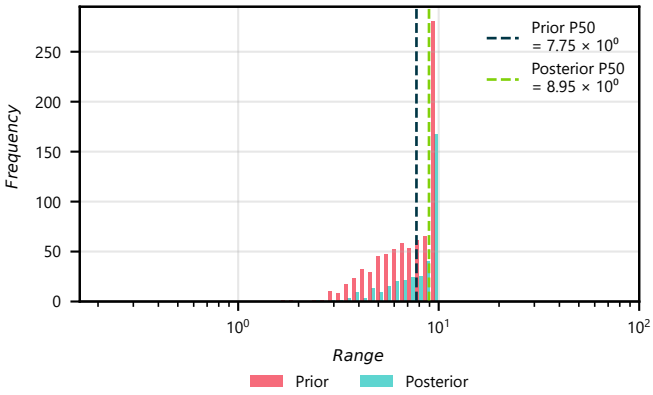

Sy:UpperTaroomC

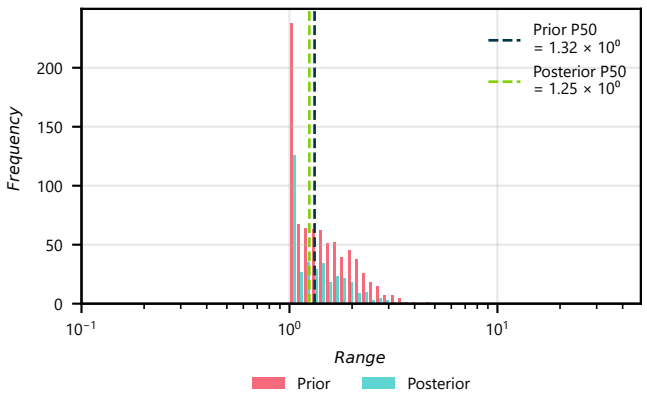

Sy:UpperTaroomIB

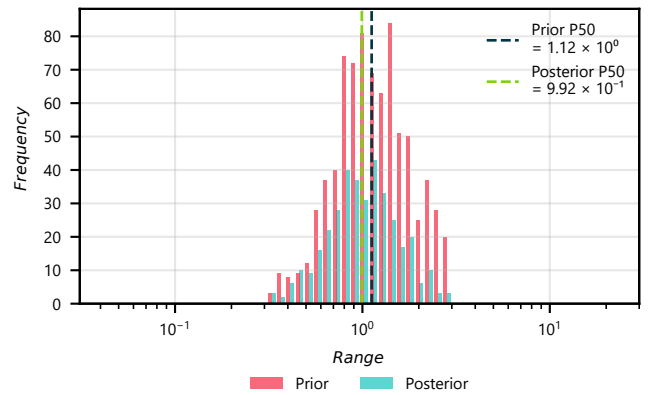

Sy:CondamineC

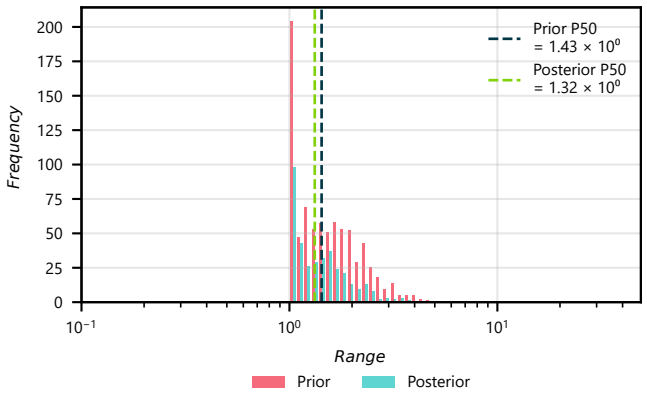

Sy:CondamineIB

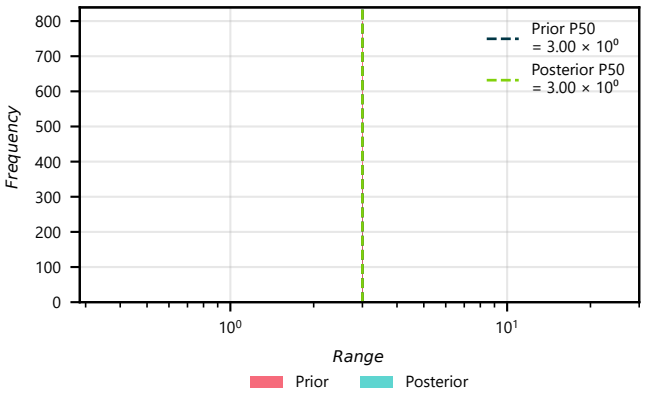

Sy:EurombahFm

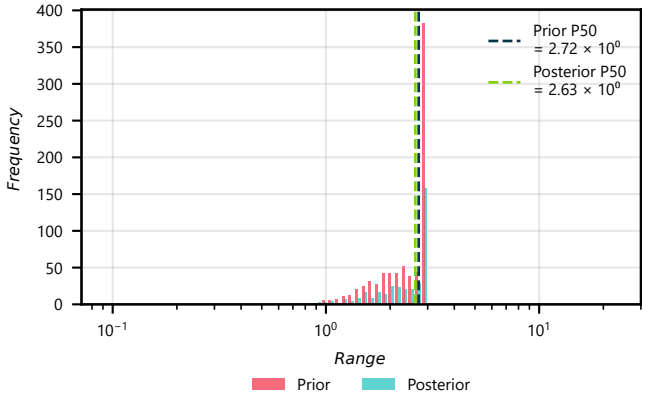

Sy:HuttonSst

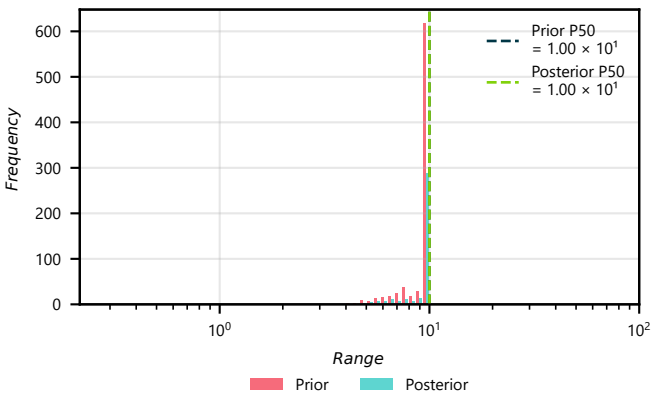

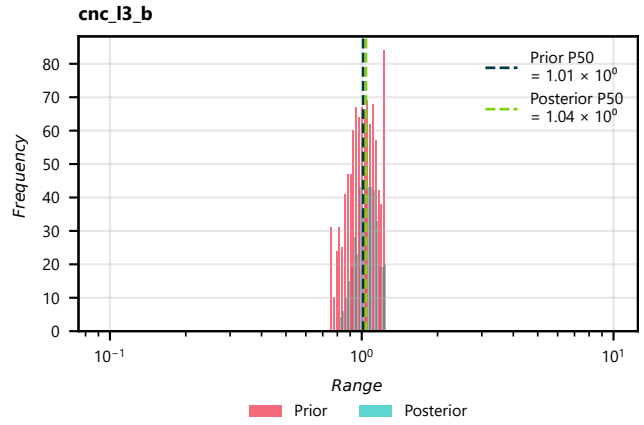
cnc_l3_b
Prior P50
= 1.01 × 10⁰
Posterior P50
= 1.04 × 10⁰
Frequency
Range
Prior
Posterior

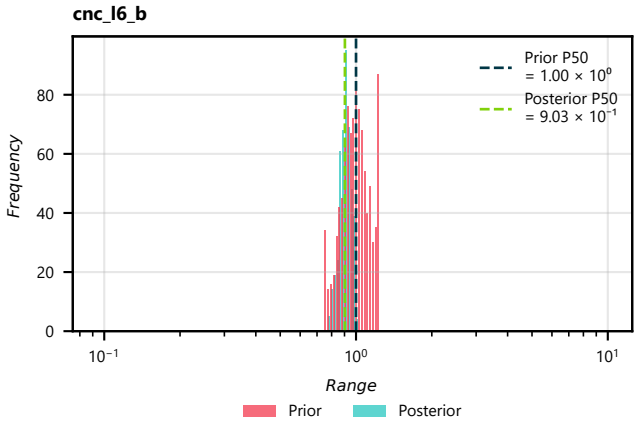
cnc_l6_b
Prior P50
= 1.00 × 10⁰
Posterior P50
= 9.03 × 10⁻¹
Frequency
Range
Prior
Posterior

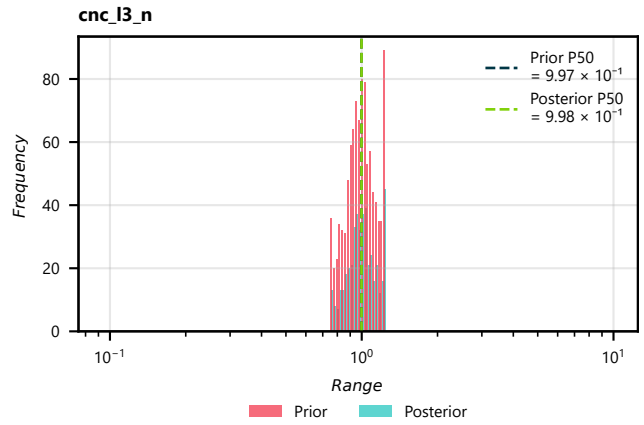
cnc_l3_n
Prior P50
= 9.97 × 10⁻¹
Posterior P50
= 9.98 × 10⁻¹
Frequency
Range
Prior
Posterior

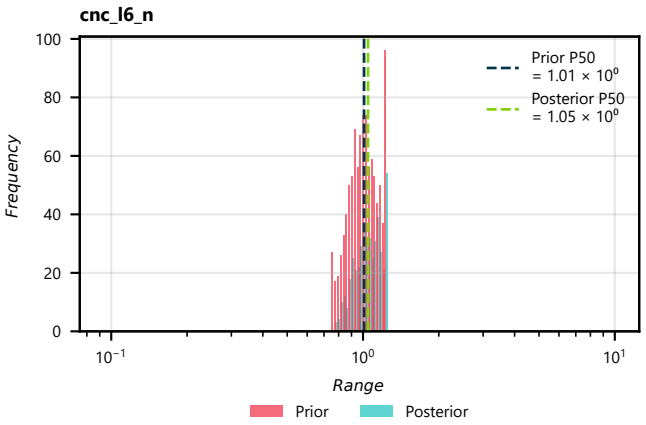
cnc_l6_n
Prior P50
= 1.01 × 10⁰
Posterior P50
= 1.05 × 10⁰
Frequency
Range
Prior
Posterior

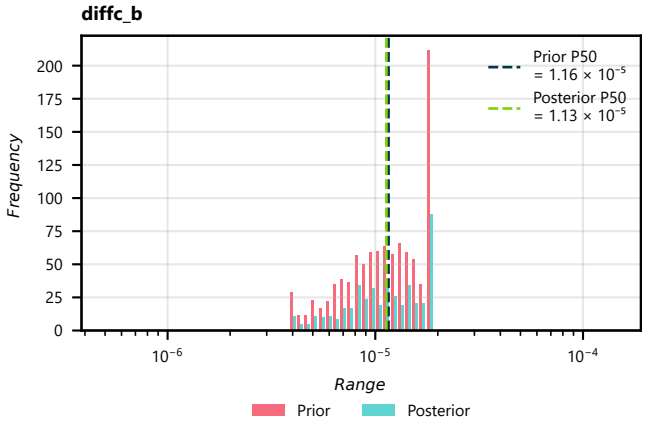
diffc_b
Prior P50
= 1.16 × 10⁻⁵
Posterior P50
= 1.13 × 10⁻⁵
Frequency
Range
Prior
Posterior

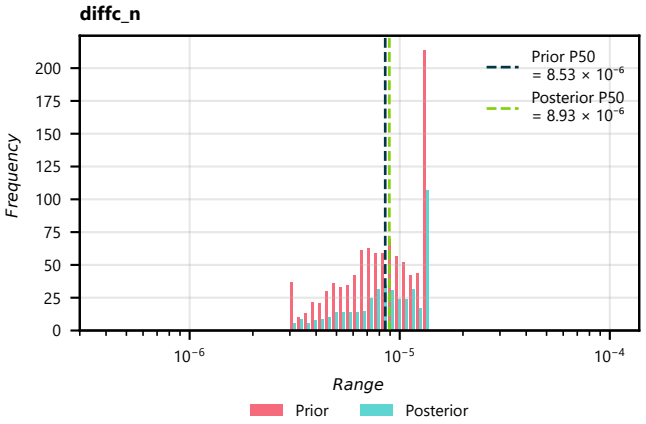
diffc_n
Prior P50
= 8.53 × 10⁻⁶
Posterior P50
= 8.93 × 10⁻⁶
Frequency
Range
Prior
Posterior

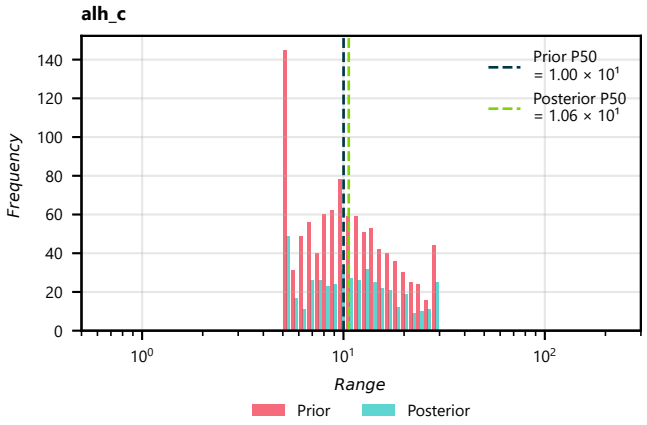
alh_c
Prior P50
= 1.00 × 10¹
Posterior P50
= 1.06 × 10¹
Frequency
Range
Prior
Posterior

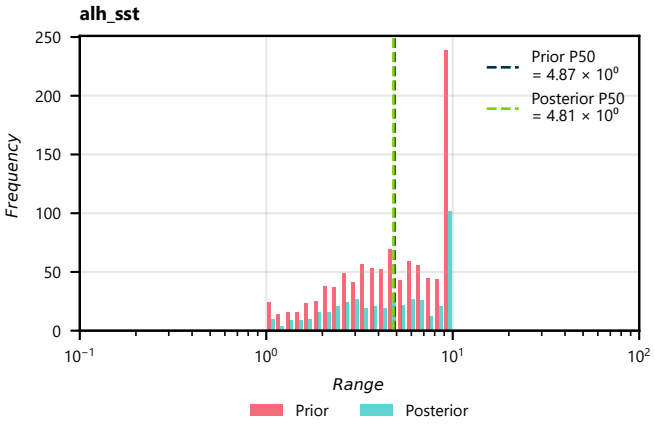
alh_sst
Prior P50
= 4.87 × 10⁰
Posterior P50
= 4.81 × 10⁰
Frequency
Range
Prior
Posterior

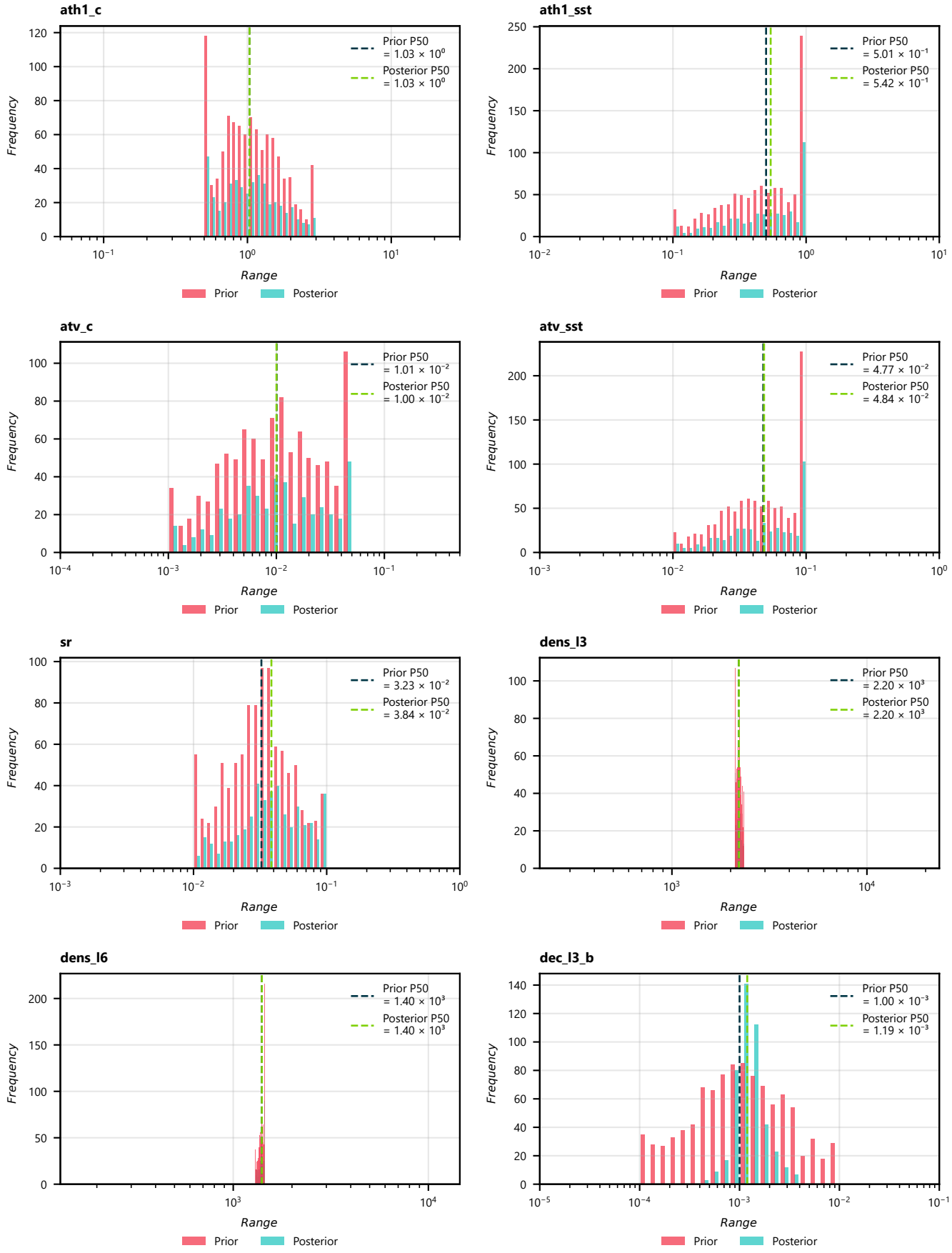
ath1_c
Prior P50 = 1.03 × 10⁰
Posterior P50 = 1.03 × 10⁰
ath1_sst
Prior P50 = 5.01 × 10⁻¹
Posterior P50 = 5.42 × 10⁻¹
atv_c
Prior P50 = 1.01 × 10⁻²
Posterior P50 = 1.00 × 10⁻²
atv_sst
Prior P50 = 4.77 × 10⁻²
Posterior P50 = 4.84 × 10⁻²
sr
Prior P50 = 3.23 × 10⁻²
Posterior P50 = 3.84 × 10⁻²
dens_l3
Prior P50 = 2.20 × 10³
Posterior P50 = 2.20 × 10³
dens_l6
Prior P50 = 1.40 × 10³
Posterior P50 = 1.40 × 10³
dec_l3_b
Prior P50 = 1.00 × 10⁻³
Posterior P50 = 1.19 × 10⁻³
Frequency
Range
Prior
Posterior

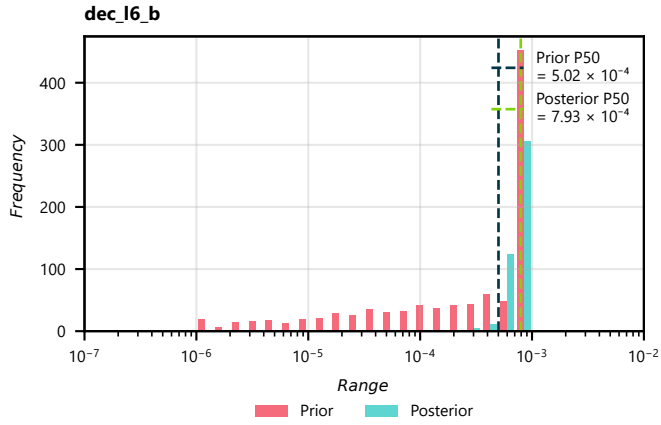
dec_l6_b
Prior P50
= 5.02 × 10⁻⁴
Posterior P50
= 7.93 × 10⁻⁴
Frequency
Range
Prior
Posterior

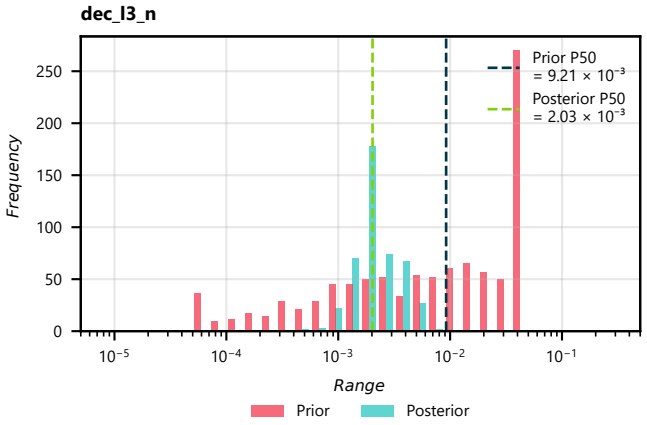
dec_l3_n
Prior P50
= 9.21 × 10⁻³
Posterior P50
= 2.03 × 10⁻³
Frequency
Range
Prior
Posterior

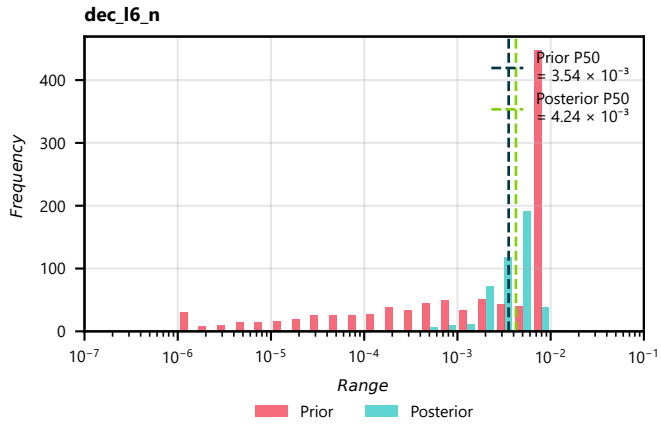
dec_l6_n
Prior P50
= 3.54 × 10⁻³
Posterior P50
= 4.24 × 10⁻³
Frequency
Range
Prior
Posterior

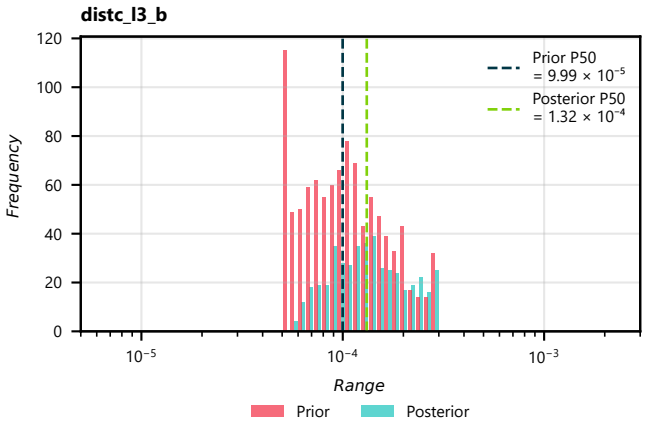
distc_l3_b
Prior P50
= 9.99 × 10⁻⁵
Posterior P50
= 1.32 × 10⁻⁴
Frequency
Range
Prior
Posterior

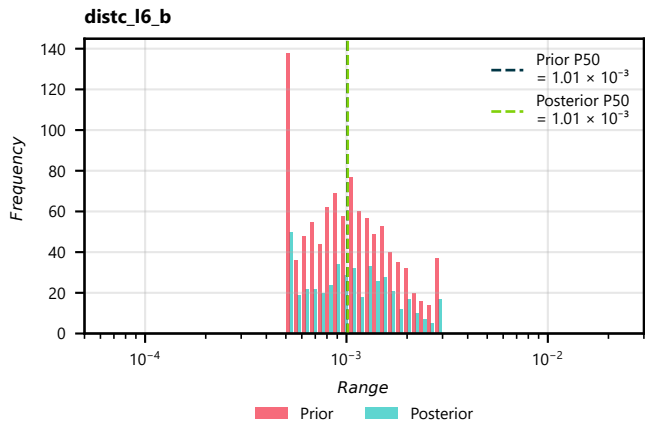
distc_l6_b
Prior P50
= 1.01 × 10⁻³
Posterior P50
= 1.01 × 10⁻³
Frequency
Range
Prior
Posterior

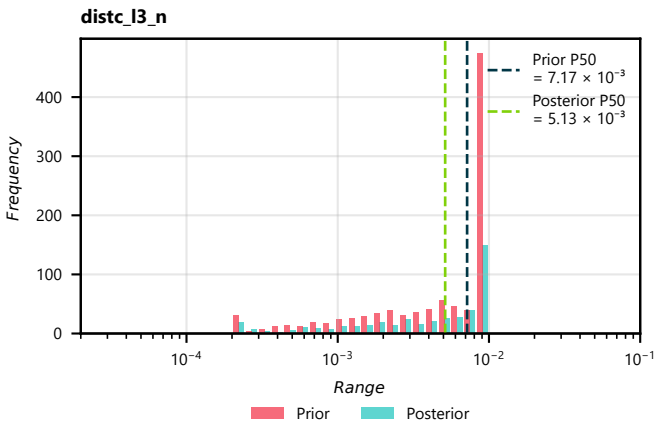
distc_l3_n
Prior P50
= 7.17 × 10⁻³
Posterior P50
= 5.13 × 10⁻³
Frequency
Range
Prior
Posterior

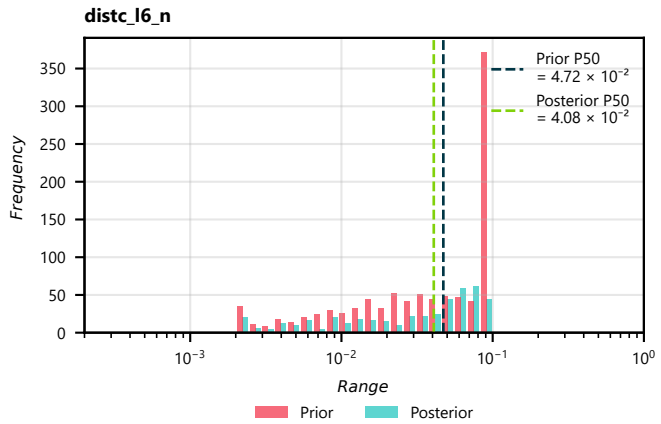
distc_l6_n
Prior P50
= 4.72 × 10⁻²
Posterior P50
= 4.08 × 10⁻²
Frequency
Range
Prior
Posterior

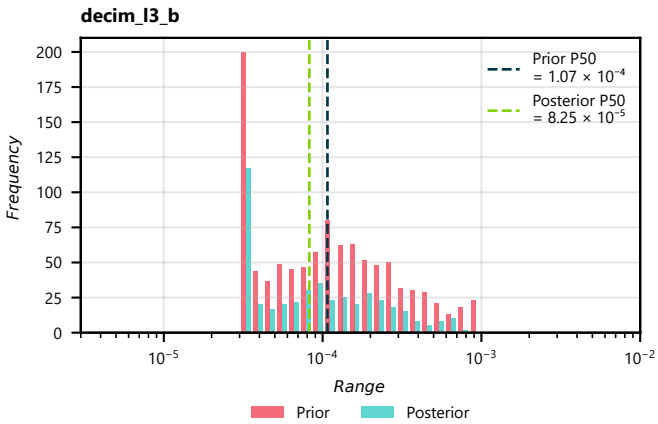
decim_l3_b
Prior P50
= 1.07 × 10⁻⁴
Posterior P50
= 8.25 × 10⁻⁵
Frequency
Range
Prior
Posterior

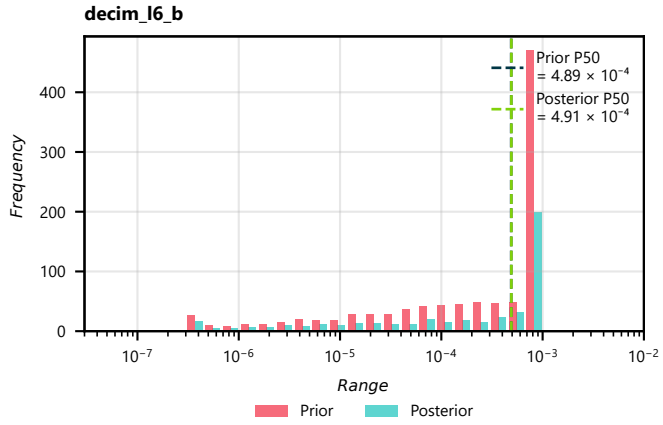
decim_l6_b
Prior P50
= 4.89 × 10⁻⁴
Posterior P50
= 4.91 × 10⁻⁴
Frequency
Range
Prior
Posterior

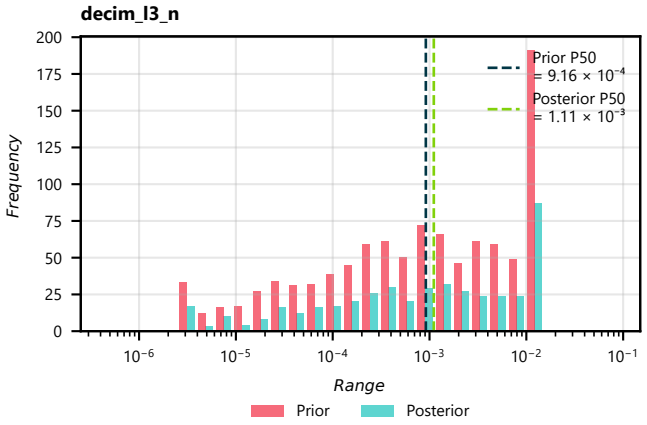
decim_l3_n
Prior P50
= 9.16 × 10⁻⁴
Posterior P50
= 1.11 × 10⁻³
Frequency
Range
Prior
Posterior

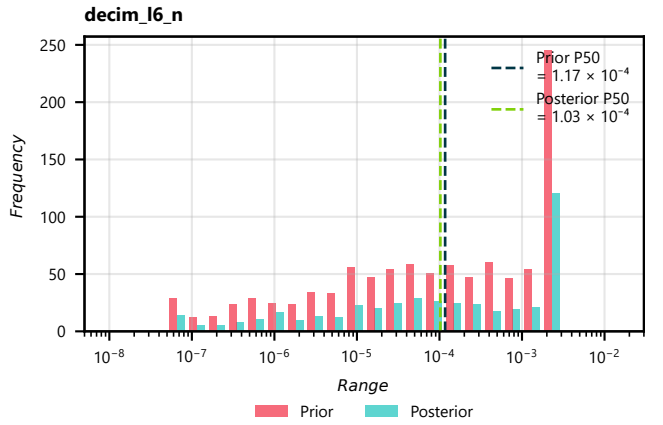
decim_l6_n
Prior P50
= 1.17 × 10⁻⁴
Posterior P50
= 1.03 × 10⁻⁴
Frequency
Range
Prior
Posterior

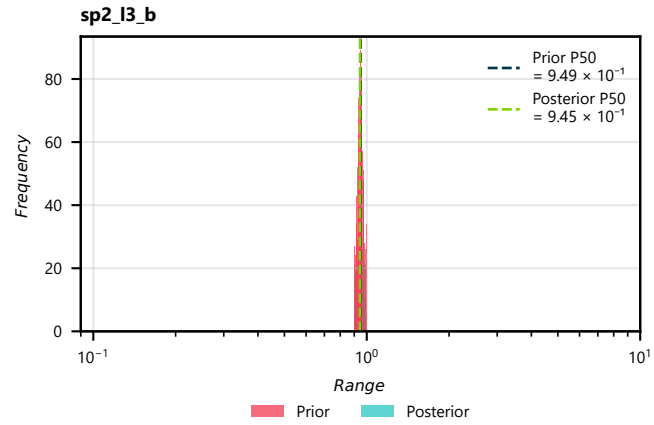
sp2_l3_b
Prior P50
= 9.49 × 10⁻¹
Posterior P50
= 9.45 × 10⁻¹
Frequency
Range
Prior
Posterior

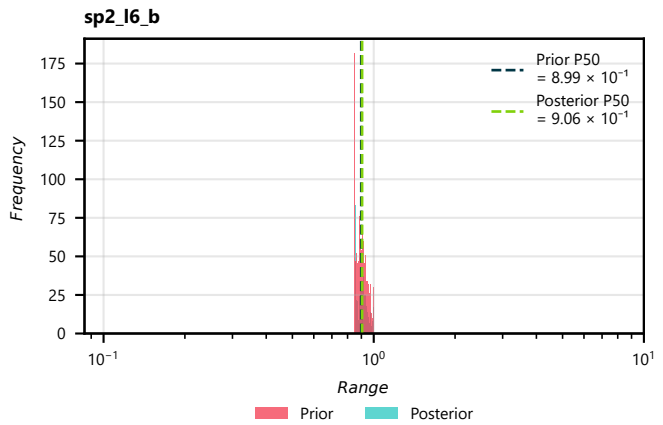
sp2_l6_b
Prior P50
= 8.99 × 10⁻¹
Posterior P50
= 9.06 × 10⁻¹
Frequency
Range
Prior
Posterior

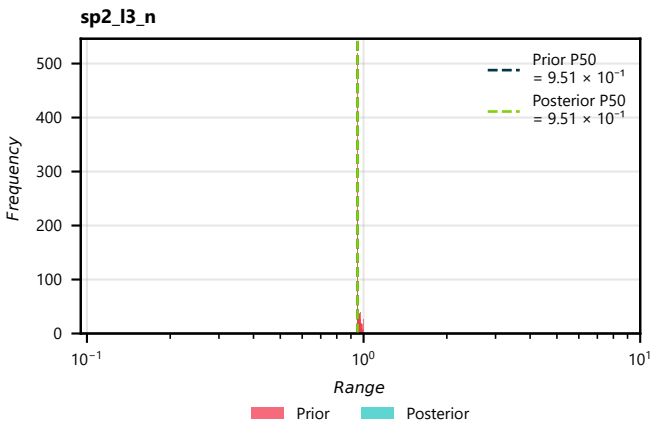
sp2_l3_n
Prior P50
= 9.51 × 10⁻¹
Posterior P50
= 9.51 × 10⁻¹
Frequency
Range
Prior
Posterior

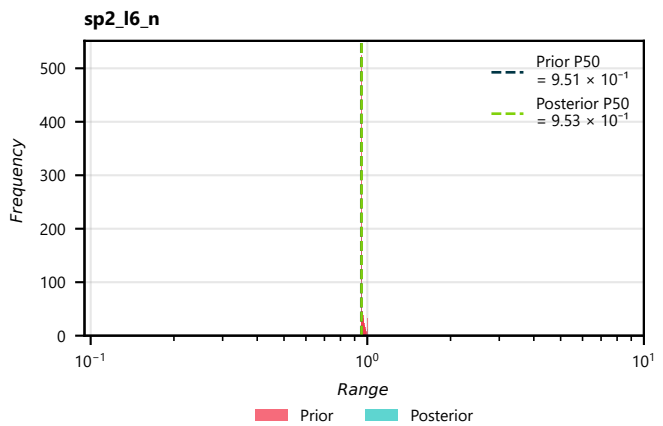
sp2_l6_n
Prior P50
= 9.51 × 10⁻¹
Posterior P50
= 9.53 × 10⁻¹
Frequency
Range
Prior
Posterior

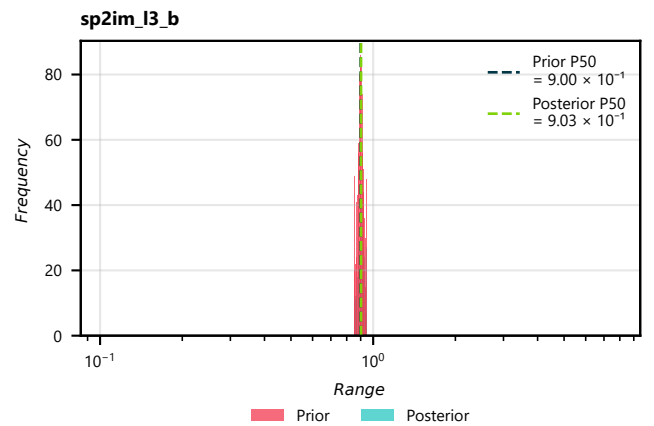
sp2im_l3_b
Prior P50
= 9.00 × 10⁻¹
Posterior P50
= 9.03 × 10⁻¹
Frequency
Range
Prior
Posterior

sp2im_l6_b

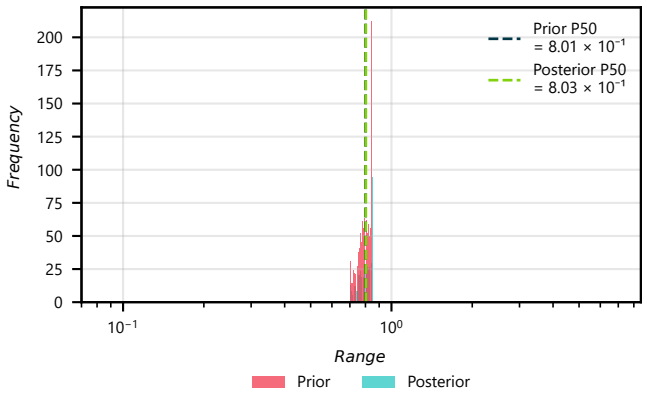

sp2im_l3_n

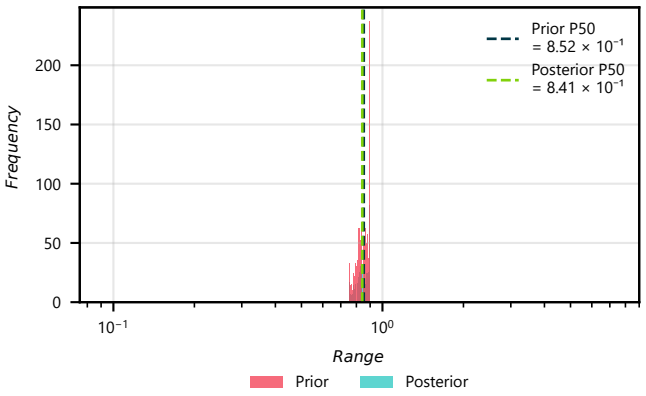

sp2im_l6_n

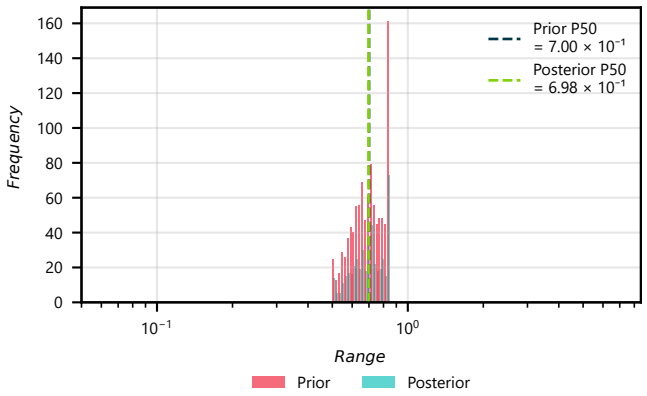

volfrac_l3

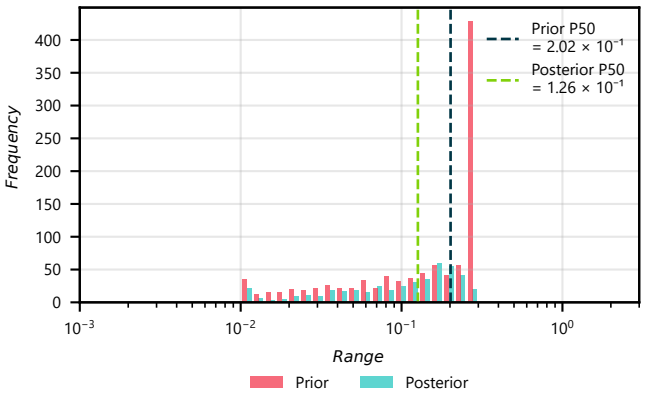

volfrac_l6

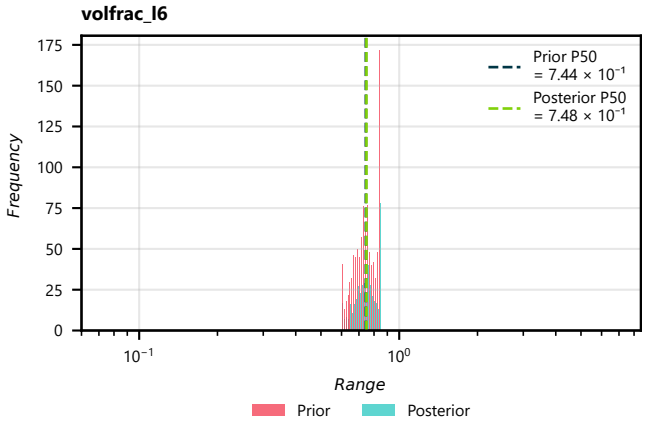

zetaim_l3

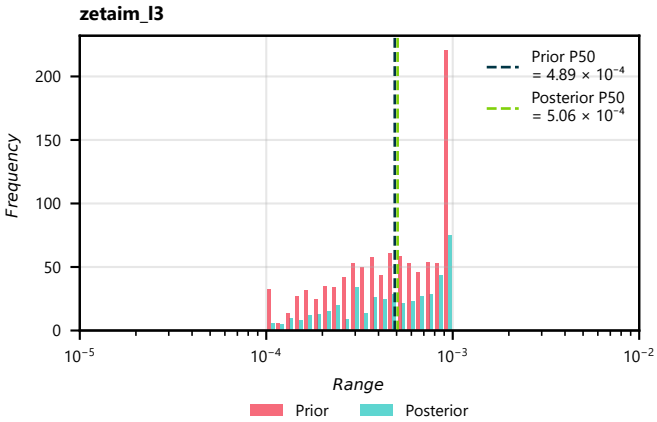

zetaim_l6

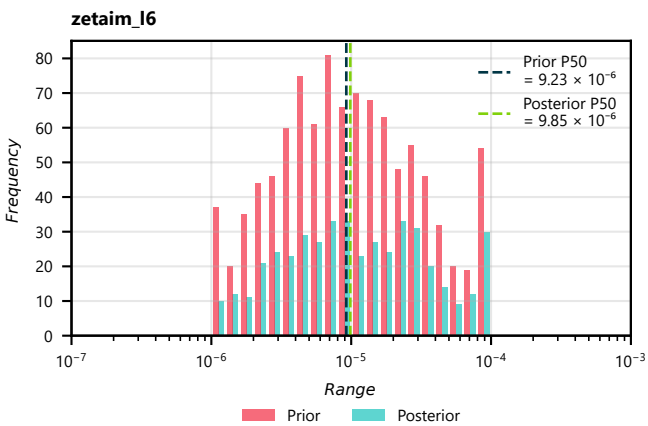

Appendix C. Modelled versus observed concentration time series plots – Benzene

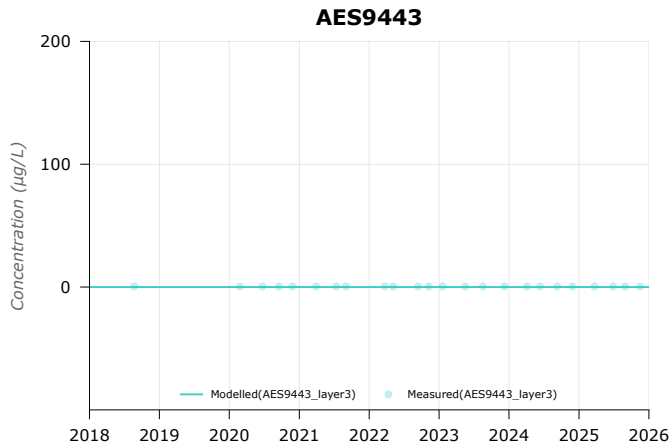
AES9443
Concentration (µg/L)
200
100
0
Modelled(AES9443_layer3)
Measured(AES9443_layer3)
2018
2019
2020
2021
2022
2023
2024
2025
2026

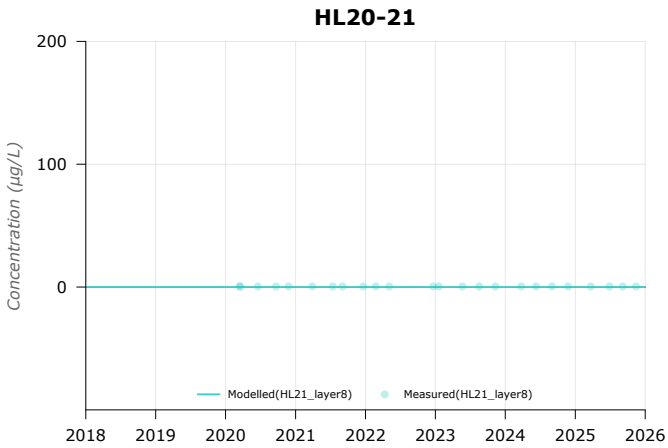
HL20-21
Concentration (µg/L)
200
100
0
Modelled(HL21_layer8)
Measured(HL21_layer8)
2018
2019
2020
2021
2022
2023
2024
2025
2026

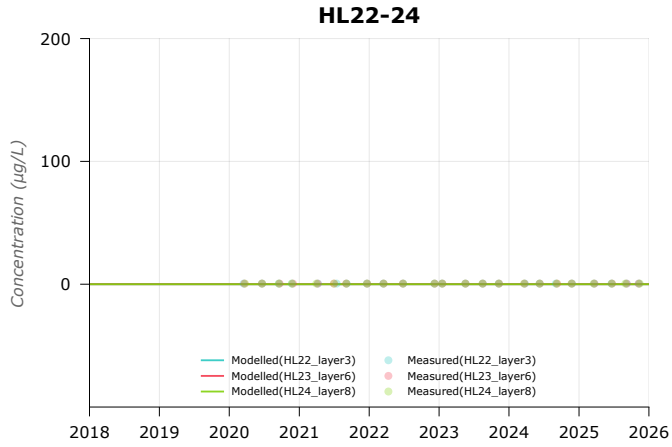
HL22-24
Concentration (µg/L)
200
100
0
Modelled(HL22_layer3)
Modelled(HL23_layer6)
Modelled(HL24_layer8)
Measured(HL22_layer3)
Measured(HL23_layer6)
Measured(HL24_layer8)
2018
2019
2020
2021
2022
2023
2024
2025
2026

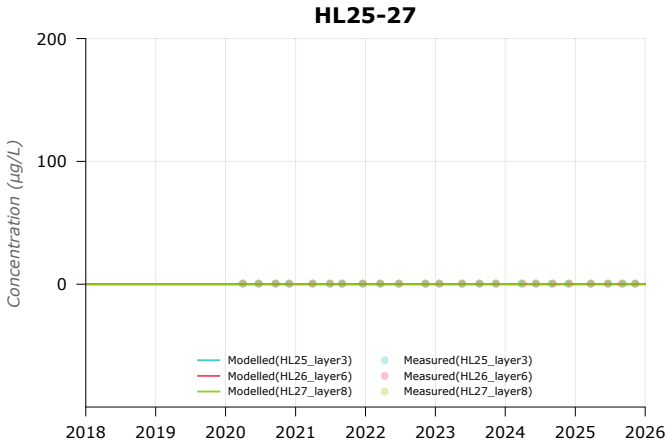
HL25-27
Concentration (µg/L)
200
100
0
Modelled(HL25_layer3)
Modelled(HL26_layer6)
Modelled(HL27_layer8)
Measured(HL25_layer3)
Measured(HL26_layer6)
Measured(HL27_layer8)
2018
2019
2020
2021
2022
2023
2024
2025
2026

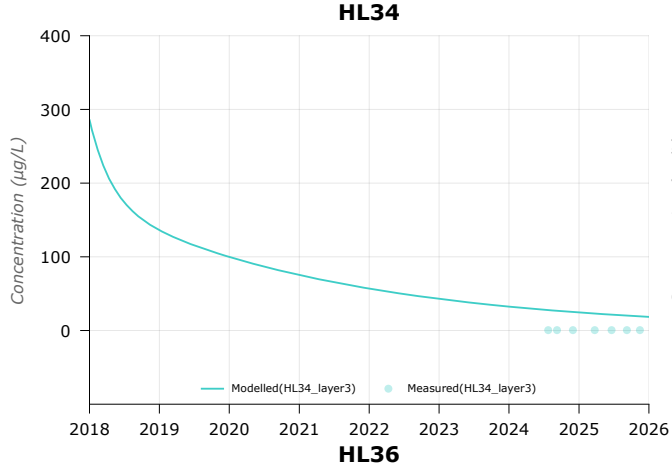
HL34
Concentration (µg/L)
400
300
200
100
0
Modelled(HL34_layer3)
Measured(HL34_layer3)
2018
2019
2020
2021
2022
2023
2024
2025
2026

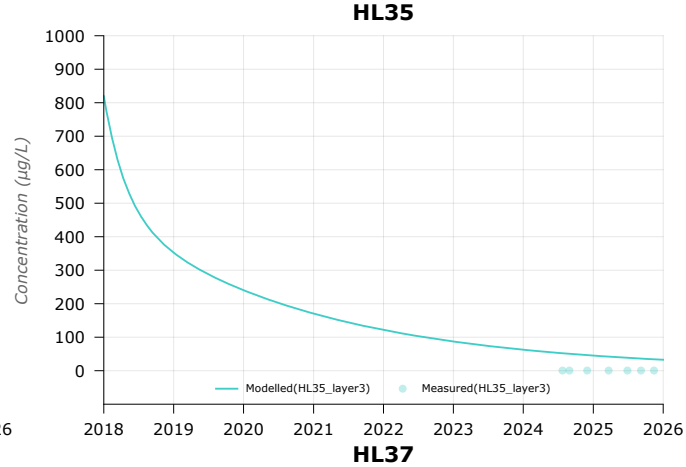
HL35
Concentration (µg/L)
1000
900
800
700
600
500
400
300
200
100
0
Modelled(HL35_layer3)
Measured(HL35_layer3)
2018
2019
2020
2021
2022
2023
2024
2025
2026

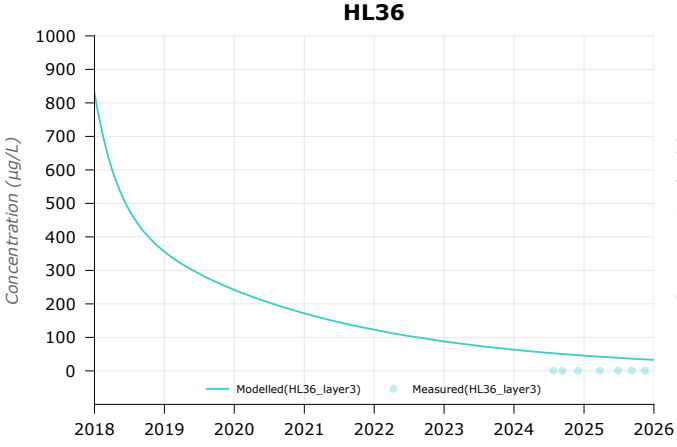
HL36
Concentration (µg/L)
1000
900
800
700
600
500
400
300
200
100
0
Modelled(HL36_layer3)
Measured(HL36_layer3)
2018
2019
2020
2021
2022
2023
2024
2025
2026

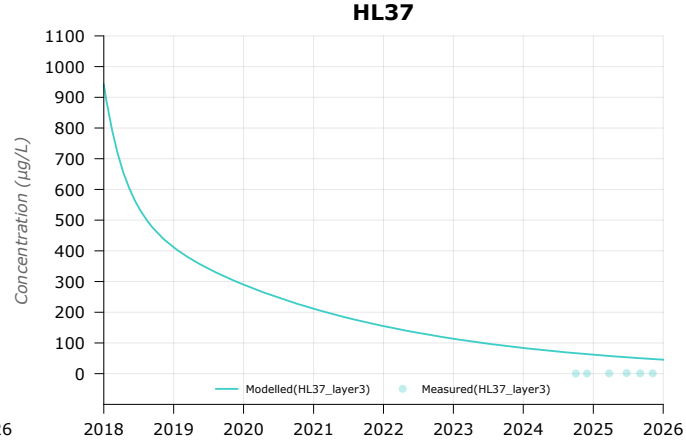
HL37
Concentration (µg/L)
1100
1000
900
800
700
600
500
400
300
200
100
0
Modelled(HL37_layer3)
Measured(HL37_layer3)
2018
2019
2020
2021
2022
2023
2024
2025
2026

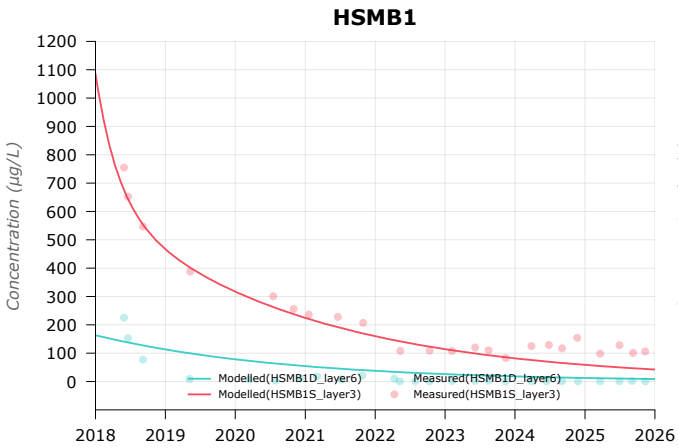
HSMB1
Concentration (µg/L)
Modelled(HSMB1D_layer6)
Modelled(HSMB1S_layer3)
Measured(HSMB1D_layer6)
Measured(HSMB1S_layer3)

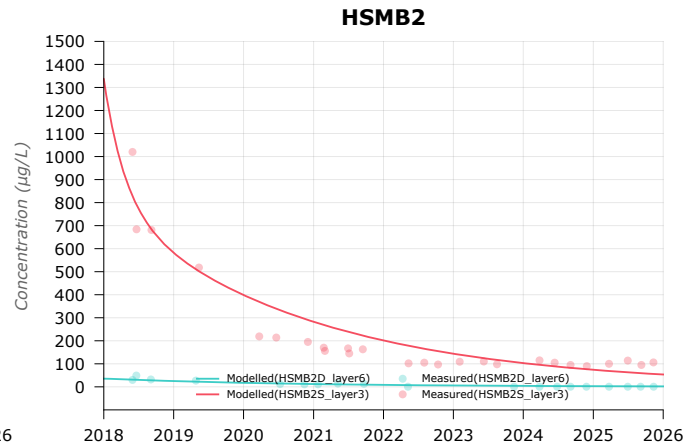
HSMB2
Concentration (µg/L)
Modelled(HSMB2D_layer6)
Modelled(HSMB2S_layer3)
Measured(HSMB2D_layer6)
Measured(HSMB2S_layer3)

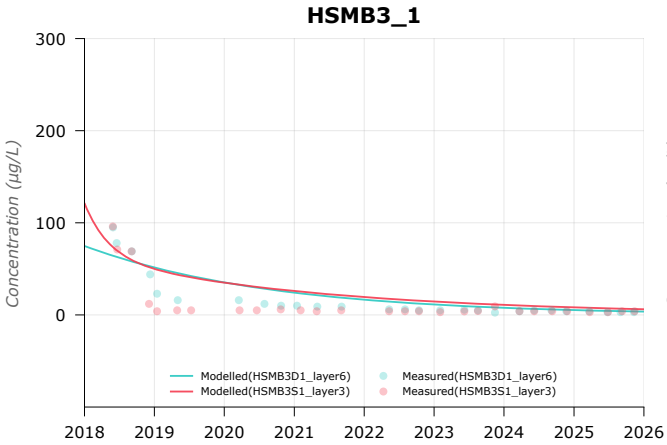
HSMB3_1
Concentration (µg/L)
Modelled(HSMB3D1_layer6)
Modelled(HSMB3S1_layer3)
Measured(HSMB3D1_layer6)
Measured(HSMB3S1_layer3)

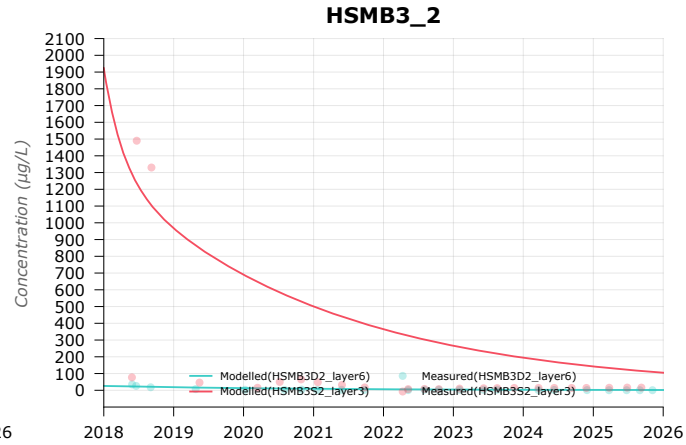
HSMB3_2
Concentration (µg/L)
Modelled(HSMB3D2_layer6)
Modelled(HSMB3S2_layer3)
Measured(HSMB3D2_layer6)
Measured(HSMB3S2_layer3)

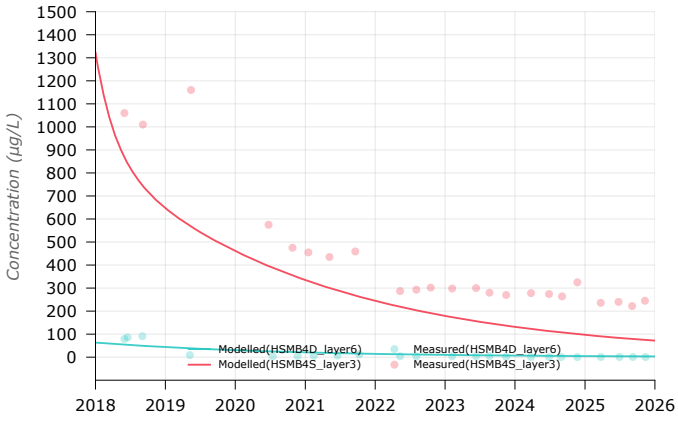
HSMB4
Concentration (µg/L)
Modelled(HSMB4D_layer6)
Modelled(HSMB4S_layer3)
Measured(HSMB4D_layer6)
Measured(HSMB4S_layer3)

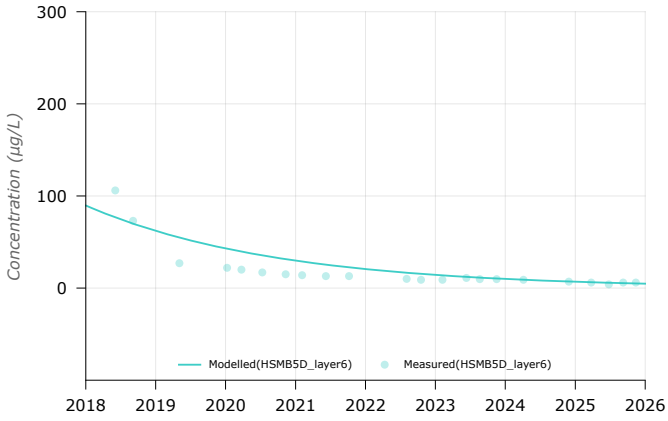
HSMB5D
Concentration (µg/L)
Modelled(HSMB5D_layer6)
Measured(HSMB5D_layer6)

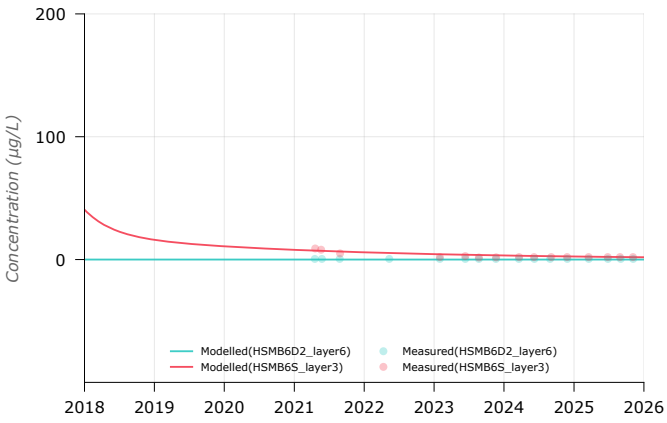
HSMB6
Concentration (µg/L)
Modelled(HSMB6D2_layer6)
Modelled(HSMB6S_layer3)
Measured(HSMB6D2_layer6)
Measured(HSMB6S_layer3)

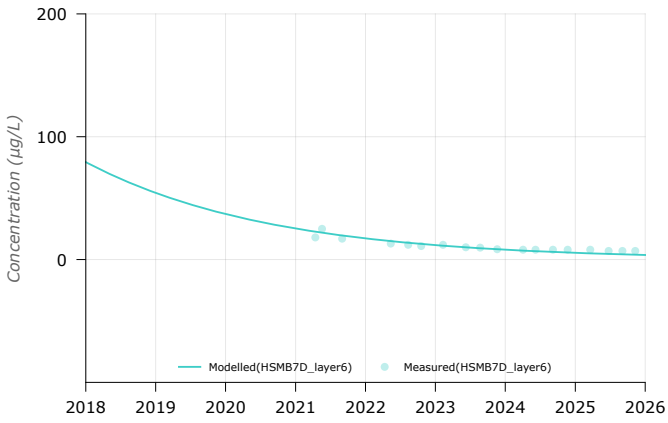
HSMB7D
Concentration (µg/L)
Modelled(HSMB7D_layer6)
Measured(HSMB7D_layer6)

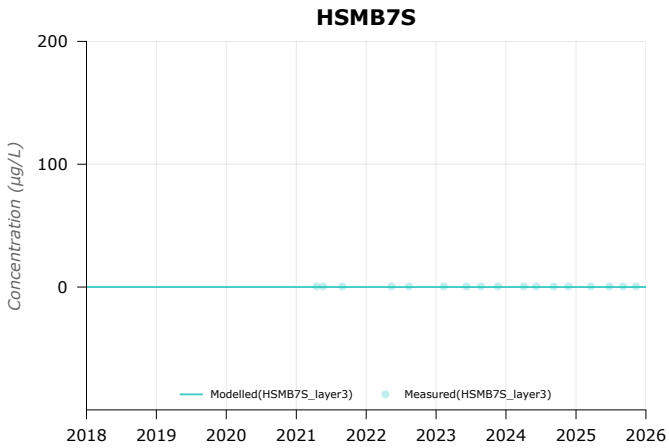
HSMB7S
Concentration (µg/L)
200
100
0
Modelled(HSMB7S_layer3)
Measured(HSMB7S_layer3)
2018
2019
2020
2021
2022
2023
2024
2025
2026

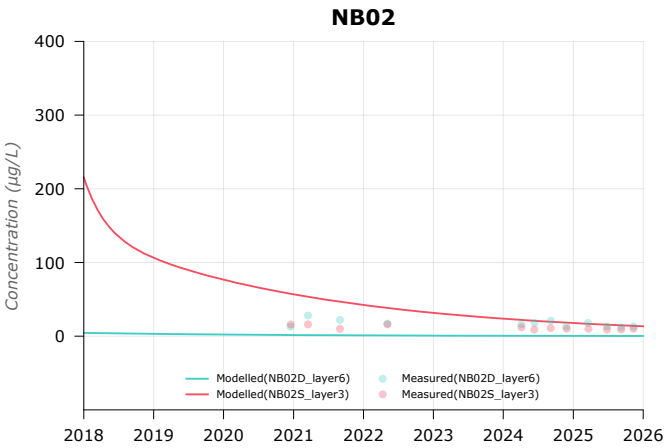
NB02
Concentration (µg/L)
400
300
200
100
0
Modelled(NB02D_layer6)
Measured(NB02D_layer6)
Modelled(NB02S_layer3)
Measured(NB02S_layer3)
2018
2019
2020
2021
2022
2023
2024
2025
2026

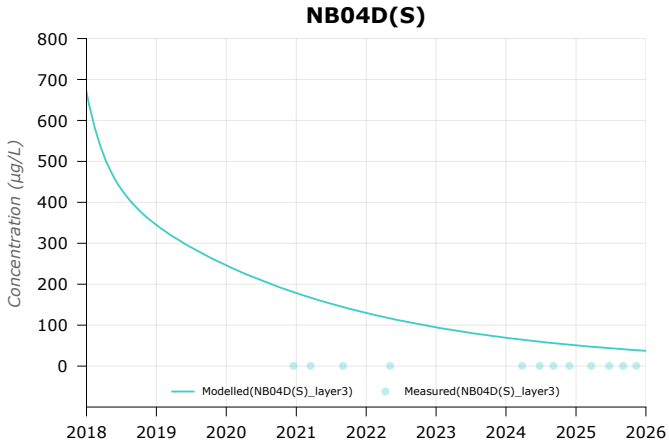
NB04D(S)
Concentration (µg/L)
800
700
600
500
400
300
200
100
0
Modelled(NB04D(S)_layer3)
Measured(NB04D(S)_layer3)
2018
2019
2020
2021
2022
2023
2024
2025
2026

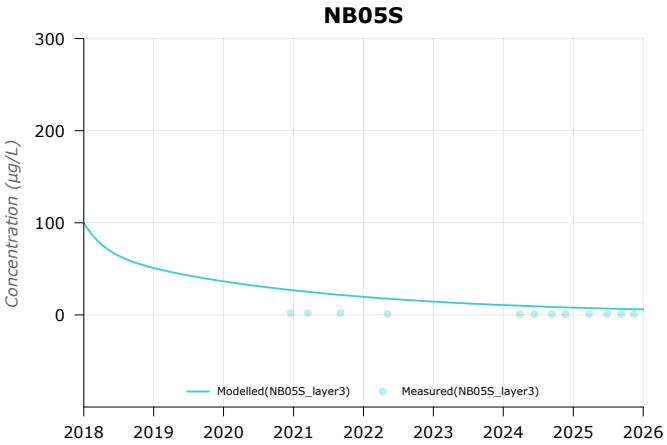
NB05S
Concentration (µg/L)
300
200
100
0
Modelled(NB05S_layer3)
Measured(NB05S_layer3)
2018
2019
2020
2021
2022
2023
2024
2025
2026

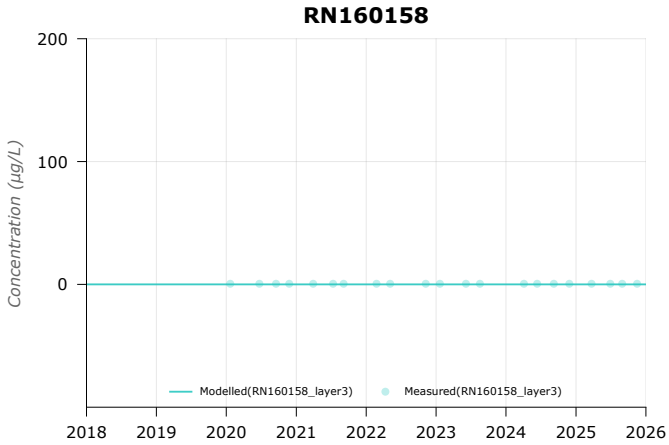
RN160158
Concentration (µg/L)
200
100
0
Modelled(RN160158_layer3)
Measured(RN160158_layer3)
2018
2019
2020
2021
2022
2023
2024
2025
2026

Appendix D. Modelled versus observed concentration time series plots - Naphthalene

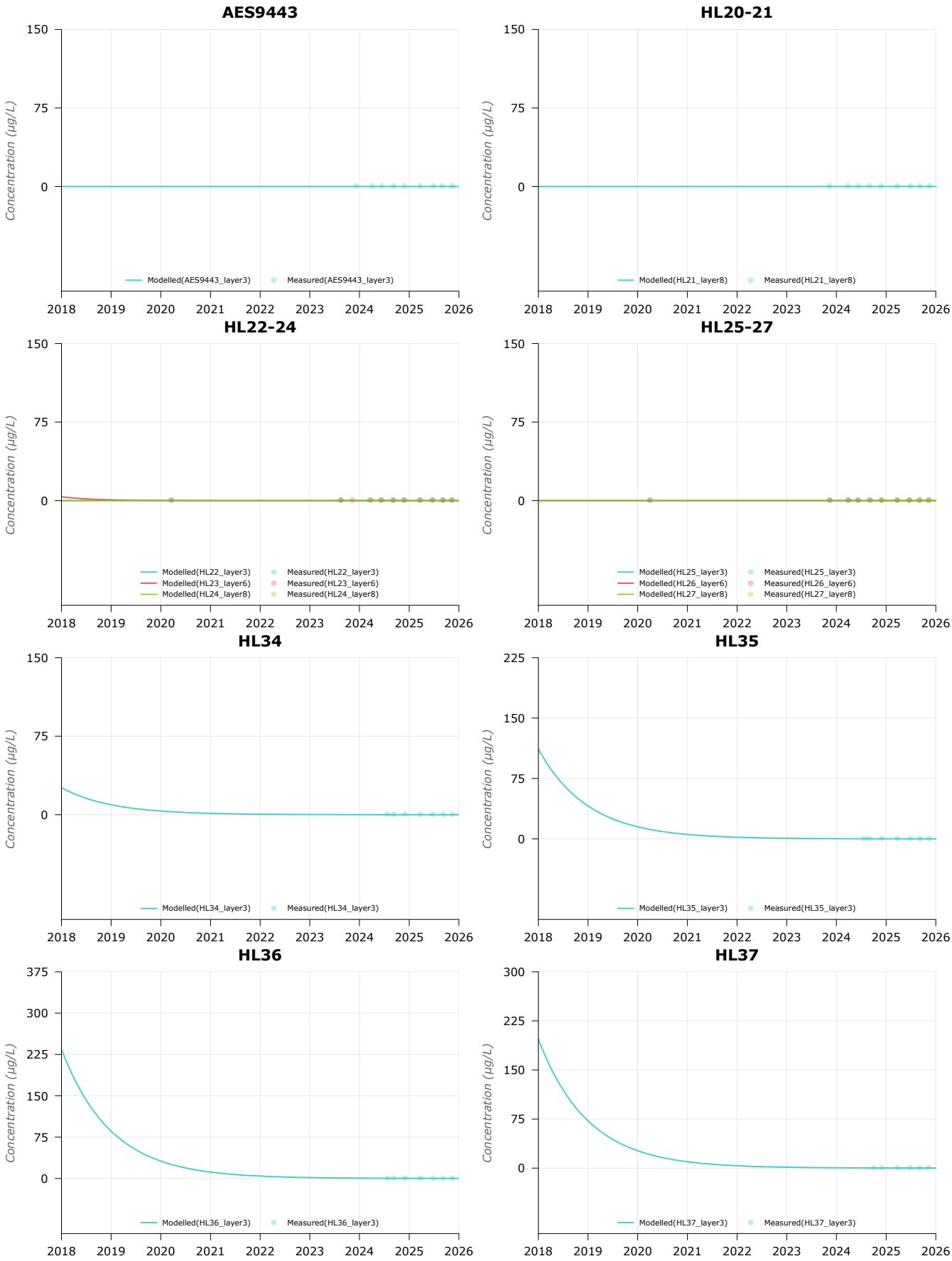
AES9443
Concentration (µg/L)
150
75
0
Modelled(AES9443_layer3)
Measured(AES9443_layer3)
2018
2019
2020
2021
2022
2023
2024
2025
2026
HL20-21
Concentration (µg/L)
150
75
0
Modelled(HL21_layer8)
Measured(HL21_layer8)
2018
2019
2020
2021
2022
2023
2024
2025
2026
HL22-24
Concentration (µg/L)
150
75
0
Modelled(HL22_layer3)
Modelled(HL23_layer6)
Modelled(HL24_layer8)
Measured(HL22_layer3)
Measured(HL23_layer6)
Measured(HL24_layer8)
2018
2019
2020
2021
2022
2023
2024
2025
2026
HL25-27
Concentration (µg/L)
150
75
0
Modelled(HL25_layer3)
Modelled(HL26_layer6)
Modelled(HL27_layer8)
Measured(HL25_layer3)
Measured(HL26_layer6)
Measured(HL27_layer8)
2018
2019
2020
2021
2022
2023
2024
2025
2026
HL34
Concentration (µg/L)
150
75
0
Modelled(HL34_layer3)
Measured(HL34_layer3)
2018
2019
2020
2021
2022
2023
2024
2025
2026
HL35
Concentration (µg/L)
225
150
75
0
Modelled(HL35_layer3)
Measured(HL35_layer3)
2018
2019
2020
2021
2022
2023
2024
2025
2026
HL36
Concentration (µg/L)
375
300
225
150
75
0
Modelled(HL36_layer3)
Measured(HL36_layer3)
2018
2019
2020
2021
2022
2023
2024
2025
2026
HL37
Concentration (µg/L)
300
225
150
75
0
Modelled(HL37_layer3)
Measured(HL37_layer3)
2018
2019
2020
2021
2022
2023
2024
2025
2026

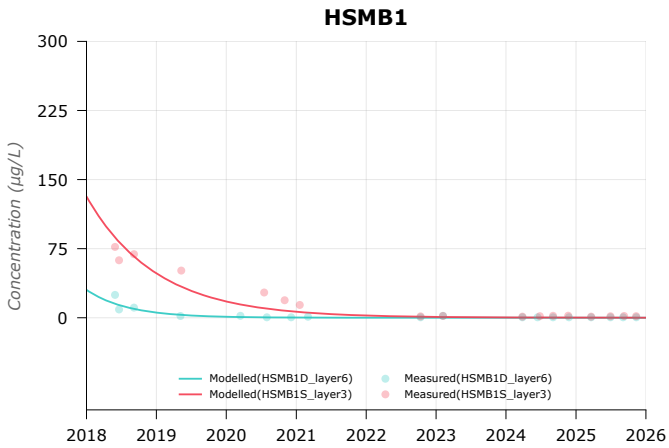
HSMB1
Concentration (µg/L)
300
225
150
75
0
2018
2019
2020
2021
2022
2023
2024
2025
2026
Modelled(HSMB1D_layer6)
Modelled(HSMB1S_layer3)
Measured(HSMB1D_layer6)
Measured(HSMB1S_layer3)

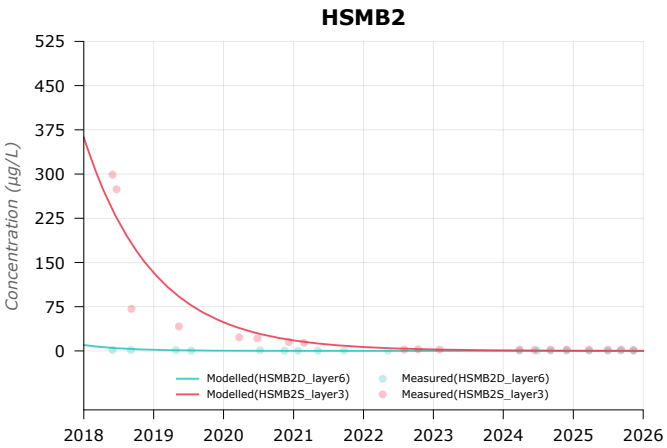
HSMB2
Concentration (µg/L)
525
450
375
300
225
150
75
0
2018
2019
2020
2021
2022
2023
2024
2025
2026
Modelled(HSMB2D_layer6)
Modelled(HSMB2S_layer3)
Measured(HSMB2D_layer6)
Measured(HSMB2S_layer3)

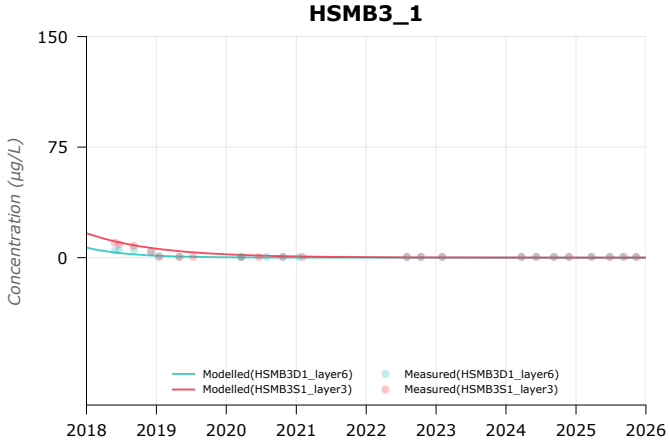
HSMB3_1
Concentration (µg/L)
150
75
0
2018
2019
2020
2021
2022
2023
2024
2025
2026
Modelled(HSMB3D1_layer6)
Modelled(HSMB3S1_layer3)
Measured(HSMB3D1_layer6)
Measured(HSMB3S1_layer3)

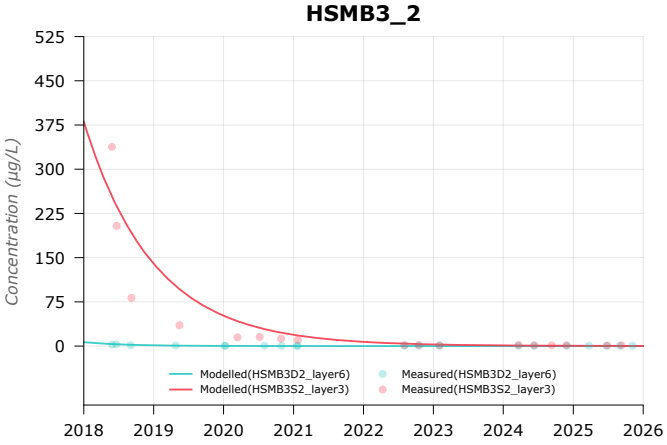
HSMB3_2
Concentration (µg/L)
525
450
375
300
225
150
75
0
2018
2019
2020
2021
2022
2023
2024
2025
2026
Modelled(HSMB3D2_layer6)
Modelled(HSMB3S2_layer3)
Measured(HSMB3D2_layer6)
Measured(HSMB3S2_layer3)

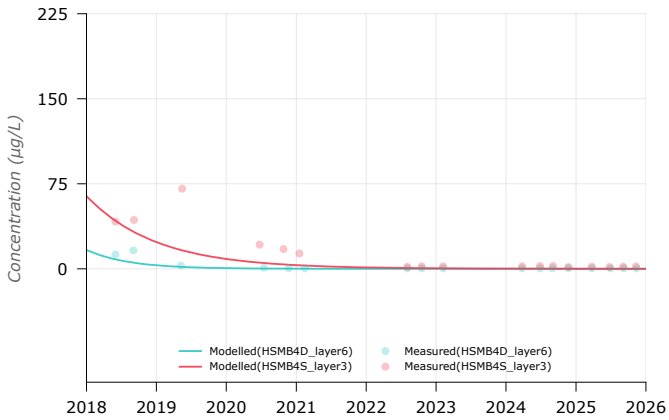
HSMB4
Concentration (µg/L)
225
150
75
0
2018
2019
2020
2021
2022
2023
2024
2025
2026
Modelled(HSMB4D_layer6)
Modelled(HSMB4S_layer3)
Measured(HSMB4D_layer6)
Measured(HSMB4S_layer3)

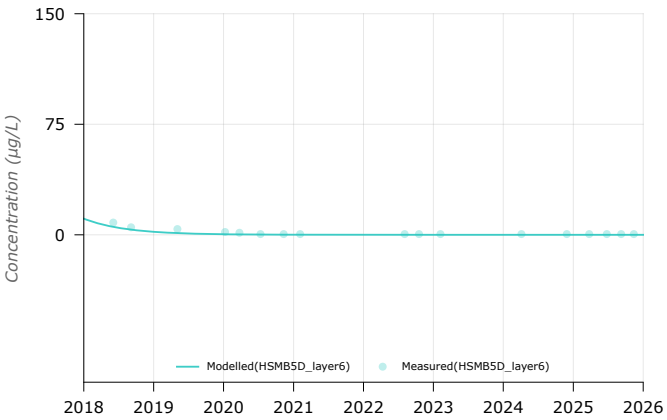
HSMB5D
Concentration (µg/L)
150
75
0
2018
2019
2020
2021
2022
2023
2024
2025
2026
Modelled(HSMB5D_layer6)
Measured(HSMB5D_layer6)

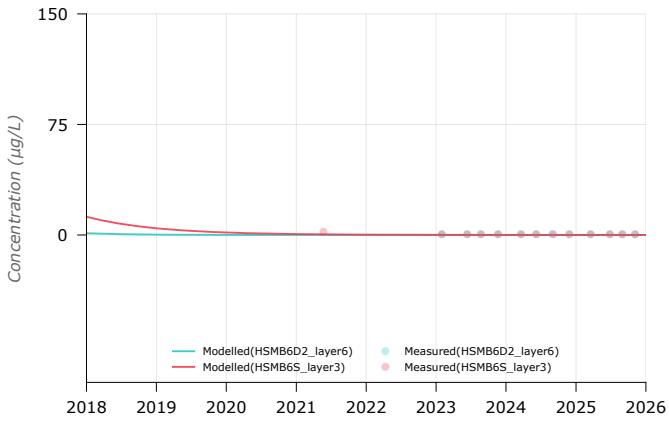
HSMB6
Concentration (µg/L)
150
75
0
2018
2019
2020
2021
2022
2023
2024
2025
2026
Modelled(HSMB6D2_layer6)
Modelled(HSMB6S_layer3)
Measured(HSMB6D2_layer6)
Measured(HSMB6S_layer3)

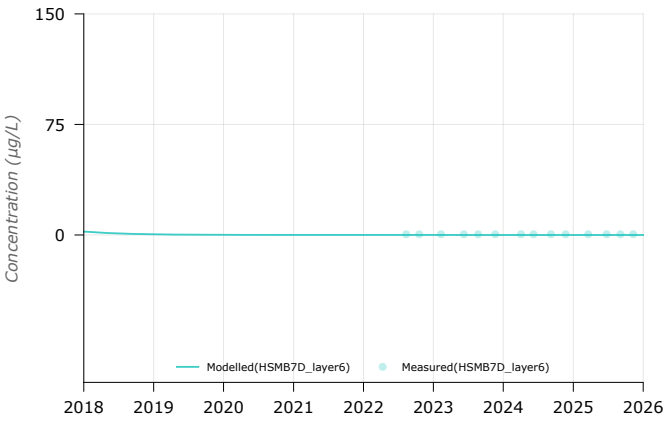
HSMB7D
Concentration (µg/L)
150
75
0
2018
2019
2020
2021
2022
2023
2024
2025
2026
Modelled(HSMB7D_layer6)
Measured(HSMB7D_layer6)

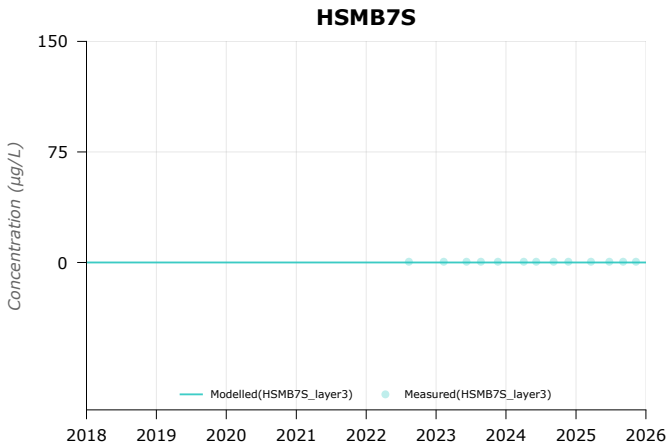
HSMB7S
Concentration (µg/L)
150
75
0
2018
2019
2020
2021
2022
2023
2024
2025
2026
Modelled(HSMB7S_layer3)
Measured(HSMB7S_layer3)

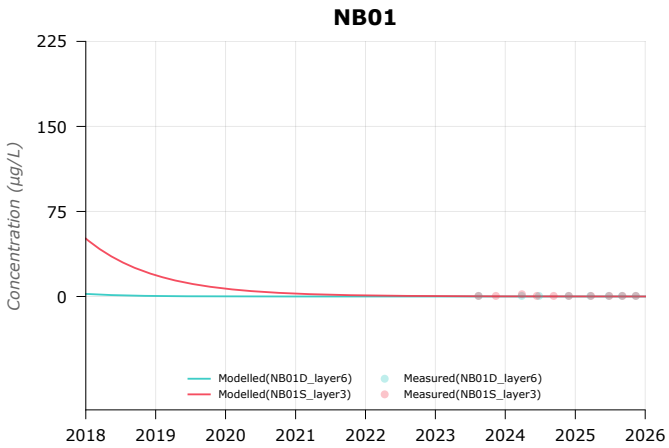
NB01
Concentration (µg/L)
225
150
75
0
2018
2019
2020
2021
2022
2023
2024
2025
2026
Modelled(NB01D_layer6)
Measured(NB01D_layer6)
Modelled(NB01S_layer3)
Measured(NB01S_layer3)

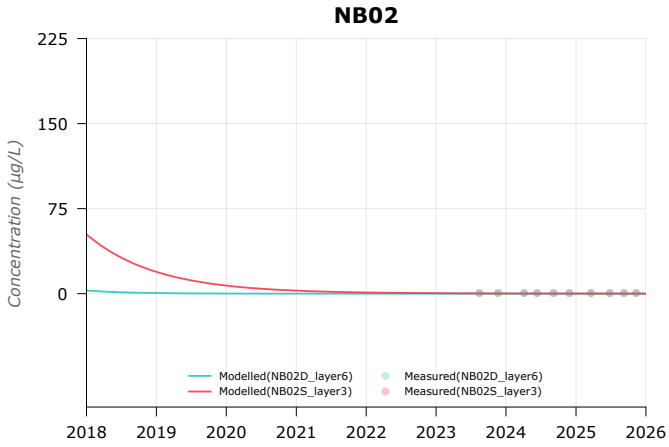
NB02
Concentration (µg/L)
225
150
75
0
2018
2019
2020
2021
2022
2023
2024
2025
2026
Modelled(NB02D_layer6)
Measured(NB02D_layer6)
Modelled(NB02S_layer3)
Measured(NB02S_layer3)

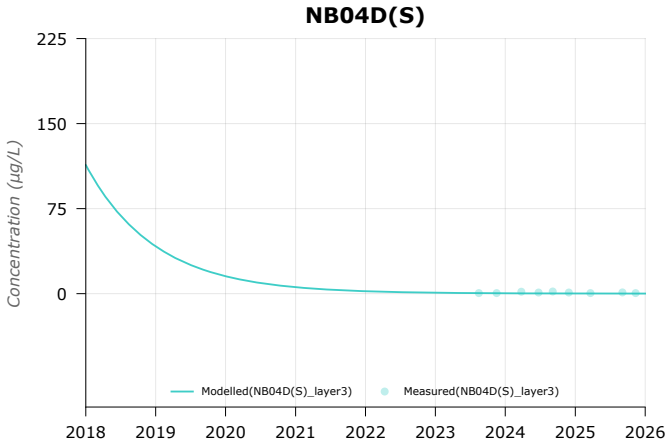
NB04D(S)
Concentration (µg/L)
225
150
75
0
2018
2019
2020
2021
2022
2023
2024
2025
2026
Modelled(NB04D(S)_layer3)
Measured(NB04D(S)_layer3)

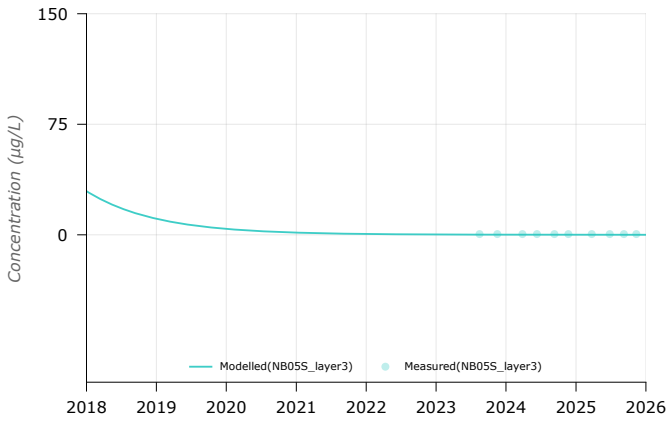
NB05S
Concentration (µg/L)
150
75
0
2018
2019
2020
2021
2022
2023
2024
2025
2026
Modelled(NB05S_layer3)
Measured(NB05S_layer3)

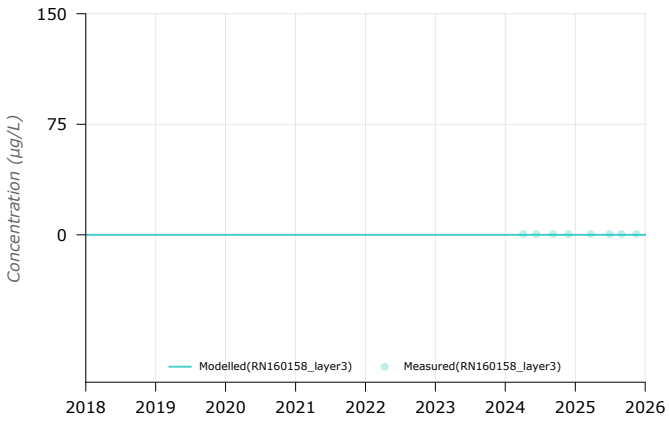
RN160158
Concentration (µg/L)
150
75
0
2018
2019
2020
2021
2022
2023
2024
2025
2026
Modelled(RN160158_layer3)
Measured(RN160158_layer3)

Appendix E. Predictive uncertainty - groundwater levels

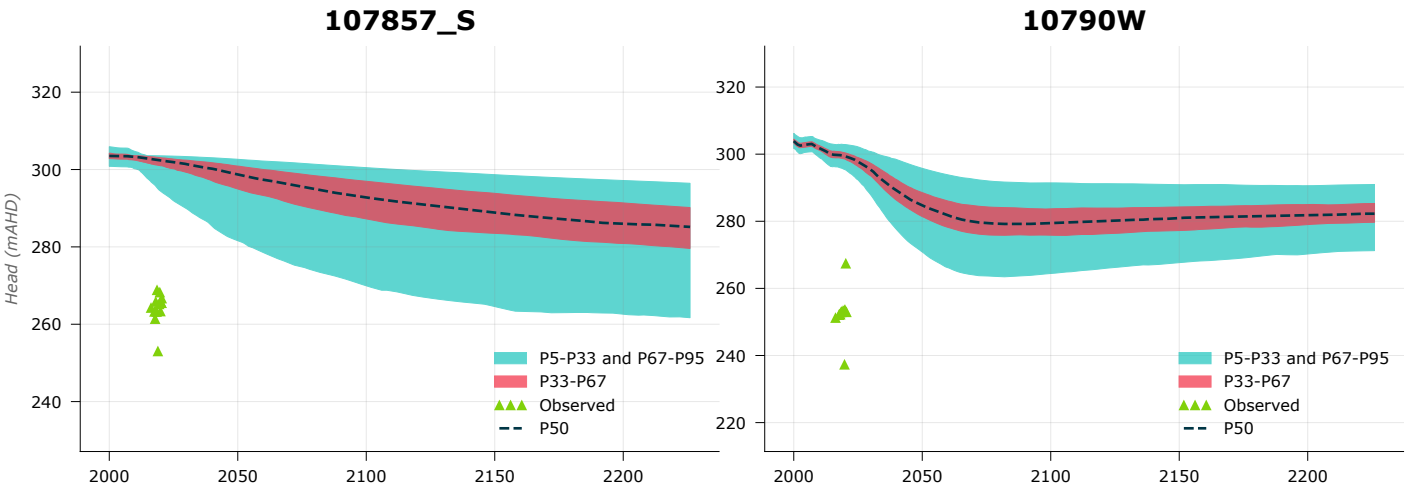
107857_S
Head (mAHD)
320
300
280
260
240
2000
2050
2100
2150
2200
P5-P33 and P67-P95
P33-P67
Observed
P50

10790W
320
300
280
260
240
220
2000
2050
2100
2150
2200
P5-P33 and P67-P95
P33-P67
Observed
P50

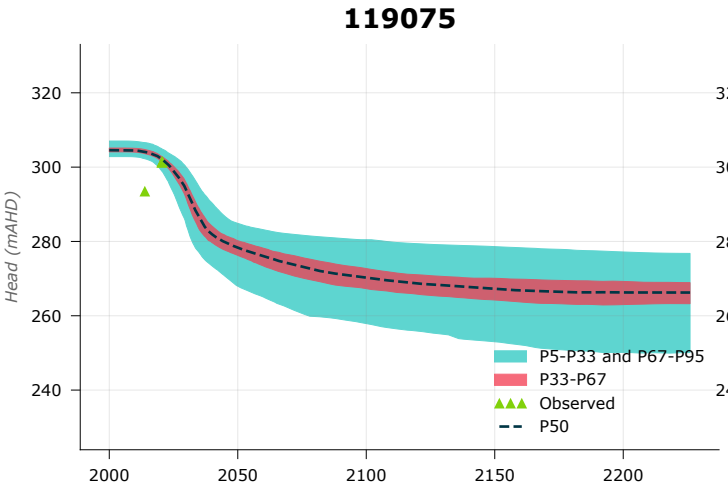
119075
Head (mAHD)
320
300
280
260
240
2000
2050
2100
2150
2200
P5-P33 and P67-P95
P33-P67
Observed
P50

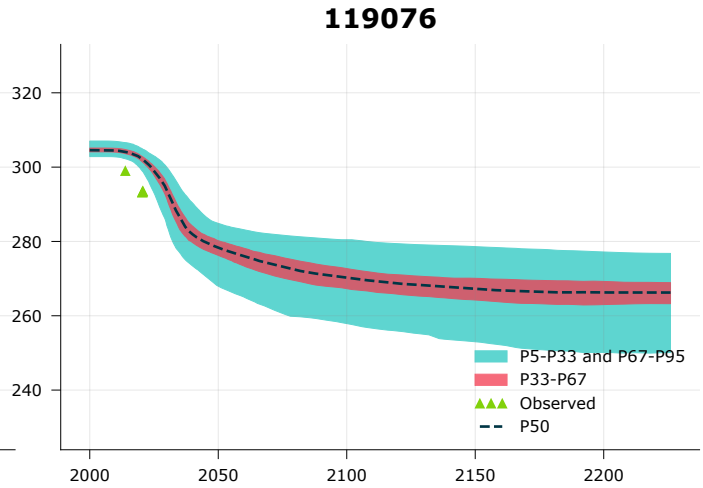
119076
320
300
280
260
240
2000
2050
2100
2150
2200
P5-P33 and P67-P95
P33-P67
Observed
P50

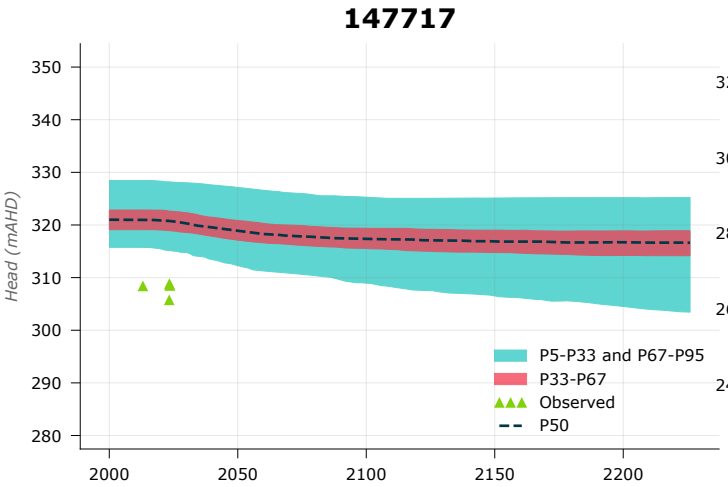
147717
Head (mAHD)
350
340
330
320
310
300
290
280
2000
2050
2100
2150
2200
P5-P33 and P67-P95
P33-P67
Observed
P50

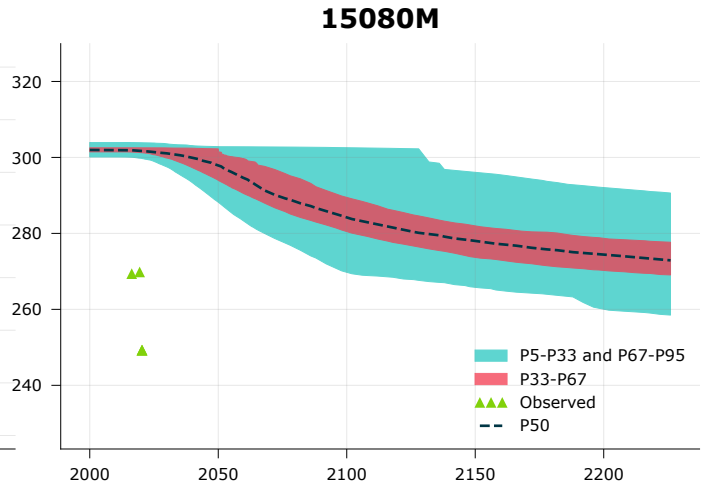
15080M
320
300
280
260
240
2000
2050
2100
2150
2200
P5-P33 and P67-P95
P33-P67
Observed
P50

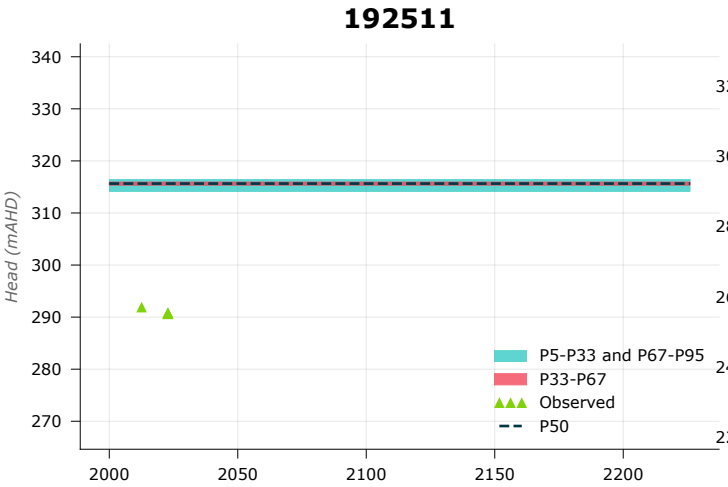
192511
Head (mAHD)
340
330
320
310
300
290
280
270
2000
2050
2100
2150
2200
P5-P33 and P67-P95
P33-P67
Observed
P50

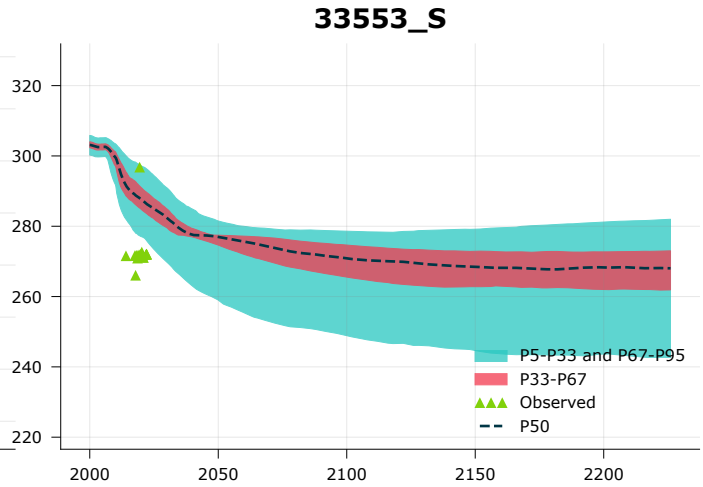
33553_S
320
300
280
260
240
220
2000
2050
2100
2150
2200
P5-P33 and P67-P95
P33-P67
Observed
P50

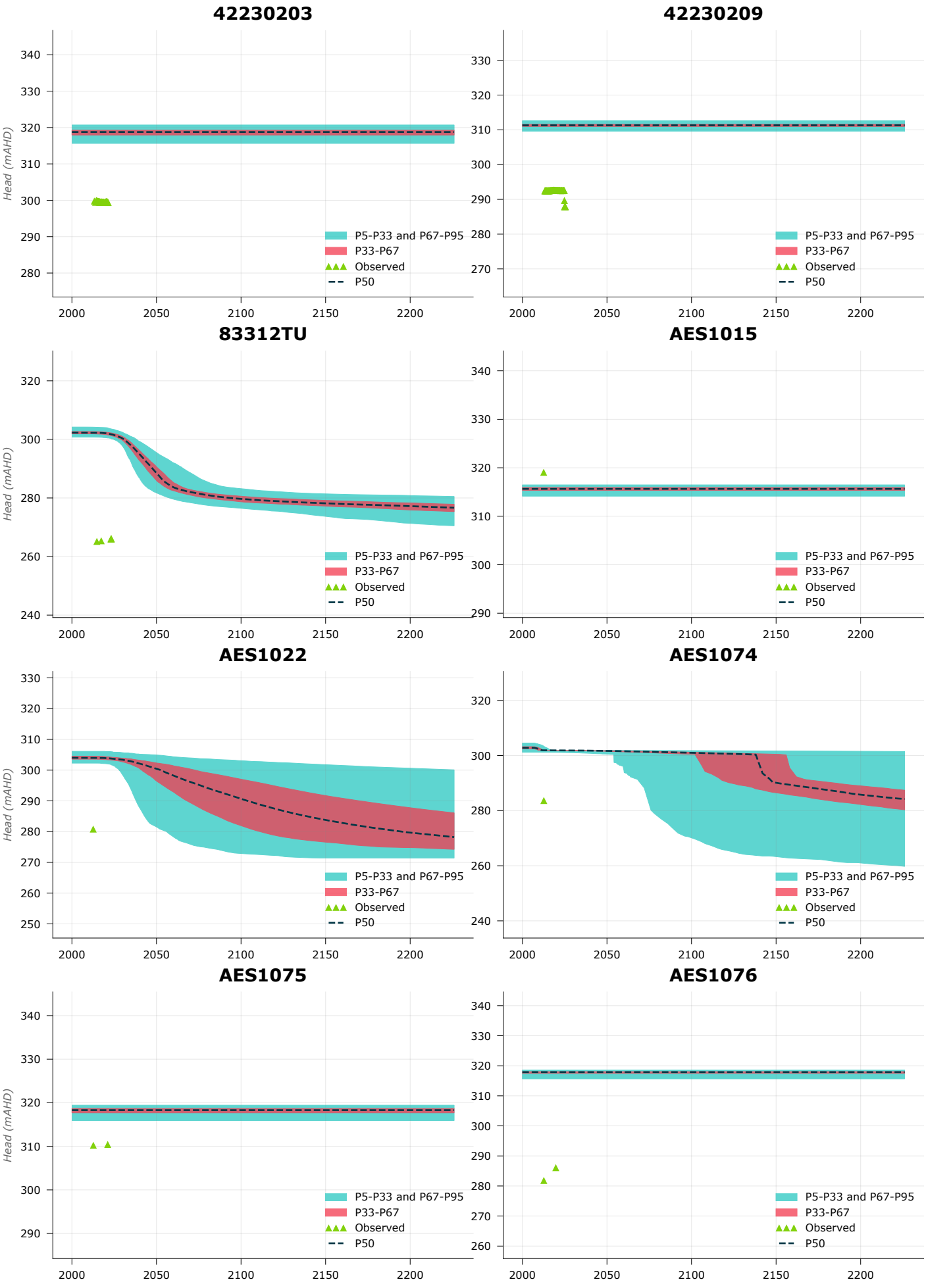
42230203
42230209
83312TU
AES1015
AES1022
AES1074
AES1075
AES1076
Head (mAHD)
P5-P33 and P67-P95
P33-P67
Observed
P50

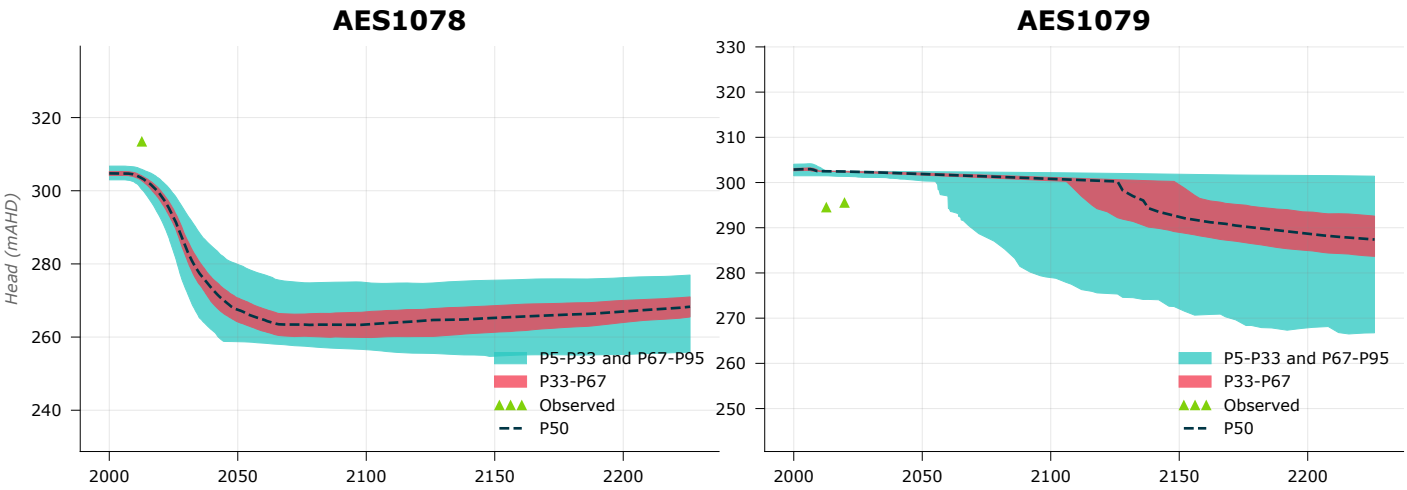
AES1078
Head (mAHD)
320
300
280
260
240
2000
2050
2100
2150
2200
P5-P33 and P67-P95
P33-P67
Observed
P50

AES1079
330
320
310
300
290
280
270
260
250
2000
2050
2100
2150
2200
P5-P33 and P67-P95
P33-P67
Observed
P50

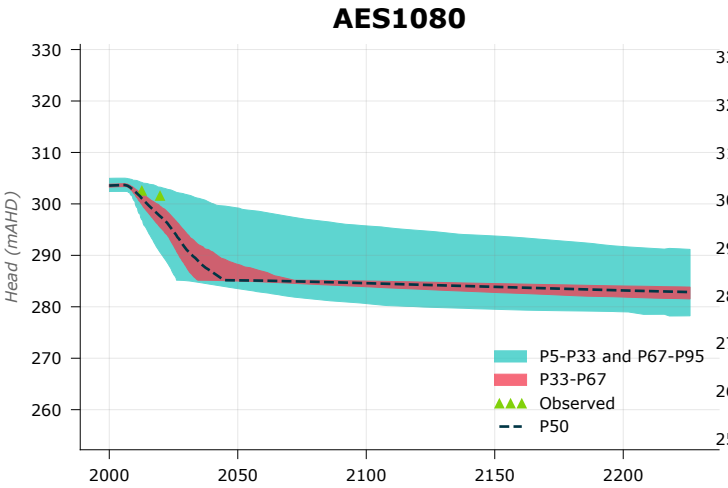
AES1080
Head (mAHD)
330
320
310
300
290
280
270
260
2000
2050
2100
2150
2200
P5-P33 and P67-P95
P33-P67
Observed
P50

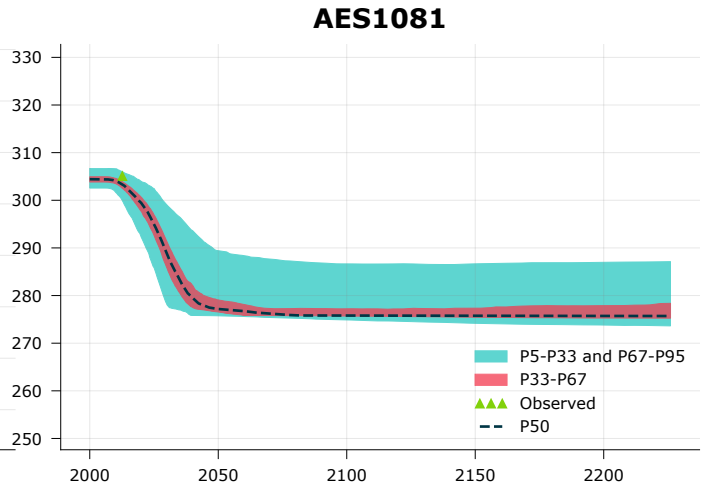
AES1081
330
320
310
300
290
280
270
260
250
2000
2050
2100
2150
2200
P5-P33 and P67-P95
P33-P67
Observed
P50

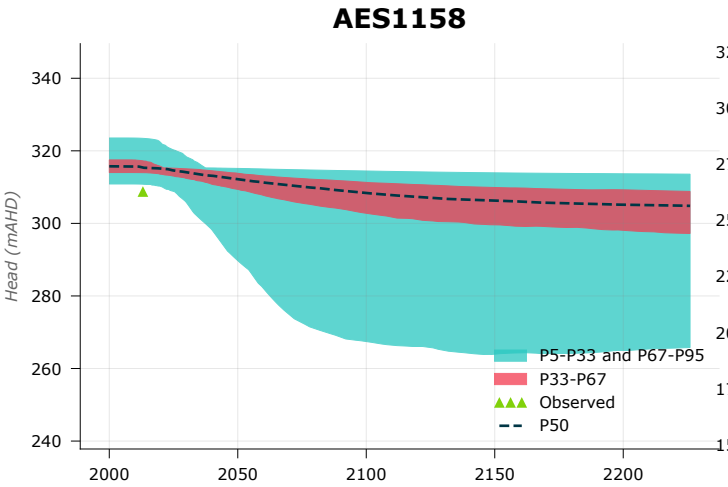
AES1158
Head (mAHD)
340
320
300
280
260
240
2000
2050
2100
2150
2200
P5-P33 and P67-P95
P33-P67
Observed
P50

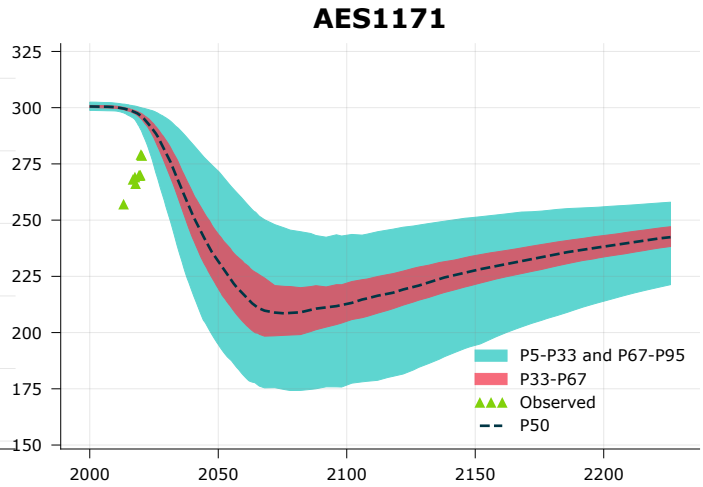
AES1171
325
300
275
250
225
200
175
150
2000
2050
2100
2150
2200
P5-P33 and P67-P95
P33-P67
Observed
P50

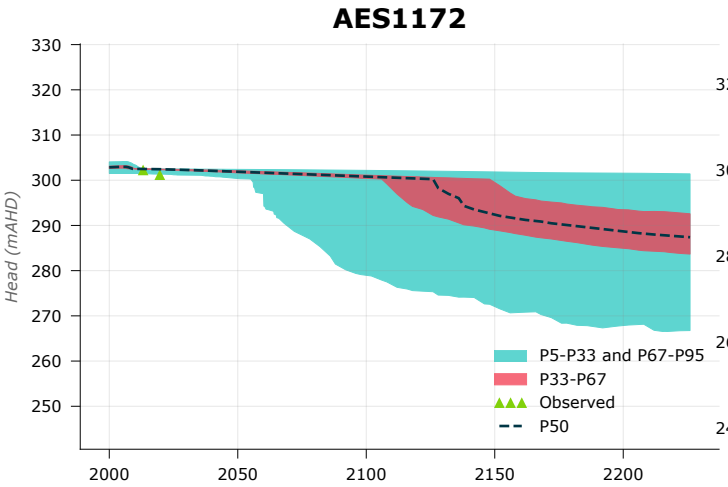
AES1172
Head (mAHD)
330
320
310
300
290
280
270
260
250
2000
2050
2100
2150
2200
P5-P33 and P67-P95
P33-P67
Observed
P50

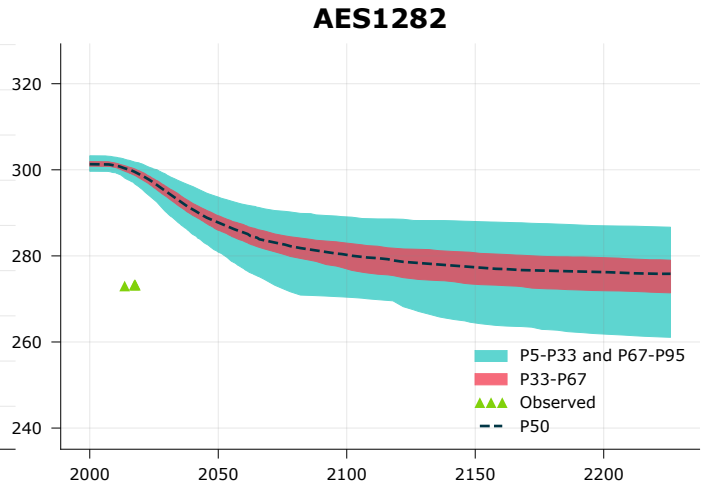
AES1282
320
300
280
260
240
2000
2050
2100
2150
2200
P5-P33 and P67-P95
P33-P67
Observed
P50

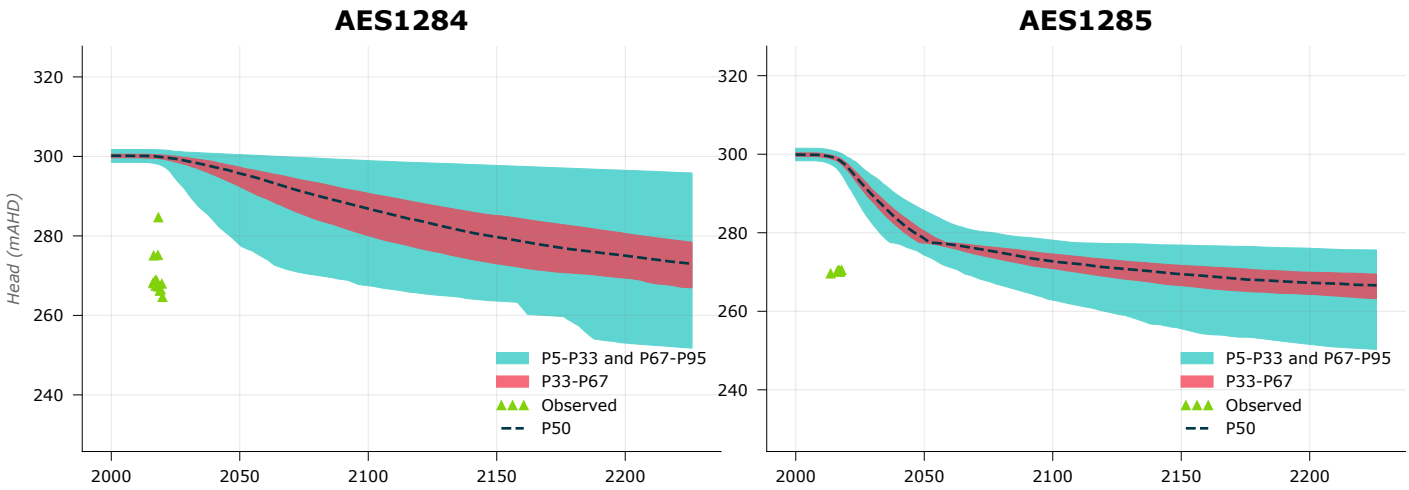
AES1284
Head (mAHD)
320
300
280
260
240
2000
2050
2100
2150
2200
P5-P33 and P67-P95
P33-P67
Observed
P50

AES1285
320
300
280
260
240
2000
2050
2100
2150
2200
P5-P33 and P67-P95
P33-P67
Observed
P50

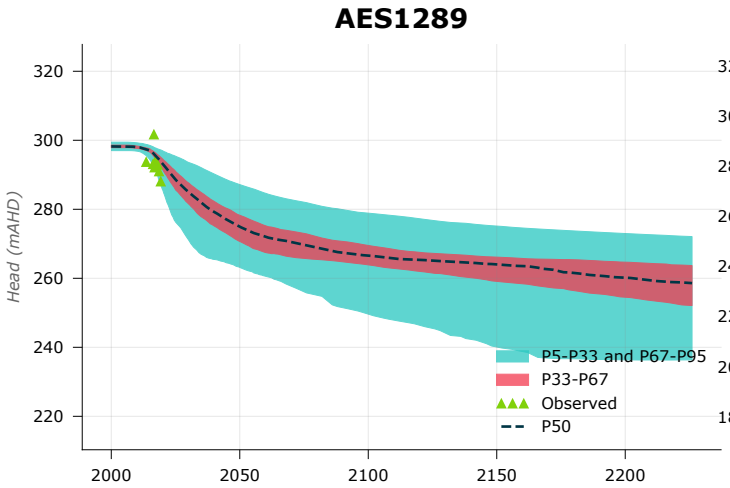
AES1289
Head (mAHD)
320
300
280
260
240
220
2000
2050
2100
2150
2200
P5-P33 and P67-P95
P33-P67
Observed
P50

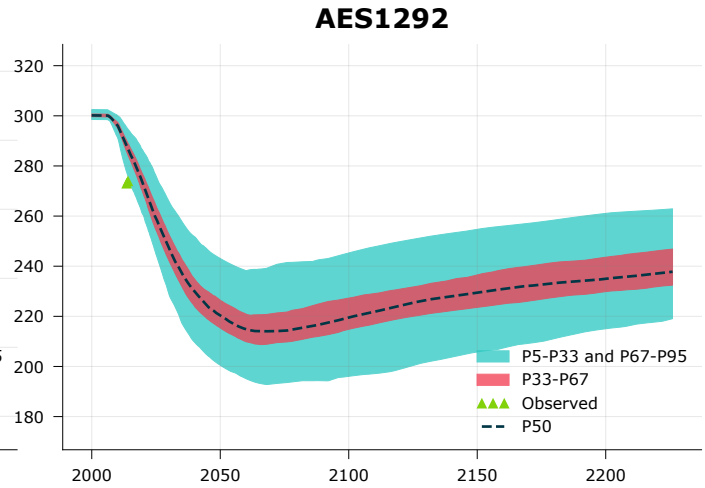
AES1292
320
300
280
260
240
220
200
180
2000
2050
2100
2150
2200
P5-P33 and P67-P95
P33-P67
Observed
P50

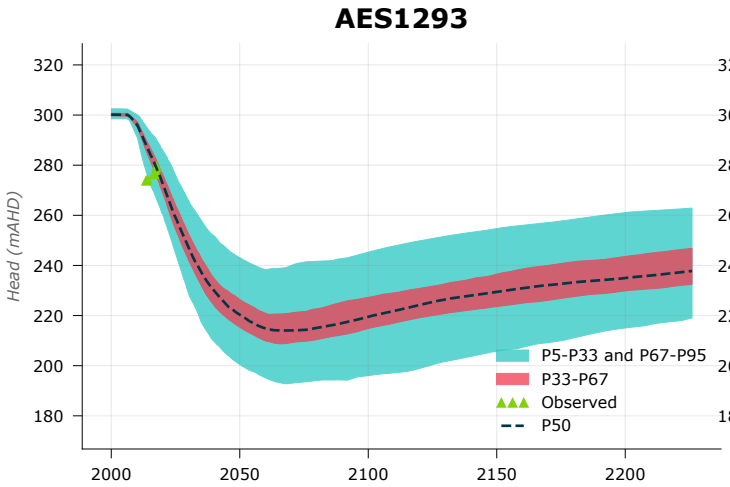
AES1293
Head (mAHD)
320
300
280
260
240
220
200
180
2000
2050
2100
2150
2200
P5-P33 and P67-P95
P33-P67
Observed
P50

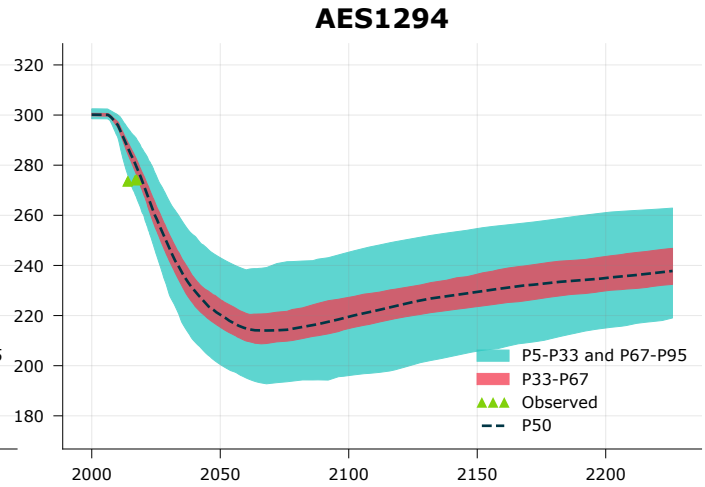
AES1294
320
300
280
260
240
220
200
180
2000
2050
2100
2150
2200
P5-P33 and P67-P95
P33-P67
Observed
P50

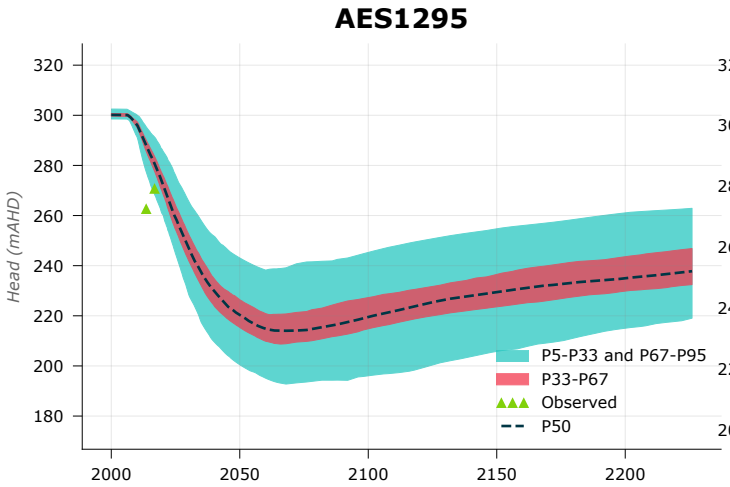
AES1295
Head (mAHD)
320
300
280
260
240
220
200
180
2000
2050
2100
2150
2200
P5-P33 and P67-P95
P33-P67
Observed
P50

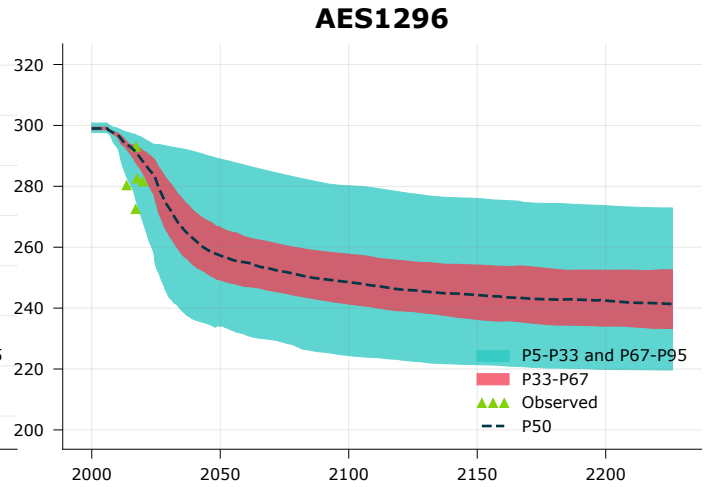
AES1296
320
300
280
260
240
220
200
2000
2050
2100
2150
2200
P5-P33 and P67-P95
P33-P67
Observed
P50

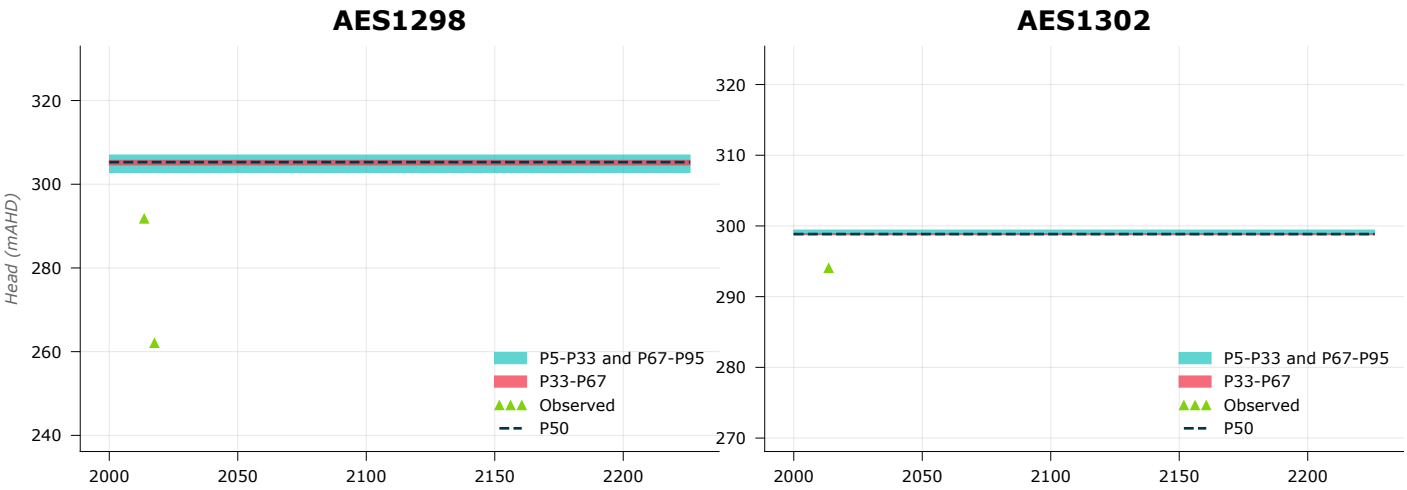
AES1298
Head (mAHD)
320
300
280
260
240
2000
2050
2100
2150
2200
P5-P33 and P67-P95
P33-P67
Observed
P50

AES1302
320
310
300
290
280
270
2000
2050
2100
2150
2200
P5-P33 and P67-P95
P33-P67
Observed
P50

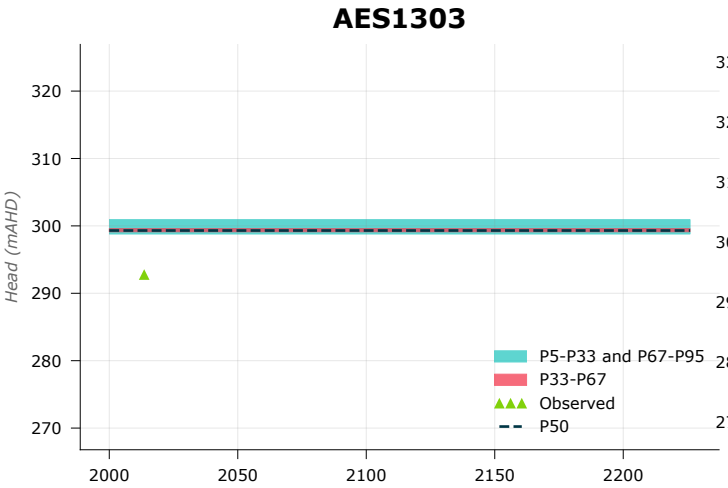
AES1303
Head (mAHD)
320
310
300
290
280
270
2000
2050
2100
2150
2200
P5-P33 and P67-P95
P33-P67
Observed
P50

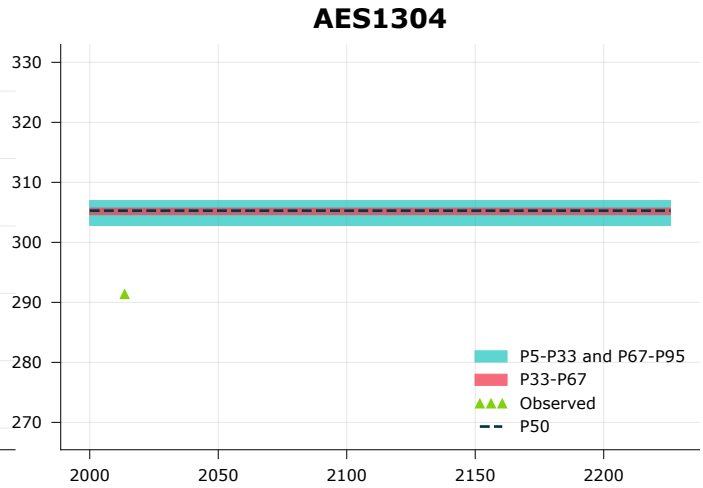
AES1304
330
320
310
300
290
280
270
2000
2050
2100
2150
2200
P5-P33 and P67-P95
P33-P67
Observed
P50

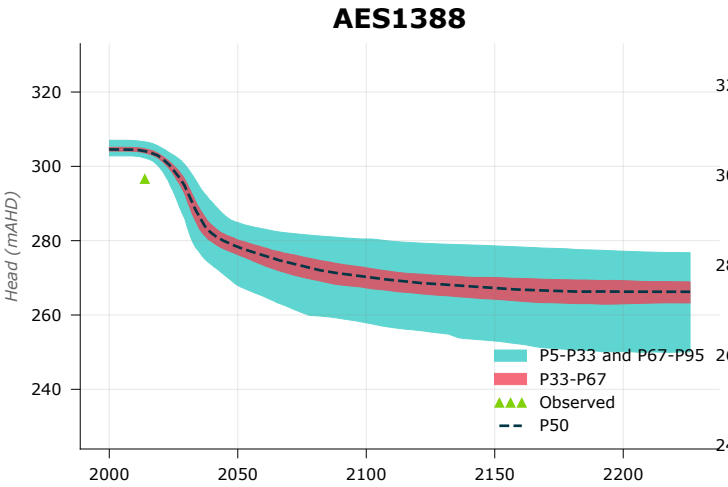
AES1388
Head (mAHD)
320
300
280
260
240
2000
2050
2100
2150
2200
P5-P33 and P67-P95
P33-P67
Observed
P50

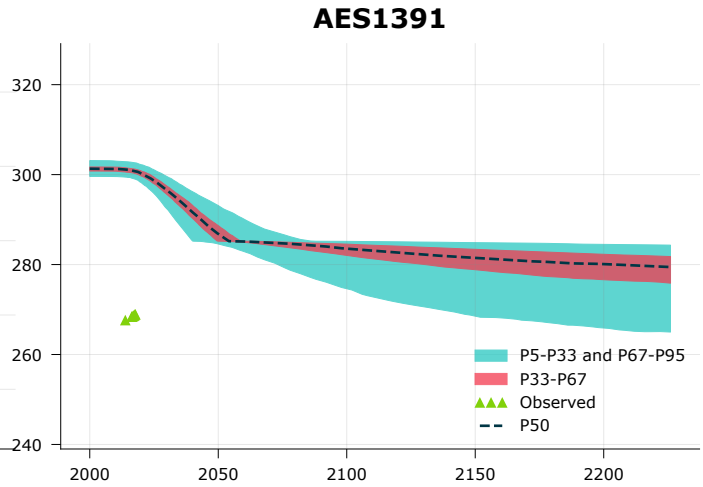
AES1391
320
300
280
260
240
2000
2050
2100
2150
2200
P5-P33 and P67-P95
P33-P67
Observed
P50

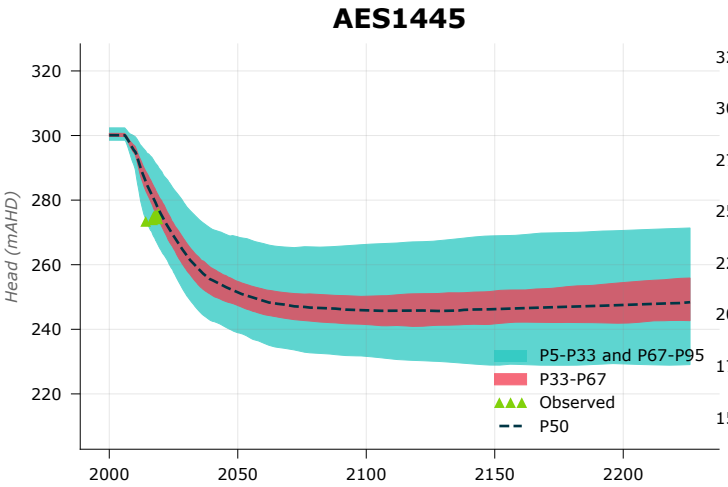
AES1445
Head (mAHD)
320
300
280
260
240
220
2000
2050
2100
2150
2200
P5-P33 and P67-P95
P33-P67
Observed
P50

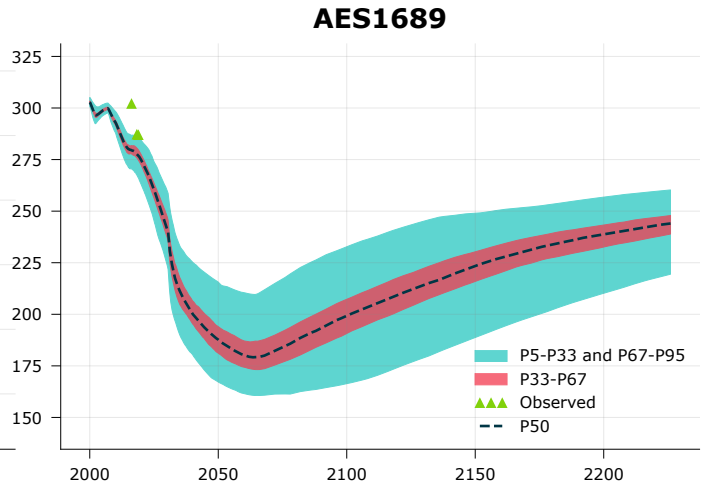
AES1689
325
300
275
250
225
200
175
150
2000
2050
2100
2150
2200
P5-P33 and P67-P95
P33-P67
Observed
P50

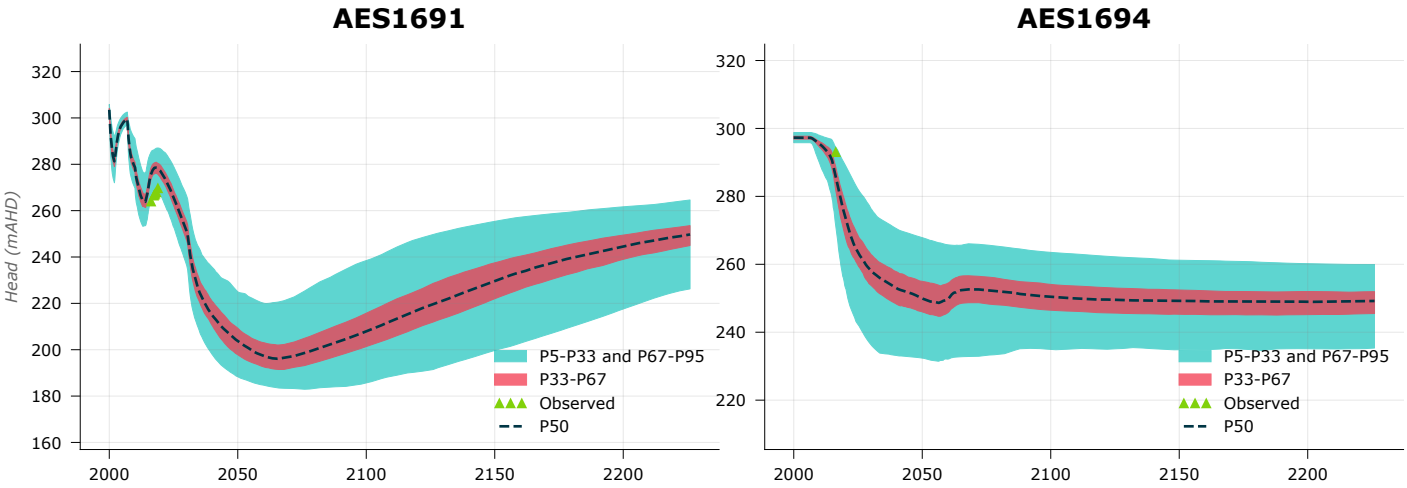
AES1691
Head (mAHD)
320
300
280
260
240
220
200
180
160
2000
2050
2100
2150
2200
P5-P33 and P67-P95
P33-P67
Observed
P50

AES1694
320
300
280
260
240
220
2000
2050
2100
2150
2200
P5-P33 and P67-P95
P33-P67
Observed
P50

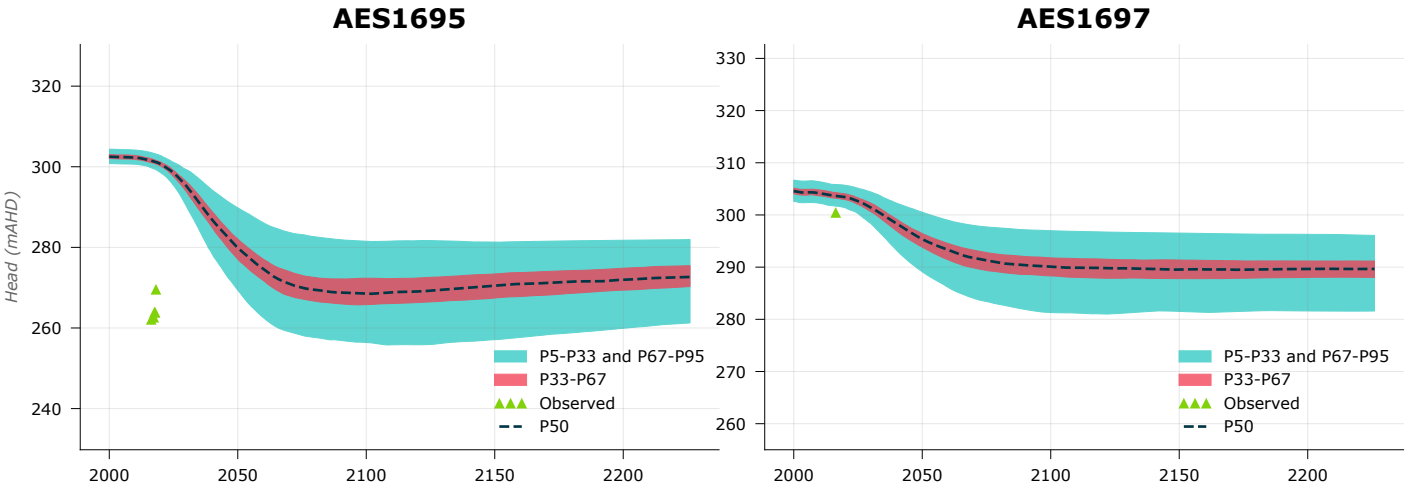
AES1695
Head (mAHD)
320
300
280
260
240
2000
2050
2100
2150
2200
P5-P33 and P67-P95
P33-P67
Observed
P50

AES1697
330
320
310
300
290
280
270
260
2000
2050
2100
2150
2200
P5-P33 and P67-P95
P33-P67
Observed
P50

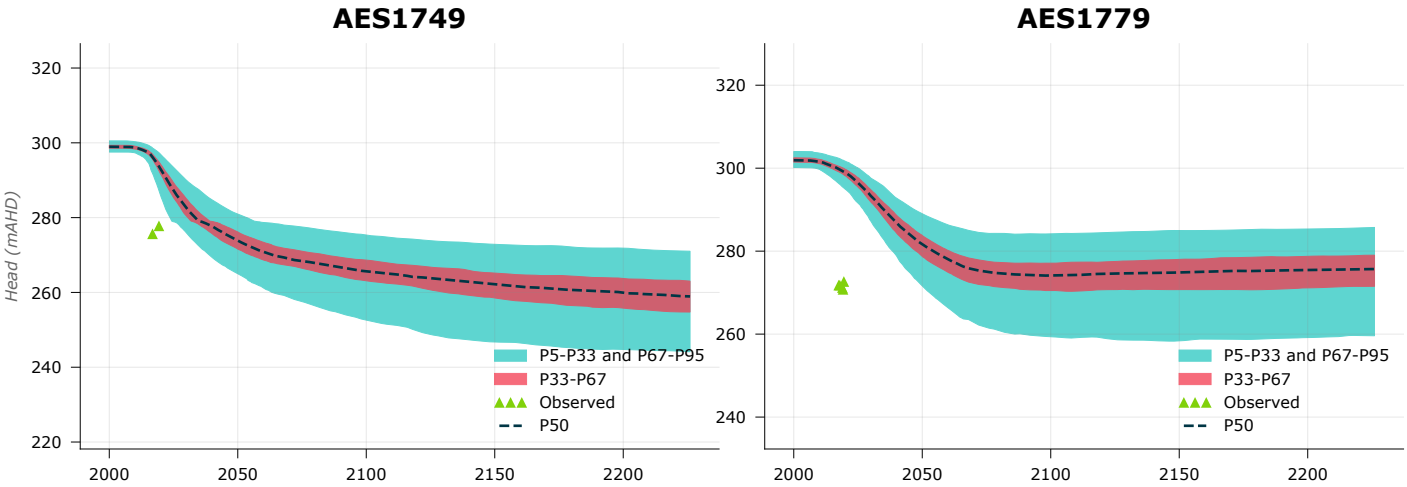
AES1749
Head (mAHD)
320
300
280
260
240
220
2000
2050
2100
2150
2200
P5-P33 and P67-P95
P33-P67
Observed
P50

AES1779
320
300
280
260
240
2000
2050
2100
2150
2200
P5-P33 and P67-P95
P33-P67
Observed
P50

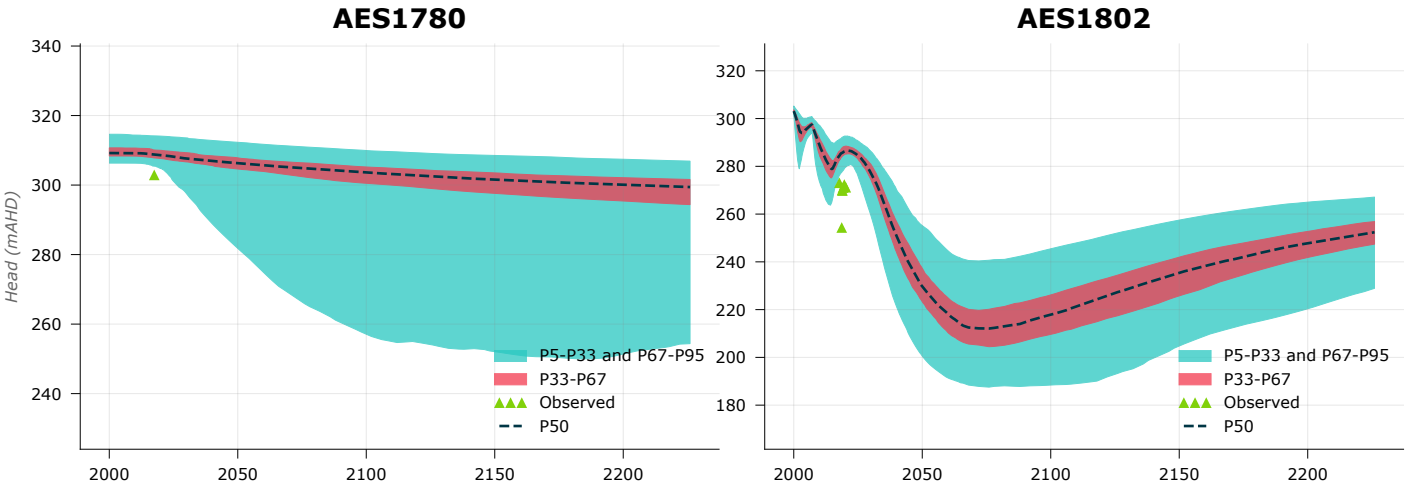
AES1780
Head (mAHD)
340
320
300
280
260
240
2000
2050
2100
2150
2200
P5-P33 and P67-P95
P33-P67
Observed
P50

AES1802
320
300
280
260
240
220
200
180
2000
2050
2100
2150
2200
P5-P33 and P67-P95
P33-P67
Observed
P50

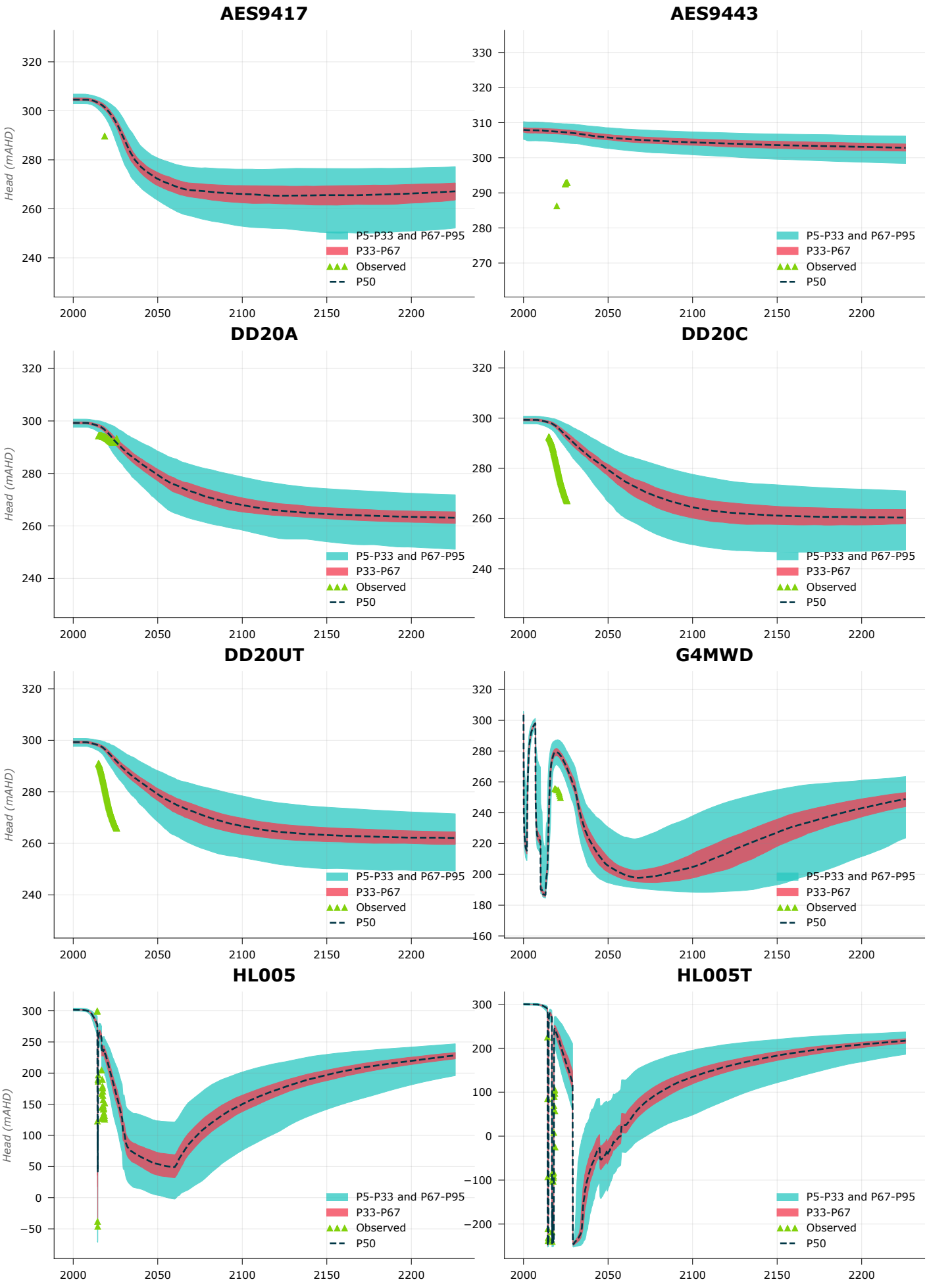
AES9417
AES9443
DD20A
DD20C
DD20UT
G4MWD
HL005
HL005T
Head (mAHD)
P5-P33 and P67-P95
P33-P67
Observed
P50

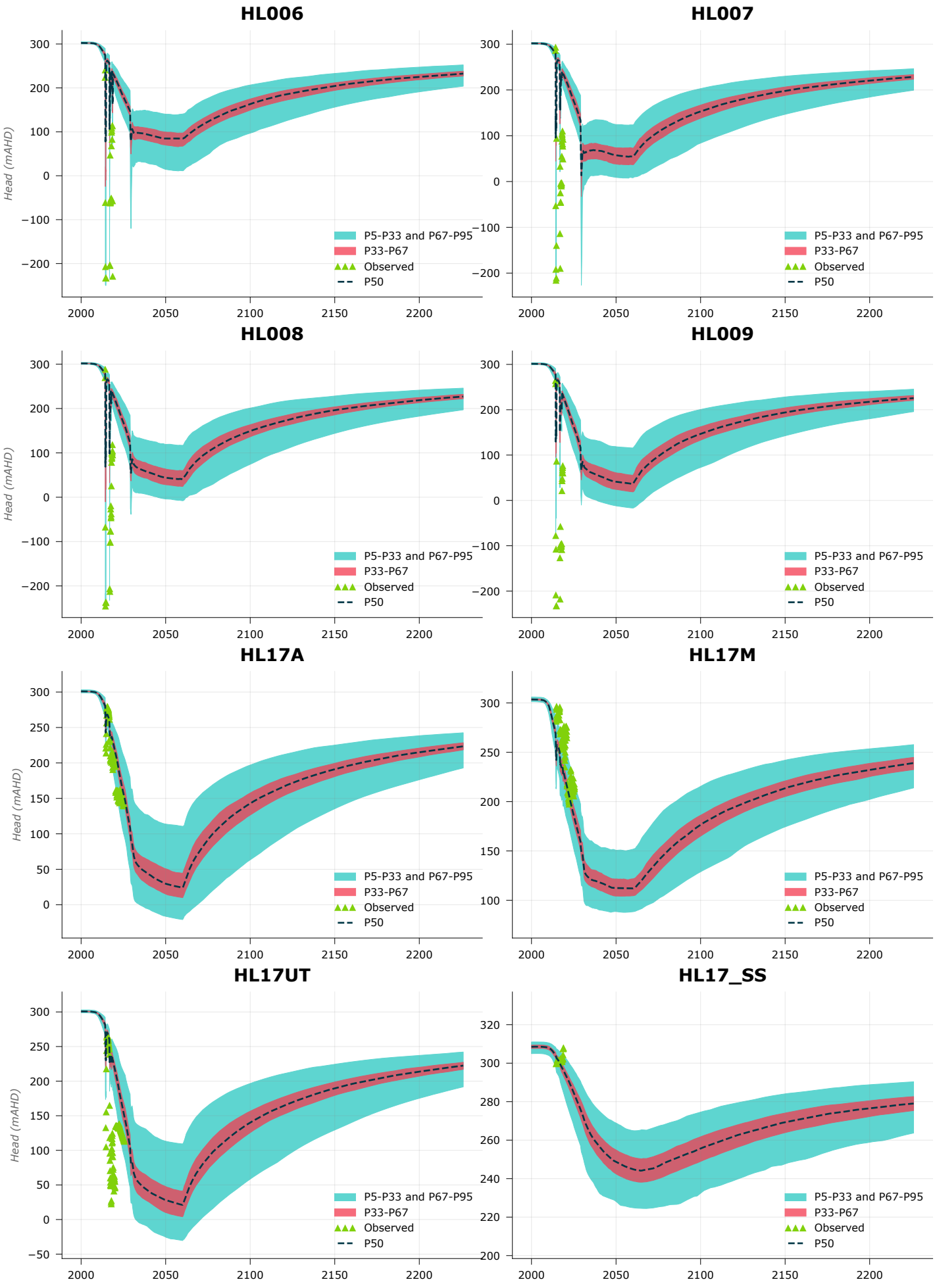
HL006
HL007
HL008
HL009
HL17A
HL17M
HL17UT
HL17_SS
Head (mAHD)
P5-P33 and P67-P95
P33-P67
Observed
P50

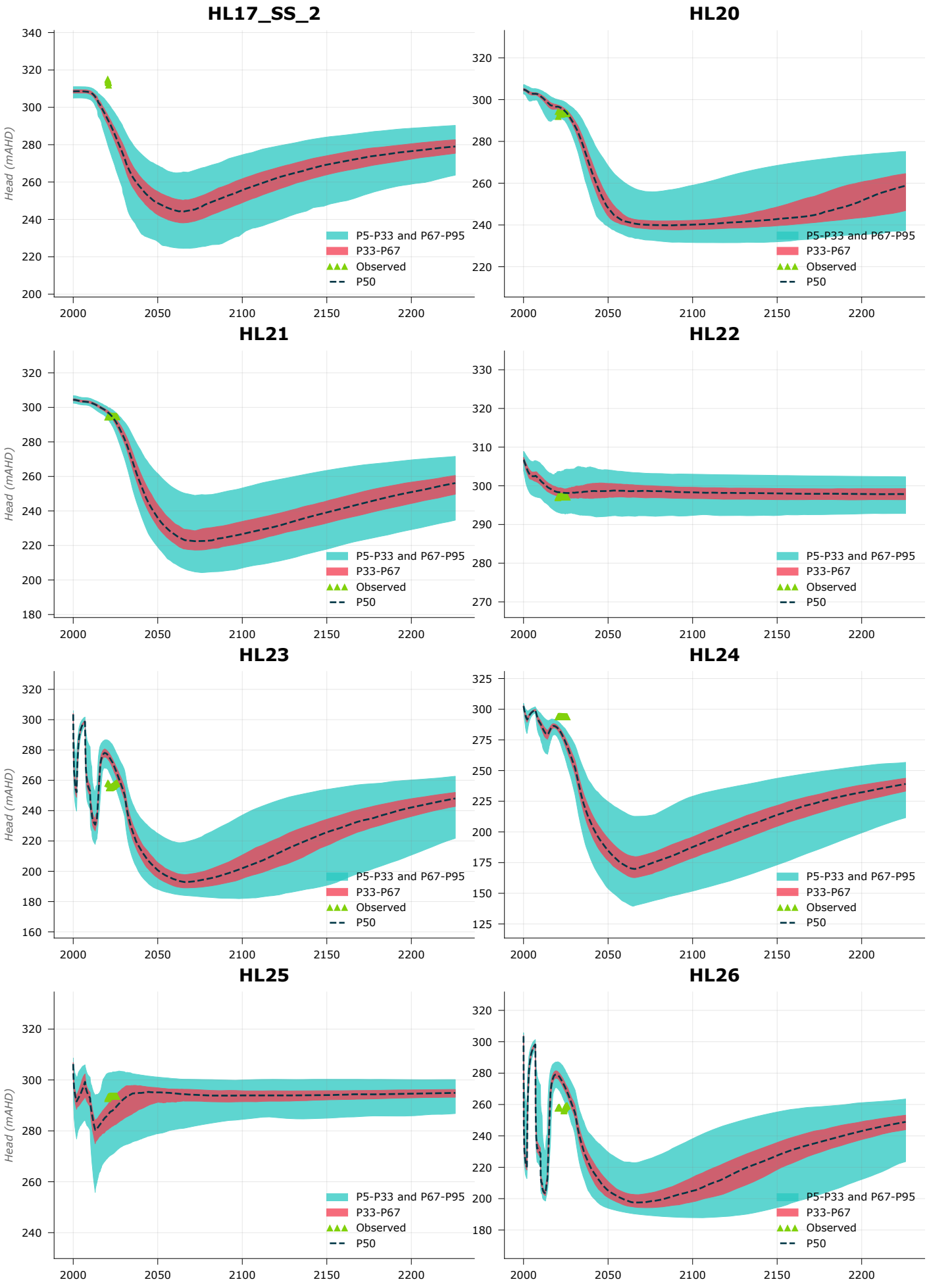
HL17_SS_2
HL20
HL21
HL22
HL23
HL24
HL25
HL26
Head (mAHD)
P5-P33 and P67-P95
P33-P67
Observed
P50
2000
2050
2100
2150
2200

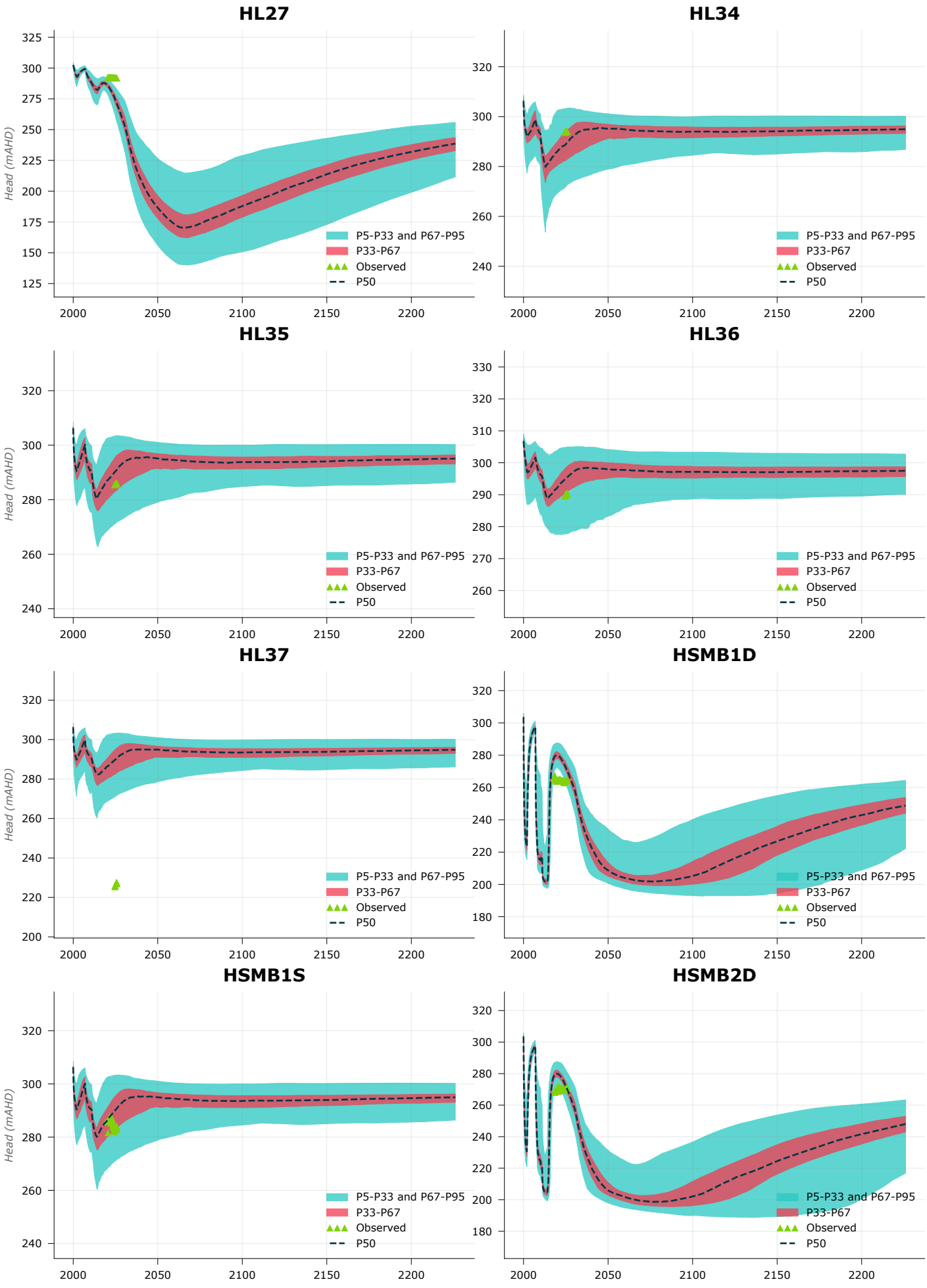
HL27
HL34
HL35
HL36
HL37
HSMB1D
HSMB1S
HSMB2D
Head (mAHD)
P5-P33 and P67-P95
P33-P67
Observed
P50

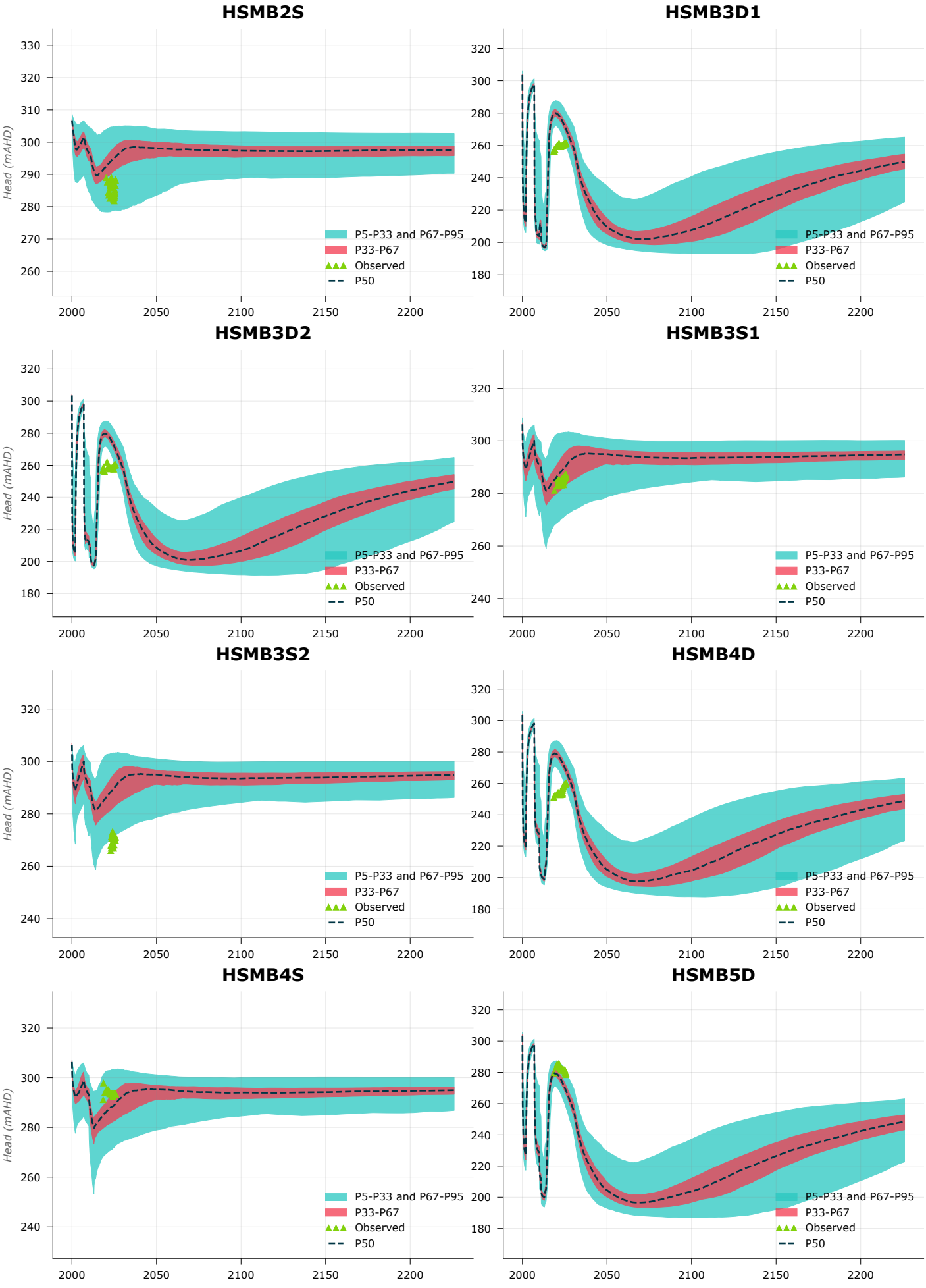
HSMB2S
HSMB3D1
HSMB3D2
HSMB3S1
HSMB3S2
HSMB4D
HSMB4S
HSMB5D
Head (mAHD)
P5-P33 and P67-P95
P33-P67
Observed
P50
2000
2050
2100
2150
2200

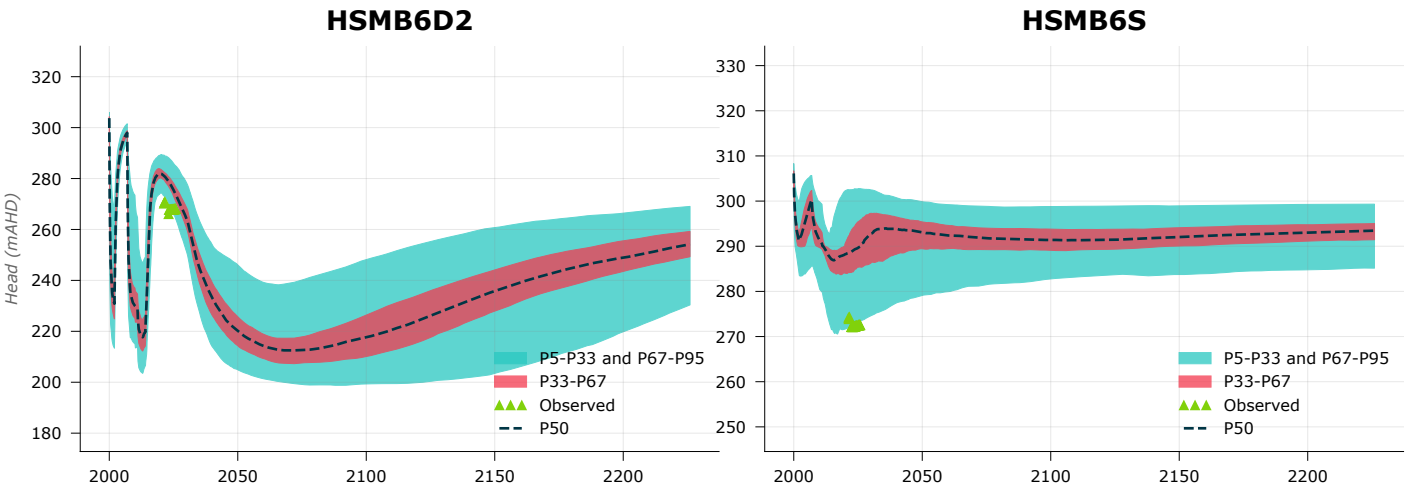
HSMB6D2
Head (mAHD)
320
300
280
260
240
220
200
180
2000
2050
2100
2150
2200
P5-P33 and P67-P95
P33-P67
Observed
P50

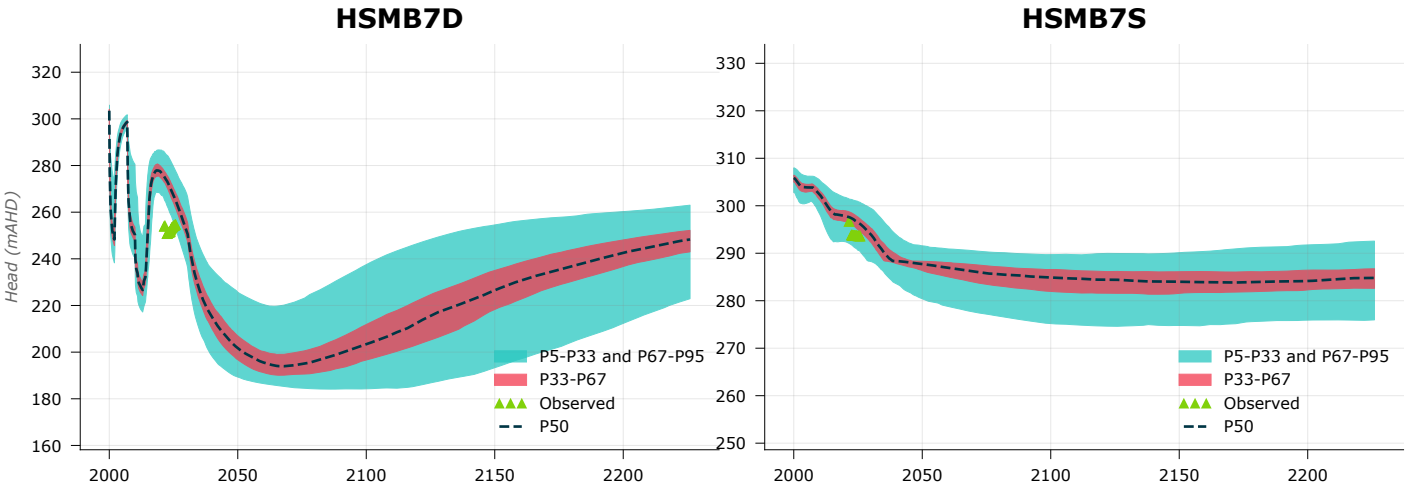
HSMB6S
330
320
310
300
290
280
270
260
250
2000
2050
2100
2150
2200
P5-P33 and P67-P95
P33-P67
Observed
P50

HSMB7D
Head (mAHD)
320
300
280
260
240
220
200
180
160
2000
2050
2100
2150
2200
P5-P33 and P67-P95
P33-P67
Observed
P50

HSMB7S
330
320
310
300
290
280
270
260
250
2000
2050
2100
2150
2200
P5-P33 and P67-P95
P33-P67
Observed
P50

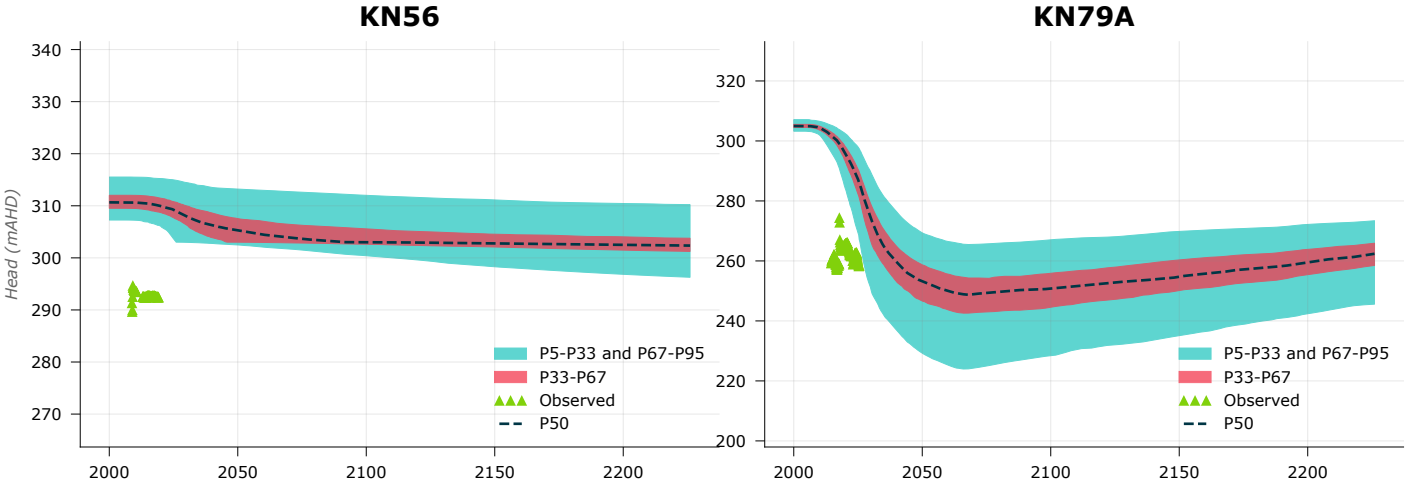
KN56
Head (mAHD)
340
330
320
310
300
290
280
270
2000
2050
2100
2150
2200
P5-P33 and P67-P95
P33-P67
Observed
P50

KN79A
320
300
280
260
240
220
200
2000
2050
2100
2150
2200
P5-P33 and P67-P95
P33-P67
Observed
P50

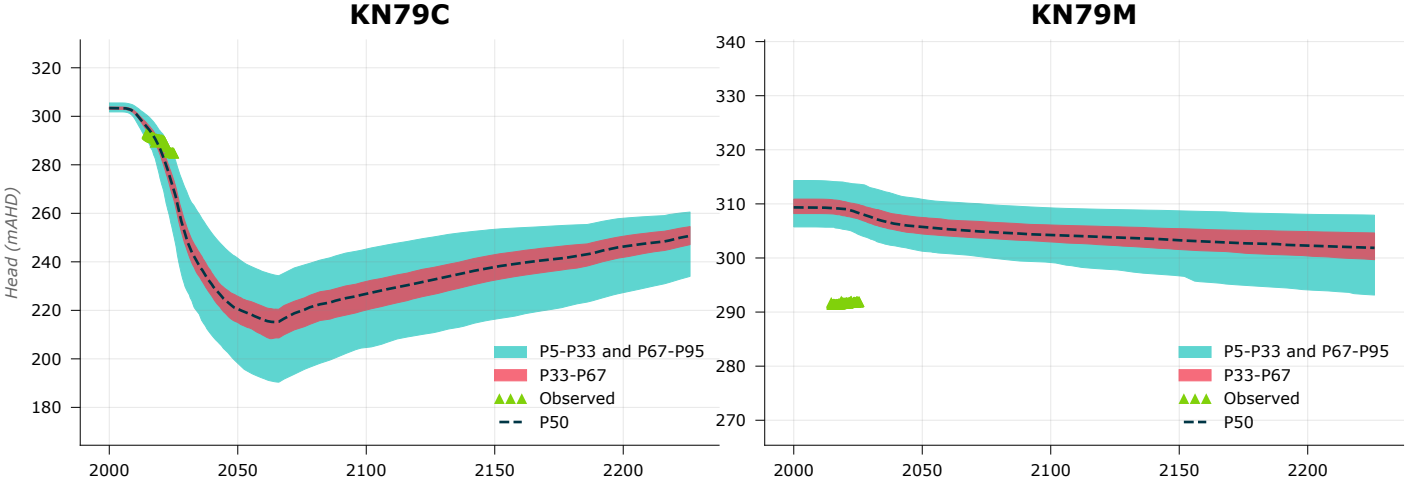
KN79C
Head (mAHD)
320
300
280
260
240
220
200
180
2000
2050
2100
2150
2200
P5-P33 and P67-P95
P33-P67
Observed
P50

KN79M
340
330
320
310
300
290
280
270
2000
2050
2100
2150
2200
P5-P33 and P67-P95
P33-P67
Observed
P50

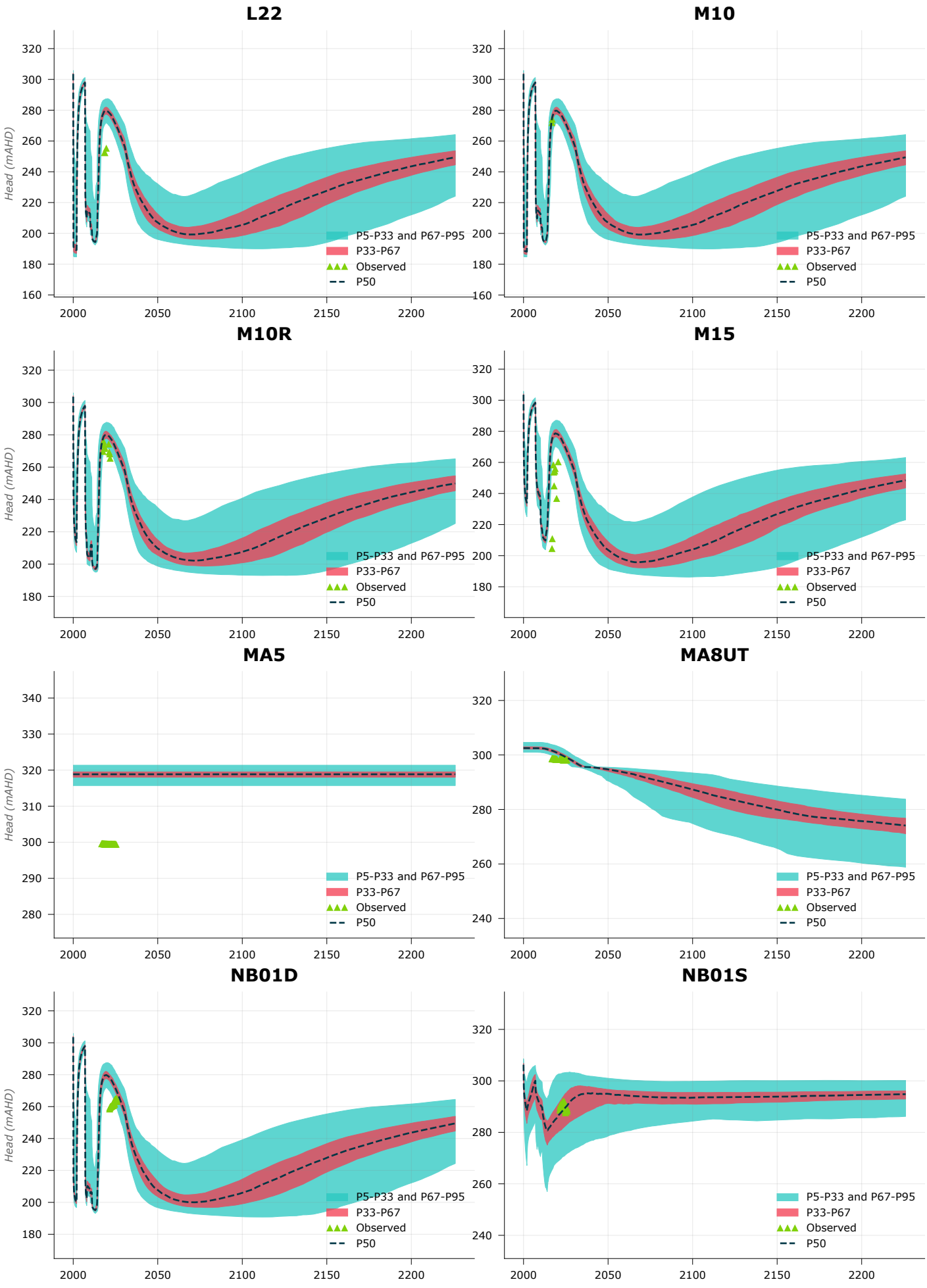
L22
M10
M10R
M15
MA5
MA8UT
NB01D
NB01S
Head (mAHD)
P5-P33 and P67-P95
P33-P67
Observed
P50
2000
2050
2100
2150
2200

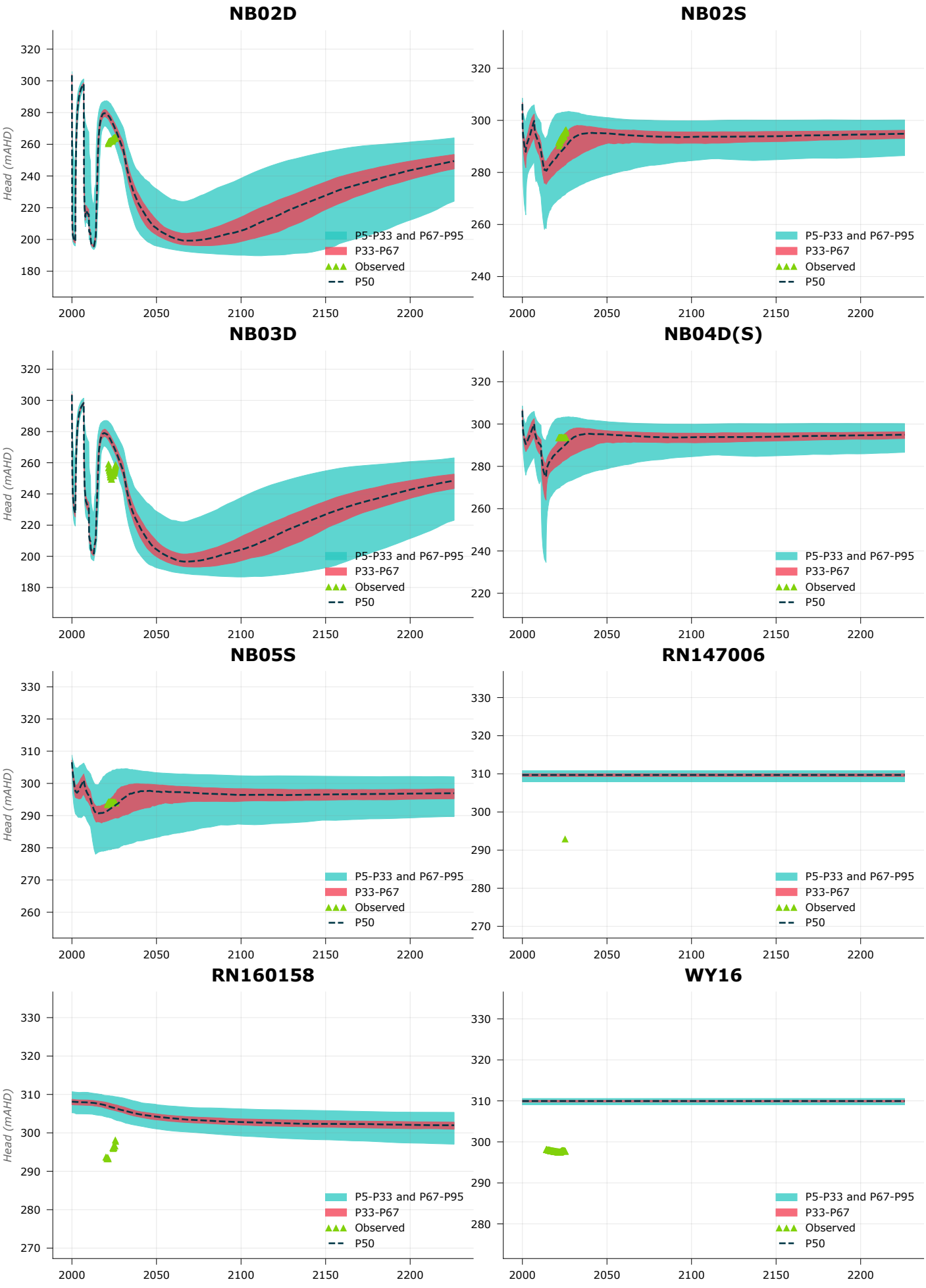
NB02D
NB02S
NB03D
NB04D(S)
NB05S
RN147006
RN160158
WY16
Head (mAHD)
P5-P33 and P67-P95
P33-P67
Observed
P50
2000
2050
2100
2150
2200

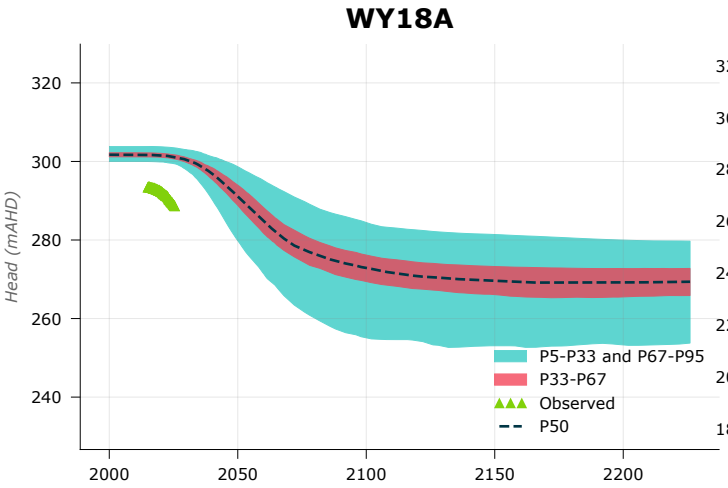
WY18A
Head (mAHD)
320
300
280
260
240
2000
2050
2100
2150
2200
P5-P33 and P67-P95
P33-P67
Observed
P50

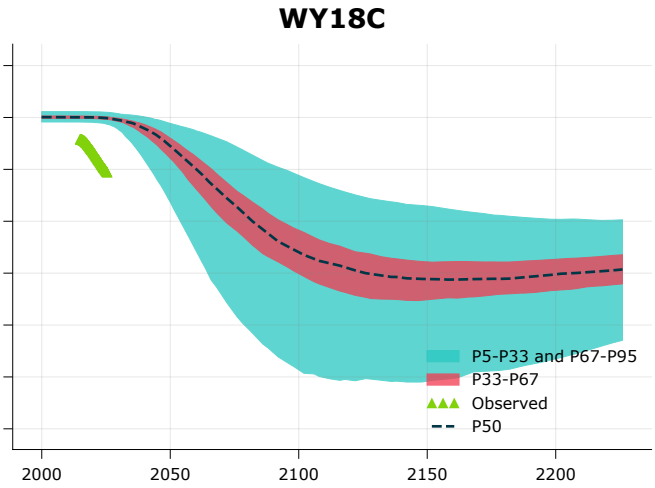
WY18C
320
300
280
260
240
220
200
180
2000
2050
2100
2150
2200
P5-P33 and P67-P95
P33-P67
Observed
P50

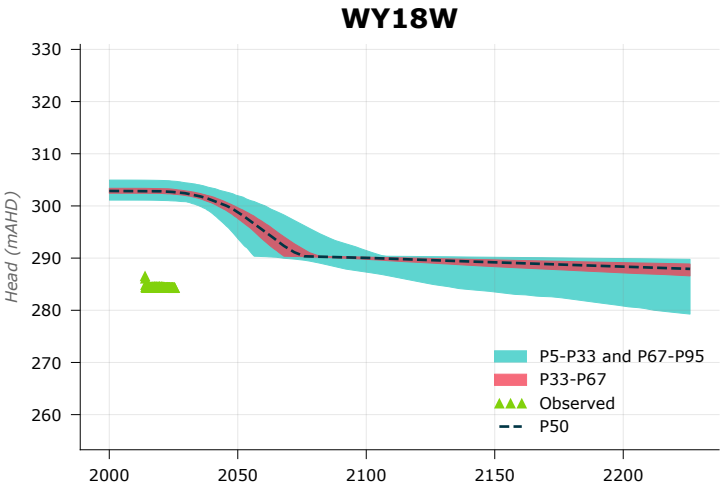
WY18W
Head (mAHD)
330
320
310
300
290
280
270
260
2000
2050
2100
2150
2200
P5-P33 and P67-P95
P33-P67
Observed
P50

Appendix F. Predictive uncertainty – Benzene concentrations

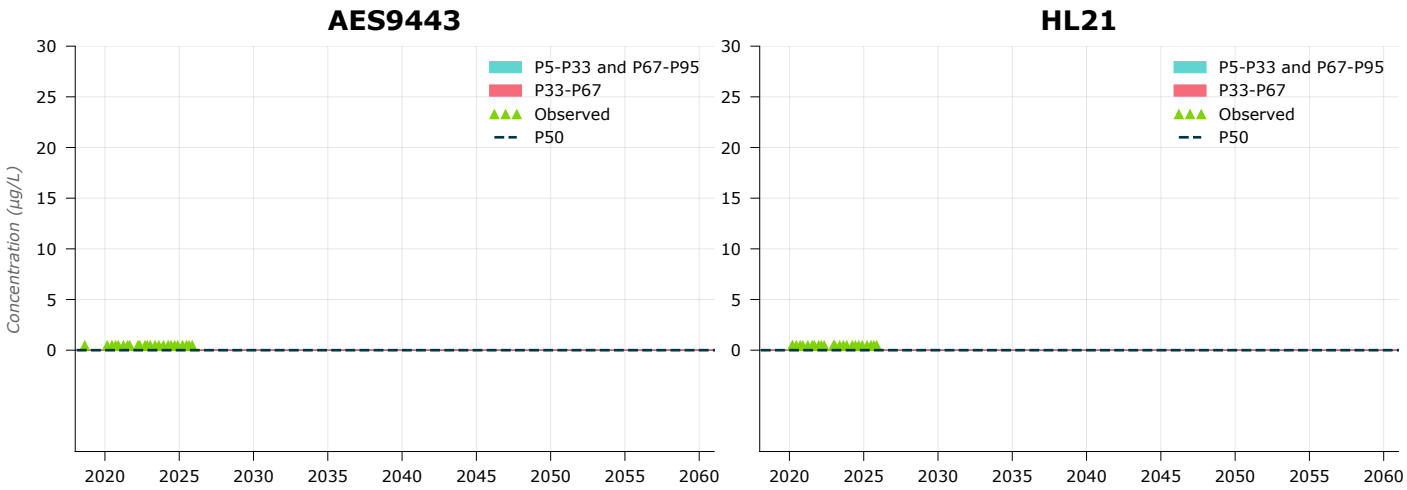
AES9443
HL21
P5-P33 and P67-P95
P33-P67
Observed
P50
Concentration (µg/L)
0
5
10
15
20
25
30
2020
2025
2030
2035
2040
2045
2050
2055
2060

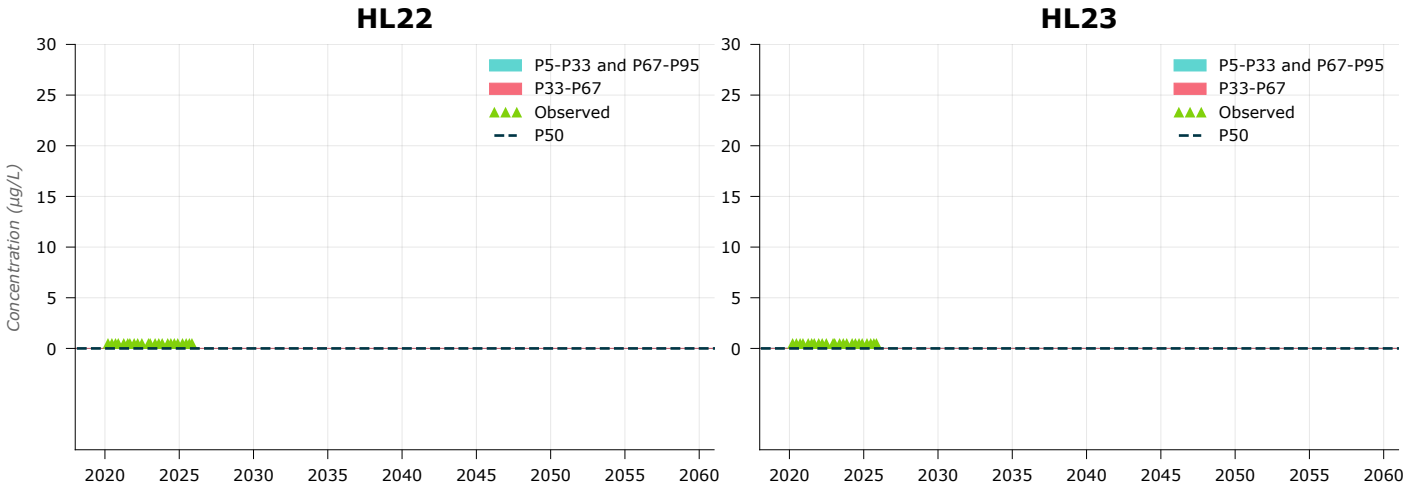
HL22
HL23
P5-P33 and P67-P95
P33-P67
Observed
P50
Concentration (µg/L)
0
5
10
15
20
25
30
2020
2025
2030
2035
2040
2045
2050
2055
2060

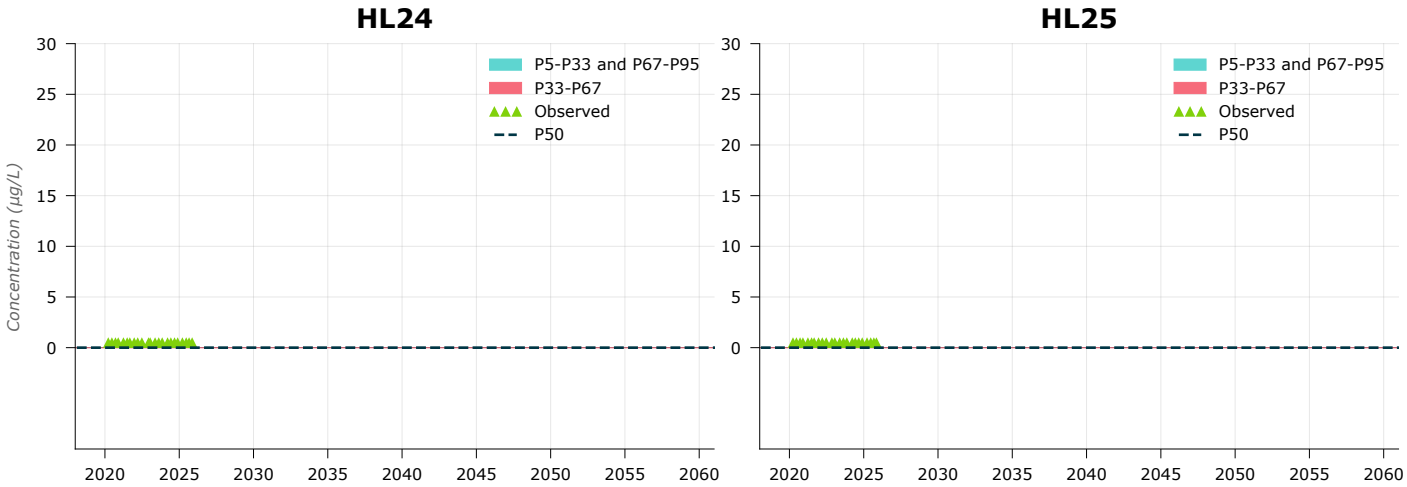
HL24
HL25
P5-P33 and P67-P95
P33-P67
Observed
P50
Concentration (µg/L)
0
5
10
15
20
25
30
2020
2025
2030
2035
2040
2045
2050
2055
2060

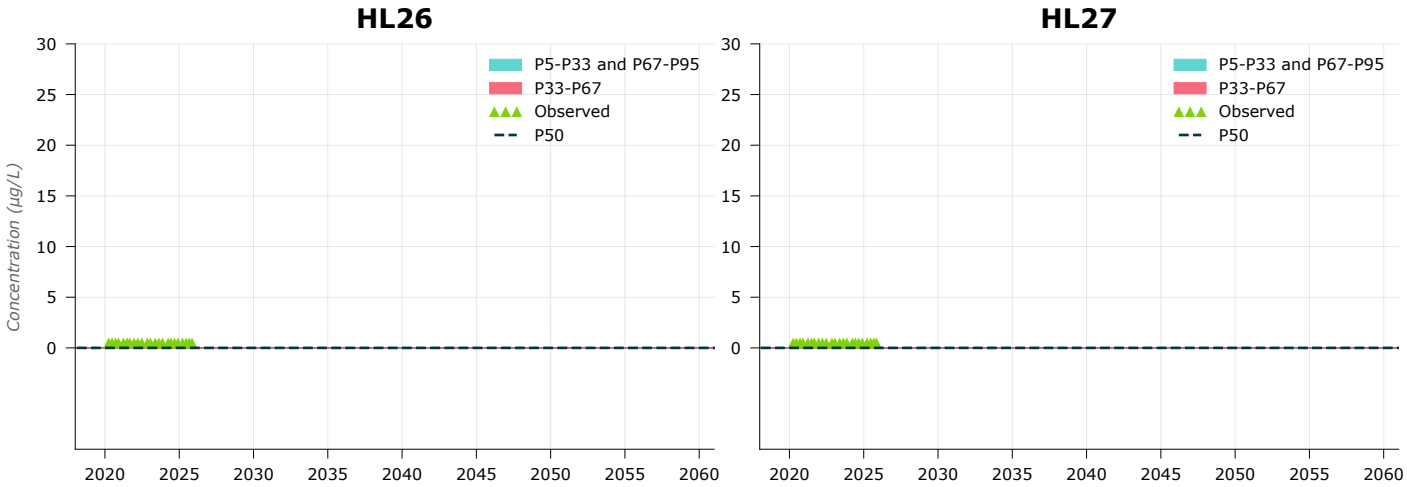
HL26
HL27
P5-P33 and P67-P95
P33-P67
Observed
P50
Concentration (µg/L)
0
5
10
15
20
25
30
2020
2025
2030
2035
2040
2045
2050
2055
2060

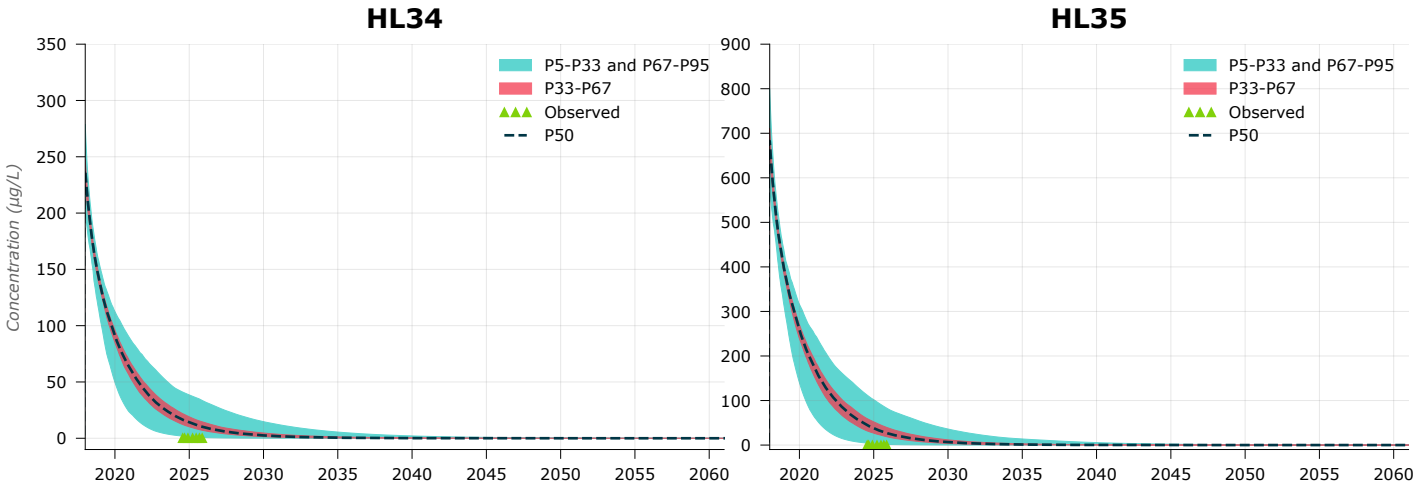
HL34
Concentration (µg/L)
P5-P33 and P67-P95
P33-P67
Observed
P50
0
50
100
150
200
250
300
350
2020
2025
2030
2035
2040
2045
2050
2055
2060

HL35
P5-P33 and P67-P95
P33-P67
Observed
P50
0
100
200
300
400
500
600
700
800
900
2020
2025
2030
2035
2040
2045
2050
2055
2060

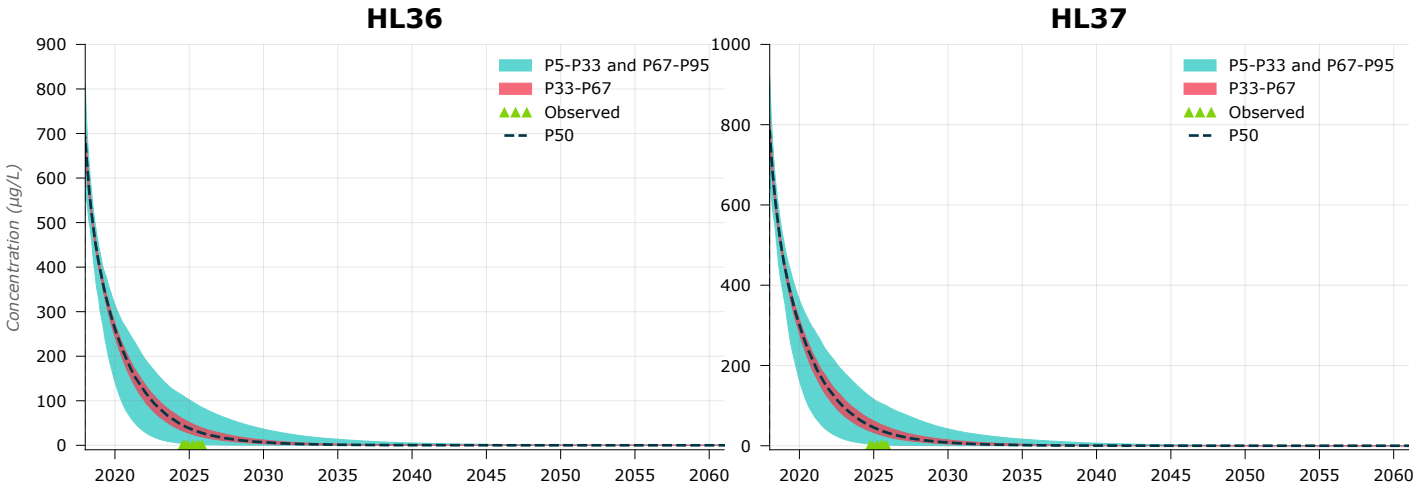
HL36
Concentration (µg/L)
P5-P33 and P67-P95
P33-P67
Observed
P50
0
100
200
300
400
500
600
700
800
900
2020
2025
2030
2035
2040
2045
2050
2055
2060

HL37
P5-P33 and P67-P95
P33-P67
Observed
P50
0
200
400
600
800
1000
2020
2025
2030
2035
2040
2045
2050
2055
2060

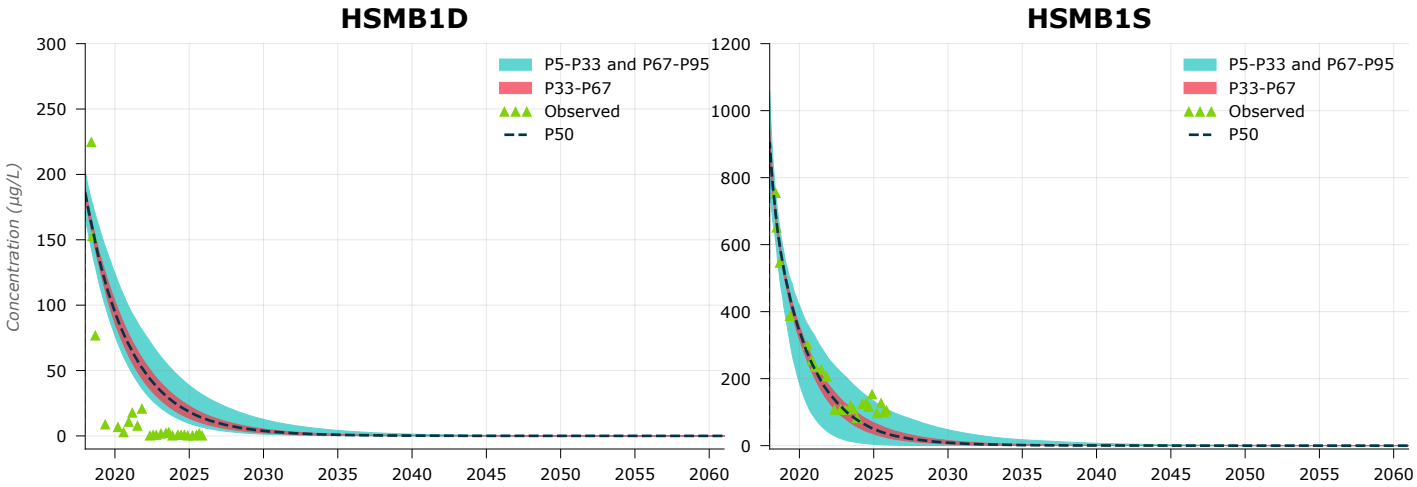
HSMB1D
Concentration (µg/L)
P5-P33 and P67-P95
P33-P67
Observed
P50
0
50
100
150
200
250
300
2020
2025
2030
2035
2040
2045
2050
2055
2060

HSMB1S
P5-P33 and P67-P95
P33-P67
Observed
P50
0
200
400
600
800
1000
1200
2020
2025
2030
2035
2040
2045
2050
2055
2060

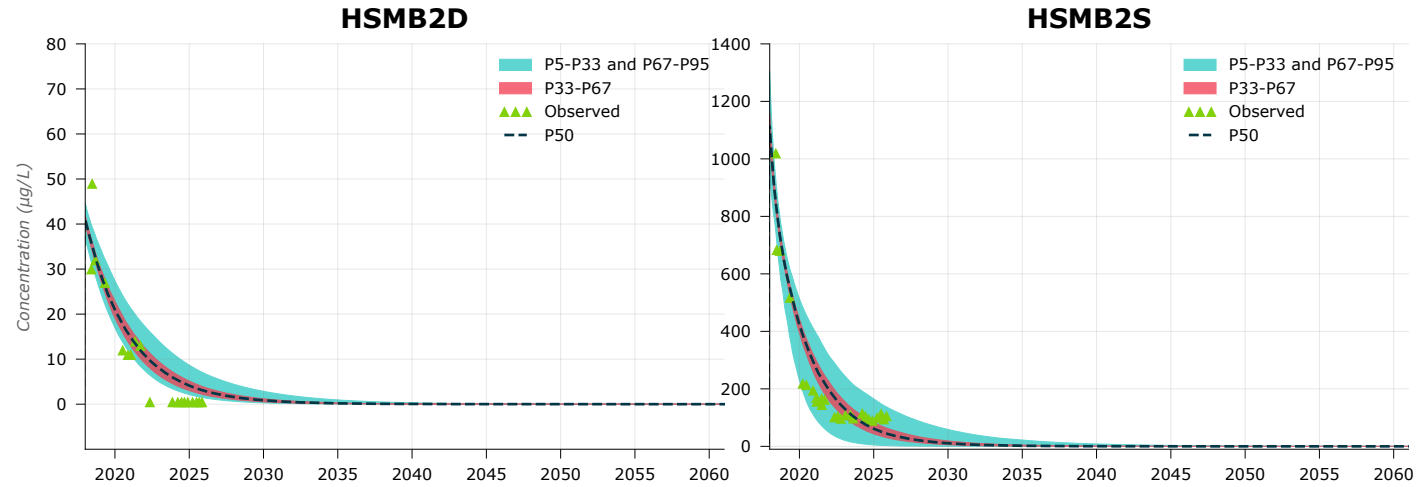
HSMB2D
Concentration (µg/L)
P5-P33 and P67-P95
P33-P67
Observed
P50
0
10
20
30
40
50
60
70
80
2020
2025
2030
2035
2040
2045
2050
2055
2060

HSMB2S
P5-P33 and P67-P95
P33-P67
Observed
P50
0
200
400
600
800
1000
1200
1400
2020
2025
2030
2035
2040
2045
2050
2055
2060

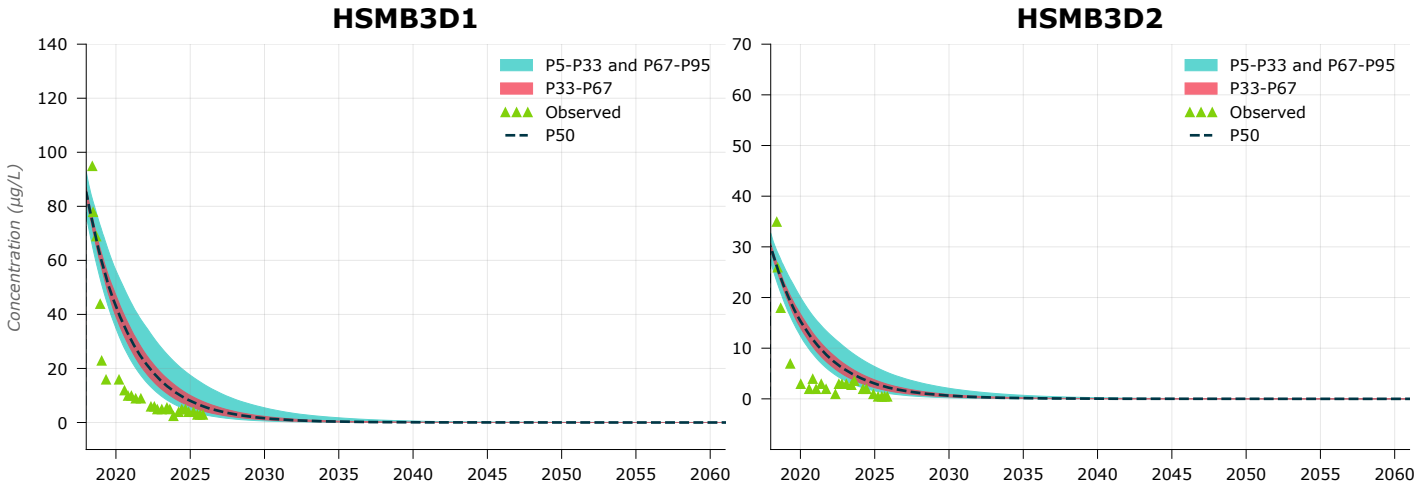
HSMB3D1
Concentration (µg/L)
P5-P33 and P67-P95
P33-P67
Observed
P50
0
20
40
60
80
100
120
140
2020
2025
2030
2035
2040
2045
2050
2055
2060

HSMB3D2
P5-P33 and P67-P95
P33-P67
Observed
P50
0
10
20
30
40
50
60
70
2020
2025
2030
2035
2040
2045
2050
2055
2060

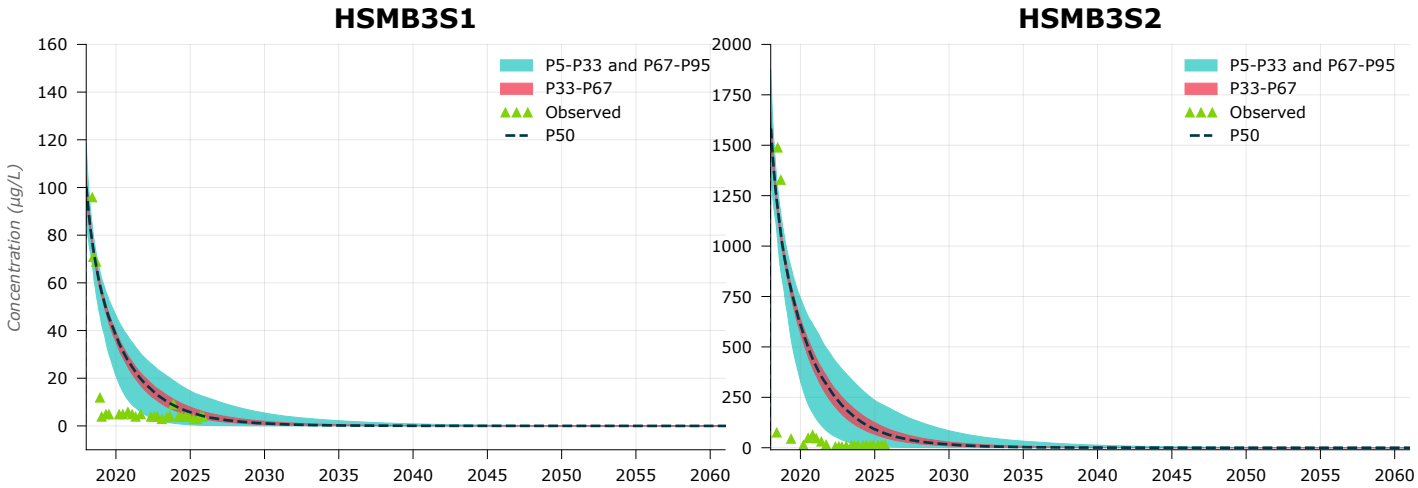
HSMB3S1
Concentration (µg/L)
P5-P33 and P67-P95
P33-P67
Observed
P50
0
20
40
60
80
100
120
140
160
2020
2025
2030
2035
2040
2045
2050
2055
2060

HSMB3S2
P5-P33 and P67-P95
P33-P67
Observed
P50
0
250
500
750
1000
1250
1500
1750
2000
2020
2025
2030
2035
2040
2045
2050
2055
2060

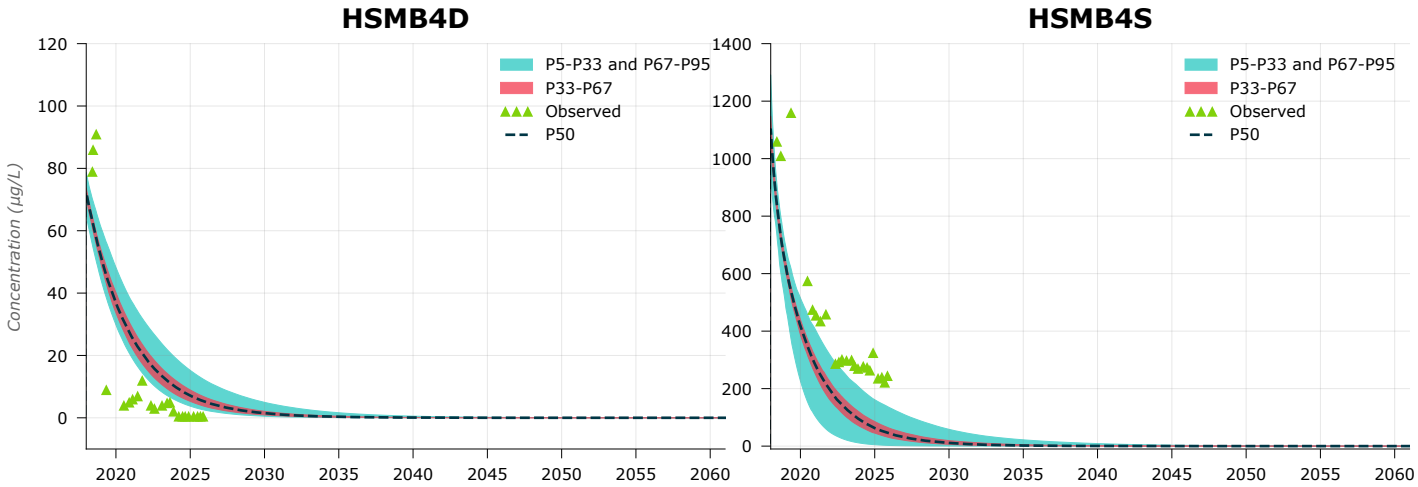
HSMB4D
Concentration (µg/L)
P5-P33 and P67-P95
P33-P67
Observed
P50
0
20
40
60
80
100
120
2020
2025
2030
2035
2040
2045
2050
2055
2060

HSMB4S
P5-P33 and P67-P95
P33-P67
Observed
P50
0
200
400
600
800
1000
1200
1400
2020
2025
2030
2035
2040
2045
2050
2055
2060

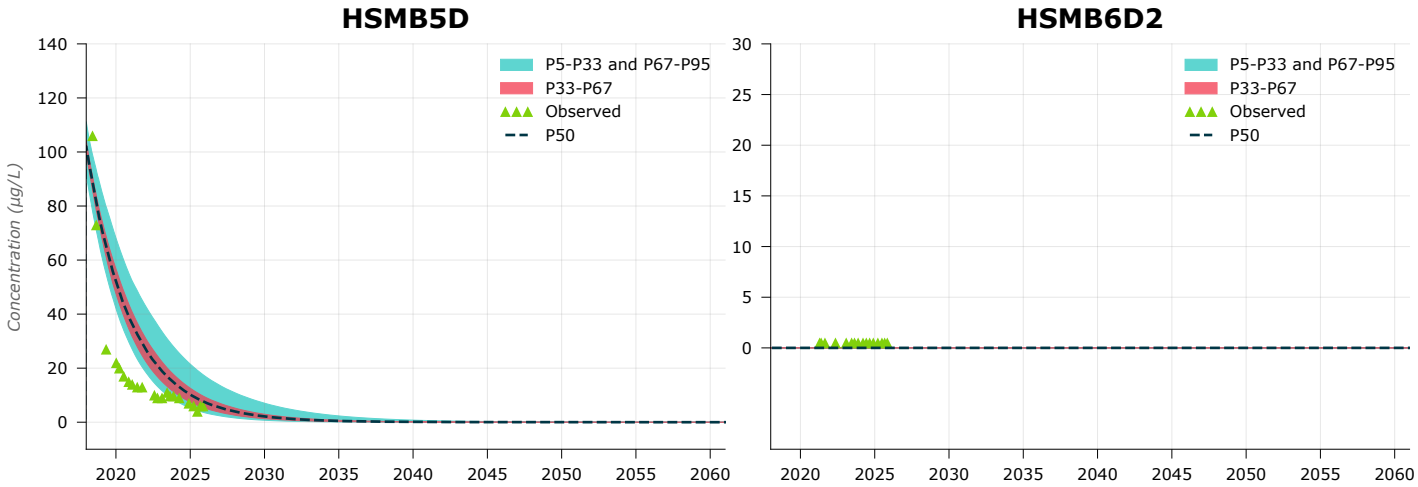
HSMB5D
Concentration (µg/L)
P5-P33 and P67-P95
P33-P67
Observed
P50
0
20
40
60
80
100
120
140
2020
2025
2030
2035
2040
2045
2050
2055
2060

HSMB6D2
P5-P33 and P67-P95
P33-P67
Observed
P50
0
5
10
15
20
25
30
2020
2025
2030
2035
2040
2045
2050
2055
2060

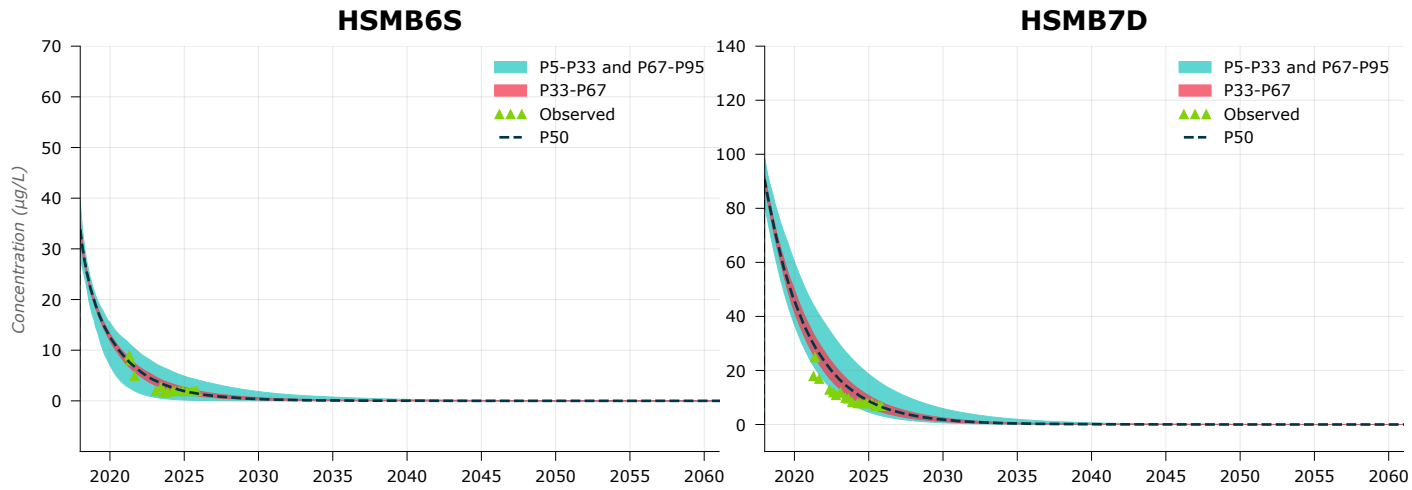
HSMB6S
HSMB7D
P5-P33 and P67-P95
P33-P67
Observed
P50
Concentration (µg/L)

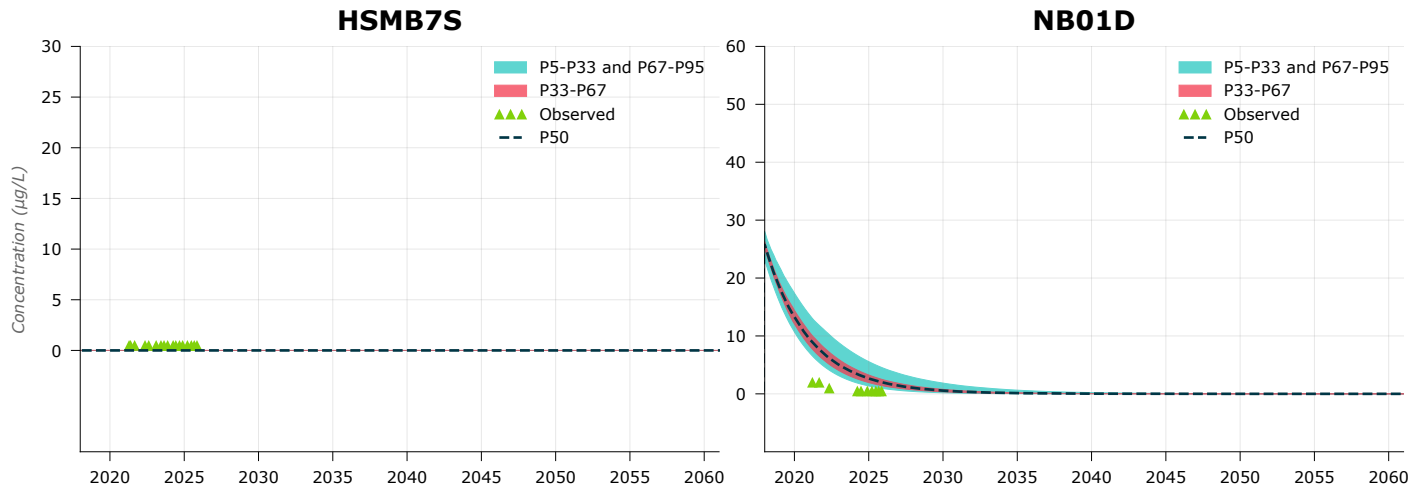
HSMB7S
NB01D
P5-P33 and P67-P95
P33-P67
Observed
P50
Concentration (µg/L)

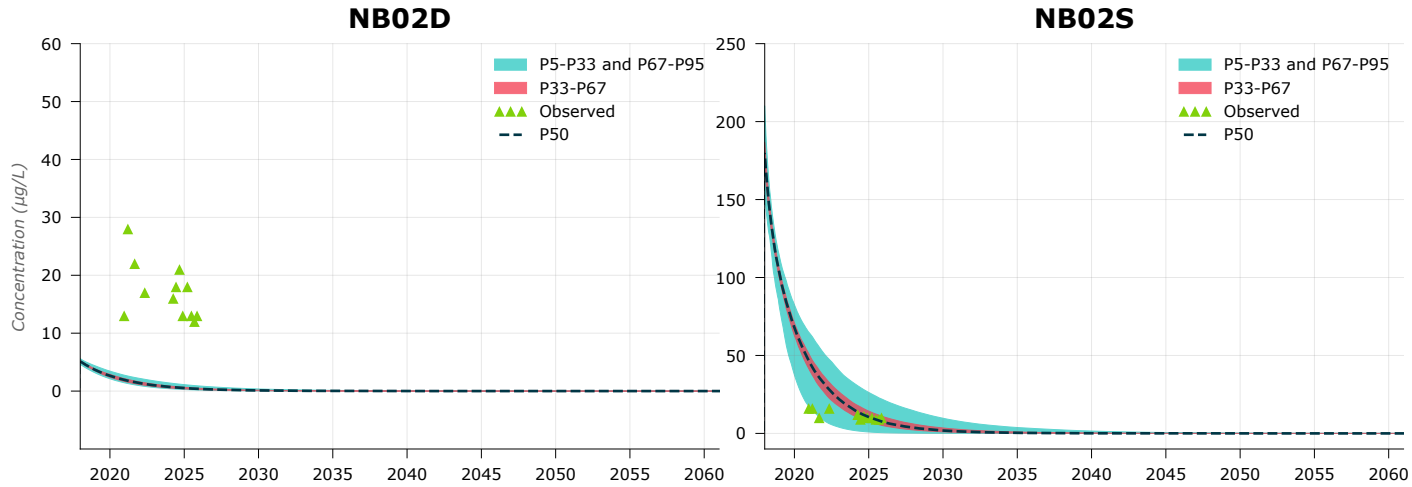
NB02D
NB02S
P5-P33 and P67-P95
P33-P67
Observed
P50
Concentration (µg/L)

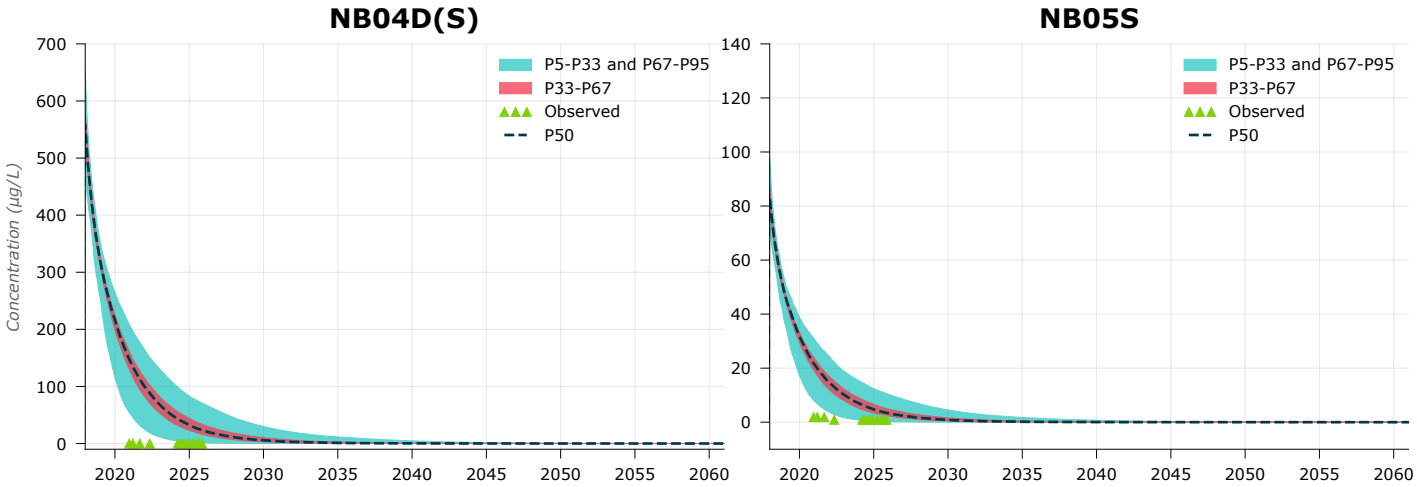
NB04D(S)
NB05S
P5-P33 and P67-P95
P33-P67
Observed
P50
Concentration (µg/L)

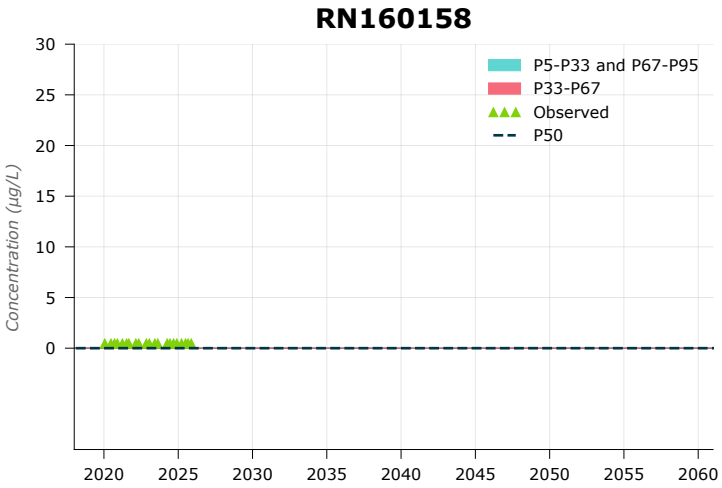
RN160158
P5-P33 and P67-P95
P33-P67
Observed
P50
Concentration (µg/L)
30
25
20
15
10
5
0
2020
2025
2030
2035
2040
2045
2050
2055
2060

Appendix G. Predictive uncertainty – Naphthalene concentrations

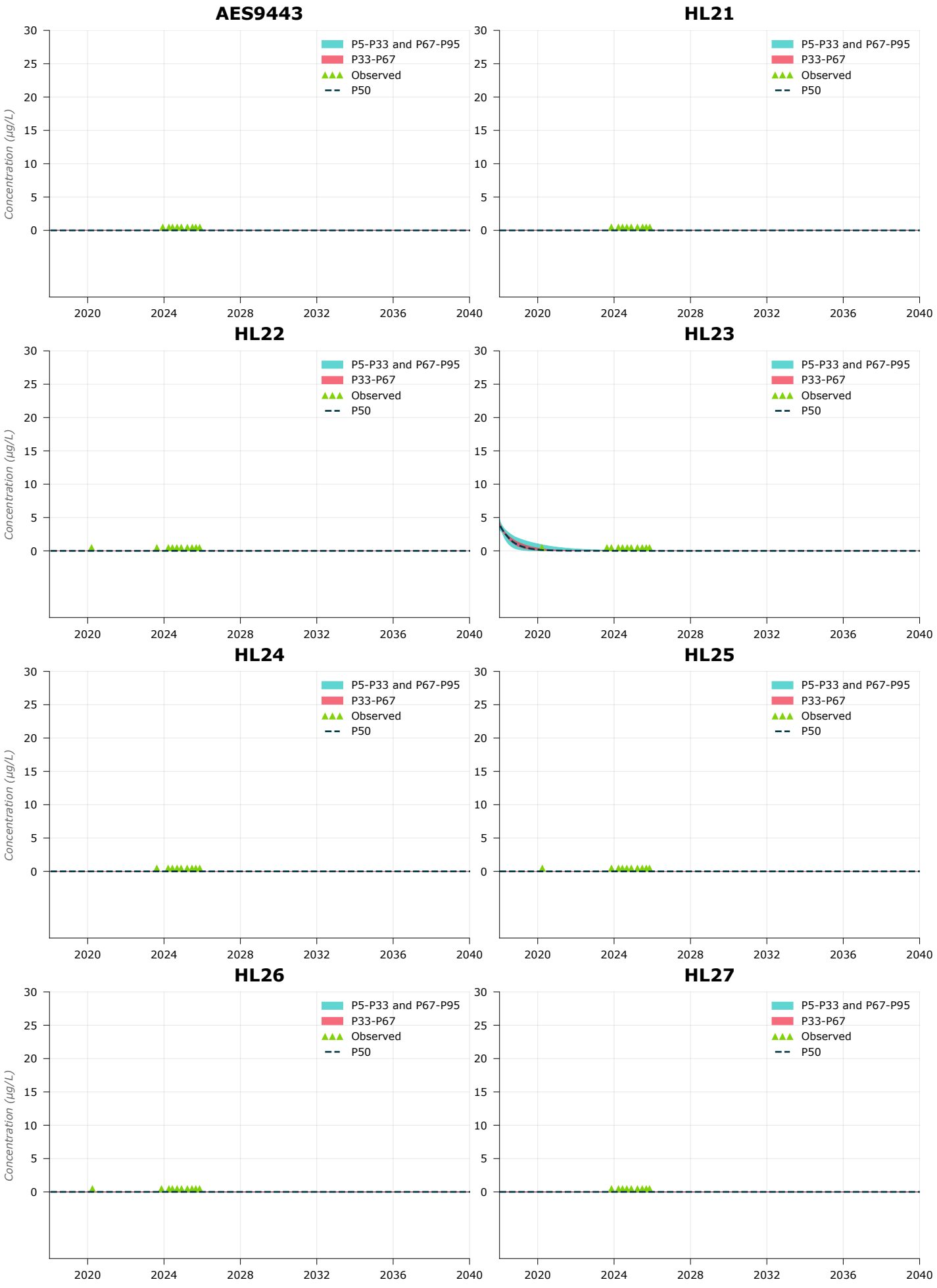
AES9443
HL21
HL22
HL23
HL24
HL25
HL26
HL27
P5-P33 and P67-P95
P33-P67
Observed
P50
Concentration (µg/L)
0
5
10
15
20
25
30
2020
2024
2028
2032
2036
2040

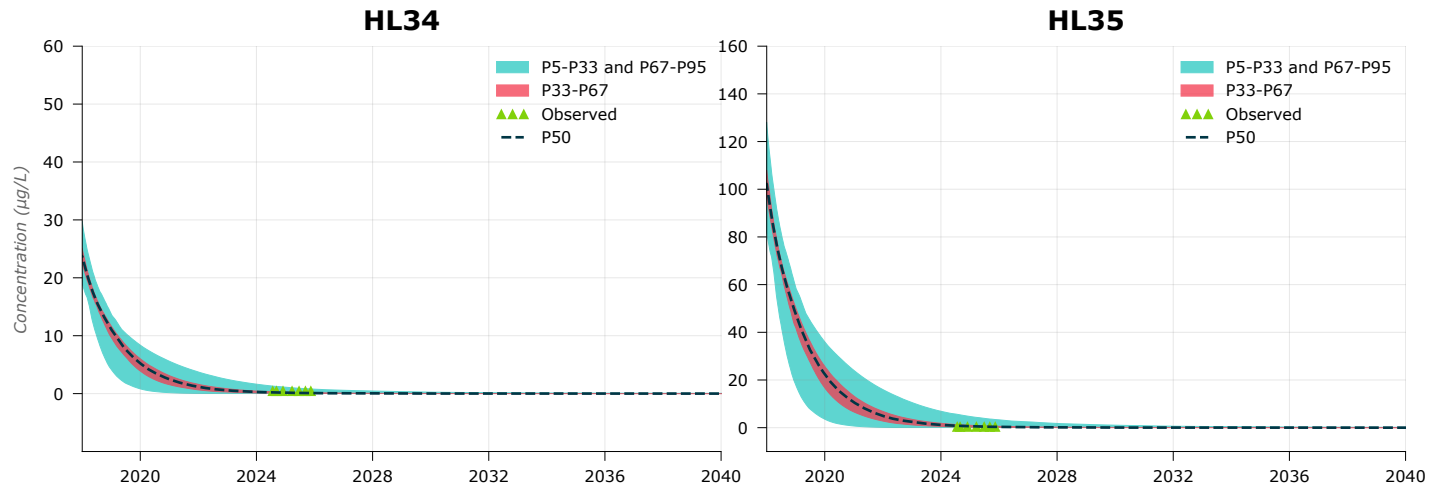
HL34
HL35
P5-P33 and P67-P95
P33-P67
Observed
P50
Concentration (µg/L)
2020
2024
2028
2032
2036
2040

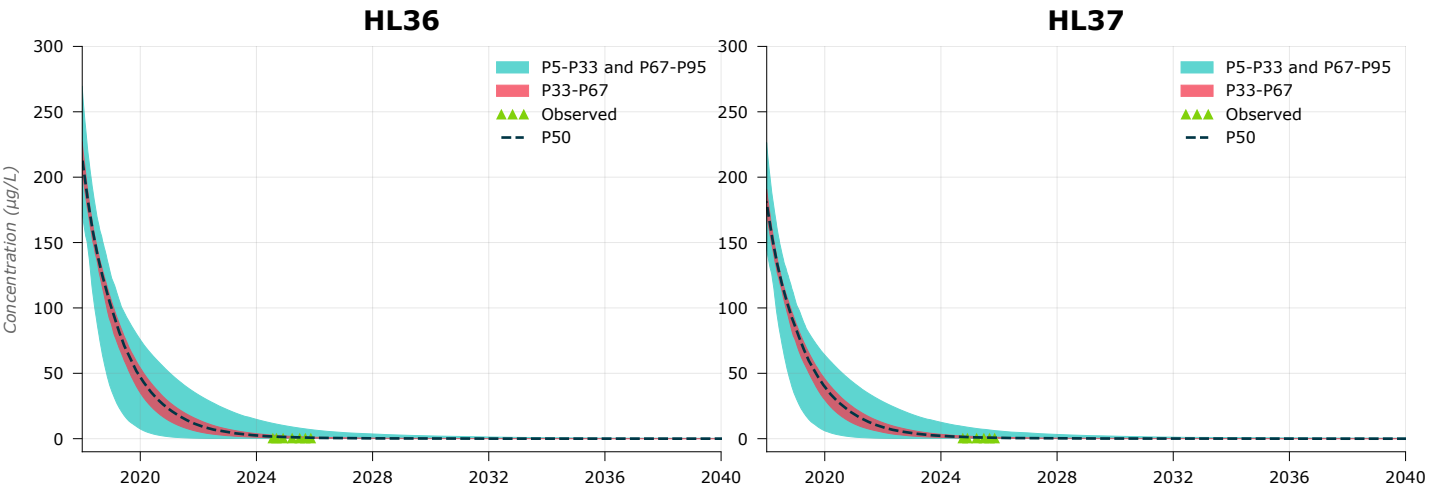
HL36
HL37
P5-P33 and P67-P95
P33-P67
Observed
P50
Concentration (µg/L)
2020
2024
2028
2032
2036
2040

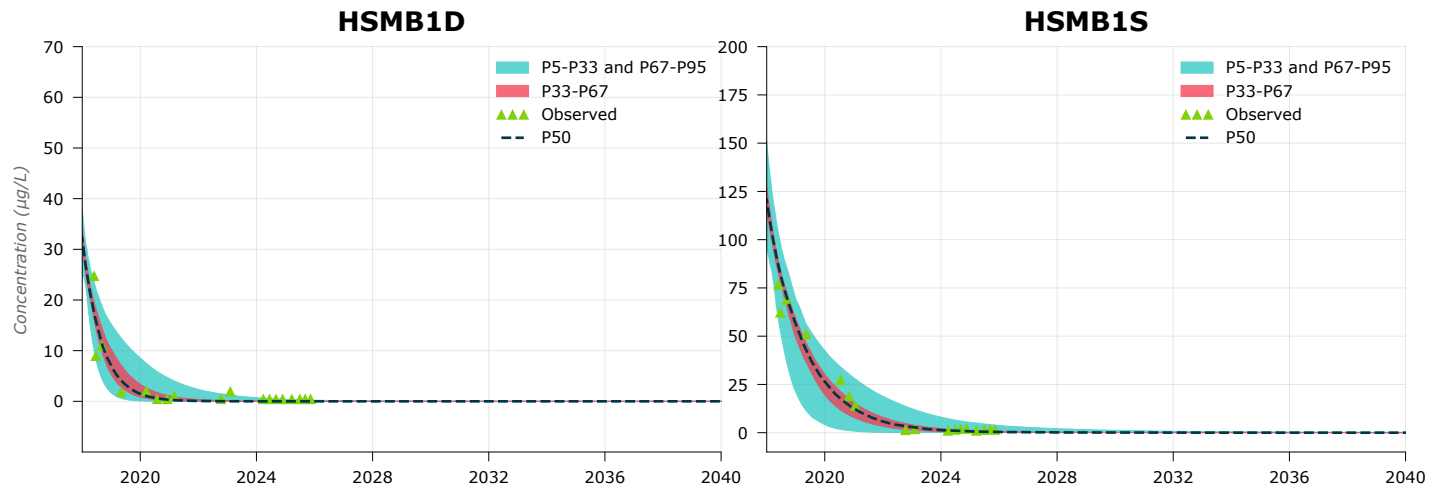
HSMB1D
HSMB1S
P5-P33 and P67-P95
P33-P67
Observed
P50
Concentration (µg/L)
2020
2024
2028
2032
2036
2040

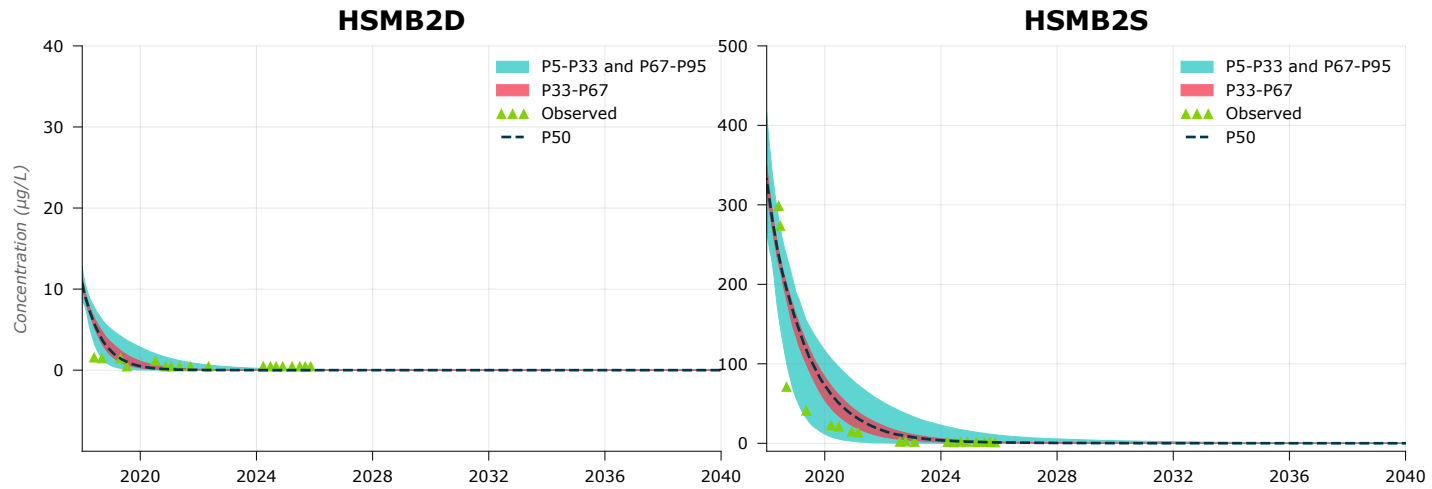
HSMB2D
HSMB2S
P5-P33 and P67-P95
P33-P67
Observed
P50
Concentration (µg/L)
2020
2024
2028
2032
2036
2040

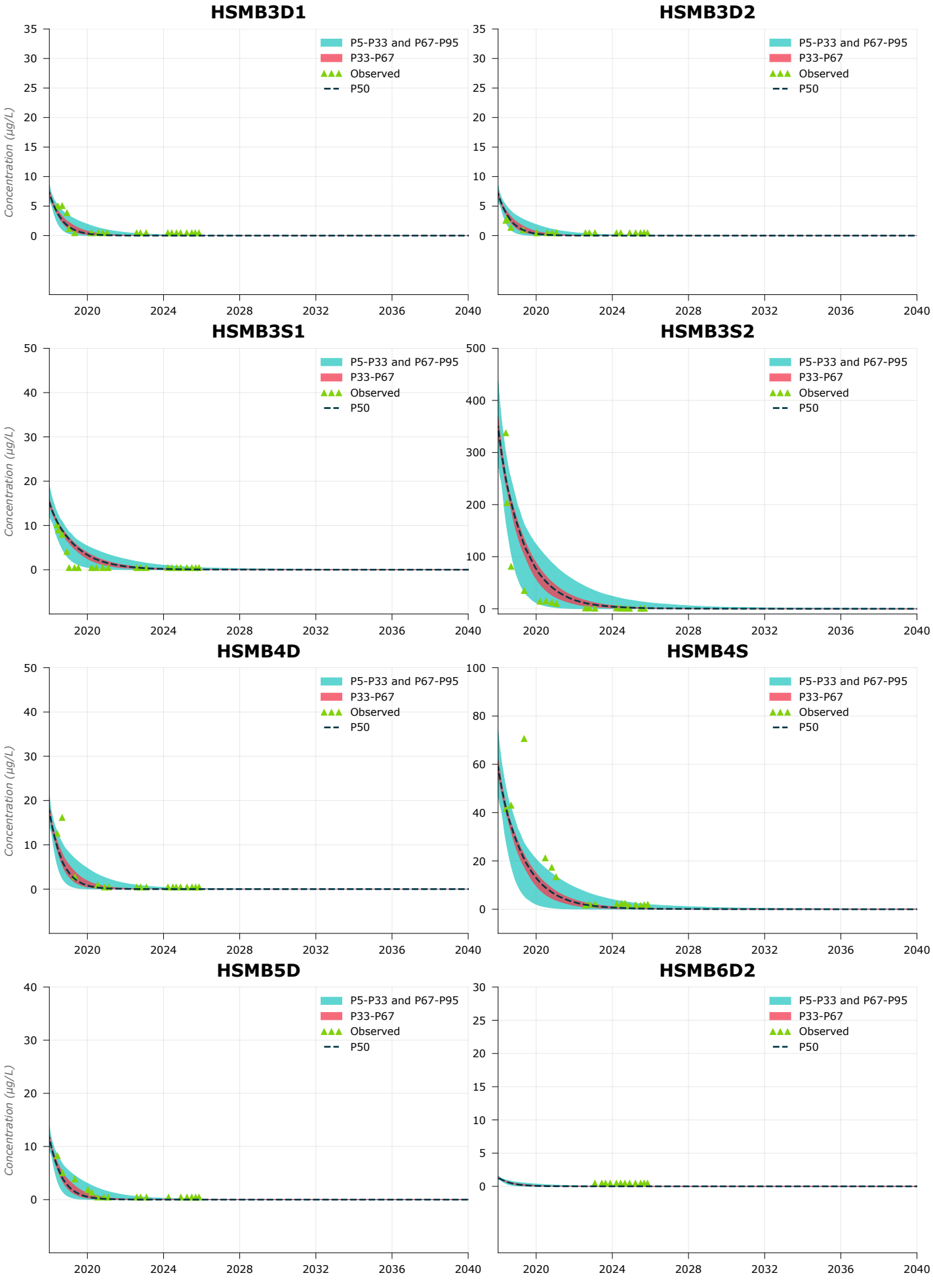
HSMB3D1
HSMB3D2
HSMB3S1
HSMB3S2
HSMB4D
HSMB4S
HSMB5D
HSMB6D2
P5-P33 and P67-P95
P33-P67
Observed
P50
Concentration (µg/L)
2020
2024
2028
2032
2036
2040

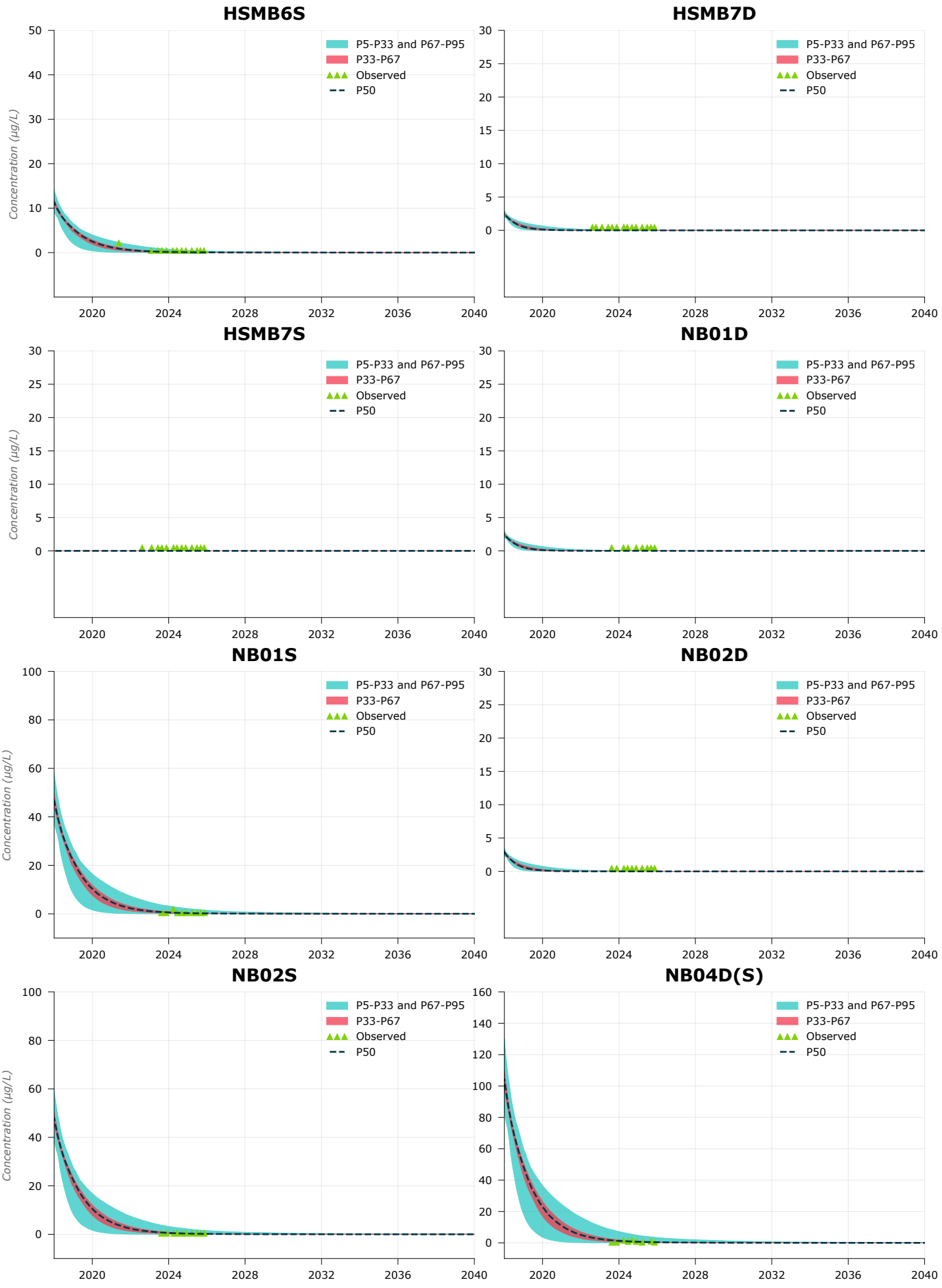
HSMB6S
HSMB7D
HSMB7S
NB01D
NB01S
NB02D
NB02S
NB04D(S)
P5-P33 and P67-P95
P33-P67
Observed
P50
Concentration (µg/L)
2020
2024
2028
2032
2036
2040

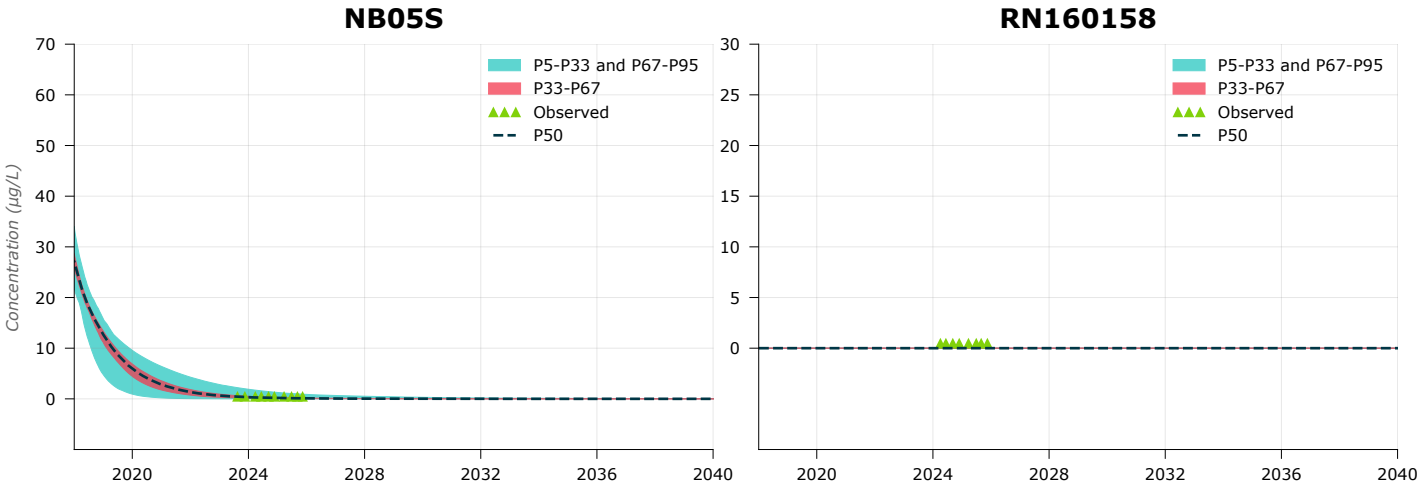
NB05S
RN160158
P5-P33 and P67-P95
P33-P67
Observed
P50
Concentration (µg/L)
70
60
50
40
30
20
10
0
30
25
20
15
10
5
0
2020
2024
2028
2032
2036
2040